Targeting β-catenin to inhibit the Wnt pathway in colorectal cancer cell lines

Laura Alexandra Colling

Hertford College



A thesis submitted to the Division of Medical Sciences, University of Oxford, in partial fulfilment of the requirements for the degree of

Doctor of Philosophy in Oncology

Trinity Term 2019

Weatherall Institute of Molecular Medicine
University of Oxford

To my parents

Thank you for all your support,
for challenging me to always give my best
and your unconditional love.

Acknowledgements

First and foremost, I would like to thank my supervisor Professor Sir Walter Bodmer for welcoming me in his lab and guiding me through the PhD. Thank you for putting your trust in me. I would also like to thank Professor Terrence Rabbitts for his valuable input into my work. My gratitude goes to Professor Valentine Macaulay who has supported and guided me over the past four years. Your help has been invaluable – thank you!

I owe heart-felt acknowledgements to Dr Djamila Ouaret and Dr Jenny Wilding. Djamila, I am deeply thankful for all your support and advice, both inside and outside the lab. I have found in you a friend and mentor which always welcomes me with open arms and ears. Jenny, thank you so much for the many supportive and encouraging discussions – they truly made a difference to me. All of this wouldn't have been possible without the two of you! I would also like to thank Dr Kamila Koprowska, who taught me in the initial steps of my studies, and Dr Viorica Liebe Lastun, who was a great help in the final months of my work. My gratitude also goes to Dr Neil Ashley, who supported me throughout my studies, and to Dr Johanna Michl and Dr Stefania Monterisi.

A big Thank You to all current and past members of the Bodmer lab, who have helped me on a scientific and personal level over the years: Jens, Peter, Tom, Hani, Haoyu, Shuhui, Mustak, Jeff and the wider POBI family. It has been a great pleasure working with you and I am grateful for you spending the long days in the lab by my side.

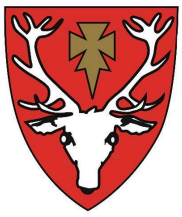
I would also like to acknowledge the help of the members of the Rabbitts lab, especially Dr Ami Miller and Dr Wilawan Bunjobpol. Furthermore, I would like to thank the Oncology Facilities team and Linda Beattie for making the day-to-day research much easier. Thank you to Andres Hueso Cuervo, Dr Abimael Cruz-Migoni, Dr David Staunton, Dr Paul Sopp, Dr Eliot Osher and Dr Ryan Beveridge for their scientific help, as well as Dr Vita Golubovskaya for her support and scientific discussions. I am grateful for the support of Professor Marella de Bruijn while being involved as the MRC Student representative.

A big *Dankeschön* to Enno and Marlene who have given me a home in Oxford and took me to unprecedented culinary explorations. Thank you to Kati, Oana, Sol, Sukhi, Andy, Luiza and all my friends for keeping up with my PhD stories and being there for me.

I want to express my gratitude to my parents and sister who showed great patience, guidance and support. And to Marcin who has shared this journey with me and made it so much more bearable. He was my safety-belt on this emotional rollercoaster ride! Thank you for everything.

This work has been funded and supported by the Medical Research Council (MRC) and the Stiftung der Deutschen Wirtschaft (SDW). I would also like to acknowledge the support from Hertford College.







Author Declaration

I, Laura Alexandra Colling, hereby declare that the work on which this thesis is based is my original work and that neither the whole work nor any part of it has been, is being, or will be submitted for another degree in this or any other university. The work is original, except where listed by reference in the text or listed as follows: computational and statistical analysis of β-catenin localisation in a panel of colorectal cancer cell lines (Chapter 3) by Ta-Chun Liu (Bodmer Lab), the creation of lentiviruses (Chapter 6) by Dr Ryan Beveridge (Lentiviral Facility, WIMM, University of Oxford), the FACS analysis of stable SW480-VHH clones (Chapter 6) by Dr Paul Sopp (FACS Facility, WIMM, University of Oxford), the Mass Spectrometry data (Chapter 6) by Dr David Staunton (Biochemistry Department, University of Oxford) and the liquid chromatography protein purifications (Chapter 6) by Andres Hueso Cuervo and Dr Abimael Cruz-Migoni (WIMM, University of Oxford).

Date: _____ Signature:_____

Abstract

In colorectal cancer (CRC), one of the post prevalent cancers, the Wnt signalling pathway is upregulated due to mutations in the key players *Adenomatous polyposis coli* (*APC*) and *CTNNB1* (β-catenin). While intensive research efforts are being placed in blocking the Wnt pathway, no inhibitors are yet in clinical use. In this project, different strategies were assessed to target β-catenin protein-protein interactions (PPIs) with the aim to inhibit the Wnt pathway in CRC cell lines.

Through 2x2 statistical analyses of known microarray gene expression and mutation data and preliminary immunofluorescence imaging of β-catenin localisation in CRC lines, low E-cadherin expression was associated with a more nuclear β-catenin subcellular localisation (**Chapter 3**).

Three different approaches to target the Wnt pathway were described: firstly, small molecule inhibitors against the β-catenin/B cell lymphoma 9 (BCL9) interaction site were tested *in vitro* (**Chapter 4**). The compounds exhibited non-specific killing on a large panel of CRC cell lines and fibroblasts. Furthermore, the compounds were also shown to be albumin dependent, limiting their further development. In **Chapter 5**, the Intracellular Antibody Capture (IAC) methodology to identify intracellular single domain antibodies (sdAb) against β-catenin is described. Through a large variable-heavy (VH) single domain library screen, three sdAb against β-catenin were identified, but subsequentially shown to be non-specific binders. Lastly, a previously described llama single-domain antibody fragment (VHH) was further characterised in SW480 CRC cells (**Chapter 6**). The VHH was shown to inhibit T-cell factor (TCF)-mediated Wnt pathway transcription and the expression of the Wnt target genes *ASCL2* and *AXIN2*. The VHH binding site was refined to the first three Armadillo repeats of β-catenin.

Overall, this work explores different routes of Wnt signalling inhibition by targeting β-catenin PPIs and discusses their advantages and potential limitations for further development (**Chapter 7**).

Table of Contents

ACKNOWLEDGEMENTS ..... **I**

AUTHOR DECLARATION ..... **III**

ABSTRACT ..... **IV**

LIST OF FIGURES ..... **XI**

LIST OF TABLES ..... **XV**

LIST OF APPENDICES ..... **XVII**

LIST OF ABBREVIATIONS ..... **XIX**

CHAPTER 1: INTRODUCTION **2**

1.1 The small intestine and the colon **2**
1.1.1 The structure of the intestinal and colonic crypts 2
1.1.2 The stem cell niche 3
1.1.3 Homeostatic control along the intestinal and colonic crypts 5

1.2 Colorectal cancer **6**
1.2.1 Epidemiology 6
1.2.2 Hereditary CRC 6
1.2.3 Wnt pathway in colorectal cancer 7

1.3 The Wnt pathway **8**
1.3.1 The canonical Wnt pathway 10

1.4 The multifunctional role of β-catenin **13**
1.4.1 The role of β-catenin in cell-cell contact 13
1.4.2 The structure of β-catenin 14

1.5 β-catenin and its interaction partners **14**
1.5.1 TCF/LEF family members 15
1.5.2 Structural details of the β-catenin/TCF4 interaction 17
1.5.3 The structure and function of BCL9/BCL9L 17
1.5.4 Structural details of the β-catenin/BCL9 interaction 20
1.5.5 Interaction partners of the β-catenin C-terminal 21

1.6 The Wnt signalling pathway as therapeutic target 22
1.6.1 Small molecules and peptides targeting the Wnt pathway 23
1.6.1.1 Targeting the β-catenin/TCF4 interaction 23
1.6.1.2 Targeting the β-catenin/BCL9 interaction 24
1.6.2 Other small molecule targets in the Wnt pathway 25
1.6.3 Antibody-based approaches 26
1.6.3.1 Conventional antibodies 26
1.6.3.2 Intracellular single domain antibodies 28
1.6.3.3 Antibodies against the Wnt signalling pathway 30
1.6.3.4 Llama antibody fragments 32
1.6.4 Characteristics of VHHs 33
1.6.5 VHHs targeting the Wnt pathway 33

1.7 Aims and scope of this work 35

CHAPTER 2: MATERIALS AND METHODS 38

2.1 Cell culture methods 38
2.1.1 Reagents and suppliers 38
2.1.2 Cell lines 38
2.1.1 Cell culture conditions and maintenance 38
2.1.2 Cell storage and retrieval 41
2.1.3 Cell counting 41
2.1.4 Mycoplasma testing 41

2.2 Drug studies 42
2.2.1 Compounds 42
2.2.2 Drug treatment 43
2.2.3 Sulphorhodamine B Protein Staining assay 43
2.2.4 Calcein-AM staining 44
2.2.5 Colony Formation Assay (CFA) 44

2.3 Lentiviral work 45
2.3.1 Lentiviral transduction of cells 45
2.3.2 Single cell selection from Lentiviral bulk cultures 46
2.3.3 Doxycycline induction 46

2.4 Microscopy 47
2.4.1 Antibodies used for immunofluorescence 47
2.4.2 Immunofluorescence 47

2.5 Luciferase reporter assay 48

2.6 RNA methods 50
2.6.1 RNA extraction 50

2.6.2 Reverse transcription 51
2.6.3 Quantitative real-time PCR (qRT-PCR) 51
2.6.4 Microarray gene expression analysis 52

2.7 DNA methods 53
2.7.1 DNA quantification 53
2.7.2 Primer design 53
2.7.3 Primers used in this thesis 53
2.7.4 Polymerase chain reaction (PCR) 55
2.7.5 Agarose gel electrophoresis 56
2.7.6 DNA purification from agarose gel 57

2.8 Cloning methods 58
2.8.1 List of vector backbones 58
2.8.2 Restriction digests 59
2.8.3 Ligations 59
2.8.4 Preparation of competent DH5α *E.coli* 60
2.8.5 Transformation of *E.Coli* 60
2.8.6 Antibiotic stock concentrations for selections 61
2.8.7 Plasmid DNA extraction from *E.Coli* 61
2.8.8 Sanger Sequencing 62

2.9 Protein methods 62
2.9.1 Preparation of whole cell protein lysates from cell lines 62
2.9.2 Preparation of cytoplasmic and nuclear protein lysates from cell lines 63
2.9.3 Bicinchoninic acid (BCA) assay 64
2.9.4 Preparation of protein lysates from yeast cells 64
2.9.5 Western Blotting 65
2.9.5.1 SDS poly-acrylamide gel electrophoresis 65
2.9.5.2 Immunoblotting 66
2.9.6 Antibodies used for Western Blotting 67
2.9.7 Immunoprecipitation of whole-cell lysates 68
2.9.8 Recombinant protein expression and purifications 69
2.9.8.1 GST-tag protein purification 70
2.9.8.2 HIS-tag protein purification 71
2.9.8.3 Coomassie stain 71
2.9.8.4 TEV digests 72
2.9.8.5 Protein purification using ÄKTA purification system 72
2.9.9 Pulldown assays with purified proteins 72
2.9.9.1 Myc-tag pulldown 72
2.9.9.2 HIS-tag pulldown 73

2.10 Yeast methods 73
2.10.1 Intracellular Antibody Capture 73

2.10.2 Preparation of yeast media 74
2.10.3 Preparation of solutions for yeast transformations 77
2.10.4 Construction and characterization of the bait vectors 78
2.10.4.1 Construction of baits and positive control preys 78
2.10.5 Yeast transformation with bait vectors 78
2.10.6 Measuring the Optical Density (OD) of a yeast culture 79
2.10.7 Glycerol stock preparation and retrieval of yeast clones 80
2.10.8 Characterization of yeast bait lines 80
2.10.8.1 Auto-activation of bait lines 80
2.10.8.2 Yeast co-transformation to assess the bait- positive control prey interaction 80
2.10.9 Large scale yeast transformation for the library screening 81
2.10.10 Plasmid DNA extraction from yeast 82

2.11 Computational and statistical analysis 83
2.11.1 Protein structures 83
2.11.2 Software use 84
2.11.3 Statistical methods 84

CHAPTER 3: B-CATENIN CHARACTERISATIONS IN A PANEL OF COLORECTAL CANCER CELL LINES 86

3.1 Introduction 86
3.1.1 Aim 87

3.2 Results 88
3.2.1 β-catenin expression in a panel of CRC cell lines 88
3.2.2 WNT transcriptional activity in SW480, HCT116 and RKO cells 92
3.2.3 Preliminary β-catenin localisation in a panel of CRC cell lines 93
3.2.4 Mutations in key WNT signalling proteins do not affect subcellular β-catenin localisation 97
3.2.5 β-catenin cellular localisation associates with E-cadherin expression 100

3.3 Discussion 107

CHAPTER 4: *IN VITRO* STUDIES OF B-CATENIN/BCL9 INHIBITORS IN COLORECTAL CANCER CELL LINES 115

4.1 Introduction 115
4.1.1 Inhibitors of the β-catenin-BCL9 interaction 115
4.1.2 Characteristics of the β-catenin – BCL9 inhibitors 116

4.2 Aims 118

4.3 Results 119

4.3.1 SRB Assays using the ZYQ-1-74 inhibitor 119
4.3.2 SRB Assays using ZYQ-2-165 and JW-2-80 122
4.3.3 ZYQ-2-165 and JW-2-80 inhibitors are affected by albumin 124
4.3.4 ZYQ-1-74 treatment of non-CRC cell lines 127
4.3.5 Assessment of WNT target genes upon β-catenin – BCL9 inhibitor treatment 131

4.4 Discussion 133

CHAPTER 5: INTRACELLULAR ANTIBODY CAPTURE TO IDENTIFY SMALL ANTIBODY FRAGMENTS AGAINST β-CATENIN 138

5.1 Introduction 138
5.1.1 Yeast-Two-Hybrid systems 138
5.1.2 Intracellular Antibody Capture (IAC) 138
5.1.2.1 General methodology 138
5.1.2.2 VH library 140

5.2 Aims 141

5.3 Results 142
5.3.1 Selection of β-catenin target domains 142
5.3.2 Cloning of bait and prey vectors 143
5.3.2.1 Construction of bait vectors 143
5.3.2.2 Construction of positive control vectors 145
5.3.3 Characterisation of bait yeast lines 147
5.3.3.1 Auto-activation test 147
5.3.3.2 Bait protein expression in yeast 150
5.3.3.3 Bait – positive control prey interaction 150
5.3.4 Large-scale yeast transformation 152
5.3.5 Optimisation trials of large-scale transformation protocol 153
5.3.5.1 Changes in the size of single-stranded carrier DNA 154
5.3.5.2 Comparison of transformation efficiencies of different bait clones 155
5.3.5.3 Effect of heat shock step on the transformation efficiency 156
5.3.6 VH library screen 157
5.3.7 Characterisation of VHs after first round of library screen 160

5.4 Discussion 164

CHAPTER 6: CHARACTERISATION OF A LLAMA VHH AGAINST B-CATENIN 168

6.1 Introduction 168
6.1.1 VHH against β-catenin 168

6.2 Aim 170

6.3 Results 171
6.3.1 Expression of LL3 and AAA in SW480 cells 171
6.3.2 VHHs are expressed in the nucleus and cytoplasm 172
6.3.3 WNT inhibition in SW480 cells by LL3 174
6.3.4 Creation of stable VHH cell lines 176
6.3.4.1 Lentiviral transduction of SW480 177
6.3.5 Expression of VHHs upon DOX induction 178
6.3.6 LL3 binds to β-catenin in SW480 cells 182
6.3.7 Characterisation of SW480-LL3-GFP and SW480-AAA-GFP stable clones 184
6.3.7.1 β-catenin – LL3 interaction in single stable clones 188
6.3.7.2 SRB viability assay and cologeneic assay data of single clones expressing LL3 and AAA 190
6.3.7.3 WNT gene expression data 195
6.3.7.4 β-catenin localisation in single clones 198
6.3.8 Assessment of LL3 Binding site on β-catenin 200
6.3.8.1 VHH and full-length β-catenin recombinant protein purifications 200
6.3.8.2 β-catenin fragment recombinant protein purifications 206
6.3.8.3 LL3 binds to Arm1-3 of β-catenin 208

6.4 Discussion 210
6.4.1 Limitation of the study 210
6.4.2 Future directions 211

CHAPTER 7: GENERAL DISCUSSION 214

7.1 E-cadherin associates with β-catenin subcellular localisation 214

7.2 Small molecules targeting β-catenin to inhibit the Wnt pathway 216

7.3 Antibody - based approaches to target β-catenin 217
7.3.1 Suggestions for the identification of VHs against β-catenin 218
7.3.2 LL3 VHH against β-catenin 219
7.3.3 Advantages of antibody fragments over monoclonal antibodies and small molecule inhibitors 221
7.3.4 Limitations of antibody fragment-based therapies 222

REFERENCES 227

APPENDICES 252
Appendix A - Supplementary data for Chapter 3 252
Appendix B - Supplementary data for Chapter 4 276
Appendix C - Supplementary data for Chapter 5 277
Appendix D - Supplementary data for Chapter 6 281

List of Figures

Figure 1.1 Schematic representation of the Intestinal and Colonic crypt structures 3
Figure 1.2 Schematic overview of the Wnt pathway. 12
Figure 1.3 Schematic structure of β-catenin and some of its binding partners. 15
Figure 1.4 Interaction between β-catenin and BCL9 20
Figure 1.5 Schematic summary of Wnt targeting strategies 23
Figure 1.6 Range of antibody fragments obtained through antibody engineering. 28
Figure 1.7 Schematic representation of the whole immunoglobin IgG and single domain antibodies (VH and VL) 29
Figure 1.8 Schematic overview of Heavy-chain antibodies compared to conventional antibodies 32
Figure 1.9 Overview of different approaches used in this thesis to inhibit β-catenin PPIs 36
Figure 2.1 TOPflash and FOPflash vectors 49
Figure 2.2 Overview of IAC workflow 74
Figure 3.1 Microarray data: β-catenin (*CTNNB1*) expression in a panel of colorectal cancer cell lines 89
Figure 3.2 Protein and mRNA expression of β-catenin in a selected panel of colorectal cancer cell lines 90
Figure 3.3 β-catenin expression and localisation in SW480, RKO and HCT116 cells 91
Figure 3.4 Baseline WNT activity in SW480, HCT116 and RKO cell lines measured by the TOPflash assay. 92
Figure 3.5 Examples of staining categories 95
Figure 3.6 β-catenin localisation score groupings 98
Figure 3.7 Correlation between β-catenin localisation with genetic data 99
Figure 3.8 Flow-chart of cell lines used for gene expression analysis: β-catenin localisation scores 1+2 vs 3+4 100

Figure 3.9 2x2 contingency table: β-catenin localisation association with CDH1 expression levels 102
Figure 3.10 E-cadherin expression in a panel of CRC cell lines 106
Figure 4.1 Representative dose-response curves to ZYQ-1-74 and JW-1-78. ... 121
Figure 4.2 Dose-response curves to ZYQ-2-165 and JW-2-80 123
Figure 4.3 Bright field images of SW480 cells in response to JW-2-80 and ZYQ-2-165 in different growth medium conditions 125
Figure 4.4 Dose-response curves to compounds JW-1-78, ZYQ-1-74, JW-2-80 and ZYQ-2-165 at different FBS concentrations 126
Figure 4.5 Dose response curves of ZYQ-1-74 and JW-1-78 in cell lines from different tissues. 128
Figure 4.6 Microarray data for *β-catenin* and *BCL9* mRNA expression in fibroblasts 129
Figure 4.7 Calcein-AM staining of CCD18-CO, JB and WFB fibroblasts after ZYQ-1-74 treatment 130
Figure 4.8 c-myc and Cyclin D1 WNT-target genes expression after ZYQ-1-74, ZYQ-2-165 and JW-1-78 treatment in SW480 cells 132
Figure 5.1 Schematic overview of the IAC mechanism of action 139
Figure 5.2 VH with randomised CDR3 region 140
Figure 5.3 PCR products of the β-catenin target regions for bait construction.... 144
Figure 5.4 pBTM116 vector map 144
Figure 5.5 PCR products of the β-catenin interaction partners BCL9, TCF4 and p300 for positive control prey construction 146
Figure 5.6 Vector map of VP16 prey vector 147
Figure 5.7 Schematic representation of bait auto-activation assessment by 3-AT 148
Figure 5.8 Auto-activation test of bait lines 149
Figure 5.9 Bait line expression 150
Figure 5.10 Bait line interactions with positive control preys 152
Figure 5.11 Single-stranded carrier DNA analysed on agarose gel 154

Figure 5.12 Amino acid sequence of VH49, VH55 and VH88 159
Figure 5.13 Schematic representation of VH binding to bait fusion protein 160
Figure 5.14 Interaction test of VH49, VH55 and VH88 with D1 and pBTM116 bait lines 162
Figure 5.15 Flow- chart overview of the VH library screen results 163
Figure 6.1 Immunoprecipitation of β-catenin by LL3-scFc 169
Figure 6.2 pNAFH-LL3 and pNAFH-AAA vector map and expected VHH structures 171
Figure 6.3 Expression of LL3 and AAA in SW480 cells 172
Figure 6.4 Cytoplasmic and nuclear expression of VHHs in transiently transfected SW480 cells 173
Figure 6.5 LL3 inhibits TOPflash signal in SW480 cells 175
Figure 6.6 TLCV2 vector map 176
Figure 6.7 Puromycin selection of SW480-LL3-GFP and SW480-AAA-GFP bulk cell lines 177
Figure 6.8 Brightfield images of stable cell lines SW480-LL3-GFP and SW480-AAA-GFP 178
Figure 6.9 VHH expression of VHHs after DOX induction in stable cell lines 179
Figure 6.10 DOX titration – Immunofluorescence 180
Figure 6.11 DOX titration in SW480-LL3-GFP_2.5 and SW480-AAA-GFP_2.5 cell lines 181
Figure 6.12 Time kinetics of VHH expression after DOX induction 182
Figure 6.13 Pulldown assay of LL3 and AAA in the bulk cell lines SW480-LL3-GFP_2.5 and SW480-AAA-GFP_2.5 183
Figure 6.14 PCR product of LL3 and AAA from single clones for sequence confirmation 185
Figure 6.15 Sequencing chromatograms of AAA clone 2D9 and LL3 clone 3D6 186
Figure 6.16 Examples of FACS analysis of LL3-GFP_5 clone 2D3 and AAA-GFP_5 clone 2D with and without DOX induction 187

Figure 6.17 VHH baseline expression in various SW480-LL3-GFP_5 and SW480-AAA-GFP_5 clones analysed by Western Blot 188
Figure 6.18 Myc-tag immunoprecipitation in single clones SW480-LL3 GFP 3C5 and SW480-AAA-GFP 1F9 189
Figure 6.19 SRB and CFA assay data of representative clones 194
Figure 6.20 Expression of Wnt target genes 197
Figure 6.21 β-catenin localisation upon DOX induction in SW480 parental, SW480-AAA-GFP_5 clones 2D9 and 1B4 and SW480-LL3-GFP_5 clones 2G10 and 2D3 (previous page) 200
Figure 6.22 pGEX-LL3 and pGEX-AAA purifications 201
Figure 6.23 Coomassie stain of pGEX-Bcatfl recombinant protein purification... 202
Figure 6.24 Pulldown assays to assess the LL3 - β-catenin interaction..... 204
Figure 6.25 HIS-TEV-Avi-LL3 and HIS-TEV-Avi-AAA protein purifications..... 205
Figure 6.26 Design of β-catenin fragments 206
Figure 6.27 Purification of pGEX-ArmR fragments 207
Figure 6.28 GST-pulldown assay with Arm1-3, Arm1, Arm2 and Arm3 β-catenin fragments 209
Figure 7.1 β-catenin sequence alignment between different species 220
Figure 7.2 Currently investigated delivery options of intracellular antibodies..... 223

List of Tables

Table 2.1 List of cell lines 40

Table 2.2 List of compounds 42

Table 2.3 List of antibodies used for immunofluorescence 47

Table 2.4 List of 20X TaqMan® Gene Expression Assay Probes 52

Table 2.5 List of primers used in this thesis 55

Table 2.6 Thermocycler set-up for the Touch-Down PCR reactions 56

Table 2.7 List of vector backbones 58

Table 2.8 T4 Ligase reaction set-up 59

Table 2.9 Antibiotic selection concentrations 61

Table 2.10 List of antibodies used for Western Blotting 67

Table 2.11 Composition of lysis, binding and washing buffers for protein purification 70

Table 2.12 Composition of selective YC dropout plates 77

Table 2.13 List of protein structures and PDB ID codes 84

Table 3.1 Overview of APC and β-catenin mutation status in a panel of CRC cell lines 94

Table 3.2 Scoring results of β-catenin localisation in a panel of colorectal cancer cell lines 96

Table 3.3 The 20 most differentially expressed probe-sets correlating with β-catenin staining analysed by membrane (localisation scores 1 and 2) vs nuclear (localisation scores 3 and 4) 2 x 2 contingency tables. 101

Table 3.4 The 20 most differentially expressed probe-sets correlating with β-catenin staining analysed by membrane (score 1) vs nuclear (score 4) 2 x 2 contingency tables. 103

Table 4.1 Characteristics of β-catenin – BCL9 inhibitors 117

Table 4.2 IC_{50} values of 28 CRC cell lines in response to ZYQ-1-74 120

Table 4.3 Non-CRC cell lines used in experiments 127

Table 5.1 List of β-catenin bait target domains 143

Table 5.2 List of β-catenin binding partner regions 145

Table 5.3 Transformation efficiency results comparing old and new carrier DNA 155

Table 5.4 Transformation efficiency results comparing D1 bait clones 4 and 5 .. 156

Table 5.5 Transformation efficiency results comparing heat shock times 156

Table 6.1 List of SW480-LL3-GFP and SW480-AAA-GFP clones used throughout this work 184

Table 6.2 Percentage cell survival at 100 ng/mL DOX treatment analysed by the SRB assay 191

List of Appendices

Appendix A.1 β-catenin expression in CC20, RKO, NCIH716, C10 and HCT116 252

Appendix A.2 p53, BRAF and KRAS mutation statuses 252

Appendix A.3 Immunofluorescence of β-catenin in a panel of 52 CRC cell lines 253

Appendix A.4 β-catenin localisation scores for 52 CRC cell lines by three assessors 257

Appendix A.5 Correlation between β-catenin localisation and position of APC and β-catenin mutations 257

Appendix A.6 List of significant differentially expressed probe-sets in correlation with β-catenin membrane (localisation scores 1 and 2) vs nuclear (localisation scores 3 and 4) 258

Appendix A.7 List of significant differentially expressed probe-sets in correlation with β-catenin membrane (localisation scores 1) vs nuclear (localisation scores 4) .. 266

Appendix A.8 CDH1 microarray expression data 274

Appendix A.9 EMT expression markers in RKO, OXCO1, SW480, SW620, LS174T and LS180 cell lines 275

Appendix B.1 Chemical structures of β-catenin/BCL9 inhibitors 276

Appendix C.1 Bait vectors sequencing results 277

Appendix C.2 Sequencing results of positive control prey vectors 279

Appendix C.3 Serial dilution of large-scale library screen on YC-WL growth control plates 279

Appendix C.4 Sequencing results of VH49, VH55 and VH88 280

Appendix D.1 DNA and Amino Acid sequences of LL3 and LL3.CDRAAA 281

Appendix D.2 Puromycin killing curve in SW480 282

Appendix D.3 Cytoplasmic and nuclear VHHs expression in stable SW480 cells 282
Appendix D.4 Sequencing data of individual SW480-AAA-GFP and SW480-LL3-GFP clones 283
Appendix D.5 FACS data of DOX-induced clones 285
Appendix D.6 Myc-tag immunoprecipitations of stable SW480-AAA-GFP and SW480-LL3-GFP clones 286
Appendix D.7 Colony formation assay results for all tested clones 287
Appendix D.8 GST-His-TEV-VHH-pGEX vector map and sequencing results ... 288
Appendix D.9 Chromatography column purification results 289
Appendix D.10 His-Tev-Avi-VHH-pRK vector map and sequencing results 290
Appendix D.11 Electronspray Ionization Mass Spectroscopy data for His-TEV-Avi-AAA, His-TEV-Avi-LL3 and pGEX-Bcatfl 291
Appendix D.12 Sequencing results of pGEX-ArmR fragments 292
Appendix D.13 Information on pET-GST-ArmR constructs from Promab Inc. 293

List of Abbreviations

µg	Microgram
µL	Microliter
µm	Micrometer
µM	Micromolar
3-AT	3-amino-1,2,4-triazole
AA	Amino acids
AAA	Mutant VHH against β-catenin
AD	Transactivation domain
ADH1	Alcohol dehydrogenase 1
APC	Adenomatous Polyposis Coli
ArmR	Armadillo Repeat
ASCL2	Achaete-scute like 2
ATCC	American Type Culture Collection
BCA	Bicinchoninic acid
BCL9	B cell lymphoma 9
BCL9L	B cell lymphoma 9 like
BMP	Bone Morphogenetic Protein
bp	Base pair
BSA	Bovine Serum Albumin
Calcein-AM	Calcein-acetoxymethyl ester
CBD	Catenin-binding domain
CBP	cAMP response element binding protein
CCND1	Encoding Cyclin-D1
CDH1	Encoding E-cadherin
cDNA	Complementary DNA
CDR	Complementarity Determining Region
CH3	Cysteine–histidine-rich region 3
CIL	Cancer and Immunogenetics Laboratory
CK1	Casein kinase 1
CO_2	Carbon dioxide
CRC	Colorectal cancer
Ct	Cycle threshold
CTNNB1	Encoding β-catenin
D	Aspartic acid
DAM	Donkey-anti-mouse
DAPI	4’,6-diamidino-2-phenylindole
DAR	Donkey-anti-rabbit
DBD	DNA-binding domain
dH_2O	Distilled water
DMEM	Dulbecco’s Modified Eagle Medium
DMSO	Dimethyl sulfoxide
DNA	Deoxyribonucleic acid

DNAse	Deoxyribonuclease
dNTP	Deoxynucleotide
DOX	Doxycyline
Dvl	Dishevelled
E-cadherin	Epithelial cadherin
ECL	Enhanced Chemiluminescence
EDTA	Ethylenediaminetetraacetic acid
EpCAM	Epithelial cellular adhesion molecule
Fab	Antigen-binding fragments
FAP	Familial adenomatous polyposis
FBS	Fetal bovine serum
FZD	Frizzled receptor
g	Gram
GAM	Goat-anti-mouse
GFP	Green-fluorescent protein
GSK3	Glycogen Synthase Kinase 3
GST	Glutathione S-transferase
H	Histidine
H_2O	Water
HCAbs	Heavy-chain antibodies
HCl	Hydrochloric acid
HD	Homology Domain
HIS	Histidine-tag
HIS3	Gene encoding Imidazoleglycerol-phosphate dehydratase
HMG	High-mobility group
HNCC	Hereditary nonpolyposis colorectal cancer
HOAc	Acetic Acid
hr	Hour
HRP	Horseradish Peroxidase
IAC	Intracellular Antibody Capture
ICAT	Inhibitor of β-catenin and TCF4
IF	Immunofluorescence
IP	Immunoprecipitations
IPTG	Isopropyl-β-D-thiogalactopyranosid
ISCOVES	Iscove's Modified Dulbecco's Medium
kDa	Kilodalton
L	Leucine
L	Liter
L40	Yeast strain
LB	Lysogeny broth
LEF	Lymphoid enhancer-binding factor
LexA	DNA-binding domain
LGR5	Leucine-rich repeat-containing G-protein coupled receptor 5
lgs	Legless, homolog of human BCL9 in Drosophila

LL3	Wild-type VHH against β-catenin
LRP5/6	Low-density lipoprotein receptor-related 5 or 6
M	Molar
mAb	Monoclonal antibody
MCR	Mutation Cluster Region
MCS	Multiple Cloning Site
mg	Milligram
min	Minutes
mL	Milliliter
mM	Millimolar
MMR	Mismatch Repair
mQ	Ultrapure water
mRNA	Messenger ribonucleic acid
MT	Mutant
NaOH	Sodium hydroxide
ng	Nanogram
nM	Nanomolar
nm	Nanometer
NP40	Nonidepet-40
NA	Numerical Aperture
OD	Optical Density
P/S	Penicillin/Streptomycin
p300	E1A-binding protein, 300 kDa
pAb	Polyclonal antibody
PBSA	Absolute phosphate buffered saline
PCR	Polymerase Chain Reaction
PDB	Protein Data Bank
PEG	Polyethylene glycol
PFA	Paraformaldehyde
PPI	Protein-Protein interactions
PVDF	Polyvinylidene Difluoride
qPCR	Quantitative real-time Polymerase Chain Reaction
R	Arginine
RE	Restriction enzymes
RNAse	Ribonuclease
RNF43	E3 ubiquitin ligase RING finger 43
RPMI	Roswell Park Memorial Institute Medium
RSPO	R-spondin
RT	Room Temperature
SAR	Swine-anti-rabbit
scFv	Single-chain variable fragments
SD	Standard deviation
sdAb	Single domain antibody
SDS	Sodium Dodecyl Sulfate

SOC	Optimal broth with catabolite repression
SRB	Sulphorhodamine B
ssDNA	Single-stranded carrier DNA
T2A	2A self-cleaving peptide
TA	Transit amplifying
TAE	Tris base, acetic acid and EDTA
TBP	TATA-box binding protein
TBS	Tris-buffered saline
TBS-T	Tris-Buffered Saline plus Tween-20
TCA	Trichloroacetic acid
TCF	T-cell factor
TD	Touch-down
TE	Tris-EDTA
Tet	Tetracycline
TEV	Tobacco Etch Virus
T_m	Melting temperature
TNK1/2	Tankyrase 1 and 2
UBC	Ubiquitin C
V	Volt
VH	Variable heavy single domain
VHH	Single domain antibodies isolated from camelids
VIM	Vimentin
VL	Variable light single domain
VP16	Transactivation domain from Herpes Simplex Virus
W	Trypotophan
WB	Western Blot
WIMM	Weatherall Institute of Molecular Medicine
WNT	*Wingless/int-1*
WT	Wild-type
Wt/vol	Weight/volume
Y2H	Yeast-2-Hybrid
YAPD	YPD medium supplemented with adenine sulfate
YC	Yeast Complete
YPD	Yeast extract peptone dextrose, complete medium for yeast growth
ZEB1	Zink Finger E-Box Binding Homeobox 1
ZNRF3	Zinc and ring finger 3
β-TrCP	Beta-transducin repeats-containing protein

Chapter 1

Introduction

CHAPTER 1: Introduction

1.1 The small intestine and the colon

The small intestine and the colon are part of the human digestive tract. The majority of food is digested in the small intestine. The intestine is structured in sheets of columnar epithelial cells with invaginations called intestinal crypts (Figure 1.1), or also known as crypts of Lieberkühn (Clevers, 2013), and finger-like projections called villi to facilitate increased absorption. The colon is the final part of the human digestive tract. Its main function is to process undigested food and waste products, reabsorb water and electrolytes and to form stool for elimination. The colon does not have villi, but is organised into functional subunits of invaginations of columnar epithelial cells called colonic crypts (Humphries & Wright, 2008).

1.1.1 The structure of the intestinal and colonic crypts

At the base of both the intestinal and colonic crypts are the stem cell niche, harbouring stem cells (SCs) with self-renewal potential. These undifferentiated SCs give rise to progenitor cells, also called Transit amplifying (TA) cells, that will migrate up towards the lumen and differentiate to form the lineage of the crypt (Crosnier, Stamataki, & Lewis, 2006; Umar, 2010). The crypts are mainly formed of three differentiated cell types – the enterocytes (absorptive), goblet cells (mucin production) and enteroendocrine (hormone secretion). Differentiated cells will eventually be shed to the lumen of the small and large intestines, which allows a rapid turnover and renewal of the crypt of 4-5 days in humans (Cheng et al., 1974; Potten et al., 1992). Mesenchymal myofibroblast cells surrounding the crypt are

thought to secrete growth factors that regulate the proliferation and differentiation of epithelial cells (Meran, Baulies, & Li, 2017).

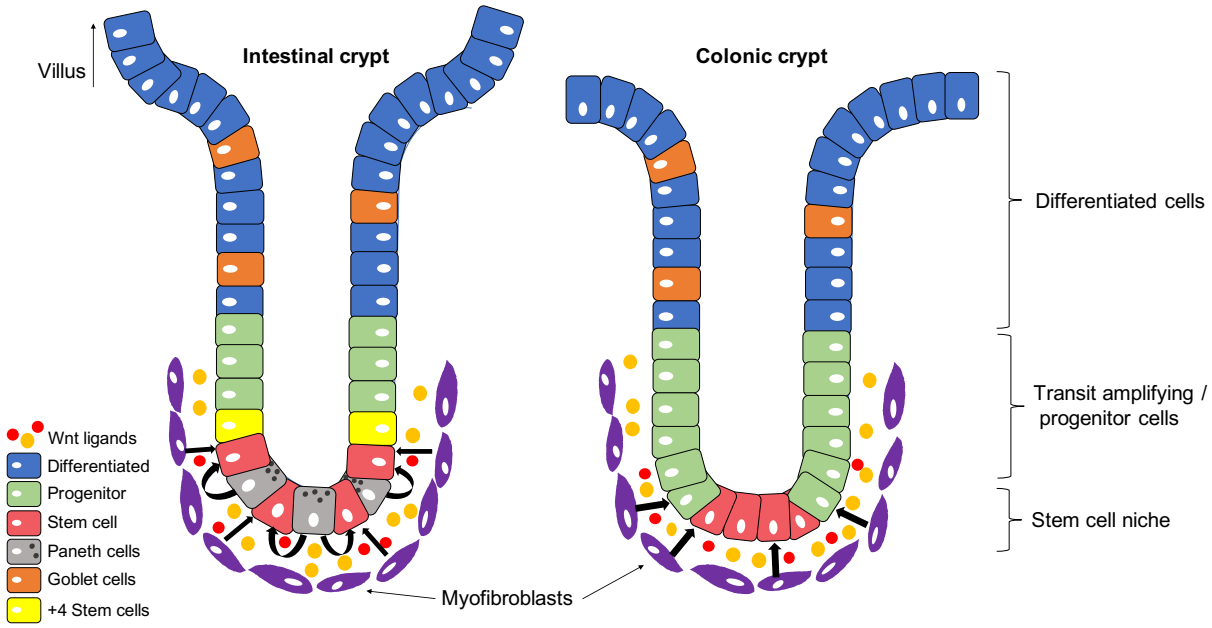


Figure 1.1 Schematic representation of the Intestinal and Colonic crypt structures
Schematic representations of the intestinal (left) and colonic (right) crypt structures. In the intestinal crypt, the Crypt Base Columnar (CBC) stem cells (red) are located at the bottom of the crypt, between Paneth cells (grey). A second stem cell population, termed +4 stem cells (yellow), are located four cell diameters above the base of the crypt. In the small intestine, Paneth cells are a major Wnt source for stem cells. In the colonic cells, CBC stem cells are located at the bottom of the crypt in the stem cell compartment. Progenitor cells (green) travel up the colonic crypt in a "conveyer belt" like fashion and are fully differentiated (blue) at the top of the crypt where they are shed into the lumen. Mucin-producing Goblet cells are represented in orange. The intestinal and colonic crypts are lined by mesenchymal stromal cells, including myofibroblasts (purple), which release cytokines, growth factors and Wnt ligands (yellow and red) essential for the normal homeostasis and Wnt signalling. (Adapted from Marahani Musa's DPhil thesis, Bodmer lab, 2018).

1.1.2 The stem cell niche

The stem cell niche at the base of the intestinal crypt harbours the intestinal stem cells. Chen and Leblond first discovered undifferentiated cycling crypt base columnar (CBC) cells at the bottom of the crypt, or the "stem cell zone" (Cheng & Leblond, 1974). Phagosome autoradiography experiments showed that all main

differentiated cell types along the crypt derived from CBC cells (Cheng & Leblond, 1974). ^{3}H-thymidine injection caused the cell death of some CBC cells that were phagocytosed by neighbouring surviving CBC cell and leading to radioactively tracible phagosomes. While initially only being tracible at the bottom of the crypt, the radioactive label was identified in more differentiated cells after hours and days (Cheng & Leblond, 1974). Later on, Leucine-rich repeat-containing G-protein coupled receptor 5 (LGR5) has been identified as adult stem cell marker in the intestinal crypt (Barker et al., 2007). A second stem cell population alongside CBCs in the small intestine has been proposed by Potten and colleagues. These DNA label-retaining cells were found four cell positions above the base of the crypt and are therefore called +4 stem cells (Potten, Hume, Reid, & Cairns, 1978).

Paneth cells reside at the bottom of intestinal crypts alongside the CBC cells (Figure 1.1, left panel). They were first discovered over a century ago through histology, owing to their distinguishable secretory granules (Clevers, 2013). Paneth cells have a crucial role in the maintenance of the stem cell niche (Meran et al., 2017) and are a major source for Wnt ligands in the small intestine, as represented in Figure 1.1. Lgr5+ single sorted stem cells do not survive in the absence of Paneth cells but are able to form “mini-gut” organoids when Paneth cells are present (Sato et al., 2011). In mouse models, the reduction of Paneth cells also displayed a significant loss of Lgr5 stem cells (Sato et al., 2011).

In contrast to the intestinal stem cell niche, there are no Paneth cells in the colonic stem cell niche. CBC stem cells reside at the base of the colonic crypt and are surrounded by the microenvironment to regulate the homeostasis of self-renewal

and production of mature progeny cells through Wnt ligand release (Vermeulen et al., 2010).

1.1.3 Homeostatic control along the intestinal and colonic crypts

The homeostasis of the intestinal and colonic crypt is a fine-tuned interplay between different signalling pathways, including Wnt, Notch and Bone Morphogenetic Protein (BMP). The orchestrated work and connections of these pathways are well described and have been extensively reviewed (Beumer & Clevers, 2016; Gehart & Clevers, 2019). While the BMP signal represents the main counterplayer of the Wnt signalling pathway along the intestinal crypt (Qi et al., 2017), the Notch signalling is vital for the cell fate decision of progenitor cells towards the absorptive and secretory lineages (Miyamoto & Rosenberg, 2011).

Numerous studies have shown that the Wnt signalling pathway is essential for the normal function of the stem cell compartment and the colonic crypt. For example, a neonatal knockout in mice of the Wnt transcription factor T-cell factor 4 (TCF4) caused a lack of proliferative crypts in the animals (Korinek et al., 1998) and conditional knockout of the key Wnt pathway protein β-catenin (*CTNNB1*) or TCF4 in adult mice caused disruption of the adult crypt proliferation as well (Fevr et al. 2007; van Es et al. 2012). A similar result was seen when Dickkopf1 (Dkk1), a Wnt receptor antagonist, was ectopically expressed in a transgenic mice model (Pinto et al., 2003). The high Wnt activity in the colonic crypt is regulated by the microenvironment through cytokines and growth factors secreted by myofibroblasts (Vermeulen et al., 2010).

1.2 Colorectal cancer

1.2.1 Epidemiology

Colorectal cancer (CRC) is a cancer of the colon or rectum. It is the third most common cancer worldwide in men and women and accounts for 6.1% of all cancer cases and 9.2% of all cancer deaths (Bray et al., 2018; Siegel, Miller, & Jemal, 2019). Most cases of CRC are sporadic, with a median patient age of 70-75 years (Yamagishi et al., 2016). Age is a main risk for sporadic CRC, along with obesity, high intake of red meat, processed food and high alcohol consumption (Pan, Yu, & Wang, 2018; Thanikachalam & Khan, 2019). Colorectal cancer is commonly staged according to the Dukes classification (Jass & Morson, 1987) or the TNM staging according to the invasion depth (T), nodal involvement (N) and metastatic spread (M) (Gelmann et al., 2000).

1.2.2 Hereditary CRC

Up to 20% of CRC cases can be attributed to a genetic hereditary predisposition (Jasperson et al., 2010; Lynch, 2003). The most common hereditary form of CRC is Hereditary nonpolyposis colorectal cancer (HNCC), also referred to as Lynch Syndrome (LS). LS is caused by mutations in the mismatch repair (MMR) genes *MLH1*, *MSH2*, *MSH6* and *PMS2* (Lynch, 2003), which leaves patients prone to the development of various tumours from early age (Stoffel et al., 2009).

Familial Adenomatous Polyposis (FAP) is the second-most prevalent form of inherited CRC (Jasperson et al., 2010). It is an autosomal dominant disorder with a germline mutation in the Adenomatous Polyposis Coli (*APC*) gene, which

encodes an important regulator of the Wnt signalling pathway. Affected patients develop hundreds of adenomatous polyps in the colon in early years and develop colon cancer by the age of 35 years if left untreated (Snyder & Hampel, 2019).

1.2.3 Wnt pathway in colorectal cancer

The Wnt pathway plays a crucial role in the development of colorectal cancer. The importance of the pathway was first elucidated in FAP, where patients presented with a germline mutation in the APC gene (Bodmer et al., 1987; Cottrell et al., 1992; Groden et al., 1991). Over 80% of sporadic CRC cases will show mutations in this gene in early adenomas (Bodmer 2006). Most of the mutations in APC occur in a specific “mutational hotspot” region between codons 1286 and 1513, also called the mutation cluster region (MCR) (Fearnhead et al., 2001; Miyoshi et al., 1992; Nagase & Nakamura, 1993). About 95% of mutations lead to the truncation of the APC protein and abnormal function due to the lack of Axin and β-catenin binding sites (Fearnhead et al., 2001).

While the great majority of sporadic cancers have a mutation in the APC protein, mutations in β-catenin itself (Morin et al., 1997) as well as in the Wnt regulators Axin2 (Liu et al. 2000) and the E3 ubiquitin ligase Rnf43 (Koo et al., 2012) have been reported. However, the APC and β-catenin mutations were shown to be mutually exclusive (Sparks et al., 1998). Taken together, there is overwhelming evidence for a key role of the Wnt pathway in the development of CRC.

1.3 The Wnt pathway

The Wnt signalling pathways have been extensively studied for over thirty years and plays a fundamental role in development, tissue homeostasis and carcinogenesis (Steinhart & Angers, 2018; Wiese, Nusse, & van Amerongen, 2018). They are highly conserved amongst the animal kingdom (metazoans) (Liu et al. 2000).

The Wnt signalling pathway can be broadly classified into β-catenin-dependent (canonical) and β-catenin-independent (non-canonical) Wnt signalling pathways. While the canonical Wnt signalling pathway is the most extensively studied, the non-canonical Wnt pathways can be further subdivided into the planar cell polarity (PCP) and the Wnt/Ca^{2+} pathways (De, 2011; Yang & Mlodzik, 2015). Historically, these pathways have been treated as separate pathways, but as research progresses, more complex interconnections between them are suggested (Ackers & Malgor, 2018; Thrasivoulou, Millar, & Ahmed, 2013; van Amerongen & Nusse, 2009). For the purpose of this thesis, the canonical Wnt pathway will be further described.

The first Wnt gene was discovered in *Drosophila melanogaster* as a segment polarity gene, and named *wingless* (wg) according to the absence of wings in mutant embryos (Sharma & Chopra, 1976). Later on, the oncogene integration-1 (*int-1*) in mice was found to be homologous to the *wg* gene (Nusse & Varmus, 1982; Rijsewijk et al., 1987). Therefore, the Wnt family name is a fusion of the *wg* and *int-1* gene names (Croce & McClay, 2008).

Wnt ligand proteins are the key signalling initiators of the Wnt pathways. They are secreted cysteine-rich glycoproteins of about 350 amino acids. So far, 19 human Wnt gene have been identified (Willert & Nusse, 2012). Wnt ligands are posttranslationally modified though palmitoylation at the endoplasmic reticulum by porcupine (PORCN), a transmembrane O-acyltransferase (Galli et al., 2007; Kadowaki et al., 1996; Zhai, Chaturvedi, & Cumberledge, 2004). This palmitoylation process was shown to be essential for the secretion of functional Wnt ligands (Komekado et al., 2007; Kurayoshi et al., 2007; Mikels & Nusse, 2006). The secreted Wnt ligands bind to various Frizzled (FZD) receptors to activate the Frizzled/low-density lipoprotein receptor-related 5 or 6 (LRP5/6) receptor (FZD-LRP) complexes, which in turn initiates a downstream intracellular signalling cascade (described in section 1.3.1).

Four secreted R-spondin (RSPO1-4) proteins have been identified to be implicated in the Wnt pathway (de Lau, Snel, and Clevers 2012). They bind to the closely related leucine-rich repeat-containing G-protein-coupled receptors (Lgr)4, Lgr5 and Lgr6 and form a receptor complex with the transmembrane E3 ubiquitin ligase RING finger 43/ zinc and ring finger 3 (RNF43/ZNRF3) (Chen et al. 2013). RNF43/ZNRF3 is responsible for a balanced FZD-LRP complex membrane clearing (Tsukiyama et al., 2015). R-Spondin induces endocytosis of the RNF43/ZNRF3 complex (Hao et al., 2012), and so stabilises the surface levels of FZD-LRP. Therefore, R-spondins are proposed to amplify the Wnt signal upon Wnt ligand binding. More recently, Yan et al. (2017) reported an essential cooperativity between Wnt and R-spondin ligands in the self-renewal potential of the colonic stem cell niche. In this study it was shown that Lgr5+ intestinal stem cells

differentiate as a default state, unless both Wnt and RSPO ligands are present (Yan et al., 2017).

1.3.1 The canonical Wnt pathway

The key effector protein of the canonical Wnt pathway is β-catenin. Cytosolic β-catenin levels are regulated by the β-catenin destruction complex. This multiprotein complex is formed principally by Glycogen Synthase Kinase 3 (GSK3), Axin, Casein kinase 1 (CK1) and APC (Behrens et al. 1998; Hart et al. 1998; Nakamura et al. 1998). CK1 and GSK3 phosphorylate β-catenin at Ser45 and Ser33/37/Thr41, respectively (Sakanaka 2002; Amit et al. 2002; Liu et al. 2002). Subsequentially, β-catenin is ubiquitinated by beta-transducin repeats-containing protein (β-TrCP) ubiquitin E3 ligase and degraded by proteasomes (Marikawa and Elinson 1998; Hart et al. 1999). The constant turnover of β-catenin keeps the Wnt effect low (Hernández, Klein, & Kirschner, 2012).

To activate the Wnt pathway, a Wnt ligand binds to a seven-transmembrane receptor Frizzled. A Wnt ligand-LRP5/6-FZD trimeric complex then forms at the cell membrane (Bourhis et al., 2010; Tamai et al., 2000), which in turn leads to the phosphorylation of the cytoplasmic domain of LRP5/6 and Dishevelled (Dvl, Dsh in *Drosophila*) (Gao & Chen, 2010; Yanagawa et al., 1995; Zeng et al., 2005). Dvl and phosphorylated LRP5/6 disrupts the β-catenin destruction complex by recruiting APC and Axin to the cell membrane (Kishida et al., 1999; Mao et al., 2001; Schwarz-Romond, Metcalfe, & Bienz, 2007; Tamai et al., 2004). Consequently, β-catenin escapes degradation, resulting in cytosolic accumulation

and nuclear translocation of the protein (Figure 1.2). The process of nuclear translocation is not fully elucidated, but the C-terminal region of β-catenin was shown to be essential for this process (Koike et al., 2004). In the nucleus, β-catenin displaces the repressor Groucho (Daniels & Weis, 2005) and recruits various transcription co-activators to the DNA-bound transcriptional regulators of the T-cell factor (TCF)/lymphoid enhancer binding factor (LEF) family. This activates the expression of different Wnt target genes, such as *c-MYC, Cyclin D1*, *AXIN2,* Achaete-scute like 2 *(ASCL2) and LGR5* (Barker et al., 2007; Jho et al., 2002; Jubb et al., 2006; Mann et al., 1999; Tetsu & McCormick, 1999).

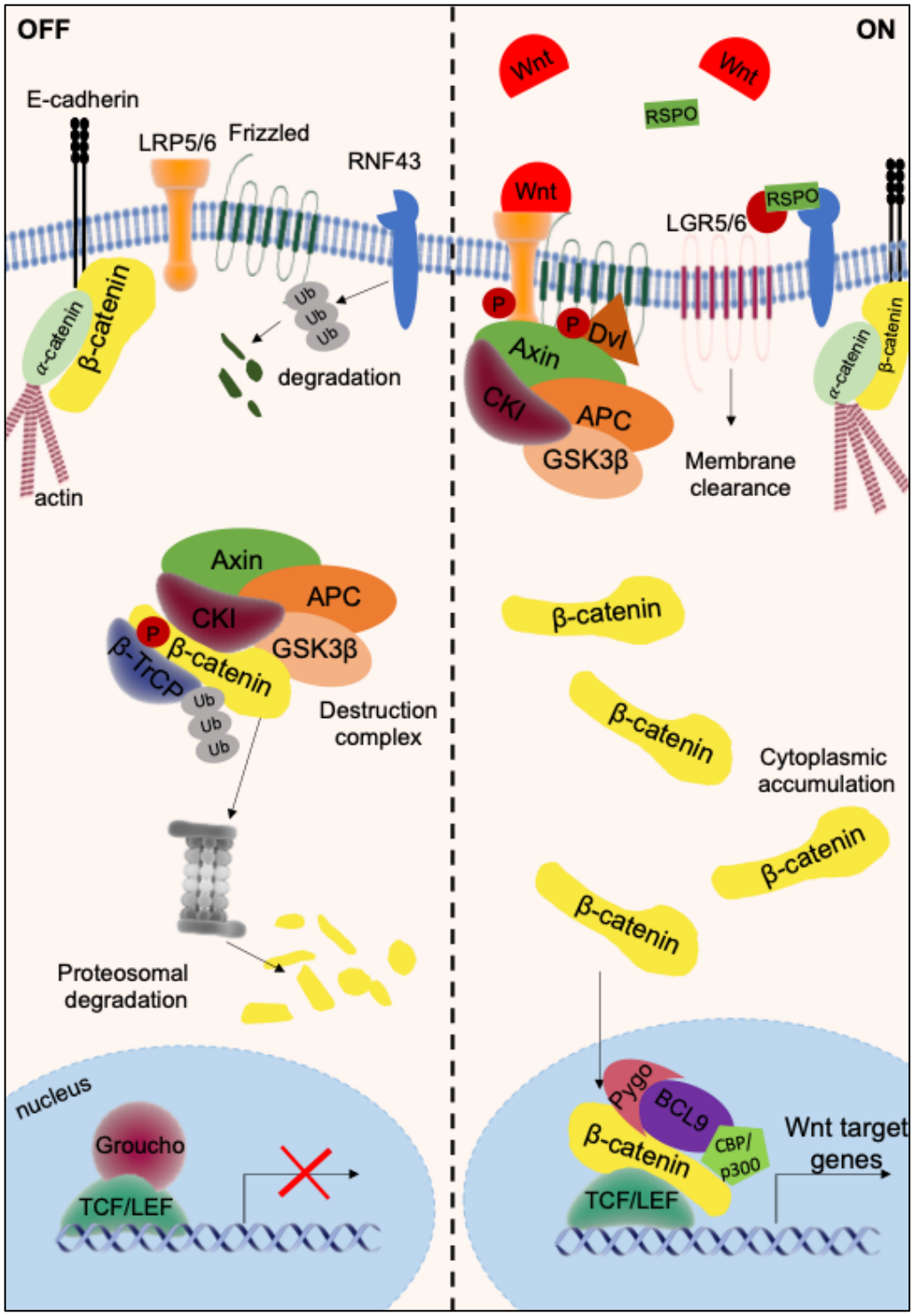


Figure 1.2 Schematic overview of the Wnt pathway.
Dvl: Dishevelled, LRP: Low-density lipoprotein receptor-related protein, β-Trcp: E3 ubiquitin ligase β-transducin repeat-containing protein, P: phosphorylation, Ub: ubiquitination, RSPO: R-spondin, RNF43: E3 ubiquitin ligase RING finger 43. Transcriptional co-activators: CBP: cAMP-responsive element binding (CREB)-binding protein (CBP), BCL9: B cell lymphoma 9, Pygo: Pygopus.

1.4 The multifunctional role of β-catenin

β-catenin is highly conserved throughout metazoan species, from sponges and cnidarians to mammals (Schippers & Nichols, 2018; Zhao, Reynolds, & Gaucher, 2011). Changes in the β-catenin expression levels of early metazoans greatly impacts their development (Gee et al., 2010; Lapébie et al., 2009), which highlights the fundamental function of this signalling pathway in development.

β-catenin has a well-established role in development (Haegel et al., 1995; Huelsken et al., 2000), adult tissue homeostasis (Fevr et al., 2007) and tissue regeneration. In order to fulfil its role, β-catenin is not only a prime mediator of the Wnt signalling pathway (as previously discussed in 1.3), but also implicated in the cell-cell adhesion complex through the interaction with Epithelial-cadherin.

1.4.1 The role of β-catenin in cell-cell contact

Epithelial cadherin (E-cadherin) is a calcium-dependent cell adhesion molecule. It is the key player of epithelial cell-to-cell adhesion through interaction of its extracellular domain. E-cadherin, encoded by the *CDH1* gene, is formed of a single transmembrane domain, a cytoplasmic domain and ectodomain of five tandemly repeated domains (Shapiro & Weis, 2009). β-catenin can bind directly to the intracellular domain of E-cadherin (Huber & Weis, 2001). This ultimately facilitates the interaction with α-catenin, forming a bridge between the cell adherens junction and the actin cytoskeleton (Desai et al., 2013). The cytoplasmic interaction of E-cadherin with the catenin-family members is essential for E-cadherin's function (Shimoyama, Nagafuchi, & Hirohashi, 1992).

1.4.2 The structure of β-catenin

β-catenin is a member of the Armadillo-repeat protein family. The human β-catenin protein is composed of 781 amino acids (AA) and can be divided into three structural areas: the flexible N- and C-terminal domains flanking the relatively rigid central Armadillo region. The Armadillo region is formed of 12 Armadillo repeats (ArmR) (Figure 1.3), each composed of 42-45 AA that are structured into three helices (Graham et al., 2000; Huber, Nelson, & Weis, 1997; Sampietro et al., 2006). The 12 ArmR form a positively charged groove, along which most of the β-catenin protein-protein interactions (PPIs) occur (Huber, Nelson, & Weis 1997). The structure of β-catenin is well described and multiple crystal structures with β-catenin-interaction partners have been published (Graham et al., 2002; Graham et al., 2000; Huber et al., 1997; Poy et al., 2001; Sampietro et al., 2006).

1.5 β-catenin and its interaction partners

β-catenin can be found at the plasma membrane, in the cytoplasm and in the nucleus, where the protein achieves its different functions. Figure 1.3 gives a schematic view of some of the known protein interaction partners of β-catenin. Cells have developed complex approaches to regulate the functions of β-catenin, notably through overlapping binding-sites allowing for competitive binding (reviewed by Valenta et al., 2012). For example, LEF-1, E-cadherin and APC all bind along the central ArmR region of β-catenin and form mutually exclusive complexes preventing the other proteins from binding (Hülsken, Birchmeier, & Behrens, 1994; Orsulic et al., 1999; von Kries et al., 2000). While many of the binding partners have been well described, no sequence homology between the β-catenin-binding domains (CBD) has been found (Graham et al., 2000).

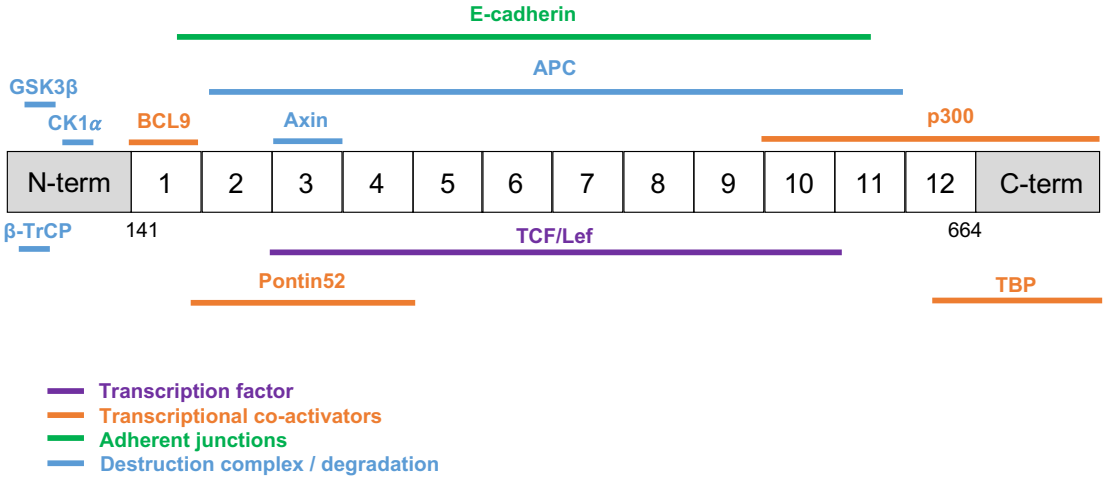


Figure 1.3 Schematic structure of β-catenin and some of its binding partners. Numbered white boxes represent the individual Armadillo repeats. Black numbers below the structure indicate the amino acid positions at the beginning and end of the central Armadillo region. APC: Adenomatous polyposis coli, TBP: TATA-box binding protein, p300: E1A-binding protein, 300 kDa. Pontin52: transcriptional co-activator, BCL9: B-Cell Lymphoma 9, GSK3β: Glycogen Synthase Kinase 3, CK1: Casein Kinase 1, β-TrCP: E3 ubiquitin ligase β-transducin repeat-containing protein. TCF/Lef: T-cell factor/lymphoid enhancer factor. Figure adapted from Valenta, Hausmann, & Basler, 2012.

Disruption of some of these PPIs can abrogate the Wnt pathway (Hahne & Grossmann, 2013a; Takada et al., 2012). Therefore, β-catenin has been proposed as valid drug target in the search of new cancer treatment approaches. Here we summarise some of the described β-catenin interactions that are subject to Wnt inhibition, including the TCF4 and BCL9/L interactions.

1.5.1 TCF/LEF family members

The T-cell factor/lymphoid enhancer factor (TCF/LEF) transcription factors are the main nuclear mediators of the Wnt signalling pathway (Cadigan & Waterman, 2012). The TCF members are part of the high-mobility group (HMG) DNA-binding factors. They bind to a consensus DNA sequence, also known as the Wnt responsive element (WRE), which can recruit transcriptional and chromatin remodelling complexes. Vertebrates have four conserved members of the

TCF/LEF family: TCF1 (encoded by *TCF7*), LEF1, TCF3 (*TCF7L1*) and TCF4 (*TCF7L2*). All family members have conserved domains including the N-terminal β-catenin binding domain, the Groucho binding domain (GBD), the HMG-domain, a nuclear localisation signal and the C-terminal tail. While the distinct roles and functions of individual TCF/LEF family members and their various splice variants are still being investigated, evidence suggest a context specific expression in development and adult homeostasis (Liu 2005; van Es et al. 2012; Arce, Yokoyama, & Waterman 2006).

The interaction between TCF/LEF family members and β-catenin was first described with LEF1 and TCF1 through a yeast two-hybrid screen (Behrens et al. 1996; Huber et al. 1996). The importance of this complex in the context of Wnt signal transduction was highlighted by the depletion of Pangolin (*Drosophila* homologue of TCF/LEF), which led to a significant reduction of the Wnt signal transduction and abnormal development of *Drosophila* (Brunner et al., 1997).

TCF4 (*TCF7L2)* is the most abundantly studied protein of the TCF/LEF family (Hrckulak et al., 2016). TCF4 is highly expressed in the intestinal epithelium (Barker et al., 1999) and was shown to be a key player in the development and homeostasis of colonic crypts. *TCF7L2* -/- mice die shortly after birth and present with only fully differentiated villus cells and a lack of the proliferative stem-cell compartment in the villi (Korinek et al., 1998). Conditional ablation of *TCF7L2* in the intestine and colon of floxed mice affected cell proliferation and intestinal homeostasis (van Es et al. 2012).

1.5.2 Structural details of the β-catenin/TCF4 interaction

The N-terminus (amino acids 1-53) of TCF4 binds along the central armadillo domains of β-catenin (Omer et al., 1999). The TCF4 residues D16 and L48 have been highlighted as important binding residues by mutagenesis studies (Fasolini et al., 2003b; Knapp et al., 2001; Omer et al., 1999). Crystal structures of the β-catenin-TCF4 complex and the closely related TCF3 revealed β-catenin residues K312 and K435 (in ArmR 5 and 8, respectively) to be crucial for the TCF interaction (Graham et al., 2000; Poy et al., 2001).

1.5.3 The structure and function of BCL9/BCL9L

B-cell lymphoma 9 (BCL9) is a transcriptional co-activator of the TCF-transcription factor complex and interacts with the first ArmR of β-catenin (Sampietro et al., 2006). Inhibiting the interaction between β-catenin and BCL9 has been described as a potential therapeutic target to inhibit the Wnt pathway (Takada et al., 2012).

The B-cell lymphoma 9 (*BCL9*) gene, and its protein product were first identified in B-cell acute lymphoblastic leukaemia (Willis et al., 1998). The gene *BCL9* is located on chromosome 1q21 and is frequently associated with chromosomal translocations and poor clinical outcome (Hyeon et al., 2013; Mani et al., 2009; Moor et al., 2015). The involvement of this protein in the Wnt pathway was first shown in *Drosophila*, where the knock-out of *legless* (*lgs*), the homolog of human *BCL9*, resulted in a Wnt negative phenotype resembling the loss of the Wnt factor *wingless* (Kramps et al., 2002). In the same study, *legless* was shown to recruit Pygopus (Pygo) to β-catenin, which allowed transcriptional activation in *Drosophila*. While Pygopus was shown to be essential for the Wnt signal cascade

in *Drosophila* (Belenkaya et al., 2002; Kramps et al., 2002; Parker, Jemison, & Cadigan, 2002), a Pygopus-independent action of BCL9L, another mammalian BCL9 gene, has been described (Brembeck 2004; Hoffmans and Basler 2007; Sustmann et al. 2008).

B-cell lymphoma 9-like (BCL9L, also known as B9L or BCL9-2), the vertebrate paralogue of BCL9, was first identified in a yeast-2-hybrid screen of a murine cDNA library using β-catenin as a bait (Brembeck 2004). The two paralogues share 60% of their amino acid sequence, with high sequence identity (up to 90%) in short conserved clusters of about 30 amino acids. These include the β-catenin and pygopus binding domains, as well as C-terminal homology domains and nuclear localisation domains (Brembeck, 2004). The distinct roles of the two mammalian paralogues are not fully elucidated. Both mammalian paralogues showed functional redundancy in *Drosophila* mutant for *legless* (Hoffmans & Basler, 2007). In contrast, BCL9L was specifically involved in early mesoderm patterning of zebrafish (Brembeck, 2004). This suggests that there might be context-specific roles for BCL9 and BCL9L, which are not fully understood yet.

BCL9 and BCL9L mRNA expressions were found to be up regulated in some colon carcinoma primary tumours (Mani et al. 2009; Brembeck et al. 2011; Adachi et al. 2004), prostate cancer (Ling et al., 2016) and multiple myeloma (Mani et al., 2009). siRNA knock-down of BCL9 caused a marked reduction of Wnt target genes and proliferation in COLO320 cells (Mani et al., 2009). BCL9L knock-down in SW480 cells repressed constitutively activated β-catenin-TCF-mediated transcription (Adachi et al., 2004). The important role of BCL9 was further highlighted by the

inhibition of Wnt signalling through dominant negative BCL9 constructs lacking their C-terminus (Adachi et al., 2004; de la Roche, Worm, & Bienz, 2008).

More recently, the relevance of the BCL9 co-factor was highlighted in a study by Mieszczanek et al. (2019), where loss of BCL9 and its interaction partner Pygo extended disease-free survival in *Apc*^{Min} mice (a model for APC loss-of-function intestinal tumorigenesis). In a further study, deletion of *BCL9/BCL9L* reduced many signs typical of APC loss and Wnt pathway upregulation (increased proliferation and uncontrolled differentiation) *in vivo* (Gay et al., 2019). Furthermore, *Bcl9*$^{fl/fl}$ *Bcl9l*$^{fl/fl}$ mice showed reduced *Lgr5* expression in *Bcl9/Bcl9L* deficient crypts and it was proposed that BCL9/BCL9L are involved in Lgr5-positive stem cell fitness. Interestingly, normal intestinal homeostasis is not affected by *Bcl9/Bcl9L* deletion (Deka et al., 2010; Gay et al., 2019).

Taken all together, there is clear evidence that BCL9 and BCL9L play a crucial role in the activation of the β-catenin/TCF transcription complex and that targeting the β-catenin/BCL9 interaction can reduce the oncogenic Wnt pathway and its target genes. As the two paralogue have conserved β-catenin binding domains (Brembeck, 2004), they are referred to as BCL9 for simplicity in this work, unless stated otherwise.

1.5.4 Structural details of the β-catenin/BCL9 interaction

The interaction between β-catenin and BCL9 has been well characterised and is restricted to the first ArmR of β-catenin (Hoffmans & Basler, 2004; Hwang et al., 2016; Sampietro et al., 2006). The homology domain 2 (HD2) of BCL9 binds to ArmR1 of β-catenin, with binding "hotspots" residues D162 and D164 on β-catenin, as visualised in Figure 1.4 (Sampietro et al., 2006).

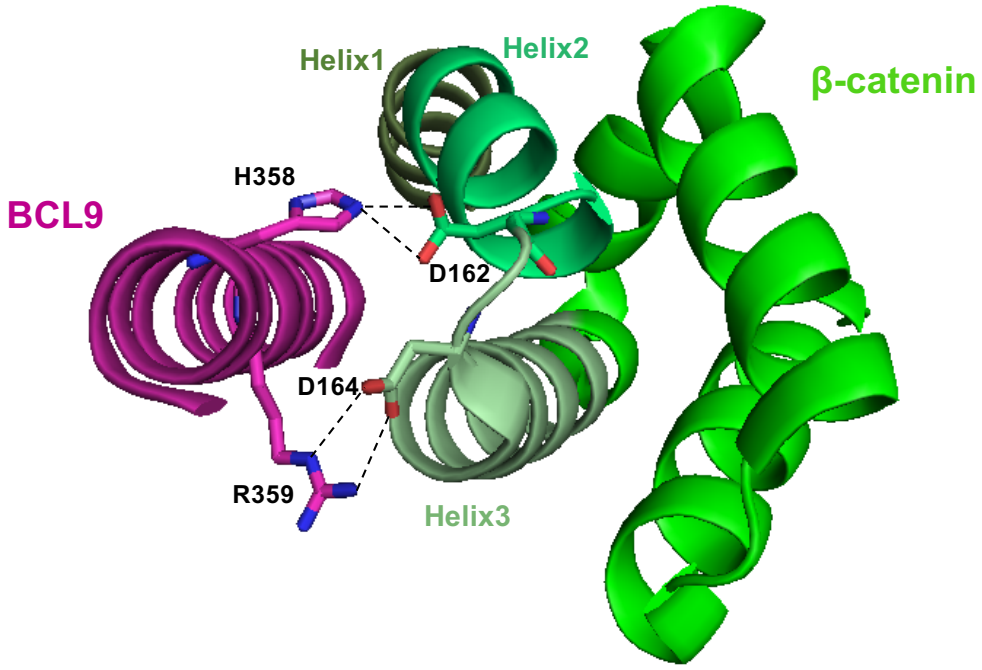


Figure 1.4 Interaction between β-catenin and BCL9
Overview of β-catenin interactions with BCL9. Helices 1-3 of ArmR1 of β-catenin are represented in different shades of green. Homology domain 2 of BCL9 is represented in magenta. Residues H358 and R359 of BCL9 form a hydrogen bond and a salt bridge with β-catenin D162 and D164, respectively. Figure adapted from Sampietro et al. 2006, Protein Data Bank ID code 2GL7.

The BCL9 binding site on β-catenin does not have any overlap with that of other known Wnt signalling proteins such as Axin or APC (Valenta et al., 2012). The only other known interaction partner at the Arm1 of β-catenin is E-cadherin, which binds along the entire length of the Armadillo repeat region of β-catenin (Arm1-Arm12) (Huber and Weis 2001). Mutations in D162 and D164 of β-catenin

did not affect the binding to E-cadherin, APC or TCF4, suggesting that ArmR1 is not essential for these interaction (Hoffmans & Basler 2004). These findings are supported by studies of Sampietro et al. (2006), where the β-catenin mutations L156A and L159A disrupted BCL9 binding, but not the E-cadherin interaction. This specific binding site makes the β-catenin-BCL9 interaction an interesting target downstream of APC or β-catenin mutations for potential therapeutic development (as discussed in section 1.6.1.2).

1.5.5 Interaction partners of the β-catenin C-terminal

The C-terminal region of the β-catenin is able to bind a multitude of transcriptional co-factors, such as the TATA-box Binding Protein, the Chromatin remodelling factor brg-1 and the histone acetyl-transferase cAMP response element binding protein (reviewed by Valenta et al., 2012). It was also shown to be involved in the nuclear translocation of the protein; a truncation of this area prevented the translocation and caused cytosolic accumulation of β-catenin (Koike et al., 2004). The Tcf-mediated transactivation was not assessed in the study, but later worked indicated inhibition of the Wnt pathway upon C-terminal truncations of β-catenin (Dar et al., 2016).

One example of an interaction partner of β-catenin at the C-terminal region is the acetyltransferase cAMP-responsive element binding (CREB)-binding protein (CBP) and closely related E1A-binding protein, 300 kDa (p300). CBP/p300 are co-activators for β-catenin mediated transcription. The cysteine–histidine-rich region 3 (CH3) of p300 interacts with the β-catenin region of AA residues 630-781 (Hecht et al., 2000a; Miyagishi et al., 2000; Sun et al., 2000; Takemaru & Moon, 2000).

1.6 The Wnt signalling pathway as therapeutic target

The constitutive activation of the Wnt signalling cascade is a main driver in the initiation and progression of colorectal cancer and has been shown to play a role in hepatocellular cancer, breast cancer and leukaemia (Zhan, Rindtorff, & Boutros, 2017). As the Wnt pathway plays a vital role in the oncogenic development, it has been proposed as a valid therapeutic target. Although many advances in the field are being reported and clinical trials are rolled out, no Wnt inhibitor is yet in clinical use (Harb, Lin, & Hao, 2019). It remains a challenge to specifically target the Wnt pathway in malignant cells without affecting the vital Wnt pathway functions in healthy tissue. Indeed, one of the main concerns targeting this pathway is its function in stem cell maintenance and tissue regeneration (Krishnamurthy & Kurzrock, 2018). Therefore, there is a high need to identify a therapy approach that can specifically target the Wnt pathway in malignant cells without inducing potentially harmful side-effects.

Multiple strategies have been exploited to target different steps of the signalling cascade, from Wnt ligands, receptors and intracellular signalling proteins (reviewed by Novellasdemunt, Antas, & Li 2015; Krishnamurthy & Kurzrock 2018; Lyou et al. 2017). A brief overview is given here on the different therapeutic approaches, including small molecules, antibody therapies and peptides. Figure 1.5 gives a graphic representation of some of the Wnt targets currently being investigated for Wnt pathway inhibition.

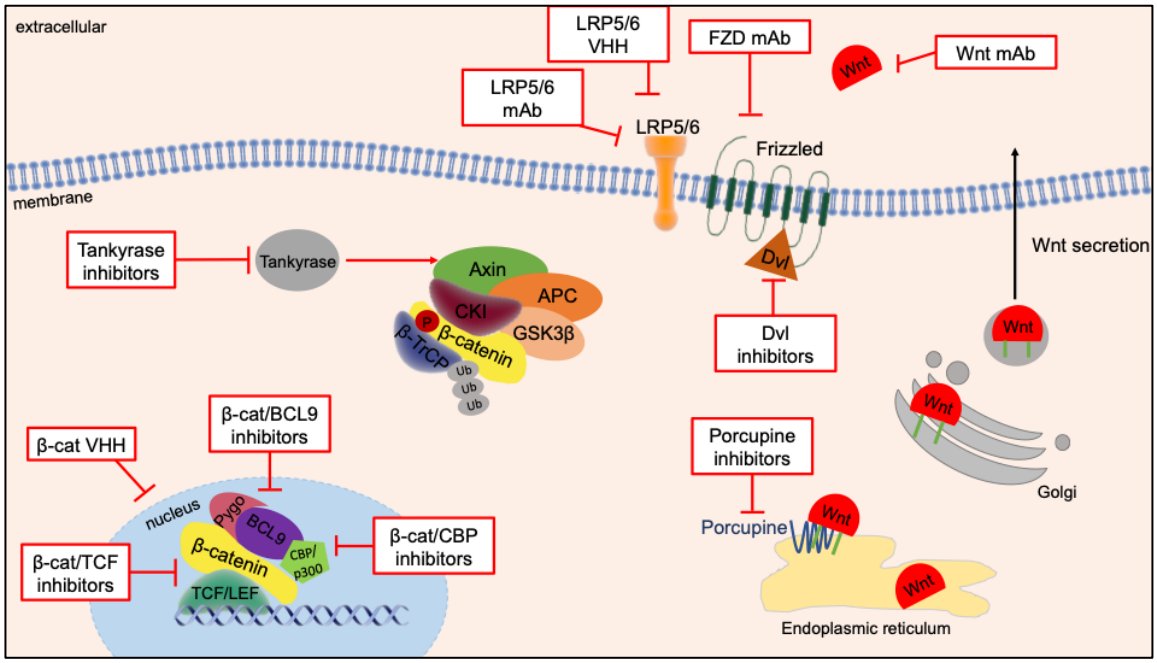


Figure 1.5 Schematic summary of Wnt targeting strategies
Overview of different Wnt pathway inhibition strategies, with extracellular and intracellular targets along the Wnt signalling cascade. Green tails on Wnt ligands represent lipid modifications. β-cat: β-catenin, mAb: monoclonal antibody, VHH: Llama single domain antibody fragment.

1.6.1 Small molecules and peptides targeting the Wnt pathway

1.6.1.1 Targeting the β-catenin/TCF4 interaction

Preventing the interaction between β-catenin and TCF4, the final step in the Wnt transduction cascade, has been suggested as potential option for specific Wnt inhibition and proof-of-concept studies have validated the target. For example, the overexpression of ICAT (endogenous inhibitor of β-catenin and TCF4) resulted in reduced Wnt target gene expression *in vitro* (Daniels & Weis, 2002; Sekiya et al., 2002; Tago et al., 2000). Various groups previously targeted the β-catenin/TCF4 complex using small molecules, showing successful Wnt-inhibition through assessment of Wnt target genes, inhibition of the TCF-mediated Wnt reporter assay TOPflash and cell growth inhibition (Zecheng Chen et al., 2009; Fang et al., 2016; Shin et al., 2017; Wei et al., 2010). However, up to date, no β-catenin/TCF4

has been reported to reach more advanced clinical assessment, which is likely due to their broad activity profile and potential off target effects (Hahne & Grossmann, 2013b).

Moreover, StAx-35R, a hydrocarbon-stapled peptide against β-catenin, was shown to inhibit the β-catenin/TCF interaction (Grossmann et al., 2012). Importantly, the peptide was described as Wnt-specific, without any significant effect on reporter gene transcription of Hedgehog, BMP or TGF-β signalling pathways. This peptide is now being further being optimised and investigated, showing good cellular uptake and inhibition of cell proliferation in Wnt-dependent cells (Dietrich et al., 2017; Held et al., 2018).

1.6.1.2 Targeting the β-catenin/BCL9 interaction

The concise and well described β-catenin/BCL9 interaction has attracted much attention for the design of specific Wnt-inhibitors. An initial approach to inhibit the β-catenin/BCL9 interaction was to synthesise triazole-stapled BCL9 α-helical peptides to dissociate endogenous BCL9 from β-catenin (Kawamoto et al., 2012). However, results of the efficacy *in vitro* and *in vivo* are still lacking from these peptides. In a similar approach, Takada et al. (2012) disrupted the β-catenin/BCL9 complex using a stabilized alpha-helix of BCL9 called SAH-BCL9$_B$ (stapled peptide) resulting in the suppression of tumour growth, angiogenesis and metastasis in mouse xenograft models of Colo320 colorectal carcinoma (Takada et al., 2012). The same group has further optimised BCL9 peptide structures to obtain a construct with half-maximal inhibitory concentration in the nanomolar range and improved pharmacological properties (Feng et al., 2019). Overall, the

research activities in the field of α-helical peptides against this interaction are flourishing, as constructs with improved stability and potency are being described and investigated (Sang et al., 2019).

Efforts have also been placed on synthesizing small molecules inhibiting the β-catenin/BCL9 interaction. Various compounds have been reported to inhibit the TOPflash assay and inhibit Wnt target genes *in vitro* (Hoggard et al., 2015; Wisniewski et al., 2016; Zhang et al., 2018), but are yet to be tested in *in vivo* models to prove efficacy and good toxicity data. Chapter 4 will discuss results obtained from different β-catenin/BCL9 inhibitors, which were kindly provided by the lab of Dr Haitao Ji at the Moffitt Cancer Centre, Florida.

1.6.2 Other small molecule targets in the Wnt pathway

Other approaches include targeting of Wnt modulating proteins, such as Axin, CK1 or Dvl, to stabilise the β-catenin destruction complex.

Tankyrase inhibitors, also known as Poly(ADP-ribose) polymerase (PARP) inhibitors, have been studied most extensively. They target Tankyrase1 and Tankyrase2 (TNK1 and 2), which are involved in the PARylation and subsequent ubiquitination of Axin. The inhibition of TNKs1 and 2 therefore stabilises the β-catenin destruction complex (Thorvaldsen, 2017). A wealth of Tankyrase inhibitors with Wnt-modulating activity *in vitro* has been described in the past decade (Chen et al., 2009; Huang et al., 2009; Lau et al., 2013; Menon et al., 2019; Scarborough et al., 2017; Waaler et al., 2012). However, the success of these

compounds has been limited by intestinal toxicity (Zhong et al., 2015) and bone loss *in vivo* (Mukai, Fujita, & Morita, 2019).

Compounds targeting Dvl interrupt its interaction with the intracellular domain of the FZD receptors, which results in the inhibition of the Wnt signal transduction and stabilisation of the β-catenin destruction complex (Fujii et al., 2007; Shan et al., 2005; Wang et al., 2015). However, it is questionable how suitable the inhibition of targets upstream of Wnt pathway activating APC and β-catenin mutations are in colorectal cancer (Masuda, Sawa, & Yamada, 2015).

Another target is the interaction between β-catenin and the cAMP-responsive element binding (CREB)-binding protein (CBP), a histone acetyltransferases and transcriptional co-activator of the β-catenin-TCF transcriptional complex (Levy et al., 2004; Sun et al., 2000). The small molecular weight compound ICG-001 was shown to specifically inhibit the CBP/β-catenin interaction, block β-catenin/TCF-mediated transcription and induce apoptosis in colon carcinoma cells *in vitro* and *in vivo* (Emami et al., 2004). The compound is now under investigation for various indication, including Multiple Myeloma and Head and Neck cancer, which have infrequent β-catenin mutations (Grigson et al., 2015; Kartha et al., 2018).

1.6.3 Antibody-based approaches

1.6.3.1 Conventional antibodies

Monoclonal antibodies (mAb) have gained significant importance as cancer therapeutics and their development is flourishing in the field of oncology (Kaplon & Reichert, 2019). mAbs are widely used as single agents or in

combination therapy (Singh et al., 2018). The development of the hybridoma technology in 1975 (Köhler & Milstein, 1975), which allows the production of specific antibodies to single targets by tissue culture from immunised mice, has been enhanced by antibody engineering technologies, which have aided the rapid and promising growth of this research sector for cancer and other treatments (Nelson & Reichert, 2009; Strohl, 2018). This has allowed the combination of different antibody domains to create antibodies with custom features, such as a specific binding affinity, altered function or different half-lives (Holliger & Hudson, 2005; Igawa et al., 2011). However, up to date, the use of mAbs has been limited to targets on the cell surface (Weiner, 2015).

A conventional antibody consists of two heavy and two light chains, which are interconnected via disulphide bonds, and each containing variable (V) and constant (C) domains (Figure 1.7). The variable single domain (VH or VL) is the smallest functional unit of an antibody that retains specific antigen binding ability through the three antigen recognition loops, also called complementarity determining regions (CDR1, CDR2 and CDR3). VHs usually have a greater variability within the CDR3 compared to VL (Tanaka & Rabbitts, 2010b). Over the years, numerous antibody fragments have successfully been engineered, ranging from antigen-binding fragments (Fab) to single-chain variable fragments (scFv) and single-domain antibodies (sdAb) (Figure 1.6).

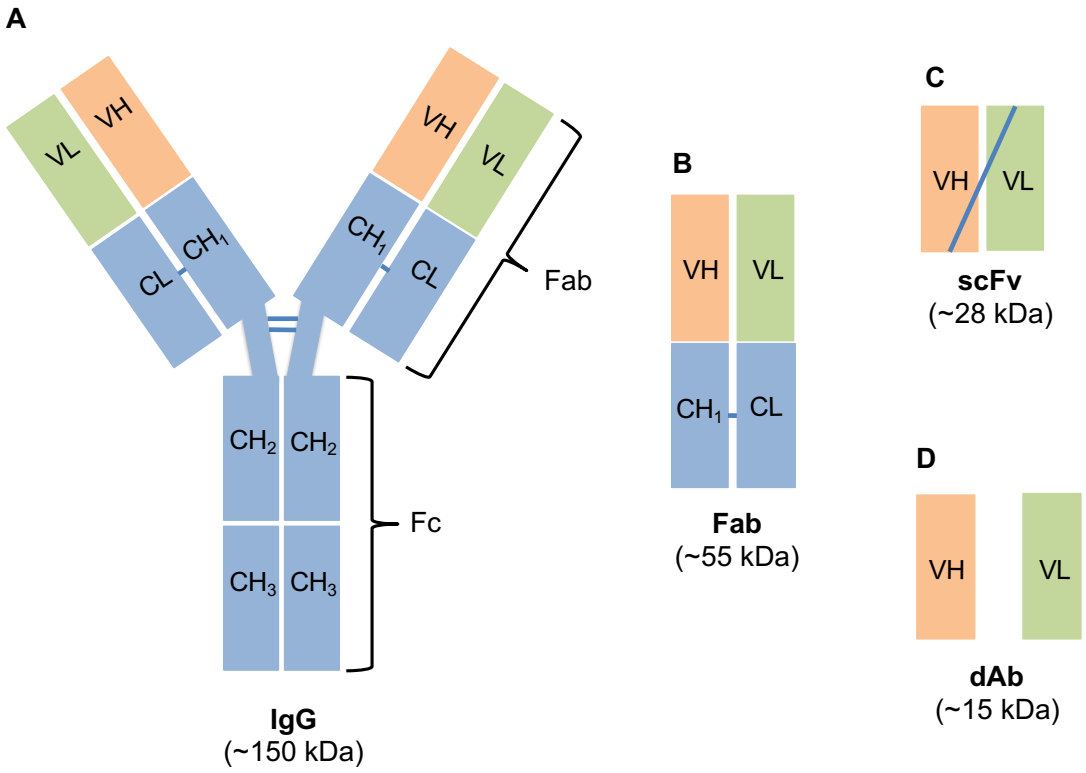


Figure 1.6 Range of antibody fragments obtained through antibody engineering
Schematic structures of **A**) the whole immunoglobulin IgG, **B**) Fab, **C**) single chain variable fragment (scFv) and **D**) single-domain antibody (dAb) VH or VL. The estimated sizes are given in kilodalton (kDa). Dark blue lines represent disulfide bonds.

1.6.3.2 Intracellular single domain antibodies

Intracellular dAbs, also called iDabs (Tanaka, Lobato, & Rabbitts, 2003), are single domain antibodies used inside the cell to inhibit cellular functions (Marschall & Dübel, 2016). They can be designed to disrupt specific protein-protein interactions for example. As previously mentioned, both VH and VL dAbs maintain their specific antigen binding properties through the CDR regions. The CDR3 loop is the most diverse region of the antibody (Kabat & Wu, 1991; Xu & Davis, 2000). Figure 1.7 shows the structure of a VH fragment.

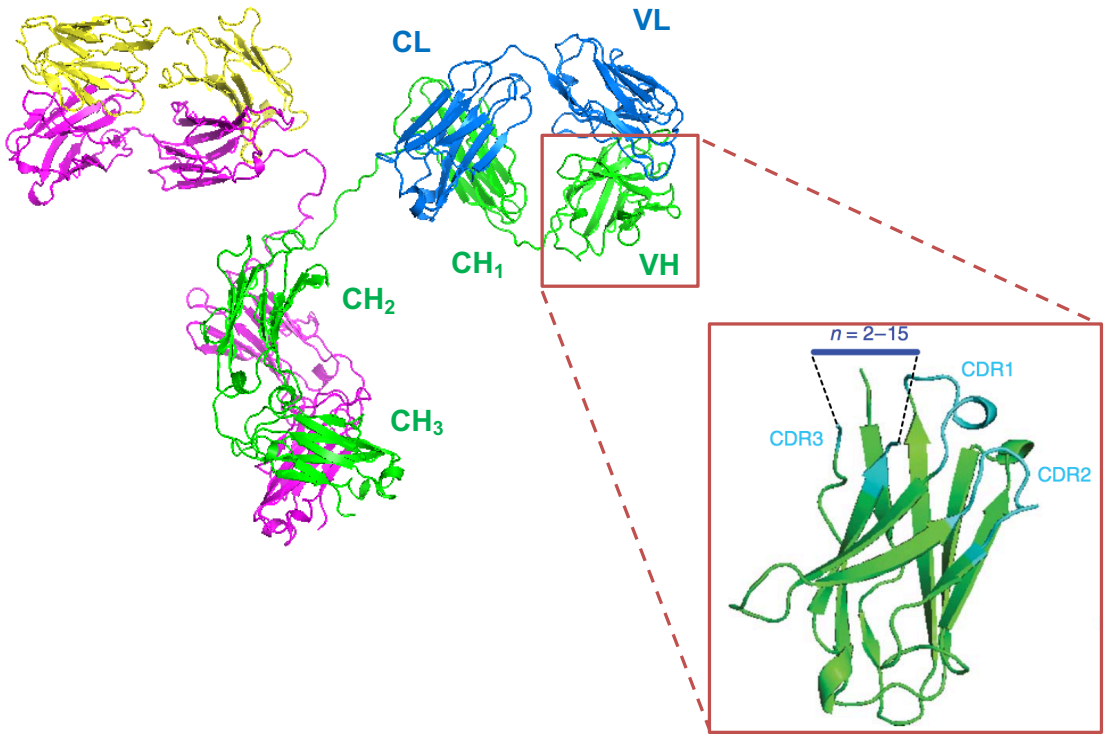


Figure 1.7 Schematic representation of the whole immunoglobin IgG and single domain antibodies (VH and VL)
Left: the whole immunoglobulin IgG (Protein Data Bank: 1IGT, Harris et al., 1997) with two heavy chains (magenta and green) and two light chains (yellow and blue). The variable domains VH and VL are located at the end of the heavy and light chains, respectively. Figure constructed using PyMol for Educational-Use. In the red box is the structure of a single variable heavy chain, with the CDR1, 2 and 3 loops indicated in light blue (figure of single domain antibody from Tanaka and Rabbitts 2010b). The CDR3 loop is the most variable region of the antibody (Kabat & Wu, 1991; Xu & Davis, 2000). This is indicated in the figure by the variable length of 2-15 amino acids (n=2-15) in the CDR3 loop of the VH.

A major concern for the progress of intracellular dAbs has been their solubility and correct folding in the reducing environment of the cell, where the native disulphide bonds cannot form (Biocca et al., 1995). Substantial efforts have been placed on engineering thermodynamically stable and functional single-chain antibody frameworks that can be expressed intracellularly without the need for disulphide bonds. Various stable scFv and dAb scaffolds that fold intracellularly have since been reported (Donini et al., 2003; Proba et al., 1998; Seo et al., 2009; Tanaka & Rabbitts, 2008; Wörn & Plückthun, 1998).

The feasibility of the use of intracellular antibodies was shown in a pre-clinical mouse-model by inhibiting RAS-dependent cancer growth (Tanaka & Rabbitts, 2010; Tanaka, Williams, & Rabbitts, 2007). In this lung cancer mouse model, a scFv specifically bound to the activated (GTP-bound) RAS, which is highly prevalent in mutated cancer pathways. The interaction between oncogenic RAS and its downstream signalling proteins were thus blocked and RAS-dependent tumorigenicity and metastasis inhibited.

Many protein-protein interactions in cell signalling pathways in human diseases have been described as “undruggable” by small molecule compounds due to selectivity, accessibility issues and challenging protein interfaces (Wells & McClendon, 2007). Intrabodies have been described as a potential alternative due to their high target affinities and their development has therefore been of an increasing research focus (Visintin et al., 2008).

1.6.3.3 Antibodies against the Wnt signalling pathway

The high target specificity and affinity of mAb is now exploited in the development of Wnt inhibitors. Initially, mAb against Wnt-1 and Wnt-2 were described and showed apoptosis of Wnt-1 and -2 overexpressing cells and growth inhibition of xenograft models (He et al., 2004; You et al., 2004).

Gong et al. (2010) generated two mAbs against different region of the extracellular LRP6 domain. Characterisation of the mAbs in cell culture showed that the antibodies had opposing effects when used in combination with different Wnt ligands: one being able to inhibit the Wnt pathway by blocking the Wnt-binding site,

while the other one enhanced the signal through facilitating the Wnt-LRP6-FZD complex (Gong et al., 2010).

The furthest developed mAb against a Wnt pathway components is OMP-18R5. Initially identified as targeting the FZD7 receptor, OMP-18R5 is now classified as a pan-FZD binder as it interacts with five FZD receptors (Gurney et al., 2012). It induces growth inhibition in various cancer types *in vitro* and exhibited synergy with commonly used chemotherapeutic agents. First-in-human evaluation of OMP-18R5 (vantictumab) for patients with advanced solid tumours showed tolerable and reversible side effects (Smith et al., 2013). Various further dose-escalation and combination studies for breast, lung and pancreatic cancer indications are being conducted (Clinicaltrials.gov NCT01973309, NCT02005315, NCT01957007 and NCT01345201).

More recently, research has been focused on identifying engineered antibodies against Wnt pathway components. scFv antibodies against FZD7 receptor have been described to induce cell death in MDA-MB-231 triple negative breast cancer cells (Nickho et al., 2017). Furthermore, a bispecific antibody against LRP6 and the tumour-associated cell surface antigen activated leukocyte cell adhesion molecule (ALCAM) has been constructed (Lee et al., 2018). The LRP6/ALCAM bispecific antibody exhibited significant Wnt-signal inhibition with an IC_{50} in the picomolar range in Wnt-activated HEK293 cells. This study explores the possibility of cell targeted Wnt inhibition, as cells with low ALCAM expression were not affected by the bispecific antibody.

Up to date, no intracellular domain antibody (VH or VL) against Wnt pathway components downstream of the Wnt receptors has been described.

1.6.3.4 Llama antibody fragments

In the 1990s it was discovered that mammals of the Camelidae family have, in addition to their conventional antibodies, antibodies composed of two identical heavy chains only (Hamers-Casterman et al., 1993). Because of the lack of the light chains, these antibodies are called heavy-chain antibodies (HCAbs). The single antigen-binding domain of a HCAb is referred to as VHH or Nanobody in order to distinguish it from the conventional VH subunit. Figure 1.8 gives a schematic representation of the HCAbs compared to conventional antibodies.

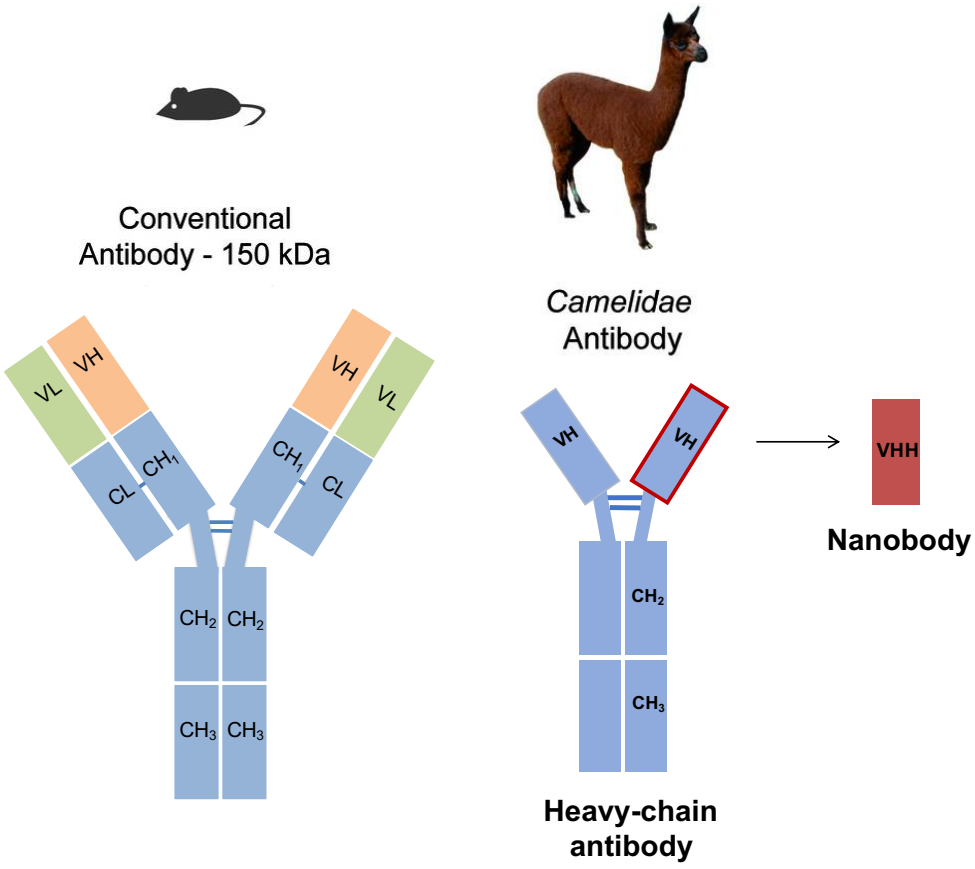


Figure 1.8 Schematic overview of Heavy-chain antibodies compared to conventional antibodies
The heavy-chain antibody lacks the light chains. The variable heavy chain is referred to as VHH, or Nanobody. Figure adapted from Labbiotech.eu .

1.6.4 Characteristics of VHHs

Similarly to VHs, the camelid VHHs contain three CDRs that are involved in antigen binding. A key difference of VHHs is that it has amino acid substitutions in the conserved residues in the framework positions compared to VHs. This region on VHs offers the hydrophobic interface with the VL domain (Harmsen & De Haard, 2007), which is absent in VHHs. These natural VHH substitutions make them more hydrophilic, highly soluble and thermodynamically stable. In fact, “camelised” human VH domains showed enhanced protein stability after the introduction of three residue substitution to mimic VHHs (Davies & Riechmann, 1996). Due to their favourable properties, VHHs are commonly used as chaperones for crystal structures (Koide, 2009). Furthermore, VHHs are characterised by longer CDR3 (Muyldermans et al., 1994), which loops along what would be the VL interface in VH fragments (Desmyter et al., 1996) and so stabilises the domain structure (Bond, Marsters Jr, & Sidhu, 2003). The extended CDR3 loop has also been attributed to the VHHs ability to recognise antigen sites that would normally not be identified by conventional antibodies (Bond et al., 2003; De Genst et al., 2006).

1.6.5 VHHs targeting the Wnt pathway

Recently, anti-LRP5/6 VHHs were isolated from a fully synthetic single-domain antibody fragment library (Fenderico et al., 2019). The VHHs specifically bind to the Wnt3 binding domain of LRP5/6 and cell-based assays resulted in IC_{50}s in the nanomolar range for Wnt3a responsive cells. The VHHs were also able to block the growth and affect cell viability of intestinal organoids.

Another approach to using an intracellular VHH has been described by Newnham et al., (2016). A llama was immunised with full-length human β-catenin and a VHH antibody was isolated that is able to inhibit β-catenin-TCF mediated transactivation in Wnt-induced HEK293 cells (Newnham et al., 2015). It is this antibody that has been studied in this thesis (Chapter 6).

1.7 Aims and scope of this work

Growing efforts are placed on targeting β-catenin protein-protein interactions to inhibit oncogenic WNT signalling. With increasing structural data and a better understanding of the β-catenin interaction partners, attempts have been made for more targeted inhibition mechanisms.

This thesis describes the characterisation of β-catenin in a panel of colorectal cancer cell lines (Chapter 3) and explores the inhibition the WNT signal by targeting the key protein β-catenin through different mechanisms (Figure 1.9):

1. The characterisation of small molecule inhibitors targeting the β-catenin/BCL9 protein-protein interaction (Chapter 4).
2. The identification of an intracellular small domain antibody (VH) targeting β-catenin using a Yeast-2-Hybrid methodology (Chapter 5).
3. The characterisation of Llama nanobodies (VHH) against β-catenin in SW480 cells (Chapter 6).

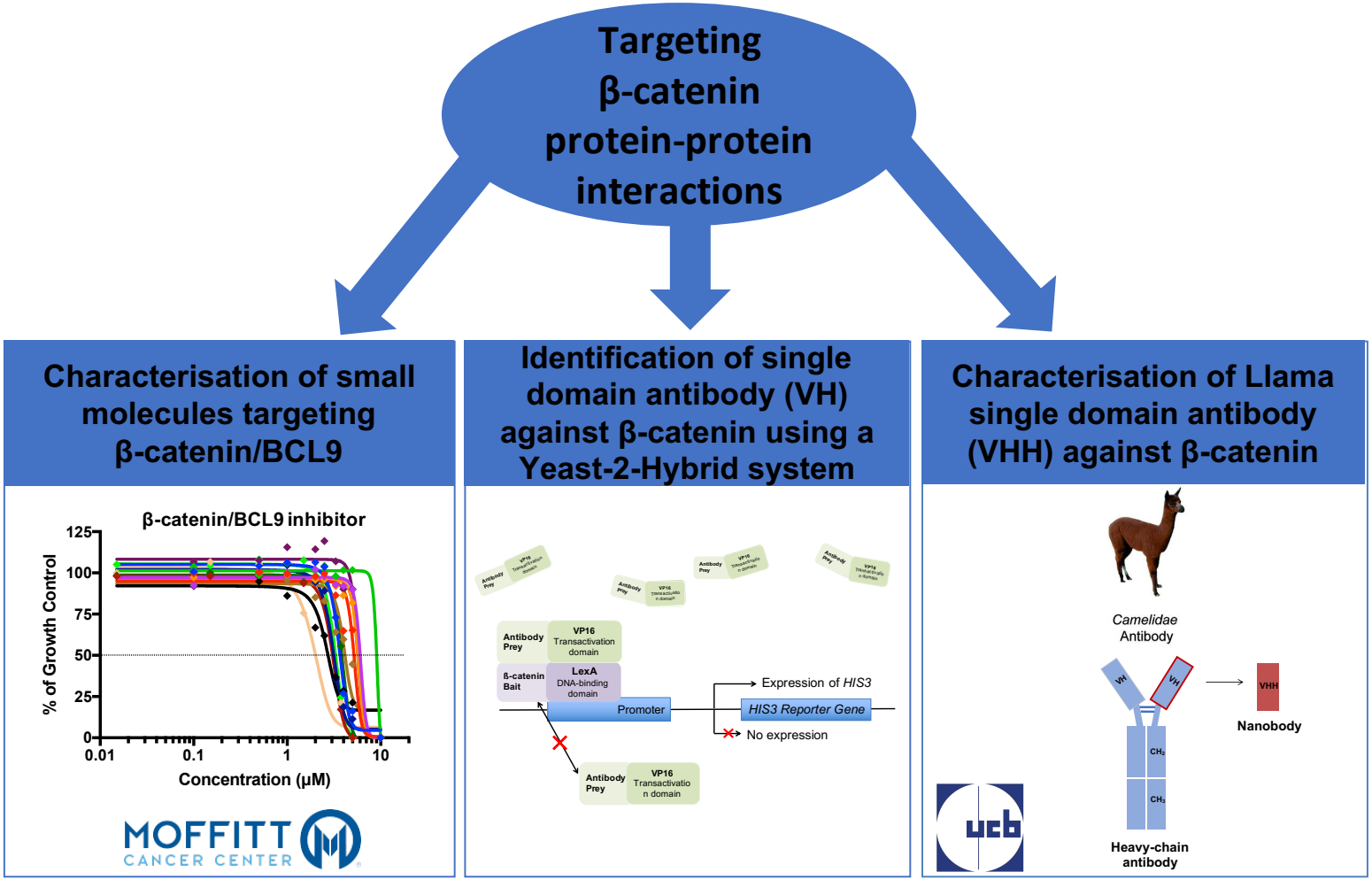


Figure 1.9 Overview of different approaches used in this thesis to inhibit β-catenin PPIs
Three different approaches to inhibit the Wnt pathway are explored in this work: **1**) the characterisation of β-catenin/BCL9 inhibitors in collaboration with the Ji lab at the Moffitt Cancer Centre, Tampa, US, **2**) Isolation of single domain antibodies against β-catenin from a VH library in collaboration with the Rabbitts lab, Weatherall Institute of Molecular Medicine, Oxford, UK, **3**) Characterisation of Llama single domain antibodies (nanobodies) against β-catenin previously developed by UCB Pharma.

Chapter 2

Materials and Methods

CHAPTER 2: MATERIALS AND METHODS

2.1 Cell culture methods

2.1.1 Reagents and suppliers

All cell tissue culture flasks and plates were supplied by Corning (USA). Cell lines were cultured in Gibco® cell culture media by Life Technologies.

2.1.2 Cell lines

The human colorectal cancer cell lines used in this study are listed in Table 2.1. All cell lines were stored at the Cancer and Immunogenetics laboratory (CIL) at the Weatherall Institute of Molecular Medicine (WIMM), Oxford, UK.

2.1.1 Cell culture conditions and maintenance

Cell lines were grown in 25 cm^2 or 75 cm^2 vented tissue culture flasks with 6 millilitre (mL) or 10 mL of the appropriate medium (see Table 2.1), supplemented with 10% fetal bovine serum (FBS, Gibco®) and 1% penicillin/Streptomycin (Lonza). Flasks were incubated at 37°C, 95% humidity and 10% CO_2.

Cells were passaged when they reached about 80-90% confluence. The flask was washed with 10 mL absolute phosphate buffered saline (PBSA) and incubated with 2 mL trypsin/Ethylenediaminetetraacetic acid (EDTA) (0.5% Trypsin-EDTA (10X), gibco® by Life Technologies) solution for 3-5 minutes (min) at 37°C to detach the cells. Five mL of complete medium was added to neutralise the trypsin. Cells were centrifuged at 160 *g* (Allegra™ 6R Centrifuge, Beckman Coulter, rotor GH-3.8) for 5 min and resuspended in 10 mL medium. Based on the cell line growth, cell suspensions were split into ratios from 1:5 to 1:20 dilution into new flasks.

Cell line name	Source	Medium
C10	CIL, Bodmer. ECACC:12022901	ISCOVES
C106	ECACC 12022906	ISCOVES
C125PM	ECACC 12022909	ISCOVES
C2BBe1	ATCC ® CRL-2102™	DMEM
C99	Developed by Bicknell, CIL. ECACC 12022905	ISCOVES
CACO2	ATCC ® HTB-37™	DMEM
CAR1	Cellbank Australia, JCRB0207	ISCOVES
CC20	A.R.Kinsella	DMEM
CCK81	Cellbank Australia, JCRB0208	DMEM
CCO7	JT Immunotech, USA	DMEM
CL40	DSMZ, ACC-535	DMEM
COLO320DM	ATCC ® CCL-220™	ISCOVES
COLO320HSR	ATCC ® CCL-220.1™	ISCOVES
COLO678	ACC-194 DSMZ	DMEM
CW2	RIKEN Cell Bank Japan RCB0778	RMPI
CX1	DSMZ, ACC-129	DMEM
DLD1	ATCC ® CCL-221™	DMEM
GP2D	ECACC: 95090714	DMEM
GP5D	ECACC: 95090715	DMEM
HCA7	Kind gift from Dr S. Kirkland, Royal Postgrad School London	DEMEM
HCT116	ATCC ® CCL-247™	DMEM
HCT15	ATCC ® CCL-225™	DMEM
HDC111	Prof. M. Schwab under MTA, DKFZ, Germany	ISCOVES
HDC114	Prof. M. Schwab under MTA, DKFZ, Germany	ISCOVES
HDC9	Prof. M. Schwab under MTA, DKFZ, Germany	ISCOVES
HT29	ATCC ® HTB-38™	DMEM
HT55	ECACC: 85061105	DMEM
LIM1215	ECACC 10092301	RPMI
LIM2405	ECACC 12062003	RPMI
LOVO	ATCC ® CCL-229™	DMEM
LS1034	Kind gift from Dr Laurent Suradet, ISREC, Switzerland	DMEM
LS123	ATCC® CCL-255™	DMEM

Cell line name	Source	Medium
LS174T	Kind gift from B.H.Tom, NW Uni. Med Centre, Chicago	DMEM
LS180	Kind gift from B.H.Tom, NW Uni. Med Centre, Chicago	DMEM
LS411	Kind gift from Dr Laurent Suradet, ISCRE, Switzerland	RPMI
LS513	ATCC® CRL-2134™	RPMI
NCIH508	ATCC® CCL-253™	RPMI
OUMS23	Cellbank Australia, JCRB1022	DMEM
OXCO1	Kind gift from Prof. E. Cerundolo, WIMM, Oxford	ISCOVES
PMFKo14	RIKEN Cell Bank Japan, RCB1426	DMEM
RKO	ATCC ® CRL-2577™	RPMI
RW2982	Prof. John Mariadason, Melbourne	DMEM
SKCO1	ATCC® HTB-29™	DMEM
SNUC2B	ATCC ® CCL-250™	RPMI
SW1116	ATCC ® CCL-233™	RPMI
SW1222	Prof. M.Herlyn, Wistar Institute	DMEM
SW1417	ATCC® CCL-238™	DMEM
SW403	ATCC® CCL-230™	DMEM
SW48	ATCC ® CCL-231™	ISCOVES
SW480	ATCC ® CCL-228™	DMEM
SW620	ATCC ® CCL-227™	DMEM
T84	ATCC ® CCL-248™	DMEM
VACO4A	Kind gift from J. McBain, VA Res.Ser. Madison, Wisconsin	ISCOVES
VACO4S	Kind gift from J. McBain, VA Res.Ser. Madison, Wisconsin	ISCOVES
VACO5	Kind gift from J.McBain, VA Res.Ser. Madison, Wisconsin	ISCOVES

Table 2.1 List of cell lines
All cell media were supplemented with 10% FBS and 1% P/S, unless otherwise stated. ECACC: European Collection of Authenticated Cell Cultures, DSMZ: German Collection of Microorganisms and Cell Cultures GmbH, DKFZ: Deutsches Krebsforschungszentrum (The German Cancer Research Centre), ISREC: Swiss Institute for Experimental Cancer Research, JCRB: Japanese Collection of Research Bioresources Cell Bank.

2.1.2 Cell storage and retrieval

Cells were stored in liquid nitrogen tanks for long time storage. 80% confluent flasks were trypsinised and centrifuged at room temperature (RT) for 5 min at 160 *g*. Cell pellets were resuspended in 1.5 mL of FBS containing 10% dimethyl sulfoxide (DMSO). The suspension was transferred into sterile cryogenic vials (Corning, USA), approximately 500 microliter (µL) into each vial. The cryovials were placed into a Nalgene®Cryo 1°C "Mr. Frosty" freezing container (VWR, UK) and stored at -80°C overnight before transferring them into cryogenic tanks with liquid nitrogen. To retrieve the culture, cryogenic vials were placed into a water bath at 37°C for 1 min, before being carefully resuspended in 5 mL of culture medium. Cells were centrifuged at 160 *g* for 5 min at RT and medium containing the leftover freezing medium with DMSO was removed. Cells were resuspended in 5 mL correct cell culture medium and transferred into either a 25 cm^2 or 75 cm^2 cell culture flask and incubated at 37°C for the cells to attach.

2.1.3 Cell counting

The Cellometer Auto T4 (Nexcelom Biosciences, USA) was used for automated cell counting. Twenty µL of the cell suspension were placed onto a disposable cell counting chamber (SD100, Nexcelom Biosciences, USA) and inserted into the Cellometer. The Cellometer Auto T4 software captures four bright field images to quantify the number of cells per mL.

2.1.4 Mycoplasma testing

Cell lines were regularly tested for Mycoplasma contamination using the MycoAlert® Mycoplasma Detection Assay (Lonza, Rockland, Maine, USA). Cells were cultured for two days before collecting 1 mL of the culture medium. The

medium was centrifuged at 160 *g* for 5 min to collect cell debris. 100 µL of the cleared supernatant was transferred to a white-walled 96-well plate. 100 µL of MycoAlert® Reagent was added and incubated for 5 min at RT. The FLUOstar Optima luminometer (BMG Labtech, Offenburg, Germany), was used to read the background luminescence of the samples ("Reading A"). Next, 100 µL MycoAlert® Substrate was added to the well and incubated for 10 min at RT. Subsequently, the luminescence of the sample was measured ("Reading B"). The ratio of Reading B to Reading A was calculated, and the cultures were considered negative if the ratio was less than 1. Ratios yielding between 1 and 2 were retested for *Mycoplasma* contamination. A ratio higher than 2 was considered as a *Mycoplasma* contamination and cells were discarded.

2.2 Drug studies

2.2.1 Compounds

Different compounds (Table 2.2) were tested in this study on a large panel of cell lines.

Name of compound	Source	Stock concentration	Comments
ZYQ-1-74	Dr Haitao (Mark) Ji, Mottfitt Cancer Centre	50 mM in DMSO	BCL9/β-catenin inhibitor
ZYQ-2-165			BCL9/β-catenin inhibitor
JW-2-80			BCL9/β-catenin inhibitor
JW-1-78			Control for BCL9/ β-catenin inhibitors

Table 2.2 List of compounds
All compounds were resuspended in DMSO and stored at -20°C. mM: millimolar

2.2.2 Drug treatment

Four thousand cells were seeded in 100 µL in triplicate into a 96-well plate, respecting the appropriate lag time of different cell lines (e.g.: GP2D cells have a lag time of 2 days and were seeded two days before drug treatment). On a separate plate, cells were seeded in triplicate as well and fixed on the day of the drug treatment (Day 0 plate, see section 2.2.3). Drugs were prepared in a 2X concentration in DMEM medium and 100 µL of the drug solution was added to 100 µL medium in the wells, resulting in a final 1X concentration of the drug. Cells were incubated with the drugs for at least three doubling times (DT).

2.2.3 Sulphorhodamine B Protein Staining assay

The Sulphorhodamine B Protein (SRB) staining assay was extensively optimized in our lab and others (Skehan et al., 1990; Vichai & Kirtikara, 2006) for cytotoxic screening by determination of relative cell numbers in a 96-well assay format by staining for proteins. Following the appropriate drug treatments and incubation of the cells (for three doubling times), 96-well cell culture plates were centrifuged at 160 *g*, RT for 15 min. Twelve µL of 50% trichloroacetic acid (TCA) were added to each well containing 100 µL of culture medium and incubated for 1 hour at 4°C. The medium/TCA was removed from the wells and washed three times with PBS. The plates were tapped on a tissue paper and let to dry overnight. One hundred µL SRB solution (0.04% SRB in 1% Acetic Acid (HOAc, Alfa Aesar), Sulforhodamine B sodium salt from Sigma, S1402) was added to each well and incubated on a rocking platform (Heidolph Titramax 100) at 600 rpm for 1 hour. The SRB solution was removed and wells were washed three times with 1% HOAc using a plate washer (ELx405) before tapping the plates on tissue paper and let to dry overnight. The SRB stain was resolved by adding 200 µL of 10 millimolar (mM)

Tris (pH 9.5). The plates were incubated on a plate shaker until the dye was fully dissolved (visual inspection). The absorbance was read at 520 nanometer (nm) on a μ-Quant spectrophotometer (Bio-Tek Instrument, USA). Plates can be stored and re-read if needed. The percentage growth of treated cells compared to DMSO control were calculated and IC_{50} were identified in GraphPad Prism 7.0.

2.2.4 Calcein-AM staining

Calcein-acetoxymethyl ester (Calcein-AM) was used to stain viable cells in culture. Calcein-AM is a non-fluorescent lipophilic ester with the ability to penetrate cellular membranes of live cells. It is cleaved intracellularly by esterases with the product calcein, a fluorescent compound (Bratosin et al., 2005). Cell cultures were incubated for 30 min at 37°C with serum-free medium and Calcein-AM (BioLegend, USA) at a dilution of 1:1000. Green fluorescence was observed using a fluorescence microscope (Axio Observer. Z1, Zeiss).

2.2.5 Colony Formation Assay (CFA)

Between 100-500 cells/well of cells of interest were seeded in a 6-well plate in triplicate. The cells were allowed to attach to the plate overnight. The medium was carefully removed the next day. Drug treatment or control was added and replaced every three days. Cells were incubated for nine days and regularly inspected for colony growth. For fixation, cells were washed once with ice-cold PBS and incubated with 100% methanol for 10 min on ice. Colonies were then stained using Crystal violet solution (0.5% crystal violet in 25% methanol) for 15 min on ice. Plates were thoroughly washed in a water bath and dried overnight. Plates were imaged using a GelCount plate reader (Oxford Optronix) and colonies were counted using the Cell Profiler Software (2.11.2). Number of colonies in treated

samples was expressed as percentage compared to untreated control. Experiments were repeated in three independent experiments.

2.3 Lentiviral work

All lentiviruses were produced by Dr Ryan Beveridge at the in-house Lentiviral Facility at the WIMM.

The sequence of interest of the VHHs LL3 and AAA (see Chapter 6) were cloned into the Tetracycline (Tet)-inducible TLCV2 lentiviral expression vector using the AgeI/BamHI restriction sites, in frame with the self-cleaving peptide T2A and Green-fluorescent protein (GFP). A vector map of TLCV2 is given in Figure 6.6.

2.3.1 Lentiviral transduction of cells

SW480 cells were plated in a 12-well plate (40,000 cells/well) in complete DMEM medium. Cells were allowed to attach overnight at 37°C. The next day, the medium was changed to antibiotic-free DMEM + 6 microgram/mL (µg/mL) polybrene (kind gift from Dr Ryan Beveridge). Different volumes (0, 2.5, 5, 25 and 50 µL/well) of lentiviruses TLCV2-LL3 or TLCV2-AAA were added to each well in duplicate. The lentivirus was left on the plates for 3 days. The cells were then expanded into 6-well plates, attached overnight and treated with 1.2 µg/mL puromycin (gibco® by Life Technologies) for selection until SW480 parental control cells were killed. The resulting bulk cell lines SW480-LL3-GFP_2.5, SW480-LL3-GFP_5, SW480-LL3-GFP_25, SW480-LL3-GFP_50, SW480-AAA-GFP_2.5, SW480-AAA-GFP_5, SW480-AAA-GFP_25, SW480-AAA-GFP_50 were expanded and a stock was frozen down.

2.3.2 Single cell selection from Lentiviral bulk cultures

Transduced and puromycin-selected SW480 bulk cultures SW480-LL3-GFP_2.5, SW480-LL3-GFP_5, SW480-AAA-GFP_2.5 and SW480-AAA-GFP_5 were trypsinised and washed twice with 1 mL PBS. Cells were incubated in a total volume of 600 µL PBS with 1:10,000 4'6-diamidino-2-phenylindole (DAPI, Invitrogen) for 10 min on ice under sterile conditions. Each bulk cell line was then single cell sorted into three 96-well plates in complete DMEM medium by the in-house FACS Facility at the WIMM, Oxford. Cells were grown until single colonies were visible in each well. The individual clones were expanded under puromycin selection and cryovial stocks were made for further characterisations.

2.3.3 Doxycycline induction

Doxycycline (DOX) was used to induce the expression of the VHH fragments LL3 and AAA in stably transformed cells. Lentiviral SW480-VHH clones and SW480 parental cells were plated in 6-well plates or 10 cm dishes and allowed to attach overnight. The next day, the cell culture medium was replaced with complete DMEM + 100 nanogram/mL (ng/mL) DOX (kind gift from Ang Koon Hwee, Harris Lab, WIMM). After 48 hours, cells were observed under the microscope for GFP induction und used for further experiments.

2.4 Microscopy

2.4.1 Antibodies used for immunofluorescence

Primary and secondary antibodies used for immunofluorescence (IF) are listed in Table 2.3.

1° mAntibody	Source	Catalogue number	Species	Dilution
β-catenin	BD Transduction Lab	610154	mouse	1:300
β-catenin	abcam	ab32572	rabbit	1:300
Myc-tag	Cell Signaling	#2276	mouse	1:1000
EpCam (AUA1)	In-house	-	mouse	1:200
2° Antibody	**Source**	**Catalogue number**	**Specifications**	**Dilution**
Alexa Fluor 488	Life Technologies	A11001	GAM	1:200
Alexa Fluor 555		A21427	RAM	1:200
Alexa Fluor 555		A31572	DAR	1:200
Alexa Fluor 647		A31571	DAM	1:200

Table 2.3 List of antibodies used for immunofluorescence
GAM: Goat anti mouse, RAM: Rabbit anti-mouse, DAR: Donkey anti-rabbit, DAM: Donkey anti-mouse

2.4.2 Immunofluorescence

5 x 10^3 cells were seeded in a 96-well plate and grown under standard cell culture condition until 70% confluent. Cells were washed with 200 µL PBS. Cells were fixed using 50 µL 4% Paraformaldehyde (PFA, VWR Chemicals) and incubated at RT in the dark for 15 min. Wells were washed three times with PBS and permeabilized with 50 µL/ well of 0.1% Triton X-100 (Sigma) for 10 min in the dark at RT. The wells were washed once using PBS and 200 µL wash buffer (PBS + 2% FBS) was added. The plate was incubated for 1 hour in the fridge. After the

incubation, the wash buffer was removed and 50 µL of the primary antibody in the appropriate dilution (Table 2.3) was added. The plate was incubated overnight at 4°C, or 1 hr at RT. The wells were washed twice using wash buffer and 50 µL of the secondary antibodies in the appropriate dilutions were added. After a 1-hour incubation at 4°C, cells were washed with 200 µL was buffer before 50 µL DAPI stain (1 µg/ml in PBS, Sigma) was added and incubated at RT for 10 min. Cells were imaged using an Axio Observer Z1 (Zeiss) microscope. The numerical apertures (NA) for the microscope objectives are as follows: 5X = 0.6 NA, 20X = 0.4 NA, 40X = 0.6 NA and 100X = 1.4 NA.

For immunofluorescence imagining performed at 100X magnifications, 12000 cells were seeded into a Nunc™ Lab-Tek™ II Chamber Slide™ System (Thermo Fisher, 154534PK). Cells were fixed and stained with 1° and 2° antibodies as previously described. For DAPI staining and mounting of the slide, Fluoromount-G™ with DAPI (Invitrogen, Ref 00-4959-52) mounting medium was used.

2.5 Luciferase reporter assay

The TOPflash assay is commonly used to measure the transcriptional activity of TCF and β-catenin through a luciferase reporter to assess the Wnt pathway activity. The TCF Reporter Plasmid Kit (TOPflash and FOPflash) was obtained from Merck, UK (17-285). The TOPflash plasmid contains two sets of three copies of the TCF binding site (wild type) upstream of the Thymidine Kinase (TK) minimal promoter and Luciferase open reading frame (Figure 2.1). FOPflash is the negative control plasmid for this assay, containing two full and one incomplete copy of the TCF binding site (mutated) followed by three copies in the reverse orientation

upstream of the TK promoter and Luciferase open reading frame. Renilla, under the control of TK promoter (pRL-TK), was used as a transfection internal control and used for normalisation of luciferase readings.

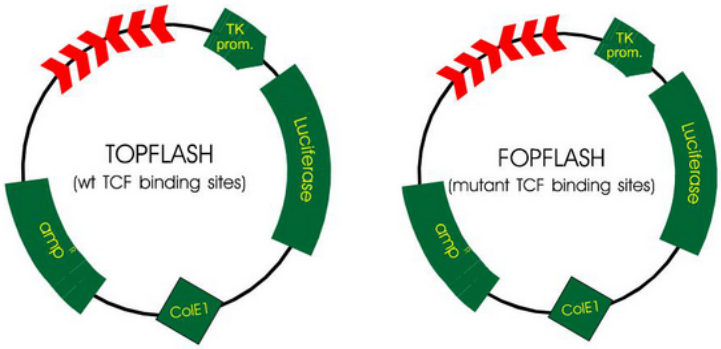


Figure 2.1 TOPflash and FOPflash vectors
TCF binding sites (red) upstream of the TK minimal promoter and Luciferase open reading frame. Image taken from the Merck-Millipore website, product 17-285.

In brief, SW480 cells were seeded in a 96-well plate at 5 x 10^4 cells per well. After the overnight attachment of the cells, they were transfected with pRL-TK (5 ng/well) with either TOPflash or FOPflash plasmids (50 ng/well) and increasing concentrations of the VHH vectors pNAFH-LL3 or pNAFH-AAA (UBC inhouse vector, received from Rabbitts lab, see Figure 6.2 and Appendix D.1) using Lipofectamine 2000 (Thermo Fischer) according to manufacturer's protocol in Gibco™ Opti-MEM™ Reduced Serum medium without P/S. Medium was changed 6-8 hours post-transfection with complete DMEM. Luciferase readings were performed 48 hours post-transfection using the Dual Luciferase Assay kit (Promega, UK) according to the manufacturer's protocol with the following modifications: cells were lysed in 20 µL 1X Passive lysis buffer for 20 min on a rocking platform at 600 rpm. After visual inspection of cell lysis, 12 µL of each well were transferred into a white 96-well plate (Nunc, 436111). Next, 25 µL of LARII reagent and 25 µL of Stop&Glow™ reagents were added to each well using the

automatic injectors of the GloMax®- Multi+ Microplate Multimode Reader (Promega). All Luciferase and Renilla readings were normalised to a blank control and Luciferase values were divided by Renilla readings to adjust for differences in the transfection efficiency.

2.6 RNA methods

2.6.1 RNA extraction

The RNeasy Mini kit (Qiagen, USA) was used according to the manufacturer's instructions to extract the total RNA from cells. All work surfaces were cleaned with RNaseZap (Ambion). Up to 1 x 10^7 cells were washed with PBS and disrupted by the addition of 350 µL Buffer RLT. One volume of 70% ethanol was added to the lysate and mixed by pipetting. Up to 700 µL of the sample was transferred to a RNeasy Mini spin column and centrifuged. All centrifugation steps were performed at 8000 *g* (benchtop centrifuge Eppendorf 5415D) for 30 seconds. Next, 700 µL of Buffer RW1 was added to the RNeasy spin column and centrifuged before the addition of 500 µL of Buffer RPE and another centrifugation. The RPE Buffer step was repeated but centrifuged for 2 min. The RNeasy column was placed in a new 1.5 mL collection tube and centrifuged for 1 min again to remove any residual buffer. The column was placed into an Eppendorf tube and 30-50 µL of RNase-free H_2O was added directly to the spin column membrane. After a 2 min incubation time, the samples were centrifuged for 1 min to elute the total RNA. The quality of the RNA was assessed using a ND-1000 spectrometer (Nano-Drop, USA) and stored at -20°C.

2.6.2 Reverse transcription

The High Capacity cDNA Reverse Transcription Kit (Applied Biosystems Inc. CA) was used to reverse transcribe total RNA to the complementary cDNA according to the manufacturer's instructions. Briefly, 10 µL of diluted RNA (10ng/µl) was mixed with 10 µL of the reverse transcriptase master mix (10x RT buffer, 25x dNTP mix, 10x random primers and reverse transcriptase) in 0.2mL thin wall PCR strip tubes (Corning). The G-STORM GS4 thermal cycler was used with the following protocol: 25°C for 10 min, 37°C for 120 min and 85°C for 5 min, storage at 4°C. The cDNA was quantified and used in further downstream experiments.

2.6.3 Quantitative real-time PCR (qRT-PCR)

Quantitative real-time PCR were performed using the TaqMan® Gene Expression Assay, 20X FAM dye-labelled kit (Applied Biosystems Inc CA). Pre-designed primers and probes for genes of interest were ordered from Life Technologies and validated by the manufacturer (Table 2.4). Briefly, cDNA of the samples of interest from reverse transcription (section 2.6.2) were diluted to 50 ng/µL and 4 µL of the sample was mixed with TaqMan® Gene Expression Assay (20X) probes, TaqMan® Universal PCR Master Mix II (2X) and nuclease-free water to a final volume of 20 µL per well in a MicroAmp Fast Optical 96-well Reaction Plate (Applied Biosystems, Ref 434606). The plates were sealed with MicroAmp Optical Adhesive film (Applied Biosystems, Ref 4311971). The qRT-PCR cycling reaction was performed using a 7500 Fast Real Time PCR System (Applied Biosystems, Ref 4351107). Experiments were performed in triplicate. Cycle threshold (Ct) values of samples were normalised to the house keeping gene *Ubiquitin C* (UBC).

Target	Probe name	Source
CCND1 (CYCLIN-D1)	Hs00765553_m1	Applied Biosystems
CTNNB1	Hs00355045_m1	
C-MYC	Hs00153408_m1	
UBC	Hs00824723_m1	
ASCL2	Hs00270888_s1	
AXIN2	Hs00610344_m1	

Table 2.4 List of 20X TaqMan® Gene Expression Assay Probes
UBC: ubiquitin-C, housekeeping gene.

Both relative (fold change) and comparative (converted ΔCt) qPCR values were calculated. For fold change calculations, the ΔCt of all samples were normalised to the untreated controls within each experiment.

The converted ΔCt (cΔCt) analysis was performed as previously reported (Hsia et al., 2016). The cΔCt method uses the actual ΔCt mean linear values, rather than an arbitrarily identified reference sample as in the ΔΔCt method. In the cΔCt analysis, the ΔCt values were deducted from the highest (arbitrary) ΔCt represented from the same experiment and converted from a logarithmic to a linear scale. The calculations are the following:

1. $\Delta Ct = Ct_{Target} - Ct_{Reference}$
2. The mean ΔCt was calculated for each sample.
3. cΔCt mean value = $2^{(n - \text{mean } \Delta Ct)}$, where n = arbitrary value greater than highest ΔCt mean value.

2.6.4 Microarray gene expression analysis

Out of the 120 colorectal cell lines at the CIL, 95 were microarrayed using the Affymetrix gene Chip Human Genome U133 Plus 2.0 Array (Affymetrix, USA). Details of the RNA submission to the Affymetrix facilities are described in Wilding

et al. (2010). Briefly, 10 µg of RNA from each cell line were sent to the Molecular Biology Core Facility of the Paterson Institute for Cancer Research (UK) for gene-expression microarray analysis containing probes to more than 54612 transcripts.

2.7 DNA methods

2.7.1 DNA quantification

DNA amount and quality were assessed using a Nano-Drop spectrometer. The DNA quality was determined by the ratios of absorbance at 260 nm to 280 nm ($OD_{260/280}$) and a value of 1.8 or greater indicated good quality DNA. Before each measurement, the instrument was blanked using the appropriate sample buffer.

2.7.2 Primer design

All oligonucleotides were purchased in lyophilized form from Life Technologies. They were validated in silico using the National Centre for Biotechnology Information Primer-BLAST tool (https://www.ncbi.nlm.nih.gov/tools/primer-blast/). Primers were resuspended in nucleotide-free H_2O to a stock of 100 µM. Working concentration stocks of 10 µM were prepared and all stored at -20°C.

2.7.3 Primers used in this thesis

Table 2.5 lists the primers used in this work for cloning and sequencing of vectors.

Primer name	Notes	Primer Sequence (5´- 3´)	Restric sites
Domain 1_F	Used to clone D1 bait	TAAGCAGAATTCGCTGAACCATCACAGATG	EcoRI
Domain 1_R		TGCTTAGTCGACTCACATGATAGCGTGTCTG	SalI
Domain 2_F	Used to clone D2 bait	GGGGCAGAATTCAATGTTAAATTCTTGGC	EcoRI
Domain 2_R		TGCTTAGTCGACTCAAGCTTCTACAATAGC	SalI
Domain 3_F	Used to clone D3 bait	GAGCAGAATTCCTTTCTAACCTCACTTGC	EcoRI
Domain 3_R		TGCTTAGTCGACTCAGTGAAGGCGAACTGCATTC	SalI
Domain 4_F	Used to clone D4 bait	GGAGCAGAATTCCACTGGCCTCTGATAAAG	EcoRI
Domain 4_R		TGCTTAGTCGACTTACAGGTCAGTATCAAAC	SalI
BCL9_F	Used to clone BCL9 prey	ATGGCCCAGCCGGCCAGCAATAGCTCTTCAGCAG	SfiI
BCL9_R		AAATATGCGGCCGCATTCTGCTGCGGTCCCC	NotI
TCF4_F	Used to clone TCF4 prey	AATGGCCCAGCCGGCCATGCCGCAGCTGAACGG	SfiI
TCF4_R		AACCATGCGGCCGCTTCTGATTCATTGACTAG	NotI
P300_F	Used to clone p300 prey	ATGGCCCAGCCGGCCACCATGGAGAAGCATAAAG	SfiI
P300_R		AAATATGCGGCCGCTTGAGTCCTGGGCAAGTAG	NotI
pBTM116_seq_F	pBTM116 sequencing	CAGAGCTTCACCATTGAA	-
pBTM116_seq_R		TCAATAAGAGCGACCTCATG	-
pVP16_seq_F	pVP16 sequencing	TTGTTTCTTTTTCTGCACAAT	-
pVP16_seq_R		CAACATGTCCAGATCGAA	-

Primer name	Notes	Primer Sequence (5´- 3´)	Restric sites
VHH_TLCV2_ AgeI_F	Cloning of VHHs into TLCV2 vector	ATCATACCGGTGCCACCATGGCTCAGGTG CAGC	AgeI
VHH-GFP-TLCV2_BamHI_R		ATCATGGATCCTGCGGCCCCATTCAGATC CTC	BamHI
pTLCV2_seq_F	Sequencing of TLCV2 vector	AGAACGTATGTCGAGTTTACTCC	-
pTLCV2_seq_R		TTTACGTCGCCGTCCAGCTCG	-
VHH_BamHI_F	Cloning of VHHs into GST-His-TEV-pGEX and HIS-TEV-Avi-MCS-pRK	TAAGCAGGATCCGGTGGCGGAGGGTCAG GTGGCGGAGGGTCAAAGCTTGCCACCATG GCTCAGG	BamHI
VHH_XmaI_R		TGCTTACCCGGGTCAGAATTCTTACTATGC GGCCCC	XmaI
VHH_EcoRI_R		TGCTTAGAATTCTCATGCGGCCCCATTCAG ATCC	EcoRI
HisTEVAviMCS_s eq_F	HIS-TEV-Avi-MCS-pRK sequencing	AGATATACATATGAGAGG	-
HisTEVAviMCS_s eq_R		CAGCAGCCAACTCAGCTTCC	-
pGEX_seq_F	GST-His-TEV-pGEX sequencing	GGGCTGGCAAGCCACGTTTGGTG	
pGEX_seq_R		AATTGTTATCCGCTGGTACCG	-

Table 2.5 List of primers used in this thesis
All primer sequences are given in 5'- 3' direction. The restriction sites are coloured within the primer sequence.'

2.7.4 Polymerase chain reaction (PCR)

The HT29 CRC cell line cDNA was used as PCR template for the cloning of β-catenin domains of interest. HT29 was selected based on its wild-type β-catenin mutation status. Sequences of interest were amplified using a touch-down (TD) PCR protocol (Table 2.6) with the Phusion® High-Fidelity DNA Polymerase (NEB, UK) according to the manufacturer's protocol on a G-STORM GS4 PCR platform.

Cycling step		Temperature (°C)	Time	Cycles
Initial denaturation		98	1 min	1
TD cycles	Denaturation	98	30 sec	15
	Annealing	68-53°C[a]	1 min	
	Elongation	72	1 min	
PCR cycles	Denaturation	98	30 sec	20
	Annealing	T_m	1 min	
	Elongation	72	1 min	
Final extension		72	10 min	1
Storage		4	Infinite	

Table 2.6 Thermocycler set-up for the Touch-Down PCR reactions
[a]In every TD cycle, the annealing temperature should be decreased by 1°C/cycle.

To assess the correct PCR product band, 5 µL of each PCR product was run on an agarose gel (agarose percentage dependent on product size, see section 2.7.5). The rest of the PCR product was purified using the QIAquick PCR Purification Kit (Qiagen, UK) according to the manufacturer's instructions. The concentration and quality of the DNA were assessed via Nano-Drop Spectrophotometry.

2.7.5 Agarose gel electrophoresis

DNA fragments were analysed by agarose gel electrophoresis. Agarose gels were prepared at a varying percentage (0.8 – 1.5%) by melting electrophoresis-grade agarose (Invitrogen, USA) in 50 mL 1X TAE buffer (Tris base, acetic acid and EDTA, prepared in the in-house facility). Next, 5 µL SYBRSafe™ (Invitrogen, USA) DNA stain was added. The solution was poured into a pre-cast mould to set with the correct sized comb. The solidified gel was placed in a MINI SUB™ DNA CELL electrophoresis unit (Bio-Rad) and the tank was filled with 1X TAE buffer. The DNA samples were mixed with 6X purple loading buffer (New England Biolabs (NEB), UK) and loaded into the wells alongside an appropriate DNA ladder (all ladders

from NEB, UK). Samples were run for 45-50 min at 85 Volt (V). Gels were visualised using a Fusion Fx gel imager (Vilber) using the Fusion Capt Advance Fx7 software.

2.7.6 DNA purification from agarose gel

DNA fragments resolved on the agarose gel and needed for further downstream applications were purified using the QIAquick Gel Extraction kit (Qiagen, UK) following the manufacturer's instructions. The gel was placed on an UV light (Transilluminator LM-26E, Alpha Innotech) and the DNA fragment was excised from it using a clean scalpel. The weight of the gel piece was measured. Three volumes of Buffer PB were added to one volume of the gel and placed in a 50°C water bath until the gel was fully melted. One gel volume of isopropanol (Fischer Scientific, UK) was added to the sample and mixed well. The sample was loaded on a QIAquick spin column and centrifuged at maximum speed (≥16000 g) for 1 min. The column was washed with 500 µL of Buffer QG and centrifuged for 1 min. Next, 750 µL of Buffer PE was used for a further washing step and centrifuged for 1 min. The QIAquick spin column was centrifuged another time for 1 min to remove the residual buffer and the column was transferred into a new Eppendorf tube. 20-30 µL of Buffer EB was used to elute the membrane bound DNA. The column was incubated for 5 min with the Buffer EB before centrifugation at maximum speed for 1 min. The quality and concentration of the DNA was analysed via Nano-Drop spectrometry. The samples were stored at -20°C.

2.8 Cloning methods

All restriction enzymes (REs) and buffers were obtained from New England Biologicals (NEB), UK unless otherwise stated. All double digest protocols can be obtained from https://www.neb.com/tools-and-resources/interactive-tools/double-digest-finder

2.8.1 List of vector backbones

Table 2.7 gives an overview of the vector backbones used in this thesis. Vector maps can be found in the indicated Figures and Appendix sections.

Vector name	Selection	Restriction sites used	Source	Notes and Vector map figure
pBTM116	CAM	EcoRI/SalI	Prof. Rabbitts Lab	Bait vector for IAC system (Figure 5.4)
pVP16	AMP	SfiI/NotI	Prof. Rabbitts Lab	Prey vector for IAC (Figure 5.6)
pNAFH-LL3	KAN	HindIII/EcoRI	Prof. Rabbitts Lab	UCB in-house vector (Figure 6.2)
pNAFH-AAA	KAN	HindIII/EcoRI	Prof. Rabbitts Lab	UCB in-house vector (Figure 6.2)
pNAFH-control	KAN	HindIII/EcoRI	Produced by cloning out LL3 from pNAFH-LL3 vector	Used as control for transfections
GST-His-TEV-pGEX	AMP	BamHI/XmaI	Prof. Rabbitts Lab	Protein expression vector (Appendix D.8)
HIS-TEV-Avi-MCS-pRK	AMP	BamHI/EcoRI	Prof. Rabbitts Lab	Protein expression vector (Appendix D.10)
TLCV2	AMP	AgeI/BamHI	Dr. Ryan Beveridge, Lentiviral Facility, WIMM	Addgene plasmid #87360 (Figure 6.6)

Table 2.7 List of vector backbones
Table provides information on the bacterial selection of the vectors, the restriction sites used for cloning, and the source of the vector. IAC: Intracellular Antibody Capture, see section 2.10.1. UCB: UCB Pharma, CAM: Chloramphenicol, KAN: Kanamycin, AMP: Ampicillin, MCS: Multiple Cloning Site.

2.8.2 Restriction digests

Vector backbones and PCR products of domains of interest were each digested using the restriction enzymes indicated in Table 2.7. With the exception of the SfiI digest, all digests were performed at 37°C for 1 hour. SfiI digests were performed at 50°C overnight. The REs were inactivated at 65°C for 10 min. The linearised backbone vector was run on a 1% ultra-pure agarose gel and purified the QIAquick Gel Extraction Kit (Qiagen, UK). The heat-inactivated digested PCR product was then ligated with the vector backbone as described in section 2.8.3.

2.8.3 Ligations

T4 Ligase was used according to the manufacturer's instructions. Restriction digested vector and insert DNA concentrations needed for the ligations were calculated using the online NEB Cloning calculator (https://nebiocalculator.neb.com/#!/ligation). The 20 µL reaction set-up is found in Table 2.8. Ligation were performed overnight at 4°C or for 1 hour at RT before heat inactivation at 65°C for 10min.

	20 µL reaction
Vector backbone	200 ng
Insert	variable
Buffer 10X	2 µL
T4 Ligase	1 µL
H_2O	Up to 20 µL

Table 2.8 T4 Ligase reaction set-up
The amount of the restriction digested DNA insert was dependent on the insert size.

2.8.4 Preparation of competent DH5α *E.coli*

Competent *DH5α* were produced from Subcloning efficient DH5α™ competent cells (Invitrogen, UK). Subcloning efficient DH5α™ competent cells were streaked onto a Lysogeny broth (LB) plate and incubated overnight at 37°C. Single colonies were inoculated in 5 mL super optimal broth (SOC) medium and grown overnight at 37°C, 225 rpm shaking (Incubator Shaker, Innova®44, New Brunswick Scientific). Seed stocks were prepared by mixing 800 µL of the culture and 300 µL 70% glycerol. Seed stocks were stored at -80°C. To prepare competent cells, 1 mL from the overnight culture was inoculated in 100 mL LB medium and grown at 37°C until an OD_{600} of 0.4. The culture was centrifuged at 1800 *g* (J6-M1 centrifuge, Beckman Coulter, JS-4.2 rotor) at 4°C for 10 min. The supernatant was discarded, and cells were carefully resuspended in 30 mL CCMB80 buffer (10 mL 1 M potassium acetate at pH7, 880 mg $CaCl_2$, 400 mg $MnCl_2.4H_2O$, 200 mg $MgCl_2.6H_20$, 10 mL glycerol, filled up to 100 mL and pH adjusted to 6.4). The suspension was incubated for 20 min on ice and centrifuged again at 4°C for 10 min. The pellet was resuspended in 5 mL of the ice cold CCMB80 buffer and 500 µL aliquots were stored at -80°C.

2.8.5 Transformation of *E.Coli*

DH5α competent cells were thawed on ice. Fifty µL of DH5α were added to pre-chilled Eppendorf tubes containing 200 ng of DNA plasmids to be transformed into *E.Coli*. If a ligation product was to be transformed, 10 µL of the ligation product was added to the Eppendorf and 100 µL of competent DH5α. The cells were mixed well by flicking the tube and incubated on ice for 20 min. Afterwards, the cells were heat shocked for 1 min in a water bath at 42°C and immediately placed on ice for

2 min. The tubes were filled with 290 µL of SOC medium and incubated for 1 hour at 37°C at 220 rpm. One hundred µL of the sample was then plated on selective agar plates and incubated overnight at 37°C.

2.8.6 Antibiotic stock concentrations for selections

Bacterial colonies were grown in LB growth medium with the appropriate antibiotics for selection. Table 2.9 lists the antibiotic stock concentrations.

Antibiotic	Stock concentration (mg/mL)	Working concentration (µg/mL)
Ampicillin	100	100
Chloramphenicol	35	35
Kanamycin	100	100

Table 2.9 Antibiotic selection concentrations
All antibiotic stocks were aliquoted and stored at -20°C. Ampicillin and Kanamycin were dissolved in H_2O, while Chloramphenicol was dissolved in ethanol.

2.8.7 Plasmid DNA extraction from *E.Coli*

Plasmid DNA was extracted and purified from single colonies using a MiniPrep kit (Qiagen, UK) according to the manufacturer's instructions. Briefly, a single transformed *E.Coli* colony was picked from a selective plate and inoculated in 5 mL antibiotic selective LB broth overnight at 37°C. The bacterial culture was pelleted by centrifugation at 3000 *g* (Avanti series centrifuge, Beckman Coulter, JA-12 rotor) for 3 min at RT. Cells were resuspended in 250 µL cold P1 buffer and transferred to an Eppendorf tube. Next, 250 µL P2 buffer were added and the tube was inverted 4-6 times. Cells were incubated for up to 5 min at RT for cell lysis to occur. To stop the lysis, 350 µL of N3 buffer were added and the tube inverted 6 times. Samples were centrifuged at 16000 *g* for 10 min at RT in a table-top

microcentrifuge. Up to 800 µL of the supernatant was applied to a QIAprep 2.0 spin column and centrifuged for 1 min. The column was washed with 500 µL PB buffer and centrifuged again for 1 min. 750 µL of PE buffer was added to the column and centrifuged for 1 min. The column was then centrifuged again for 1 min to remove the residual wash buffer. The column was placed into a new Eppendorf tube and 50 µL EB buffer was incubated for 5 min before centrifugation for 1 min to elute the DNA. The DNA concentration and quality were assessed by Nano-Drop Spectrophotometry. The DNA plasmids were sent for Sanger Sequencing to confirm the correct vector sequence.

If large amounts of DNA vectors were required, the Endo-Free MaxiPrep Kit (Qiagen, UK) was used, following the manufacturer's instructions.

2.8.8 Sanger Sequencing

DNA was given for sequencing analysis to the in-house DNA Sequencing Core Facility at the WIMM. Sequencing primers are provided in Table 2.5. Sequences were analysed and visualised using the MacVector Software.

2.9 Protein methods

2.9.1 Preparation of whole cell protein lysates from cell lines

Cells were grown in 6-well plates or 10 cm cell culture dishes until 80% confluent. Plates were placed on ice and cells were washed with ice-cold PBS to remove any leftover medium. Cells were scraped using a cell scraper in a small amount of PBS and transferred to 15 mL Falcon tube. Cells were pelleted by centrifugation at 160 *g* for 5 min and the supernatant was removed. The cell pellet was lysed in 100-400 µL RIPA buffer (150 mM NaCl, 1% NP40, 0.5% sodium deoxycholate,

0.1% SDS, 50mM Tris-HCl pH8, 2 mM EDTA). Samples were incubated on ice for 30 min, briefly vortexing every 10 min. Cell lysates were then centrifuged at 20000 *g* (Eppendorf, Centrifuge 5417R) for 20 min at 4°C to pellet the cell debris. The total cell lysate in the supernatant was collected, transferred into a new Eppendorf tube and stored at -20°C.

2.9.2 Preparation of cytoplasmic and nuclear protein lysates from cell lines

Cells were grown in 6-well plates and treated with the desired compounds. When cells were 80-90% confluent, they were washed with PBS once and trypsinised. Cells were collected in a 15 mL falcon tube and centrifuged for 3 min at 160 *g*. The supernatant was removed, and the cell pellet was washed with PBS once more. Cells were transferred in a 1.5 mL Eppendorf tube and centrifuged at 500 *g* for 3 min. The supernatant was removed to leave the cell pellet as dry as possible. The NE-PER™ extraction kit (Pierce Biotechnology) was used to extract the cytoplasmic and nuclear protein fractions according to the manufacturer's protocol. In brief, the cell pellet was re-suspended in 100 µL ice-cold CER I solution, vortexed for 15 sec and incubated on ice for 10 min. Next, 5.5 µL of CER II was added, vortexed for 15 sec and incubated on ice for 1 min. Samples were then centrifuged at top speed (20000 *g*) at 4°C for 5 min. The supernatant (cytoplasmic protein fraction) was transferred into a new chilled Eppendorf tube and the cell pellet was left as dry as possible, before re-suspending the pellet in 50 µL NER solution. The samples were vortexed for 15 sec and incubated on ice for 40 min. Every 10 min the samples were vortexed. The nuclear protein fraction was obtained by centrifuging the samples at top speed at 4°C for 10 min and

transferring the supernatant into a new chilled Eppendorf tube. Both cytoplasmic and nuclear protein samples were stored at -20°C until further use.

2.9.3 Bicinchoninic acid (BCA) assay

The quantification of the protein extracted from cell lines was performed using the bicinchroninic acid colorimetric assay, BCA™ Protein Assay (Pierce, USA). This methodology is based on the Biuret reaction, which is the reduction of Cu+2 to Cu+1 by a protein in an alkaline medium. Cu+1 can be detected colometrically when in combination with bicinchoninic acid (BCA) and forms a purple colour.

Protein standards ranging from 0-2000 µg/mL were prepared from the supplied Albumin Standard ampoule (2 mg/mL). The BCA™ working reagent was prepared by mixing 50 parts of BCA™ solution A with 1 part of BCA™ solution B. Twenty-five µL of the protein samples of unknown concentration and standards in duplicates were added to a 96-well plate. Two hundred µL of the working reagent was added to each standard or sample well. The plate was wrapped in foil and incubated at 37°C for 30 min. The plate was read at an absorbance of 562 nm on a plate reader (µQuant, Bio-Tek Instrument, USA). The blank standard measurement was subtracted from all measurements and a standard curve was plotted using the average standard measurement vs. its concentration in µg/mL. The standard curve was used to determine the concentration of each unknown sample.

2.9.4 Preparation of protein lysates from yeast cells

The yeast protein extraction was followed as described by Matsuo et al. (2006). A single yeast clone was inoculated in 5 mL of the appropriate selective medium overnight at 37°C and 220 rpm. The next day, yeast was diluted to an OD_{600} of

0.25 in 10 mL selective medium and grown until an OD_{600} of 0.4-0.6. The culture was centrifuged at 3000 *g* for 5 min, washed with 1 mL distilled water (dH_2O) and transferred into a clean 1.5 mL Eppendorf tube. Cells were centrifuged at 3000 *g* for 5 min and first re-suspended in 0.3 mL dH_2O. An equal amount of 0.6 M NaOH was added and incubated for 10 min at room temperature. This two-step suspension is important because direct suspension of cells in 0.3 M NaOH causes inefficient extraction (Matsuo et al., 2006). Cells were collected by centrifugation and the supernatant was carefully removed. Next, 70 µL of sodium dodecyl sulfate (SDS)-sample buffer (60 mM Tris-HCL, pH 6.8, 4% β-mercaptoethanol, 4% SDS, 0.01% bromophenol blue, 5% glycerol) was used to re-suspend the sample. After boiling at 95°C for 3 min, samples were stored at -20°C.

2.9.5 Western Blotting

2.9.5.1 SDS poly-acrylamide gel electrophoresis

SDS-gel concentration ranged from 10-15% depending on the size of the protein of interest. Protein samples were boiled for 5 min in 5x SDS sample buffer (3.12 mL of 2 M Tris HCl (pH 6.8), 5 mL β-mercaptoethanol, 1.88 mL milliQ H_2O, 10 mL glycerol, 2 g SDS and a small amount of bromophenol blue) and briefly centrifuged.

About 15-20 µL of the yeast protein extract or 30 µg of cell protein lysate per lane were run in a Mini-PROTEAN®-II vertical electrophoresis unit (Bio-Rad, UK) in 1X Running Buffer (1 L of 10X Running Buffer: 250 mM Tris base, 192 mM glycine, 1% SDS, adjusted to pH 8.3). Proteins were loaded into the stacking gel wells along with a molecular weight marker and run at 80 V until the proteins reached

the separating gel. Proteins were then resolved at 120 V until good protein separation was reached.

2.9.5.2 Immunoblotting

The proteins from the SDS poly-acrylamide gel electrophoresis were transferred to a polyvinylidene difluoride (PVDF) membrane (Amersham Biosciences, USA) using a semi-dry transfer machine (TE 77, Amersham Bioscience). The PVDF membrane was first soaked in 100% methanol and washed in transfer buffer (100 mL methanol, 7.2 g glycine, 12.5 mL 1 M Tris at pH 7.5, fill up to 500 mL with MilliQ H_2O). The membrane was placed on three transfer buffer soaked Whatman papers and the SDS gel was placed on top, followed by another three Whatman filter papers. The transfer was run for 1 hour at RT at 20 V. After the transfer, the proteins on the membranes were visualized using Ponceau Red Stain (0.1% Ponceau S (Sigma) in 5% glacial acetic acid) for 10 min on a rocking platform. The membrane was rinsed with MilliQ water before being blocked using 5% semi-skimmed milk (prepared in Tris-buffered saline (TBS) with 1% Tween-20 (TBS-T)) for 1 hour on a rocking platform at RT. The membrane was then incubated with the primary antibody of interest at appropriate dilution overnight at 4 °C. After three 10 min washes with TBS-T, the membrane was incubated with the appropriate secondary antibody for 1 hour at RT on a rocking platform. The membrane was washed again for three times 10 min with TBS-T and finally incubated with Clarity™ Western ECL Substrate (Bio-Rad) or ECL Prime Western Blotting Detection System solution (GE Healthcare, UK) for 5 min. The blot was then imaged using light-sensitive films (SuperRX-N, Fuji Medical X-Ray Film, Fujifilm) and developed in a dark room using the ECOMAX X-Ray Film Processor (Protec-Med).

2.9.6 Antibodies used for Western Blotting

All antibody dilutions for WB were prepared in 5% semi-skimmed milk in TBS-T.

Table 2.10 lists the antibody used for Western Blotting in this thesis.

1° mAb	Species	Source and catalogue number	Dilution	2° pAb	Source	Dilution for WB
Anti-LexA	mouse	SantaCruz, sc-7544	1:500	GAM	Dako	1:10000
Anti-VP16	mouse	SantaCruz Sc-7545	1:500	GAM	Dako	1:10000
α-tubulin (DM1A)	mouse	Abcam ab7291	1:2000	GAM	Dako	1:10000
β-catenin	mouse	BD Bioscience 610154, Clone 14	1:8000	GAM	Dako	1:10000
Cyclin D1 (pAb)	rabbit	NeoMarkers RB-0-10-P0	1:300	SAR	Dako	1:10000
c-myc (9E10.3)	mouse	NeoMarkers MS-139-P0	1:500	GAM	Dako	1:10000
Axin2 (76G6)	rabbit	Cell Signaling #2151S	1:1000	SAR	Dako	1:10000
Lamin A/C (4C11)	mouse	Cell Signaling #4777S	1:2000	GAM	Dako	1:10000
β-actin (AC-15)	mouse	Sigma A5441	1:4000	GAM	Dako	1:10000
β-tubulin (TUB 2.1)	mouse	Sigma T5201	1:6000	GAM	Dako	1:10000
c-myc tag (9B11)	mouse	Cell Signaling #2276	1:4000	GAM	Dako	1:10000
GFP	mouse	SantaCruz Sc9996	1:500	GAM	Dako	1:10000
GST (pAb)	rabbit	Sigma G7781	1:6000	SAR	Dako	1:10000
HIS-tag HRP	mouse	Sigma A7098	1:5000	n/a	n/a	n/a

Table 2.10 List of antibodies used for Western Blotting
GFP: Green-fluorescent protein, GST: Glutathione-S-Transferase, GAM: Goat-anti mouse, SAR: Swine anti-rabbit.

2.9.7 Immunoprecipitation of whole-cell lysates

Dynabeads® protein G (Invitrogen, UK) were used to perform immunoprecipitations. Cells were grown and treated appropriately in 10 cm dishes. Protein lysates were prepared using a Nonidet-P40 (NP40) lysis buffer (150 mM NaCl, 1% NP40, 50 mM Tris-HCl pH 8, 1 mM EDTA, add protease inhibitor tablets (Roche) before use). Cells were briefly washed in ice-cold PBS before being scraped off and transferred into an ice-cold 15 mL falcon tube. Cells were centrifuged at 160 *g* for 3 min and PBS was removed. Cells were re-suspended in 1 mL NP40 lysis buffer, transferred into a new 1.5 mL Eppendorf tube and incubated on ice for 30 min. Samples were then centrifuged at 20,000 g for 20 min at 4°C and supernatant containing soluble proteins was collected. The protein concentration of samples was measured using the BCA assay. Samples were pre-cleared with 10 µL of Dynabeads® for 25 min at 4°C on a rotor. Lysates were separated from magnetic beads using a magnetic rack. 500 µg of the pre-cleared lysates were then incubated with the antibody of interest (1:1000) or an IgG control overnight at 4°C on a rotor in a total volume of 600 µL NP40 lysis buffer. Input controls (5%) were taken before the addition of the antibodies. After the overnight incubation on a rotor at 4°C, 30 µL of Dynabeads® were added to the antibody-antigen lysate and incubated for 4 hours at 4°C. The magnetic beads were carefully separated from the lysates using the magnetic rack and the supernatant was removed. The beads were washed 3 times using with 0.8 mL of NP40 lysis buffer. The beads were transferred to a new Eppendorf tube for the last wash to avoid unspecific protein contamination. Proteins were eluted from the beads using 30 µL of 5X SDS loading buffer and boiling at 90°C for 5min. Samples were then stored at -20°C until further use.

2.9.8 Recombinant protein expression and purifications

Sequences of interest were cloned into expression vectors (Table 2.7) and cloned into OverExpress^{TM} C41 (DE3) chemically competent cells (Sigma Aldrich, kind gift from Dr Ami Miller, Rabbitts Lab), as previously described. A single clone was inoculated overnight in 50 mL LB + antibiotic at 30°C, 225 rpm. The next day, 1 L of LB + antibiotic was inoculated with 10 mL of the overnight culture and grown until OD_{600} of 0.8. A 3 mL "uninduced" sample was taken and the pellet resuspended in 200 µL H_2O. The bacterial culture was induced with 0.8 mM Isopropyl β-D-1-thiogalactopyranoside (IPTG, Sigma) and grown at 16°C overnight, 225 rpm. The next day, a 3 mL "induced" sample was collected and the pellet re-suspended in 200 µL H_2O. A further 3 mL sample was collected, re-suspended in 500 µL H_2O, sonicated 6 x 6 sec on/off (Soniprep 150 Plus, MSE) and centrifuged at maximum speed for 25 min at 4°C. The supernatant (soluble fraction) was collected, while a fraction of the pellet (insoluble) was re-suspended in 200 µL H_2O. The rest of the 1 L culture was collected at 4°C, 1800 *g* for 10 min and the pellet was stored at -80°C overnight to aid lysis.

The bacterial cell pellets were re-suspended in 20 mL lysis buffer supplemented with protease inhibitors and lysozymes (Table 2.11A). The samples were sonicated 8 x 6 sec on/off on ice. DNAaseI (Thermo Scientific, #90083) was added and carefully mixed. The samples were centrifuged at 14000 *g* for 90 min at 4°C. Depending on the affinity tag on the recombinant protein to be purified, the purification methods differ and are described in sections 2.9.8.1 and 2.9.8.2.

Table A - Lysis buffer	GST- tagged proteins	HIS - tagged protein
Tris-HCl, pH 7.4	20 mM	20 mM
NaCl	200 mM	300 mM
Glycerol	5%	5%
Imidazole	-	20 mM
Lysozymes	100 µg/mL	100 µg/mL
Protease inhibitors (tablets)	+	+

Table B – Binding and wash buffer	GST- tagged proteins	HIS - tagged protein
Tris-HCl, pH 7.4	20 mM	20 mM
NaCl	200 mM	300 mM
Glycerol	5%	5%
Imidazole	-	30 mM
Protease inhibitors (tablets)	+	+

Table 2.11 Composition of lysis, binding and washing buffers for protein purification
Table A – lysis buffers for GST- and HIS-tagged proteins. Table B – binding and wash buffers for GST- and HIS-tagged proteins. Protease inhibitor tablets (cOmplete, EDTA-free, Roche, one tablet per 10 mL) were used according to manufactures' instructions. Lysozymes from Thermo Scientific (#90082).

2.9.8.1 GST-tag protein purification

For GST-tagged protein purifications, 1 mL of 4B Sepharose beads (GE Healthcare) were washed with PBS twice and pre-equilibrated in binding buffer (Table 2.11B). The separated soluble fraction (section 2.9.8) was incubated with the 4B Sepharose beads at 4°C, for 4 hours, rotating. Next, the sample was poured into a Poly-Prep® chromatography column (Bio-Rad, #731-1550) and the flow-through was collected. The beads were washed twice with 10 mL binding buffer at 4°C, collecting the flow-through of the washes each time for later gel analysis. The protein was eluted from the beads using 500 µL GST elution buffer

(10 mM reduced glutathione (Serva, 23150.02) in 50 mM Tris-HCl, pH 8), for 10 min at RT. The elution step was repeated 3 times and eluates were collected in separate Eppendorf tubes. Elution samples were run on an SDS gel, alongside fractions from the uninduced, induced, insoluble, soluble, flow-through and wash samples to assess the protein purification results. The gel was stained for proteins using the Coomassie stain (see section 2.9.8.3). Protein concentrations (A280) were measured using a Nano-Drop.

2.9.8.2 HIS-tag protein purification

HIS-tagged proteins were purified as described in section 2.9.8.1, with the following modifications: 1 mL Ni-NTA resin (Thermo Fischer Scientific) was used, twice washed with PBS according to manufactures' instructions and pre-equilibrated in binding buffer (Table 2.11B). The elution from the beads was performed using HIS elution buffer (20 mM Tris-HCl, pH 7.4, 300 mM NaCl, 5% glycerol, 250 mM imidazole) for 10 min at RT.

2.9.8.3 Coomassie stain

After separation of the proteins by gel electrophoresis, the gel was briefly rinsed using milliQ H_2O. The gel was then incubated on a shaker for 20 min with a fixation and de-stain solution (50% methanol, 40% milliQ H_2O, 10% acetic acid), before incubating with the Coomassie stain (50% methanol, 10% acetic acid, 0.25% Brilliant Blue R-250) for at least one hour. The gel was de-stained by 4x 20 min washes on a shaker using the fixation solution (approx. 25 mL to cover the gel). Alternatively, the Pierce® Silver Stain kit (Thermo Scientific) was used to stain the gel, according to the manufactures' instructions.

2.9.8.4 TEV digests

Recombinant proteins including the Tobacco Etch Virus (TEV) sequence E-X-X-Y-X-Q-G/S were cleaved using TEV protease (kind gift from Dr Ami Miller, Rabbitts lab), if required. TEV protease was added 1:1000 to the protein of interest overnight at 4°C, rotating. The protein cleavage was confirmed on a SDS acrylamide gel by Coomassie staining.

2.9.8.5 Protein purification using ÄKTA purification system

An ÄKTA pure chromatography system (GE Healthcare) was used to purify the proteins of interest (removal of glutathione, imidazole, TEV protease). The purifications were kindly performed by Dr Abimael Cruz Migoni and Mr Andres Hueso Cuervo at the WIMM. Proteins were purified using a Superdex75 10/300 column (GE Healthcare) and fractions of interest were analysed on a SDS acrylamide gel and Coomassie stain. Proteins were aliquoted and stored at -80°C.

2.9.9 Pulldown assays with purified proteins

2.9.9.1 Myc-tag pulldown

Proteins of interest (5 µg) were mixed and a 5% input control was taken. Protein mixtures were incubated in 500 µL binding buffer (20 mM Tris-HCl pH 8, 300 mM NaCl, 5% glycerol) with myc-tag antibody (Cell Signaling, 1:1000), overnight at 4°C, rotating. The next day, 20 µL pre-equilibrated Dynabeads Protein G were added to each sample for 1.5 hours at 4°C, rotating. Beads were separated from the solution using a magnet and washed 3 times with 700 µL binding buffer. The beads were transferred into a new Eppendorf tube for the last wash. Proteins were eluted off the beads using 30 µL 5X SDS sample buffer and boiled at 95°C for 5 min. Pulldown results were analysed by Western Blot.

2.9.9.2 HIS-tag pulldown

Dynabeads™ His-Tag Isolation and Pulldown beads (Thermo Fischer Scientific) were used for HIS-tag pulldowns. Proteins of interest (10 µg each) were mixed and a 5% input control was taken. Mixtures were incubated in a final volume of 500 µL binding buffer (20 mM Tris-HCL, pH7.4, 300 mM NaCl, 20 mM imidazole, 5% glycerol) for 1 hour at 4°C, rotating. His-Tag Dynabeads™ beads were washed and pre-equilibrated in binding buffer and 20 µL beads were added to the protein mixtures for 20 min, 4°C, rotating. Beads were separated from the mixture using magnets and washed 3x 1 mL with binding buffer. Proteins were eluted from the beads using 30 µL HIS elution buffer (20 mM Tris-HCl, pH 7.4, 300 mM NaCl, 5% glycerol, 250 mM imidazole) for 10 min at RT.

2.10 Yeast methods

2.10.1 Intracellular Antibody Capture

The Intracellular Antibody Capture (IAC) is an adapted Yeast-two-Hybrid (Y2H) screen used to generate single-domain antibody fragments (VH). The protocol used was published by Tanaka and Rabbitts, 2010. The VH single domain antibody library was obtained by Professor Terence Rabbitts, Molecular Heamatology Unit at the WIMM, Oxford, UK. Please refer to Chapter 5 for a more detailed background. A general workflow of the protocol is given in Figure 2.2.

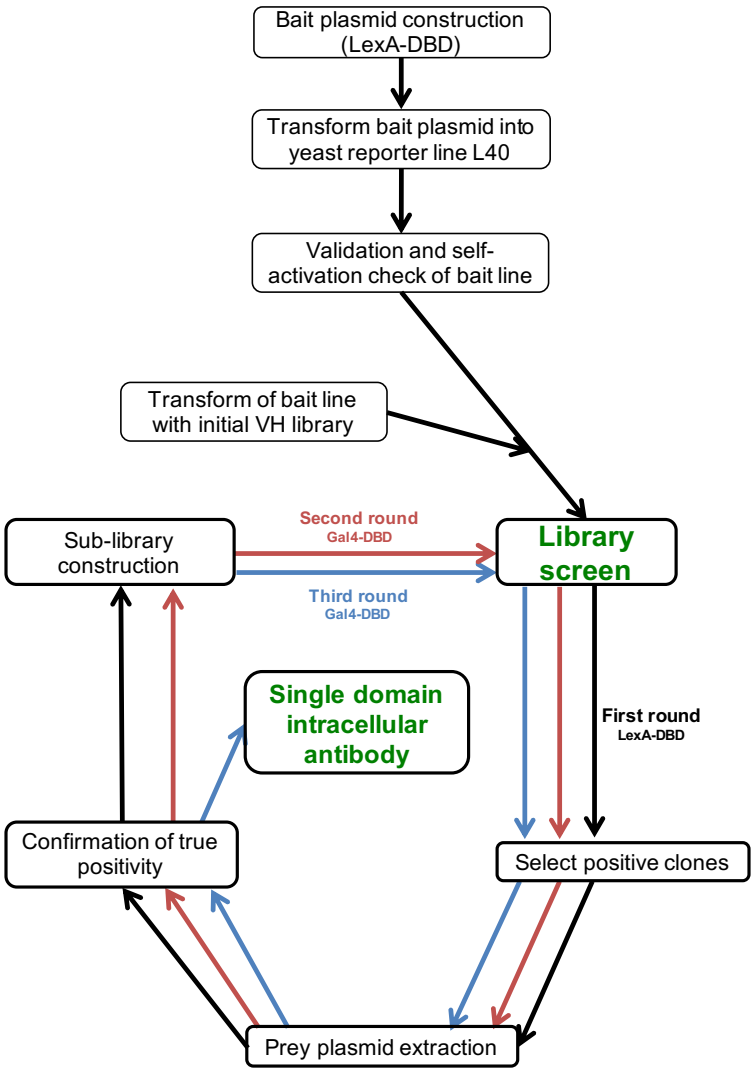


Figure 2.2 Overview of IAC workflow
The yeast-2-hybrid methodology is sub-divided in three separate library screen rounds to allow for single-domain antibody affinity maturation. Gal4-DBD: alternative DBD used in second and third round of screening.

2.10.2 Preparation of yeast media

All the amino acids (AA) were purchased from MP Biologicals unless otherwise stated.

20% glucose solution (wt/vol): 100 g of D-glucose (Scientific Laboratory Supplies) were dissolved in 500 mL dH_2O and passed through a 0.2 micrometre (µm) filter system (Corning). Solution was stored at RT for up to 3 months.

Yeast Extract-Peptone-Dextrose (YPD) medium – 50 g of YPD broth (Fischer BioReagents, UK) was dissolved in 1 L of dH_2O. The solution was autoclaved and stored at RT for 1 month. Before use, 1X adenine hemisulfate was added to make YAPD medium.

YPD agar – 10 g of yeast extract (Sigma), 20 g of peptone (BD Bioscience) and 20 g of agar (BD Bioscience) were dissolved in 900 mL of dH_2O and autoclaved. Before pouring YPD plates, 100 mL 20% glucose solution *and 1X* adenine hemisulfate were added.

5x Yeast complete (YC) medium without amino acids (5x YC w/o AA) - 2.4 g of yeast nitrogen base lacking amino acids and ammonium sulphate (Appleton Woods), 10 g of ammonium sulphate (Fisons Scientific Equipment), 20 g of succinic acid (Acros Organics), 0.1 g of tyrosine (Sigma) and 12 g of NaOH (Sigma) were dissolved in 400 mL dH_2O. The pH was adjusted to 7.0 by adding more NaOH pellets. The solution was autoclaved and stored at RT.

Amino acid supplements mix minus 7 dropout (AA mix-7) – Prepared as a 100X stock solution. One g of phenylalanine, 1 g of isoleucine (Sigma), 2 g of arginine, 1 g of valine, 1 g of aspartic acid, 1 g of proline, 1 g of serine and 2 g of threonine were dissolved in 200 mL of dH_2O. The solution was sterile filtered (0.2 µm), aliquoted in 50 mL falcon tubes and stored at 4°C for up to 6 months.

Amino acid (AA) and nucleoside supplements – All AA and nucleoside stocks were made as 100X solutions, except for uracil, which is made as a 10X solution. Either 2 g of tryptophan (abbreviated as W, Sigma), 2 g of lysine (Sigma), 1 g of methionine, 2 g of adenine, 1 g of histidine (abbreviated as H) or 2 g of leucine (abbreviated as L) were each dissolved in 200 mL of dH_2O. The solutions were

sterile filtered, aliquoted and stored at 4°C for up to 6 months. For the uracil stock, 1 g of uracil was dissolved in 1 L of dH_2O, sterile filtered, aliquoted and stored at 4°C.

2 M 3-amino-1,2,4-triazole (3-AT) – 168.2 g of 3-AT (MP Biological) were measured in a fume hood and dissolved in 1 L of dH_2O, 0.2 µm sterile filtered and stored at 4°C for up to 6 months.

YC dropout medium – 20 mL of 5xYC w/o AA, 10 mL of 20% glucose solution, 1 mL of AA mix-7, 1 mL of each 100x amino acid supplement (except uracil) and 10 mL of 10x uracil were mixed. The amino acid supplement of interest to make selective dropout medium was omitted. Autoclaved dH_2O was added to make 100 mL and stored at RT for up to 1 month.

YC dropout plates – 20 g of agar were dissolved in 200 mL 5x YC w/o AA and 400 mL of dH_2O and autoclaved. The agar was cooled down to 55°C in a water bath. Amino acid supplement, glucose and 3-AT (when needed) where then added to the agar in the appropriate concentrations based on the number of plates and plate sizes needed (Table 2.12). Plates were poured in a hood and plates were dried with open lids for at least 30 min. Large square plates for the IAC screen were purchased from Thermo Scientific.

	9 cm round dish	Large square plate (25 x 25 cm)
20% glucose solution	2.5 mL	25 mL
AA - 7mix & AA supplements (except uracil)	250 µL	2.5 mL
Uracil	2.5 mL	25 mL
3-AT	When required	When required
Agar	Up to 2 5mL	Up to 250 mL

Table 2.12 Composition of selective YC dropout plates

2.10.3 Preparation of solutions for yeast transformations

20 mg/mL salmon sperm DNA stock - 0.25 g of salmon sperm DNA (AppliChem, A2159,0001) was dissolved in 12.5 mL of 1X TE using a magnetic stirrer at 4°C overnight. Aliquots (1 mL) were prepared and stored at -20°C. Before use, the salmon sperm DNA was boiled at 95°C for 10 min and immediately placed on ice.

50% PEG solution (wt/vol) – 250 g of PEG3350 (Sigma) was dissolved in 500 mL of dH_2O and passed through a 0.2 µm filter. The solution was stored at RT for up to 3 months.

1 M Lithium Acetate (LiAc) solution – 12.25 g of LiAc (Sigma) was dissolved in 100 mL of dH_2O. The pH was adjusted to 7.5 with glacial acetic acid and the final volume was adjusted to 125 mL. The solution was autoclaved and stored at RT for up to 3 months.

10X TE – 1.21 g of Tris base (Fisher Scientific) and 0.37 g of EDTA (Sigma) were dissolved in 90 mL of dH_2O, adjusted to pH 7.5 with concentrated HCl and finally adjusted to the final volume of 100 mL. The solution was autoclaved and stored at RT.

TE-LiAc solution – The solution was prepared fresh before each use. Ten mL of 1 M LiAc, 10 mL of 10X TE and 80 mL of dH_2O were mixed.

LiAc-TE-PEG solution – 10 mL 1 M LiAc, 10mL of 10X TE and 80 mL of 50% PEG solution were mixed freshly each time before use.

2.10.4 Construction and characterization of the bait vectors

2.10.4.1 Construction of baits and positive control preys

All vectors for the IAC methodology were obtained from the Rabbitts Laboratory and summarised in Table 2.7.

Antigen domains of interest were cloned as in-frame fusion with the LexA DNA-binding domain (DBD) in the pBTM116 vector (Figure 5.4, Chapter 5) using the EcoRI/SalI restriction sites. The positive control sequences of interaction partners were cloned in-frame with the VP16 – activation domain (AD) of the pVP16* vector (Figure 5.6, Chapter 5) using the SfiI/NotI restriction sites to replace the VH antibody domain.

2.10.5 Yeast transformation with bait vectors

The L40 yeast strain (*MATa, leu2-3,112, his3Δ200, trp1Δ1, ade2, LYS2 (LexA-op)$_4$-HIS3, URA3(LexA-op)$_8$-lacZ*) was obtained from the Rabbitts laboratory. A single L40 colony was inoculated in 2 mL YAPD medium (contains 0.01% adenine hemisulfate) and incubated overnight at 30°C in a shaking incubator at 220 rpm.

The following day, the yeast culture was diluted in 15 mL YAPD to a starting point of OD_{600} 0.2-0.3. The culture was grown at 30°C and 225 rpm until the culture

reached an OD_{600} 0.5-0.6. Transformation efficiencies are reduced if yeast cultures grow above a density of OD_{600} = 0.6. The culture was pelleted by centrifugation at 1000 *g* for 5 min at RT. The supernatant was removed, and the pellet resuspended in 10 mL dH_2O. Cells were centrifuged again for 5 min at 1000 *g* and the yeast pellet was resuspended in 1 mL freshly made TE-LiAc. The competent yeast cells were kept on ice for no longer than 1 hour.

Two hundred ng of bait plasmid and 100 µg of salmon sperm carrier DNA were mixed in an Eppendorf tube. Next, 100 µL of the competent yeast cells were added to the bait plasmid-carrier DNA mixture and mixed well by flicking the tube. Six hundred µL freshly made PEG-TE-LiAc solution were added and mixed well by vortexing for 15 sec. The mixture was incubated at 30°C, 225 rpm for 30 min. After the incubation, 70 µL of DMSO (Fisher Bioreagents) were added and mixed by gently inversion of the tube (no vortexing). The sample was heat shocked for 15 min in a 42°C water bath. Afterwards, tubes were directly placed on ice for 2 min, filled with dH_2O and centrifuged for 5 min at 3000 *g* at RT. The supernatant was removed, and the cell pellet was resuspended in 200 µL 1X TE. Transformed yeast (100 µL) was plated on selective YC-W plate, as the pBTM116-cam vector carries the tryptophan selection marker. Plates were incubated at 30°C for 2-3 days. 25% Glycerol stocks were prepared from single bait line colonies and stored at -80°C (see 2.10.7).

2.10.6 Measuring the Optical Density (OD) of a yeast culture

The OD_{600} of yeast culture was measured by diluting 100 µL of the overnight culture in 900 µL of the appropriate medium (1:10 dilution). This 1 mL sample was placed in a cuvette (Fischer Scientific, UK) and OD_{600} measurements were

performed on a spectrophotometer (Ultraspec 10, Amersham Biosciences). The machine was blanked with the appropriate medium without yeast culture. The OD_{600} was calculated by multiplying the OD_{600} measurement by the appropriate dilution factor of 10.

2.10.7 Glycerol stock preparation and retrieval of yeast clones

Single yeast clones of interest were inoculated in 5 mL selective medium (YC-W for bait lines, YC-L for positive control prey and VH single-domain library) overnight at 30°C, 225 rpm. The overnight cultures were mixed in a ratio of 1:1 with 50% glycerol and placed on dry ice. Glycerol stocks were stored at -80°C. A small amount of the glycerol stock was streaked out onto the appropriate selective plate and grown for 2-3 days at 30°C in order to retrieve the clones.

2.10.8 Characterization of yeast bait lines

2.10.8.1 Auto-activation of bait lines

Single yeast clones from different bait lines (and pBTM116 line as empty vector control) were streaked on YC-WL plates containing 0 mM, 5 mM, 10 mM, 30 mM, 50 mM and 100 mM of 3-AT. The plates were incubated at 30°C for 2-3 days and yeast growth was assessed to determine the minimal 3-AT concentration needed to prevent the auto-activation of the different bait lines.

2.10.8.2 Yeast co-transformation to assess the bait- positive control prey interaction

Single clones from the yeast bait lines were inoculated in 5 mL of YC-W selective medium and cultured overnight at 30°C, 225 rpm. The yeast transformation protocol was followed, except that 200 ng of the positive control prey plasmid

instead of the bait plasmid was used. Transformed yeast was grown on selective YC-WL plates for 2-3 days at 30°C. Clones were selected and streaked onto YC-WLH selective dishes and incubated at 30°C for 2-3 days in order to assess the bait-prey interactions.

2.10.9 Large scale yeast transformation for the library screening

Between 5 - 10 colonies of the established bait line were inoculated in 1 mL of autoclaved dH_2O and resuspended by vortexing. The yeast suspension was inoculated in 200 mL of YC-W selective media in a 500 mL Erlenmeyer flask and cultured overnight at 30°C, 225 rpm. Alongside, 1 L of YAPD medium was placed at 30°C to pre-warm the medium for the next day. The screening plates were pre-warmed overnight in a 30°C incubator.

Between 100-200 mL of the YC-W overnight culture was inoculated in 1 L of pre-warmed YAPD medium in a 2.5 L Erlenmeyer flask in order to produce a starting OD_{600} between 0.2-0.3. The culture was incubated at 30°C, 225 rpm for 3-4 hours until the OD_{600} reached 0.5-0.6. The yeast culture was transferred into a 225 mL conical tube (Corning) and centrifuged at 1000 *g*, RT for 2 min, and repeated until collected into one pellet. The pellet was washed 3 times in 200 mL dH_2O and centrifuged for 5 min at 1000 *g*, RT. Cells were then re-suspended in 8 mL freshly prepared TE-LiAc. The competent cells were kept on ice up to a maximum of 1 hour. The entire 300 µg of the yeast single domain library DNA (Rabbitts lab) was mixed with 10 mg of salmon sperm carrier DNA. The library DNA-carrier DNA mixture was added to the 8 mL of competent yeast and mixed well by inversion. Next, 60 mL of freshly prepared PEG-LiAc-TE was added and mixed again by inversion. The mixture was incubated at 30°C, 225 rpm for 30 min.

Seven mL of DMSO was added and mixed by inversion (no vortexing). The yeast was heat shocked for 15 min in a 42°C water bath and tubes were swirled around every 5 min to ensure a good temperature distribution in the flask. The flask was placed on ice for 2 min and filled with dH_2O. The cells were pelleted by centrifugation at 2500 *g,* RT for 5 min. The supernatant was removed by pipetting. Cells were washed again in 200 mL dH_2O and centrifuged at 2500 *g,* RT for 5 min. Supernatant was removed by pipetting and the cell pellet was resuspended in 5 mL 1X TE. More 1X TE was added to make a final volume of 10 mL. This transformant yeast was now plated out onto five large YC-WLH screening plates (25 x 25 cm) by using 1.5 mL of the yeast mixture per plate.

To determine the total number of transformants, 100 µL of the transformed yeast was used to make 100 µL serial dilutions (1:10, 1:100, 1:1000 and 1:1000 dilutions) in 1X TE and 100 µL was plated on 9 cm YC-WL plates. The large YC-WLH screening plates and 9 cm YC-WL dishes were incubated at 30°C for 4-5 days and 3 days, respectively. The number of yeast colonies growing on each YC-WL plates were counted multiplied by the dilution factor of the plate in order to determine the number of total yeast transformants (ex.: 234 colonies were counted on 1:100 dilution plate and a 100 µL was spread out on the plate, therefore calculate 234 x 100 x 100 = 2.34 $x10^6$ transformants). The transformation efficiency of the screen was calculated by dividing the number of total transformants by the amount of DNA used and expressed as transformants/ µg DNA.

2.10.10 Plasmid DNA extraction from yeast

The Zymoprep™ Yeast Plasmid MiniPrep II kit (Zymo Research, USA) was used to extract the plasmid DNA from yeast according to the manufacturer's protocol.

Positive yeast colonies from the first screening round were separately inoculated into 5 mL of YC-L medium in a 50 mL sterile Falcon tube over night at 30°C, 225 rpm. YC-L medium was used for cultures when extracting prey plasmids from yeast, as the bait plasmid will preferentially be lost in culture medium containing tryptophan. On the next day, the overnight culture was diluted in YC-W to a starting OD_{600} of 0.2-0.3 and 1.5 mL harvested at 600 *g* for 2 min when an OD_{600} of 0.5-0.6 was reached. The supernatant was carefully removed and 200 µL of Solution 1 was added. Three µL of Zymolase™ was added and the tube was flicked to resuspend the pellet. After a 45 min incubation at 37°C, 200 µL of Solution 2 and 400 µL of Solution 3 were added and mixed well. The microcentrifuge tube was spun at the maximum speed for 3 min and the supernatant was transferred to a Zymo-Spin-I column. The column was centrifuged for 1 min and washed with 550 µL of Wash Buffer. The column was centrifuged for 2 min before being placed into a new microcentrifuge tube. 10 µL of TE was added to the column membrane, incubated for 5 min and centrifuged for 1 min at maximum speed to elute the DNA. The amount and quality of the DNA was assessed via Nano-Drop Spectrophotometry.

2.11 Computational and statistical analysis

2.11.1 Protein structures

Protein structures were obtained from the Protein Data Bank (PDB, https://www.rcsb.org/pdb/home/home.do) and visualised using PyMol (for Educational-use only, https://pymol.org/). Table 2.13 gives an overview of the relevant protein structures in this thesis.

Name of structure	PDB ID code	Reference
Whole IgG structure	1IGT	Harris et al., 1997
β-catenin/Tcf complex	1JDH	Graham et al. 2000
β-catenin/BCL9/Tcf4	2GL7	Sampietro et al. 2006

Table 2.13 List of protein structures and PDB ID codes

2.11.2 Software use

Sequencing results were visualised using the MacVector software (https://macvector.com) and SnapGene (https://www.snapgene.com).

The protein sequence alignments were performed using the Jalview software (http://www.jalview.org/). The ImageJ software was used to visualise immunofluorescence images (https://imagej.net). The colony counting for the CFA images was performed using the CellProfiler Software and the "Yeast Colony Classification" cell counting pipeline (https://cellprofiler.org/previous_examples/%23yeast-colony-classification). DNA sequences of genes of interest were obtained from Ensembl (https://www.ensemble.org). Some figures in this thesis were produced with images from a Library of Science and Medical Illustrations and can be accessed here: https://www.somersault1824.com/science-illustrations/ .

2.11.3 Statistical methods

GraphPad Prism 8.0 Software (La Jolla, Carlifornia, USA) was used to perform all data analysis. All data are presented as the mean values + standard deviation (SD). P-values were obtained using a two-tailored student's t-test from biological replicates. p-values below $p \leq 0.05$ (*) were considered as statistically significant. $p \leq 0.01$ and $p \leq 0.001$ were denoted by ** and ***, respectively.

Chapter 3

Characterisation of β-catenin in a panel of colorectal cancer cell lines

CHAPTER 3: β-catenin characterisations in a panel of colorectal cancer cell lines

3.1 Introduction

Mutations in APC or β-catenin are common in CRC and are known to stabilise β-catenin, resulting in the nuclear translocation of the protein and hyperactivation of the Wnt signal transduction. Hence, nuclear β-catenin has been widely described as the hallmark of Wnt activity (Zeng et al., 2017).

β-catenin localisation has been investigated through immunohistochemical staining of patient samples in a wide range of cancers, including colorectal cancer, hepatocellular cancer, ovarian cancer, cervical cancer and non-small cell lung cancer (Chen et al., 2014; Chen et al., 2013; Li et al., 2013; Wong et al., 2004; Zhang et al., 2014). While some investigations found an association between nuclear β-catenin localisation and favourable prognosis in ovarian cancer (Gamallo et al., 1999; Nagy et al., 2017; Wang et al., 2019) and melanoma (Kageshita et al., 2001), many studies associated a poor survival prognosis for patients with nuclear β-catenin accumulation in colorectal cancers (Baldus, 2004; Chen et al., 2014; Chen et al., 2013; Wong et al., 2004; Zhang et al., 2016), cervical cancer (Zhang et al., 2014) and lung cancer (Li et al., 2013). Furthermore, various studies show no link between β-catenin nuclear localisation and the tumour grade or β-catenin mutation status (Chen et al., 2013; El-Bahrawy et al., 2004; Hugh et al., 1999).

β-catenin has a prominent role in canonical Wnt signalling and readily shuttles between the cytoplasm and the nucleus. β-catenin itself does not have a recognisable

nuclear localisation sequence (Fagotto, Glück, & Gumbiner, 1998) and the exact nuclear translocation mechanism is still being investigated. Different proteins, including APC (Henderson, 2000; Rosin-Arbesfeld et al., 2003) and Axin (Cong & Varmus, 2004), have been described as nuclear "shuttling chaperones" for β-catenin. On the other hand, some studies suggest that these proteins influence β-catenin localisation by compartmental retention (Krieghoff, Behrens, & Mayr, 2006) and that nuclear β-catenin levels are mainly regulated by the level of cytoplasmic degradation. Furthermore, β-catenin was shown to interact directly with nuclear pores for passage (Koike et al., 2004; Yang et al., 2015). These reports reflect a complex balance between import and export of β-catenin, influenced by cytoplasmic and nuclear retention (Yokoya et al., 1999).

3.1.1 Aim

In this chapter, we aimed to characterise the β-catenin expression and subcellular localisation in a panel of colorectal cancer (CRC) cell lines. A localisation analysis of β-catenin using immunofluorescence (IF) in CRC cell lines can give valuable information on the mechanisms and factors involved in the subcellular distribution of the protein. Microarray and mutation status data for the CRC cell lines available in our lab was used to search for correlations with β-catenin localisation.

3.2 Results

3.2.1 β-catenin expression in a panel of CRC cell lines

The Cancer and Immunogenetics Laboratory (CIL) has microarray expression profiles of about 120 CRC cell lines. mRNA expressions of β-catenin (*CTNNB1*) were ranked from lowest to highest, as shown in Figure 3.1, and show that β-catenin is widely expressed across the CRC cell line panel.

The β-catenin protein expression was verified by Western Blot. As seen in Figure 3.2A, β-catenin was detected at the protein level for all cell lines tested, with the exception of RKO. This stands in contrast to the microarray data (Figure 3.1 and Figure 3.2B), where RKO expressed high mRNA levels for *CTNNB1*. The mRNA expression of β-catenin in RKO cells was confirmed by qPCR (Figure 3.2C). RKO is a colon carcinoma cell line with wild-type (wt) *APC* and *CTNNB1* (Sparks et al., 1998). This genotype is comparatively uncommon in colorectal cancer, as most carry either an *APC* or *CTNNB1* mutation (Sparks et al., 1998). As RKO is wild-type for both *APC* and *CTNNB1*, it might be possible that there is a high turn-over of the protein, which is not detected by the antibody. Furthermore, different-sized bands can be identified in multiple of the tested cell lines. These might be breakdown products of the protein that are recognised by the antibody, as caspase-cleaved β-catenin products were previously described with a mass of about 70 kDa (Steinhusen et al., 2000).

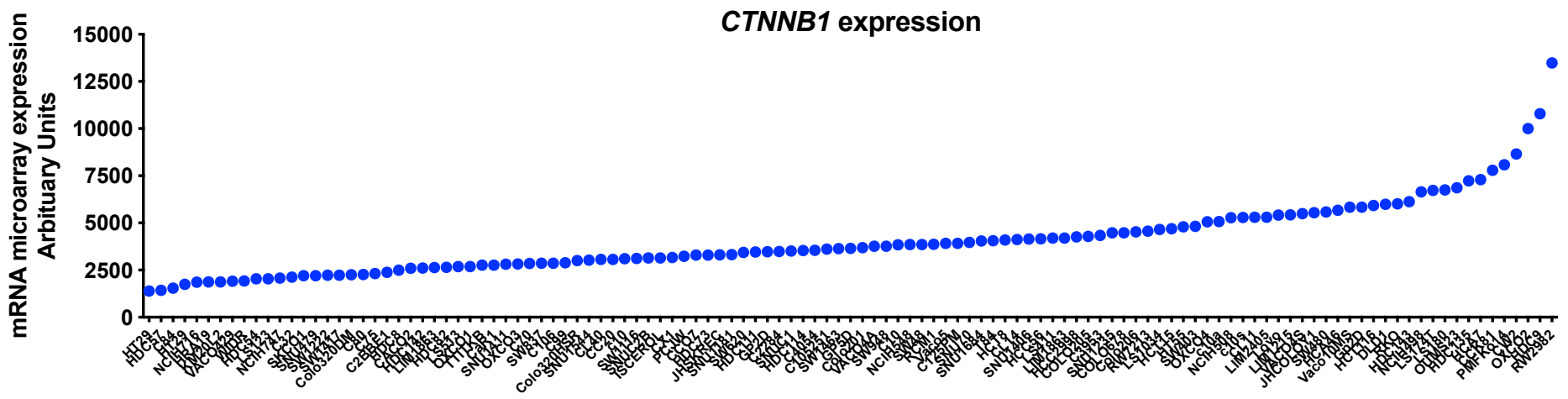


Figure 3.1 Microarray data: β-catenin (*CTNNB1*) expression in a panel of colorectal cancer cell lines
CTNNB1 expression data of 119 colorectal cancer cell lines was obtained by Affymetrix Human Genome U133 plus 2.0 microarray. Data are expressed as arbitrary units and arranged in ascending order. x-axis: CRC cell lines, y-axis: mRNA level

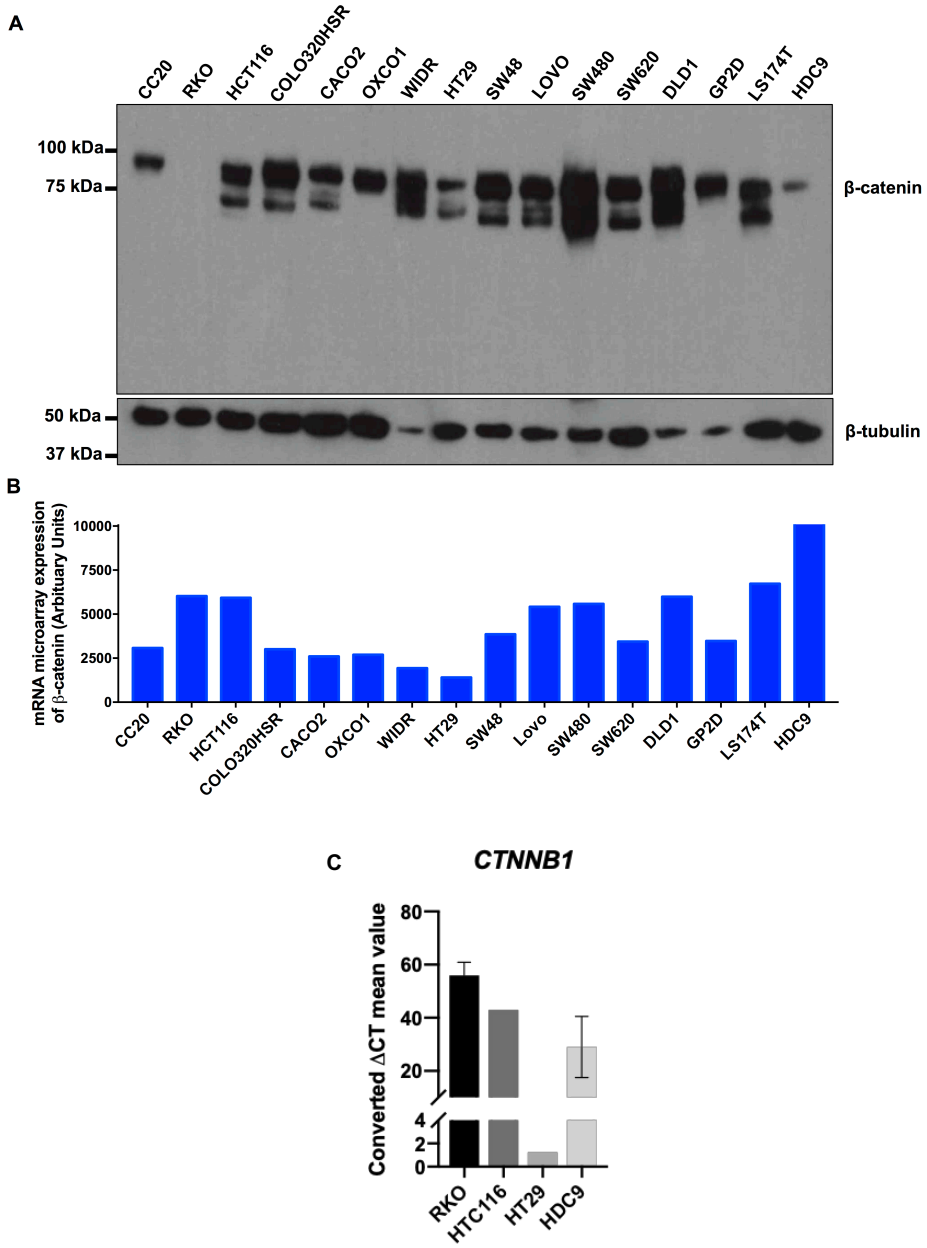


Figure 3.2 Protein and mRNA expression of β-catenin in a selected panel of colorectal cancer cell lines

A) Representative Western Blot of β-catenin in a panel of colorectal cancer cell lines. Proteins were extracted using RIPA buffer and 20 µg were loaded on a 12% SDS acrylamide gel, transferred on a PVDF membrane and probed for β-catenin (BD Technologies, 1:5000) for 1hr at RT. RKO cell lysates from independent experiments were blotted and were negative for β-catenin at the protein expression level (another WB example is given in Appendix A.1). A shorter time exposure would potentially have benefited the assessment of β-catenin levels in the panel of cell lines **B**) *CTNNB1* mRNA microarray expression data from the indicated cell lines. **C**) *CTNNB1* expression in RKO (n=2), HCT116 (n=1), HT29 (n=1) and HDC9 (n=2) cells assessed by qPCR.

The absence of β-catenin protein expression in RKO cells was further validated by immunofluorescence (IF). While β-catenin could be detected with varying localisation in most of the colorectal cancer cell lines, RKO gave a completely negative signal

(Figure 3.3, middle panel). Both SW480 and HCT116 cell lines showed β-catenin expression throughout the cytoplasm. However, while a dominant nuclear localisation of the protein was visible in SW480 cells (Figure 3.3, top panel), β-catenin also aggregated at the cell membrane in HCT116 cells. F-actin staining was used as counter stain to visualise the cells.

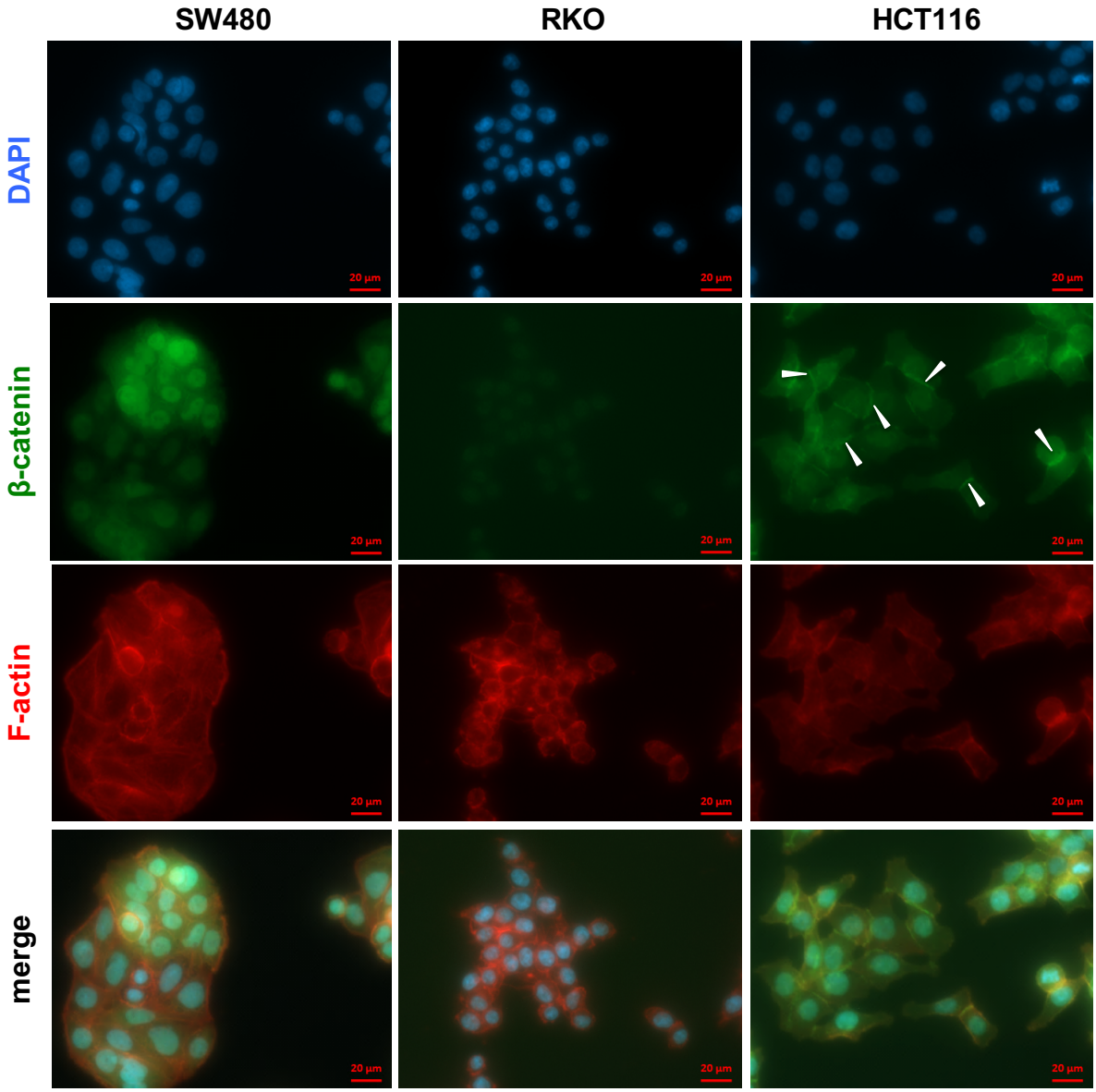


Figure 3.3 β-catenin expression and localisation in SW480, RKO and HCT116 cells
SW480, RKO and HCT116 cells were stained for DAPI (blue), β-catenin (green), F-actin (red). SW480 cells exhibited ubiquitous β-catenin localisation, with a strong focus on nuclear staining. β-catenin expression was visible throughout the cells in HCT116 cells, but a distinctive accumulation at the cell membranes with cell-cell contact could be observed (white arrow heads). β-catenin could not be detected by IF in RKO cells, even at long (1 sec) exposure. F-actin staining was performed as counter stain to visualise the cells. 40X magnification, NA = 0.6,. Scale bars: 20 µm.

3.2.2 WNT transcriptional activity in SW480, HCT116 and RKO cells

Based on the different β-catenin localisations in SW480, HCT116 and RKO cell lines, it was hypothesised that these cells also show differences in their Wnt transcriptional activity. In order to assess this, the Wnt activity in SW480, HCT116 and RKO cells was measured through TCF-mediated transcription using the TOPflash assay (Korinek et al., 1997). As expected, by this criterion, SW480 cells (APC mutant) have higher baseline transcriptional Wnt activity compared to HCT116 (heterozygous β-catenin mutation) and RKO cells are negative (wild-type for both *CTNNB1* and *APC* and β-catenin protein not detectable) (Figure 3.4).

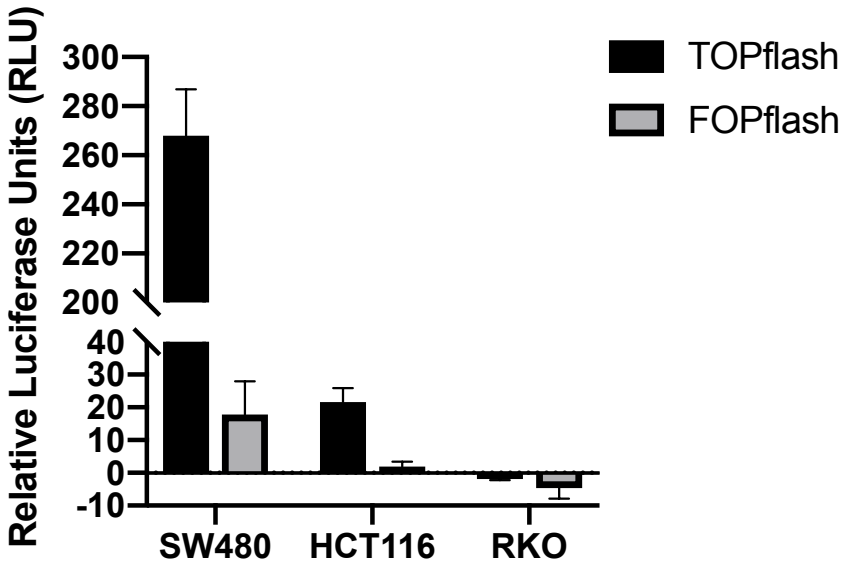


Figure 3.4 Baseline WNT activity in SW480, HCT116 and RKO cell lines measured by the TOPflash assay.
TCF-mediated transcription in SW480, HCT116 and RKO cells was measured via the TOPflash assay. Given are relative Luciferase:Renilla units, also called Relative Luciferase Units (RLU), averaged from two technical replicates of a representative experiment. Results were confirmed in three independent experiments.

This luciferase reporter result is consistent with the nuclear localisation of β-catenin obtained by IF (Figure 3.3) and in line with what might be expected from previously published data in cell lines (Qu et al. 2016; Rosin-Arbesfeld et al. 2003; da Costa et al. 1999). However, immunohistochemistry staining of CRC patient samples and cell lines for β-catenin showed no correlation between staining patterns and APC or β-catenin mutation status (Chen et al., 2013; El-Bahrawy et al., 2004; Hugh et al., 1999). This prompted us to assess a larger panel of CRC cell lines with known *APC* and *CTNNB1* mutation status to get a better understanding of the functional implications and mutational associations of β-catenin subcellular localisation.

3.2.3 Preliminary β-catenin localisation in a panel of CRC cell lines

Given the previously presented preliminary β-catenin localisation data in SW480, HCT116 and RKO cells, a panel of 52 CRC cell lines was stained for β-catenin via immunofluorescence. Epithelial cellular adhesion molecule (EpCAM) was stained using the in-house AUA1 antibody to visualise individual cells. Table 3.1 lists the cell lines used in this study, indicating their APC and β-catenin mutation status.

Cell line	APC mutation status	β-catenin mutation status	Cell line	APC mutation status	β-catenin mutation status
C10	WT	WT	**LIM1215**	WT	MT§
C106	MT	WT	**LIM2405**	MT§	WT
C125PM	MT	WT	**LOVO**	MT	WT
C2BBe1	MT	MT§	**LS123**	MT	WT
C99	WT	WT	**LS1034**	MT	WT
CACO2	MT	MT§	**LS174T**	WT	MT
CC20	WT	WT	**LS180**	MT§	MT
CCK81	MT§	MT§	**LS513**	WT	MT§
CCO7	MT	WT	**NCIH508**	WT	WT
CL40	MT	?	**OUMS23**	MT	?
COLO320DM	MT	WT	**OXCO1**	MT	WT
COLO320HSR	MT	WT	**PMFKo14**	WT	MT
COLO678	MT	WT	**RKO**	WT	WT
CW2	MT	MT§	**RW2892**	MT	WT
CX1	MT	WT	**RW7213**	MT	WT
DLD1	MT	WT	**SKCO1**	MT	WT
GP2D	MT	WT	**SNUC2B**	WT	WT
HCA7	MT	WT	**SNU1746**	MT	?
HCT116	WT	MT	**SW1417**	MT	WT
HCT15	MT	WT	**SW403**	MT	WT
HDC111	?	?	**SW48**	MT§	MT
HDC114	MT	?	**SW480**	MT	WT
HDC54	MT	MT§	**SW620**	MT	WT
HDC57	MT	MT§	**VACO4A**	MT	WT
HT29	MT	WT	**T84**	MT	WT
JHCOLOYI	?	?	**WIDR**	MT	WT

Table 3.1 Overview of APC and β-catenin mutation status in a panel of CRC cell lines
Cell lines derived from the same patient are shaded in the same colour. MT: mutant within mutation cluster region, WT: wild-type, MT§: mutant outside of cluster region, ? = unknown mutation status. Mutation statuses of p53, KRAS and BRAF for all listed cell lines can be found in Appendix A.2.

β-catenin localisation was scored independently by three assessors into the following categories: 1) clearly membrane, 2) cytoplasmic / membrane, 3) cytoplasmic / nuclear, 4) nuclear, 5) non-quantifiable, 6) no staining. Representative staining patterns are visualised in Figure 3.5. The β-catenin staining of all other cell lines and the scoring of individual assessors can be found in Appendix A.3, and Appendix A.4, respectively. Poor imaging quality and insufficient magnification are an important reason for non-quantifiable β-catenin localisation.

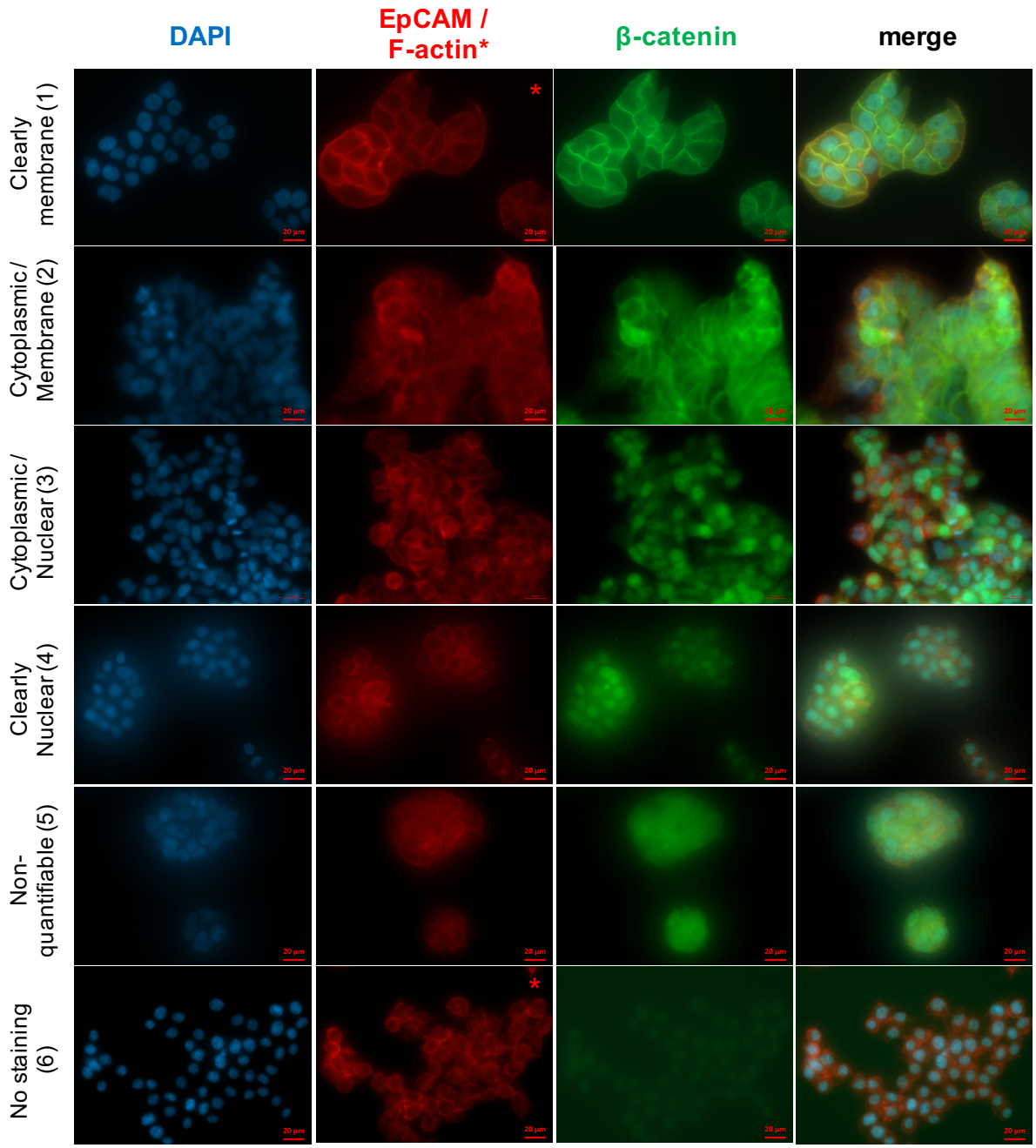


Figure 3.5 Examples of staining categories
Representative examples of different β-catenin staining patterns in a panel of CRC cell lines. Cell lines were stained for β-catenin (green), EpCAM (red) and DAPI (blue) according the methods described in Chapter 2. Phalloidin (staining F-actin) was used as counterstain in some cell lines and indicated by * in this figure. Cells were imaged using a Zeiss Observer z1 fluorescence microscope. Scale bar: 20 μm, 40X magnification, NA = 0.6.

The scoring consensus from the three assessors for all stained cell lines is listed in Table 3.2. The six cell lines with no clear agreement between the assessment scores

(no consensus), namely CC20, COLO678, DLD1, LS1034, LS180 and T84, were left out of further analysis.

Cell line	β-catenin localisation scoring results	Cell line	β-catenin localisation scoring results
C10	1	**LIM1215**	3
C106	1	**LIM2405**	1
C125PM	1	**LOVO**	1
C2BBe1	1	**LS1034**	No consensus
C99	3	**LS123**	1
CACO2	1	**LS174T**	4
CC20	No consensus	**LS180**	No consensus
CCK81	1	**LS513**	4
CCO7	4	**NCIH508**	2
CL40	1	**OUMS23**	1
COLO320DM	4	**OXCO1**	4
COLO320HSR	4	**PMFKo14**	1
COLO678	No consensus	**RKO**	6
CW2	1	**RW2892**	5
CX1	1	**RW7213**	1
DLD1	No consensus	**SKCO1**	1
GP2D	2	**SNUC2B**	1
HCA7	1	**SNU1746**	1
HCT116	2	**SW1417**	1
HCT15	1	**SW403**	5
HDC111	1	**SW48**	5
HDC114	2	**SW480**	4
HDC54	1	**SW620**	4
HDC57	1	**VACO4A**	No consensus
HT29	1	**T84**	No consensus
JHCOLOY1	1	**WIDR**	1

Table 3.2 Scoring results of β-catenin localisation in a panel of colorectal cancer cell lines
A total of 52 CRC cell lines were stained for β-catenin. Images were scored by three individuals for the β-catenin localisation, where 1 = clearly membrane, 2 = cytoplasmic/membrane, 3 = cytoplasmic/nuclear, 4 = clearly nuclear, 5 = non-quantifiable, 6 = no staining. Cell lines with different scoring from all three scorers (no consensus) were excluded from further analysis. Individual assessor scores can be found in Appendix A.4. Duplicate cell lines are visualised in colours.

3.2.4 Mutations in key WNT signalling proteins do not affect subcellular β-catenin localisation

In the first instance, we aimed to assess any potential correlation between β-catenin subcellular localisation and mutation status of key Wnt pathway effectors such as APC and β-catenin itself. We also included known mutation data of other relevant proteins known to be frequently mutated in CRC, namely p53, KRAS and BRAF, as well as the cell line replication error (RER) status (Liu & Bodmer, 2006; Wilding et al., 2010). Our lab has established a broad database of known mutation statuses in the panel of colorectal cell lines, which is validated against commonly available data from the Broad Institute's Cancer Cell Line Encyclopedia (CCLE) (Barretina et al., 2012), The Cancer Genomic Atlas (TCGA) (Garnett et al., 2012; The Cancer Genome Atlas Network, 2012) and COSMIC (Catalogue of Somatic Mutations In Cancer) data base (Tate et al., 2019), as well as sequencing data from our collaborators (Mouradov et al., 2014).

The β-catenin localisation scores (Table 3.2, no consensus removed) were used to broadly group the cell lines into β-catenin membrane (clearly membrane (1) and membrane/cytoplasmic (2)) and β-catenin nuclear (cytoplasmic/nuclear (3) and nuclear (4)) categories (Figure 3.6). The cell lines RKO, RW2892, SW403, and SW48 did not fall into either group as they showed diffuse or no staining. Furthermore, duplicate cell lines derived from the same patient were removed for statistical analysis (COLO320HSR, SW620, CX1, WIDR, HDC54, HCT15, C2BBe1). Duplicate cell lines can serve as good positive controls but bias statistical analyses (Bracht et al., 2010).

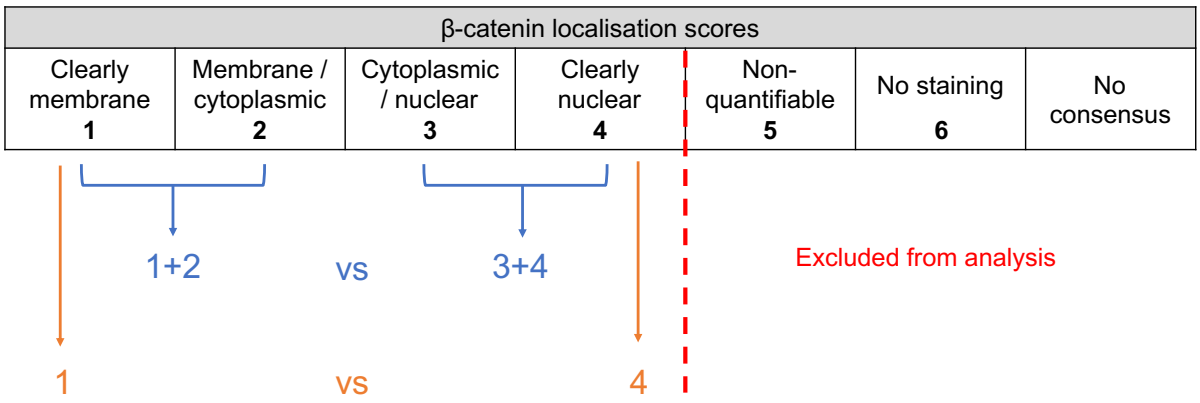


Figure 3.6 β-catenin localisation score groupings
In a first round of analysis (blue), cell lines with localisation scores 1 and 2 were grouped into "membrane" staining, while cell lines with scores 3 and 4 were grouped into "nuclear" staining. In a further analysis (orange), only cell lines with clearly membrane staining were assessed against cell lines with clearly nuclear staining. Cell lines with diffuse staining, no staining or no consensus between the assessment scores were excluded from the analysis.

Ta-Chun Liu (Bodmer lab) performed all the computational analysis of the data in this chapter. Using 2 x 2 contingency tables, we showed that there is no correlation between the subcellular localisation of β-catenin and any of the analysed mutations in the cell lines (Figure 3.7, top panel). The data were also reassessed when only the clearly membrane (1) and nuclear (4) cell lines were compared (Figure 3.7, lower panel), as well as taking the position of the mutation in APC (inside or outside of MCR) and β-catenin (mutation hotspot in exon 3) into consideration (Appendix A.5).

These results stand in line with previous published data, showing no correlation between APC or β-catenin mutation status and β-catenin subcellular localisation (Chen et al., 2013; El-Bahrawy et al., 2004; Hugh et al., 1999). Our analysis on a large panel of CRC cell lines strengthen these observations.

Correlation of β-catenin localisation with genetic data – subgroups 1+2 vs 3+4

P=0.154	APC	
	WT	MT
β-catenin localisation		
membrane	4	19
nuclear	4	4

P=1.00	β-catenin	
	WT	MT
β-catenin localisation		
membrane	13	7
nuclear	4	3

P=0.433	p53	
	WT	MT
β-catenin localisation		
membrane	8	16
nuclear	4	4

P=1.00	KRAS	
	WT	MT
β-catenin localisation		
membrane	11	13
nuclear	3	4

P=1.00	BRAF	
	WT	MT
β-catenin localisation		
membrane	16	7
nuclear	5	3

P=0.672	RER status	
	-	+
β-catenin localisation		
membrane	13	9
nuclear	6	2

Correlation of β-catenin localisation with genetic data – subgroups 1 vs 4

P=0.239	APC	
	WT	MT
β-catenin localisation		
membrane	2	17
nuclear	2	4

P=1.00	β-catenin	
	WT	MT
β-catenin localisation		
membrane	12	5
nuclear	3	2

P=1.00	p53	
	WT	MT
β-catenin localisation		
membrane	6	14
nuclear	2	4

P=0.615	KRAS	
	WT	MT
β-catenin localisation		
membrane	9	11
nuclear	1	4

P=0.344	BRAF	
	WT	MT
β-catenin localisation		
membrane	14	5
nuclear	3	3

P=0.621	RER status	
	-	+
β-catenin localisation		
membrane	11	7
nuclear	5	1

Figure 3.7 Correlation between β-catenin localisation with genetic data
Top panel shows the 2 X 2 contingency tables for mutation status of APC, β-catenin, p53, KRAS, BRAF and the mismatch repair (RER) status for β-catenin localisation subgroups membrane/ cytoplasmic (1+2) vs cytoplasmic/nuclear (3+4). The lower panel shows the results for the same analysis only considering β-catenin localisation subgroups clearly membrane (1) vs clearly nuclear (4). *P*-values for Fisher's exact test for the 2 x 2 tables are given. Note that the number of cell lines vary, as not all cell lines have a known mutation status for the genes of interest and were therefore not included in the specific 2 x 2 tables.

3.2.5 β-catenin cellular localisation associates with E-cadherin expression

Next, we wanted to address the possibility that the β-catenin subcellular localisation is correlated with the gene expression profile in the cell lines. Our lab previously developed a Gaussian Mixture Modelling (GMM) method to detect and characterise bimodally distributed genes based on the microarray expression data in a panel of 78 CRC cell lines (MPhil thesis of Peter Kalugin, 2017). The CRC cell line data set for the GMM does not contain any duplicate cell lines (derived from the same patient). Of note, three cell lines stained in this study, namely LIM1215, LIM2405 and SNU1746, were not part of the GMM data set and were removed from this specific analysis, leaving a total of 31 cell lines for the localisation grouping 1+2 vs 3+4 analysis (Figure 3.8A).

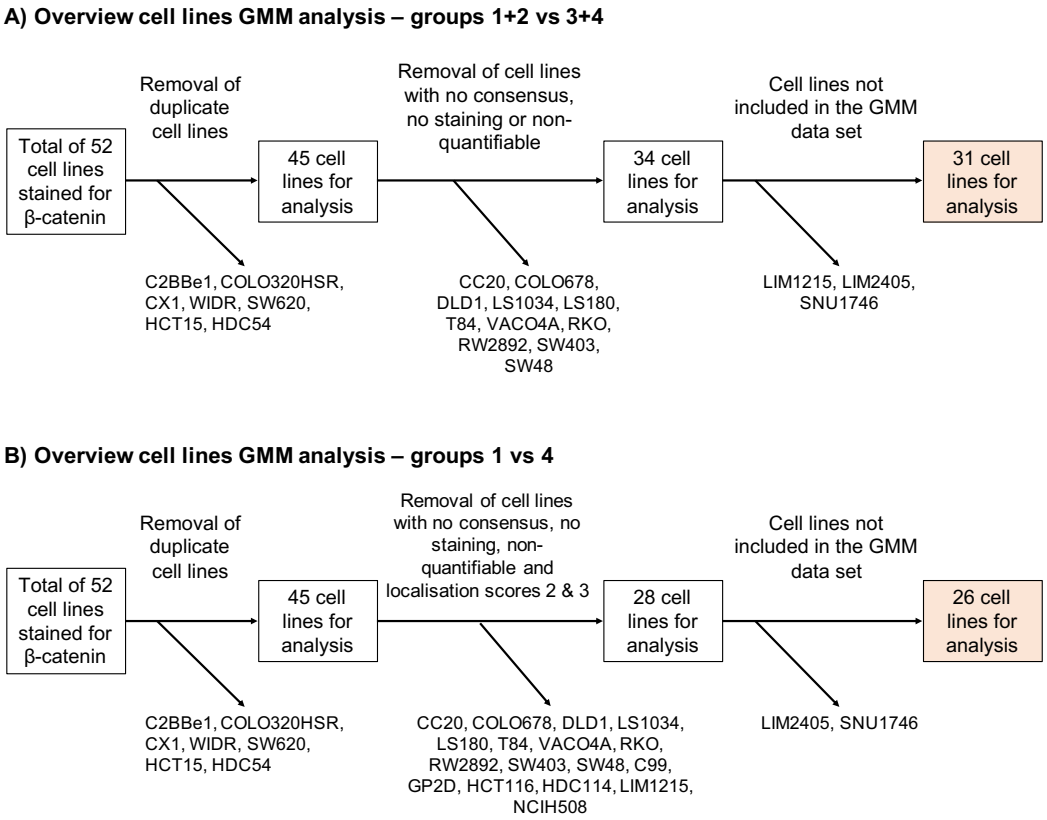


Figure 3.8 Flow-chart of cell lines used for gene expression analysis: β-catenin localisation scores 1+2 vs 3+4
A) Flow-chart explaining which cell lines were removed for the gene expression analysis using the localisation grouping 1+2 vs 3+4. **B**) Flow-chart explaining which cell lines were removed for the gene expression analysis using the localisation scores 1 vs 4 only.

The localisation data (clearly membrane (1) and cytoplasmic/membrane (2) vs cytoplasmic/nuclear (3) and nuclear (4)) were analysed against a total of 4392 bimodal expressing genes (a total of 6482 probe-sets). In total, 278 differentially expressed probe-sets significantly associated with the β-catenin localisation. Table 3.3 lists the most 20 significant differentially expressed probe-sets (the entire list is given in Appendix A.6).

Significantly correlated probe-sets to membrane staining (localisation scores 1 and 2) compared to nuclear staining (localisation scores 3 and 4)					
Gene Symbol	Membrane / low gene expression	Membrane / high gene expression	Nuclear / low gene expression	Nuclear / high gene expression	p-value
CDH1--1	0	24	5	2	0.00012359
CDH1--2	0	24	5	2	0.00012359
C1orf172	1	23	5	2	0.00069403
AP1M2--1	0	24	4	3	0.00111235
AKT3--2	24	0	3	4	0.00111235
nan--711	24	0	3	4	0.00111235
MAP7--3	0	24	4	3	0.00111235
RAB25	0	24	4	3	0.00111235
AP1M2--2	0	24	4	3	0.00111235
MAP7--1	0	24	4	3	0.00111235
MAP7--2	0	24	4	3	0.00111235
GRHL2	0	24	4	3	0.00111235
IRF6--1	0	24	4	3	0.00111235
LOC100506844	24	0	3	4	0.00111235
nan--5366	24	0	3	4	0.00111235
OVOL1--2	0	24	4	3	0.00111235
AIM1	0	24	4	3	0.00111235
SPINT1--1	0	24	4	3	0.00111235
MARVELD3--2	2	22	5	2	0.00226843
CD24--4	2	22	5	2	0.00226843

Table 3.3 The 20 most differentially expressed probe-sets correlating with β-catenin staining analysed by membrane (localisation scores 1 and 2) vs nuclear (localisation scores 3 and 4) 2 x 2 contingency tables.
p-values uncorrected for multiple comparisons are given. Values in columns 2-5 are the number of cell lines falling into each category.

Notably, the expression of E-cadherin (CDH1) strongly correlated with the localisation of β-catenin ($p \leq 0.0001$, not corrected for multiple testing, see Table 3.3). As E-cadherin is known to interact with β-catenin (Huber & Weis, 2001), it is an *a priori* candidate gene in this analysis and therefore no multiple correction adjustments were performed. The two probe-sets for the CDH1 gene in the microarray data set both topped the significance list. In cell lines expressing high levels of CDH1, β-catenin was primarily bound to the cell membrane. β-catenin was accumulated in the nucleus in low *CDH1* expressing cells (2 X 2 contingency table in Figure 3.9). The cell lines C99 and LS513 are the only exceptions to this observation. Notably, C99 expressed high levels of CDH1 on a mRNA level (Appendix A.8).

Analysis groups 1+2 vs 3+4	**β-catenin membrane group**	**β-catenin nuclear group**
CDH1 low	-	CCO7, LS174T, OXCO1, SW480, COLO320DM
CDH1 high	C106, C125PM, CACO2, CCK81, CL40, CW2, GP2D, HCA7, HCT116, HDC111, HDC114, HT29, JHCOLOY1, LOVO, LS123, NCIH508, OUMS23, PMFK014, SKCO1, SNUC2B, SW1417, C10, HDC57, RW7213	C99, LS513

Figure 3.9 2x2 contingency table: β-catenin localisation association with CDH1 expression levels
Correlation between CDH1 expression level and β-catenin localisation, individual cell lines given in each category. Analysis was performed on localisation subgroups 1+2 vs 3+4. No cell lines had β-catenin membrane staining and low CDH1 expression levels.

Another gene that was significantly associated in our analysis was *MAP7* (three probe-sets were represented in the top 20 differentially expressed genes). The *MAP7* gene codes for Ensconsin (also known as MAP7 or E-MAP-115), a microtubule-associated protein predominantly expressed in epithelial cells (Bulinski & Bossler,

1994; Chaudhary et al., 2019; Yadav, Verma, & Panda, 2014). Just as the association with E-cadherin, when MAP7 expression is low, β-catenin localises to the nucleus of cells.

When the gene expression analysis was performed using only the clearly membrane vs nuclear β-catenin localisation subgroups (scores 1 vs 4, 26 cell lines in total), the correlation with CDH1 was even stronger (*p*-value = 0.0000912). The full list of the 304 significantly associated probe-sets can be found in Appendix A.7. The 20 most significant probe-sets for this analysis are represented in Table 3.4.

Significantly correlated probe-sets to membrane staining (score 1) compared to nuclear staining (score 4)					
Gene Symbol	Membrane / low gene expression	Membrane / high gene expression	Nuclear / low gene expression	Nuclear / high gene expression	p-value
CDH1--1	0	20	5	1	9.12E-05
CDH1--2	0	20	5	1	9.12E-05
MARVELD3--2	1	19	5	1	0.00052556
CD24--4	1	19	5	1	0.00052556
F11R--3	0	20	4	2	0.00100334
RAB25	0	20	4	2	0.00100334
nan--5366	20	0	2	4	0.00100334
AKT3--2	20	0	2	4	0.00100334
AP1M2--1	0	20	4	2	0.00100334
nan--711	20	0	2	4	0.00100334
RTEL1/TNFRSF6B	20	0	2	4	0.00100334
GRHL2	0	20	4	2	0.00100334
IRF6--1	0	20	4	2	0.00100334
AP1M2--2	0	20	4	2	0.00100334
AIM1	0	20	4	2	0.00100334
OVOL1--2	0	20	4	2	0.00100334
MAP7--3	0	20	4	2	0.00100334
LOC100506844	20	0	2	4	0.00100334
FHL1--1	20	0	2	4	0.00100334
MAP7--1	0	20	4	2	0.00100334

Table 3.4 The 20 most differentially expressed probe-sets correlating with β-catenin staining analysed by membrane (score 1) vs nuclear (score 4) 2 x 2 contingency tables.
p-values uncorrected for multiple comparisons are given. Values in columns 2-5 are the number of cell lines falling into each category.

Low or absent E-cadherin expression in combination with high Vimentin (Vim), Zink Finger E-Box Binding Homeobox 1 (ZEB1) and N-cadherin expression is a hallmark of Epithelial-to-mesenchymal transition (EMT). EMT is a process during which epithelial cells with usually strong cell-cell adhesion gain mesenchymal properties with weaker cell-cell adhesion, increased motility and possibly a metastatic phenotype (Vu & Datta, 2017). It was previously suggested that nuclear β-catenin might be associated with an EMT phenotype (Basu, Cheriyamundath, & Ben-Ze'ev, 2018; Schmalhofer, Brabletz, & Brabletz, 2009).

Previous work in our lab identified a distinct group of cell lines with EMT expression profiles, which we term "EMT cell lines" (Appendix A.9). The tested EMT cell lines in this study, namely CCO7, OXCO1, COLO320DM and COLO320HSR exhibited nuclear β-catenin, with the exception of RKO (no β-catenin expression) and CC20 (no consensus). All the EMT cell lines lack E-cadherin expression, as assessed by the microarray data available in our lab (Figure 3.10 and Appendix A.8). SW480 and SW620 cell lines are classified as "borderline EMT" cell lines, because their pattern of expression of EMT markers (ZEB1, Vimentin…) is less consistent (Appendix A.9). They also show significant nuclear β-catenin localisation. It can be clearly seen in Figure 3.10A that E-cadherin protein expression is absent in all the EMT cell lines (indicated in orange), which is in good agreement with the mRNA expression from the microarray data (Figure 3.10B). However, it should be noted that the nuclear β-catenin-staining cell line LS174T is not an EMT cell line, as it does not follow the EMT expression patterns. For example, it has low Vimentin and ZEB1 expression, which are key features of EMT cell lines (Appendix A.9). Instead, this cell line carries two different heterozygous nonsense mutations in E-cadherin: i) exon 8 splice donor

site mutation and ii) frameshift mutation in exon 3 resulting in a premature stop codon at codon 216 (Efstathiou et al., 1999). LS174T does not express E-cadherin either on a protein or message level, due to its mutations in the E-cadherin coding gene (Figure 3.10A, purple). This lack of E-cadherin expression might explain the nuclear β-catenin staining in LS174T cells. Of note, the cell line HDC9 also contains two different heterozygous mutations in E-cadherin and, just as LS174T, does not express E-cadherin (Figure 3.10, purple).

Interestingly, β-catenin in LS513 is detected at a notably faster electrophoretic mobility than in the other cell lines on a WB (Figure 3.10A), consistent with a molecular mass of about 70 kDa. This cell line harbours an amino acid pA5-A80del deletion in β-catenin, which could explain the size difference. LS513 is the cell line that showed nuclear β-catenin localisation, even though it has detectable E-cadherin expression. It could be further investigated if the mutation has an effect on the E-cadherin-binding, which could explain the more nuclear localisation of β-catenin.

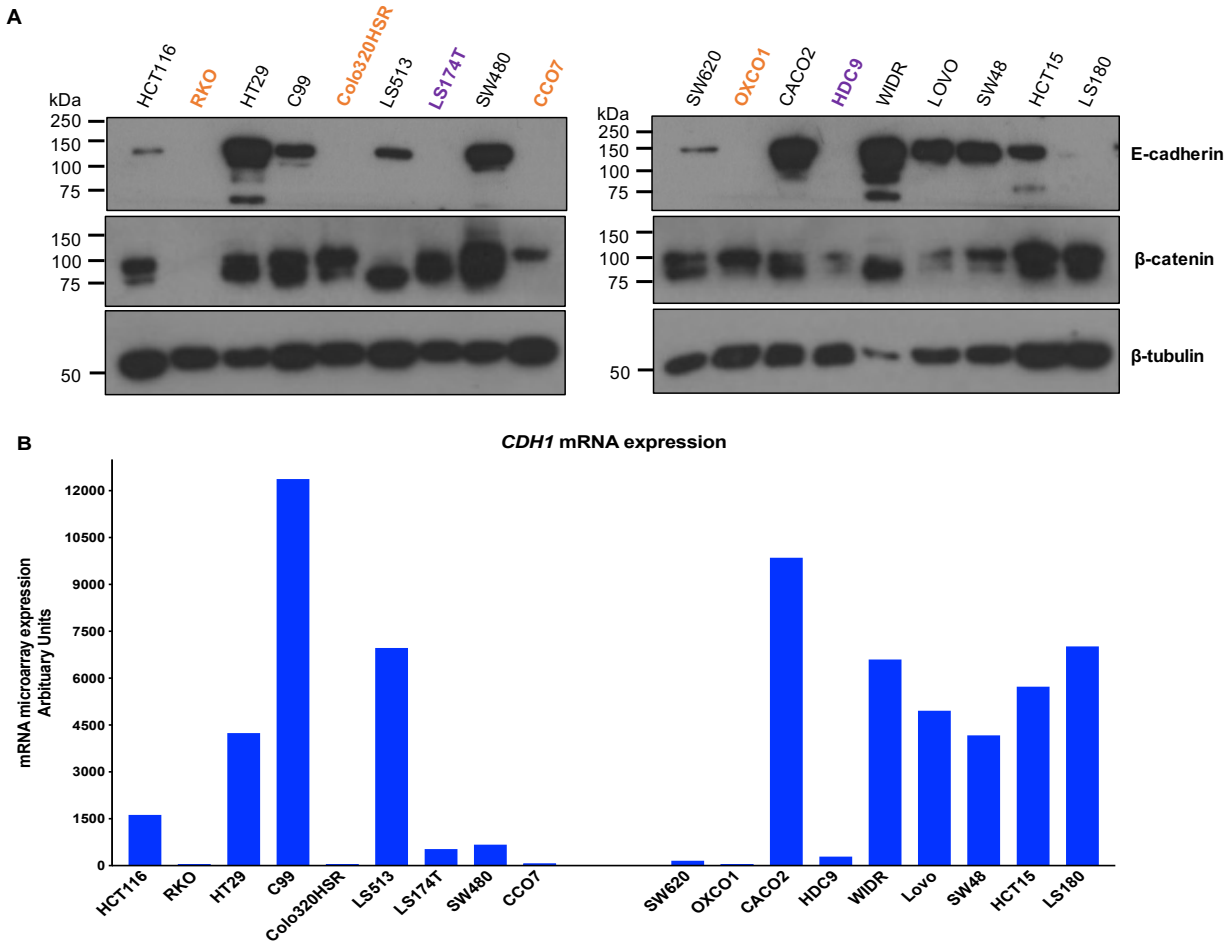


Figure 3.10 E-cadherin expression in a panel of CRC cell lines
A) E-cadherin protein expression in different CRC cell lines, analysed by Western Blot. Total cell lysates (30 µg / lane) were separated on a 10% SDS gel. The membrane was probed using primary antibodies against E-cadherin (Cell Signalling, 1:1000) and β-tubulin (Sigma, 1:5000). EMT cell lines are highlighted in orange, cell lines with two different heterozygous E-cadherin mutations in purple. A shorter time exposure would have benefited the interpretation of protein expression across cell lines. **B**) mRNA microarray expression data for the cell lines analysed in A). Note the following cell lines derived from the same patients: HT29 - WIDR, LS174T - LS180, SW480 - SW620. kDa: kilo Daltons.

.

3.3 Discussion

β-catenin is a key mediator of the Wnt signalling pathway and the expression levels are likely to have effects on the transcriptional activation. Here we characterised a panel of CRC cell lines for their β-catenin gene mRNA and protein expressions. Microarray expression data show that β-catenin mRNA is expressed in all cell lines, though at varying levels (Figure 3.1). When the protein expression was assessed by WB, different levels of β-catenin expression were observed. Most notably, we could not detect any expression of the protein in RKO cells (Figure 3.2A), even though β-catenin mRNA was highly expressed in this cell line (Figure 3.2B and C). These results were confirmed by IF (Figure 3.3). This is in accordance with previous work by Li et al. (2014) and Tanaka et al. (2017), where no β-catenin protein expression could be detected in RKO cells by WB. As the RKO cell line does not harbour any APC or β-catenin mutations, β-catenin is rapidly degraded (Li et al. 2014). This would also explains the absence of detectable Wnt activity measured by the TOPflash assay by us (Figure 3.4) and others (da Costa et al., 1999; Qu et al., 2016).

The analysis of subcellular β-catenin localisation in the panel CRC cell lines showed no association between APC, β-catenin, p53, BRAF or KRAS mutation status with the β-catenin localisation in cells. Rosin-Arbesfeld et al. (2003) suggested that the location of the APC mutation has an influence on β-catenin localisation in a panel of CRC cell lines. Cell lines with truncating mutations in the MCR and lacking the nuclear export signal (NES) immediately behind the MCR showed varying degrees of nuclear β-catenin and APC staining, while APC wild-type cell lines did not (Rosin-Arbesfeld et al., 2003). When we specifically analysed our β-catenin localisation data with cell lines with APC mutations inside and outside the APC mutation cluster region, we did

not find any significant correlation (Appendix A.5). Furthermore, some discrepancies in the β-catenin localisations between the two studies became apparent. While we observed nuclear β-catenin accumulation in LS174T cells, Rosin-Arbesfeld et al. (2003) described efficient nuclear exclusion of the protein in this cell line. Similarly, while we obtained strong membrane staining for LOVO cells, their study showed nuclear staining in this cell line. On the other hand, their study confirms the strong nuclear β-catenin localisation in COLO320 cell lines and clear membrane staining in HT29 and HCT116 cells.

Some studies showed that the confluency of the cells is a decisive factor for β-catenin localisation (Brabletz et al., 2001; Dietrich et al., 2002), as tight cell adherens junctions are formed, involving intracellular β-catenin attached to E-cadherin. When we grew SW480 cells at increasing confluence and clearly visible cell-cell contact, we only rarely observed membranous β-catenin staining in the cells (see Figure 3.3 and Appendix A.3). This finding stands in line with immunocytochemistry data in SW480 and SW620 cells, where little membrane staining for β-catenin was observed in either dispersed or clustered cells (El-Bahrawy et al., 2004). In the same study, HCT116, HT29 and CACO2 cells showed membrane β-catenin staining at points of cell-cell contact. Very faint or no β-catenin signal was obtained in sparsely growing cells. Similar results are seen in our study, where β-catenin localisation was observed at sites of cell-cell interactions and not on the "free borders" of the cells. This staining pattern was frequently observed in membranous β-catenin staining in our study. For example, CX1 cells show strong β-catenin membrane staining at points of cell contact, with weaker staining at the

membranes without contact (Figure 3.5). Further similar examples are the β-catenin staining in HCT15, HCT116, RW2892, SNUC2B and WIDR cell lines (Appendix A.3).

The microarray expression analysis of cell lines with membrane or nuclear β-catenin showed a clear negative association with E-cadherin (Table 3.3). When E-cadherin is present, it is able to sequester β-catenin to the cell membrane, thus escaping the destruction complex and subsequent protein degradation. This E-cadherin-β-catenin complex can be observed independently of the APC mutation status. For example, the APC-mutant cell lines CX1 and CACO2 show clear β-catenin membrane staining, while APC wild-type HCT116 cells show some degree of membrane localisation as well.

An important role of E-cadherin in the β-catenin subcellular localisation has previously been postulated. Orsulic et al., (1999) showed that E-cadherin binding can prevent the nuclear localisation of β-catenin and subsequent β-catenin/LEF1-mediated transactivation. The nuclear localisation of β-catenin in E-cadherin -/- embryonic stem cells was prevented by the transient expression of wild-type E-cadherin. The mutated E-cadherin construct E$\Delta\beta\alpha$C lacking the β-catenin binding domain (Δ carboxy-terminal 70 amino acids of E-cadherin) did not have the same effect. Similar effects were also shown in SW480 colorectal cancer cells (Orsulic et al., 1999). Furthermore, a different study showed significant growth-inhibition of SW480 cells after expression of wild-type E-cadherin (Gottardi, Wong, & Gumbiner, 2001). This inhibitory effect was not seen in cells with an E-cadherin construct lacking the β-catenin binding site.

More recently, E-cadherin has been described as a “sink” for β-catenin by binding even mutated β-catenin and preventing it from translocating to the nucleus and performing its downstream signalling functions (Huels et al., 2015). In mouse knock-out models, it was shown that, especially when there are β-catenin activating mutations, the reduction of E-cadherin aided malignant transformation.

The current preliminary immunofluorescence staining observations in a panel of colorectal cancer cell lines supports the significance of the dual role of β-catenin as key Wnt pathway signal mediator, as well as important interaction partner at the cell adhesion junction complex. While Wnt activity is most commonly associated with APC mutations leading to nuclear β-catenin and transcriptional activation, the crucial involvement of E-cadherin for the subcellular localisation of β-catenin is highlighted here. The large panel of CRC cell lines covers a spectrum of endogenous E-cadherin expression levels and mutations, reflecting a wide range of genetic backgrounds. More importantly, some of our preliminary experiments suggest that while EMT is characterised by low or absent E-cadherin expression, nuclear β-catenin localisation is associated to the lack of E-cadherin expression. The non-EMT LS174T cell line is a good example for this, with no E-cadherin expression and nuclear β-catenin localisation. HDC9 also carries two E-cadherin mutations and does not have E-cadherin protein expression (Figure 3.10 and Olymbia Dikomitou, DPhil Thesis, Bodmer Lab). It would be of interest to assess the β-catenin localisation by IF in this cell line to confirm the hypothesis that the lack of E-cadherin expression results in nuclear β-catenin. Furthermore, the β-catenin staining in LS180 cells should be repeated. The β-catenin localisation scoring in this cell line was without consensus, largely due to diffuse staining and insufficient image magnification. LS180 is derived

from the same patient as LS174T but does express E-cadherin. This would serve as a good control for the hypothesis that E-cadherin is a key driver of nuclear β-catenin localisation.

Several cell lines, namely SW620, SW480, COLO320DM, COLO320HSR, RKO, C2BBe1, LOVO and LS174T, were repeatedly stained for β-catenin to confirm the observed results. In addition, immunofluorescence staining was performed without the EpCAM staining (β-catenin alone) to validate the observed β-catenin localisation is not a signal leakage from the other fluorescence channels. Furthermore, a different antibody (β-catenin anti-mouse, BD Technology) against the C-terminal region of β-catenin was used for some of the immunofluorescence staining to confirm the previously obtained β-catenin localisation results using the rabbit antibody against N-terminal β-catenin. If time had permitted, the β-catenin staining should have been repeated in more biological replicates, as many cell lines were only imaged in a single experiment. In addition, low and high cell density samples should have been assessed in the panel of cell lines to control for the potential change in β-catenin localisation upon cell-cell contact (Dietrich et al., 2002). One major drawback of the initial results presented in this chapter is the imaging quality and lack of quantifiable results. The imaging should be performed using confocal microscopy to allow for clearer definition of intracellular localisation. This would have allowed for mid-nuclear images to be taken, which reduces the chance that the nuclear signal was due to β-catenin in the overlying cytoplasm. The use of 3D imaging techniques and appropriate image analysis tools would have allowed for proper quantification of the β-catenin localisation throughout the cells

Nuclear β-catenin is associated with high β-catenin-TCF-mediated transactivation (Cong et al., 2003). It would be of interest to investigate if the β-catenin localisation in this study correlates with the baseline Wnt signal activation in these cell lines. In this case, it would suggest that cell lines with nuclear β-catenin localisation, such as LS174T, COLO320HSR and COLO320DM exhibit higher Wnt pathway activation. This could be assessed using the TOPflash assay across the panel of the tested cell lines. Previous studies indicated an inhibition of the Wnt signalling pathway upon E-cadherin overexpression in Drosophila and Xenopus (Fagotto et al., 1996; Sanson, White, & Vincent, 1996), as well as SW480 CRC cells (Gottardi et al., 2001). Initial experiments using SW480, HCT116 and RKO cells do align with the hypothesis of a link between β-catenin localisation and Wnt-mediated transactivation (Figure 3.4). In contrast, other studies did not find any association between Tcf-mediated transactivation of the Wnt pathway and the expression or mutation status of E-cadherin in a panel of breast, gastric and pancreatic cancer cell lines (Caca et al., 1999; van de Wetering et al., 2001). In light of these conflicting findings, it would be of interest assess the constitutive Wnt-activation in the panel of CRC cell lines. However, as the transfection efficiencies greatly vary between cell lines, transfection protocols would need to be adapted for each cell line, which might make the comparison between cell lines more difficult. Furthermore, while nuclear β-catenin is an important factor in the Wnt activation, expression levels of other members of the transcription factor complex, such as TCF4 and BCL9, vary between cell lines and are likely to affect the level of β-catenin-dependent Wnt pathway activation.

Further experiments to help elucidate the link between E-cadherin and Wnt signalling in CRC cell lines could include the siRNA knock-down of E-cadherin, followed by

TOPflash assessments and β-catenin localisation visualisation by IF. Furthermore, it would be of interest to assess the levels of active and phosphorylated pools of β-catenin using specific antibodies for each β-catenin population. It has previously been described that E-cadherin is able to promote N-terminal phosphorylation of β-catenin, and thus reducing the levels of the free signalling (active) form of the protein (Maher et al., 2009).

The preliminary results presented in this chapter support the hypothesis of an association between E-cadherin and β-catenin subcellular localisation in CRC cell lines. The fact that low E-cadherin expression is a hallmark of EMT may cause the nuclear β-catenin phenotype in the EMT cell lines. These data open a line for further investigations to elucidate the exact impact of E-cadherin expression levels and mutation status on the Wnt pathway activation.

Chapter 4

In vitro studies of β-catenin/BCL9 inhibitors in colorectal cancer cell lines

CHAPTER 4: *IN VITRO* STUDIES OF β-CATENIN/BCL9 INHIBITORS IN COLORECTAL CANCER CELL LINES

4.1 Introduction

4.1.1 Inhibitors of the β-catenin-BCL9 interaction

As the BCL9-β-catenin interaction is the penultimate step in the Wnt signalling pathway in the nucleus, this interaction has been described as a potential target to inhibit WNT signalling (Cui et al., 2018; Takada et al., 2012).

Efforts to inhibit the β-catenin-BCL9 interaction have included the identification of the natural compound carnosic acid (CA) through a high-throughput screen (de la Roche et al., 2012). In this study, 25 μM CA inhibited Wnt target genes such as *AXIN2* and the TOPflash Wnt reporter assay by over 50% in SW480 cells compared to untreated controls. CA can be found in high amounts in rosemary (*Roasmarinus officinalis*) and is known for its antioxidative properties (Loussouarn et al., 2017). However, its catechol structural core reacts with protein nucleophiles and is known as a pan-assay interference compound (PAINS) (Baell, 2016; Baell & Walters, 2014; Hoggard et al., 2015) and is likely to interfere with many biological activities.

In another study Triazole-Stapled BCL9 α-helical peptides (Kawamoto et al., 2012) and hydrocarbon stapled BCL9 peptides (Takada et al., 2012) have both been designed in an attempt to inhibit the Wnt signalling pathway. The inhibition of the BCL9-β-catenin interaction by the hydrocarbon stapled BCL9 peptide reduced the Wnt-specific reporter assay by close to 60% in Colo320 and HCT116 colorectal

cancer cells, as well as leading to a decreased expression of various WNT target genes including *Axin2*, *c-myc* and *LEF1* (Takada et al., 2012).

Recently, the laboratory of Dr Haitao (Mark) Ji at the H. Lee Moffitt Cancer Centre & Research Institute (Tampa, USA) has designed and synthesised small molecules targeting the β-catenin-BCL9 binding hotspot region in ArmR1 (Hoggard et al., 2015; Wisniewski et al., 2016). We have received three of their compounds to be tested on a panel of colorectal cancer (CRC) cell lines at the Bodmer lab, as will now be described.

4.1.2 Characteristics of the β-catenin – BCL9 inhibitors

ZYQ-1-74, ZYQ-2-165 and JW-02-80 were provided as inhibitors of the β-catenin – BCL9 interaction, while JW-1-78 was given to us as a control compound and thought not to affect the protein-protein interaction. The Ji Lab provided us with their previous experimental results and information on the β-catenin – BCL9 inhibitors, including MTS cell growth inhibition assays and TOPflash data (inhibition of the Wnt pathway). These data are summarised in Table 4.1 and the chemical structures of the compounds can be found in Appendix B.1.

		ZYQ-1-74	ZYQ-2-165	JW-02-80	JW-1-78 (control)
Biochemical K_i (Alpha Screen Assay)		1.4 μM	1.6 μM	5.2 μM	<500 μM
MTS cell growth inhibition assay (IC_{50})	**SW480**	2 μM	18 μM	22 μM	-
	HCT116	7.5 μM	27 μM	26 μM	-
	A549	9.4 μM	92 μM	300 μM	-
TOPflash (IC_{50})	**HEK293**	6.2 μM	12μM	52% inhibition at 25 μM	-
	SW480	1.2 μM	-	-	-
FOPflash	**HEK293**	58% inhibition at 12.5 μM	No inhibition at 200 μM	No inhibition at 100 μM	-

Table 4.1 Characteristics of β-catenin – BCL9 inhibitors
Summary of the previous experimental data on the β-catenin – BCL9 inhibitors from the Ji Lab. The indicated compounds were tested on SW480 and HCT116 colorectal cancer cell lines (WNT active) and A549 non-small cell lung cancer cells (Wnt-independent). Cell-free assay AlphaScreen™: Amplified Luminescent Proximity Homogeneous Assay, commonly used for High-Throughput screening for small molecules (Yasgar, Simeonov, & Coussens, 2016), MTS: MTS tetrazolium cell proliferation assay, TOPflash and FOPflash: see Materials & Methods chapter for detailed description.

4.2 Aims

The β-catenin-BCL9 inhibitors obtained from the Ji lab were tested on a panel of 28 CRC cell lines using the Sulforhodamine B (SRB) Assay, which is used as a measure of cytotoxicity screening (Skehan et al., 1990). The aim was to assess if the small molecules exhibit any differential activity in cell lines dependent on mutation and expression data available in the lab.

It should be noted that after the completion of the experiments for this chapter, the Ji lab published their experimental data for the compounds ZYQ-1-74 and ZYQ-2-165 (Zhang et al. 2018). The results presented here were based on the initial unpublished data that we have received (Table 4.1) and were then compared and discussed in the light of the publication in the Discussion part of this chapter (section 4.4).

4.3 Results

4.3.1 SRB Assays using the ZYQ-1-74 inhibitor

The compound ZYQ-1-74 was tested on a panel of 28 CRC cell lines with different APC and β-catenin mutation statuses (Table 3.1). Cells were treated with increasing concentrations of ZYQ-1-74 and JW-1-78 (control compound) and incubated for three cell-doubling times (DTs). DTs are well characterised in our laboratory and differ from cell line to cell line (Bodmer lab, unpublished data). The IC_{50}s for each cell line are summarised in ascending order in Table 4.2**.** Representative dose-response curves of ZYQ-1-74 and JW-1-78 (control) for all APC and β-catenin mutation statuses are visualised in Figure 4.1. ZYQ-1-74 inhibited cell viability in all 28 cell lines tested, with an IC_{50} range of 2.2 - 9.1 μM (Table 4.2). This IC_{50} range is comparable to previous data from the Ji lab (IC_{50} = 2 μM in SW480). We found an IC_{50} of 3.4 μM ZYQ-1-74 for SW480 cells. At 10 μM, visual inspection showed that no viable cells were present in any of the cell lines. Various duplicate cell lines with different mutational profiles and gene expression levels were tested in the experiment to assess any potential differential drug responses. Duplicate cell lines include HT29 - WIDR - CX1, SW620 - SW480, DLD1 - HCT15, GP2D - GP5D and COLO320HSR - COLO320DM.

Cell line	IC_{50} ZYQ-1-74 (μM)	Cell line	IC_{50} ZYQ-1-74 (μM)
HT29	2.203	**C10**	5.162
SW620	2.377	**LOVO**	5.245
CCO7	2.937	**PMFKo14**	5.396
SW48	3.021	**GP5D**	5.637
OXCO1	3.083	**HCT15**	5.653
WIDR	3.084	**CC20**	5.66
HCT116	3.157	**LS180**	5.715
CX1	3.244	**SNUC2B**	5.786
SW480	3.418	**LS174T**	6.049
CAR1	4.439	**VACO5**	6.114
DLD1	4.813	**RKO**	6.434
LS411	4.839	**COLO320HSR**	6.532
GP2D	4.959	**HT55**	6.648
C2BBe1	5.134	**COLO3320DM**	9.141

Table 4.2 IC_{50} values of 28 CRC cell lines in response to ZYQ-1-74
IC_{50} values were derived from SRB assays and determined using Prism 7. Cell lines are ranked by increasing IC_{50} values. Colours indicate cell lines from the same tumour. For ZYQ-1-74 SW480, the number of replicates was n = 5, SW620 n = 2, HCT116 n = 3, all other cell lines n = 1.

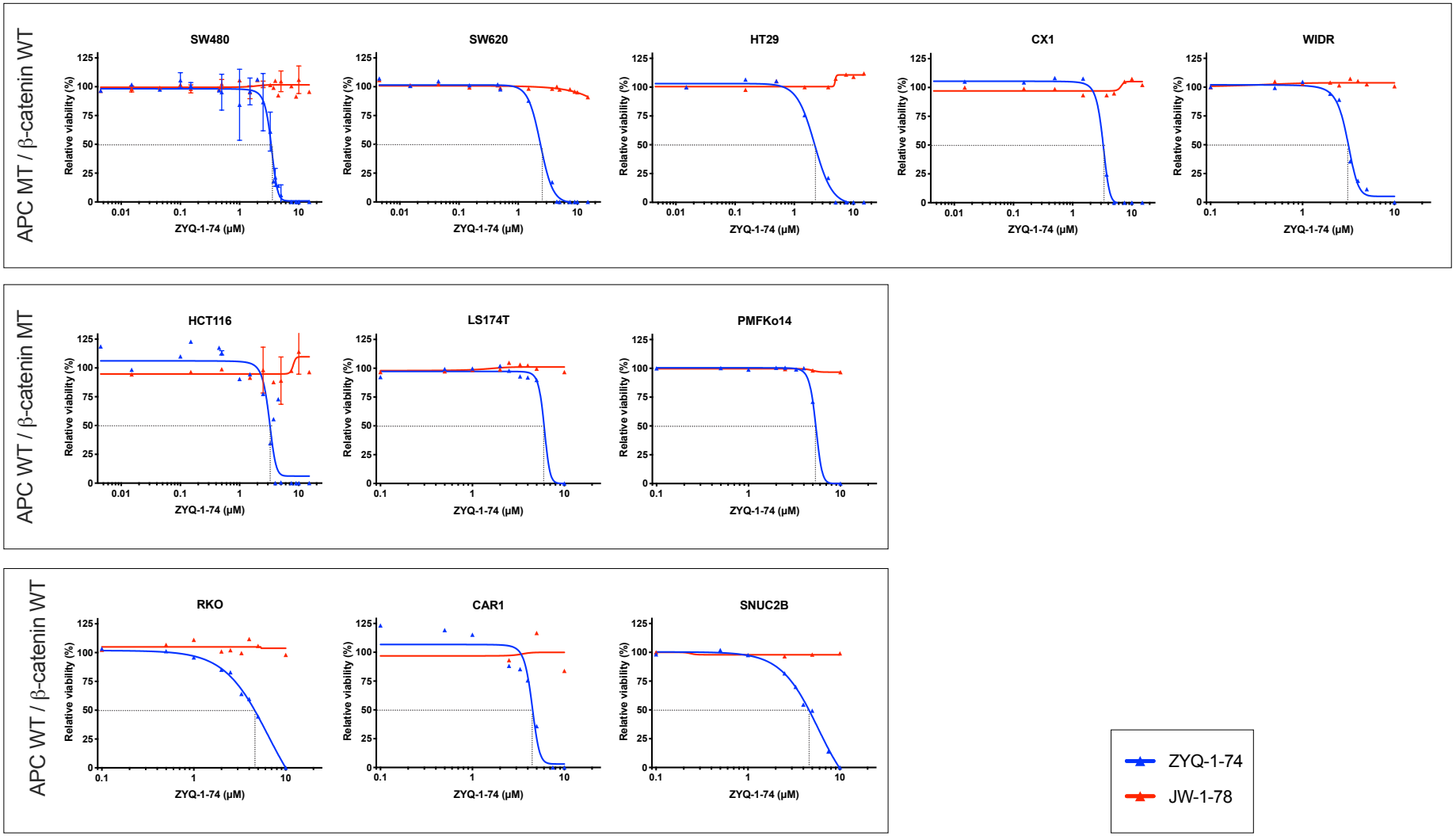


Figure 4.1 Representative dose-response curves to ZYQ-1-74 and JW-1-78.
Representative dose-response curves for APC MT/ β-catenin WT cells (SW480, SW620, HT29, CX1, WIDR), APC WT/ β-catenin MT cells (HCT116, LS174T, PMFKo14) and APC WT/ β-catenin WT cells (RKO, CAR1, SNUC2B). Cell lines were treated with increasing concentrations of ZYQ-1-74 (blue) and JW-1-78 control (red) for three cell doubling times. An SRB assay was performed to assess the effect on cell viability. SW480 n= 5, SW620 n=2, HCT116 n=3, all other cell lines n=1.

4.3.2 SRB Assays using ZYQ-2-165 and JW-2-80

Based on initial results from the Ji lab, the compounds ZYQ-2-165 and JW-2-80 exhibited different inhibitory properties and resulted from a different chemical series (Wisniewski et al., 2016; Zhang et al., 2018). ZYQ-2-165 and JW-2-80 were tested on a small panel of CRC cell lines, including SW480, SW620, HCT116, HT29 and CX1. The dose-response curves to these compounds are shown in Figure 4.2. According to previously obtained data from the Ji lab, ZYQ-2-165 treatment resulted in IC_{50}s of about 18 μM and 27μM were expected for SW480 and HCT116, respectively. For the compound JW-2-80, IC_{50}s of 22 μM to 26 μM for the same cell lines were predicted. However, in our hands, the compounds resulted in much higher IC_{50}s over 100 μM (Figure 4.2).

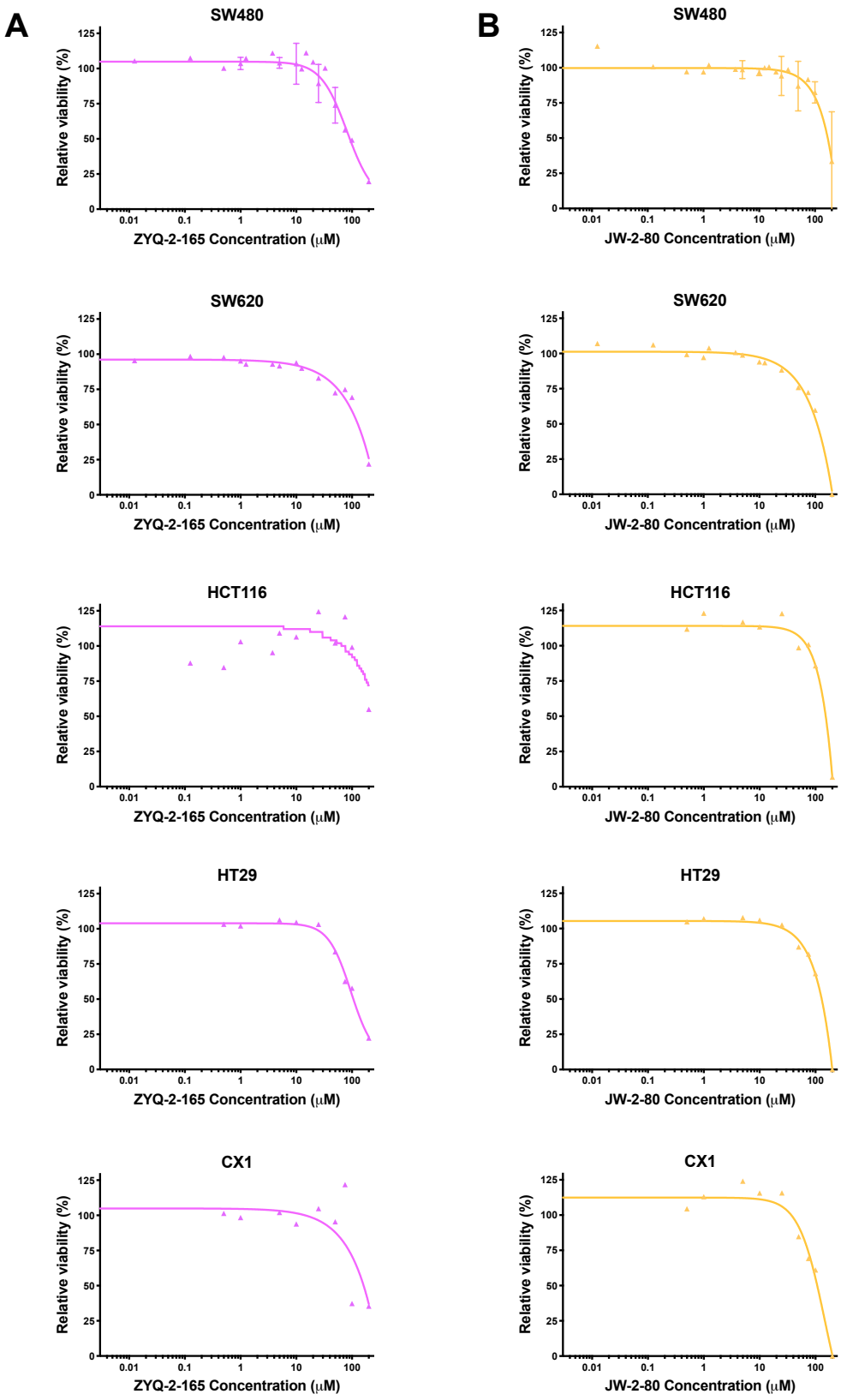


Figure 4.2 Dose-response curves to ZYQ-2-165 and JW-2-80
SW480, SW620, HCT116, HT29 and CX1 cell lines were treated with **A**) ZYQ-2-165 and **B**) JW-2-80 for three cell doubling times and the SRB assay was performed. For ZYQ-2-165: SW480 n=3, SW620 n=2, HCT166 n=2, all other cell lines n=1. For JW-2-80: SW480 n=3, SW620 n=2, all other cell lines n=1.

4.3.3 ZYQ-2-165 and JW-2-80 inhibitors are affected by albumin

As seen in Figure 4.2, there is a striking discrepancy between the experimental results we obtained in our lab with the compounds ZYQ-2-165 and JW-2-80 compared to the data received from the Ji lab (Table 4.1). The expected IC_{50}s for ZYQ-2-165 and JW-2-80 in SW480 were 18 μM and 22 μM, respectively, based on their previously performed MTS cell growth inhibition assay. Upon discussion with our collaborators, we discovered that the compounds were previously tested in growth medium supplemented with 1% fetal bovine serum (FBS) as compared to the 10% FBS we use in our standard media. This raised the question of whether the compounds were affected by the serum concentration in the growth medium. FBS contains albumin, an abundant plasma protein (Hortin, Sviridov, & Anderson, 2008), which is known to bind to various different drugs, influencing their pharmacokinetics and ultimately impacting their efficacy both *in vivo* and in standard tissue culture media that contain 10% FBS (Vallner, 1977). In order to test the hypothesis that the compounds in this study might be affected by the FBS concentration in the growth medium, SW480 cells were grown and treated with the inhibitors ZYQ-1-74, JW-2-80 and ZYQ-2-165 in 10% FBS, 5% FBS, 1% FBS and 1% FBS supplemented with 1% albumin. The control compound JW-1-78 and DMSO treatments were used as control conditions.

The compound effects on SW480 cells in different FBS concentrations were imaged after four days of drug treatment (Figure 4.3). ZYQ-2-165 caused visible cell death of SW480 cells in 1% FBS, which did not occur in the 10% FBS, 1% FBS + 1% albumin or DMSO and JW-1-78 control groups. While 100 μM ZYQ-2-165 had to be used to achieve 50% cell killing in 10% FBS medium, the IC_{50} dropped to 47 μM in 1% FBS medium (Figure 4.4D). In contrast, the FBS concentration in the growth medium did

not affect the JW-2-80 inhibitor effect, with an undetermined IC_{50} (>100 μM) in both 10% and 1% FBS medium (Figure 4.3 and Figure 4.4C). Reducing the FBS concentrations in the ZYQ-1-74 treatment group caused a minor reduction in IC_{50} from 3.21 μM to 1.67 μM at 10% and 1% FBS, respectively (Figure 4.4B).

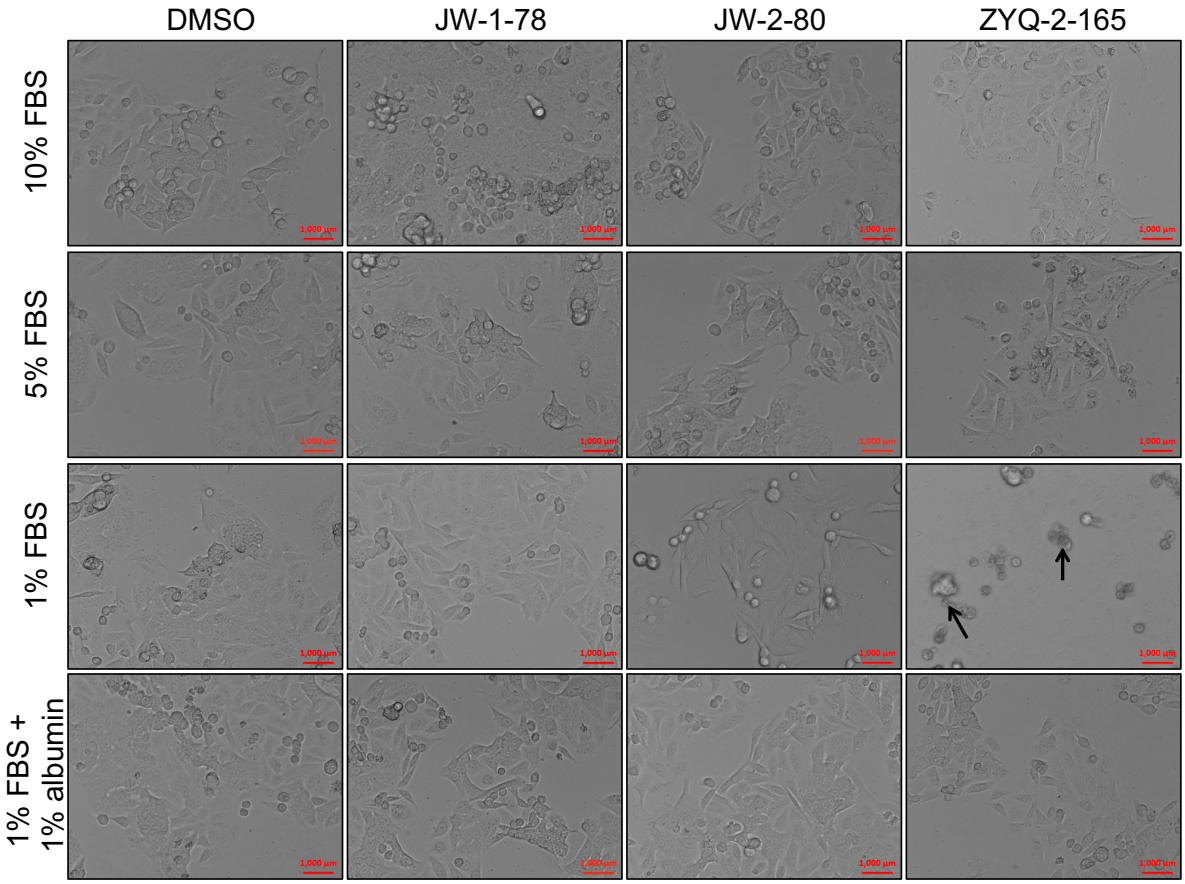


Figure 4.3 Bright field images of SW480 cells in response to JW-2-80 and ZYQ-2-165 in different growth medium conditions
Representative images of SW480 cells grown in 10%, 5%, 1% FBS and 1% FBS + 1% albumin (BSA, gibco by Life Technologies) treated with 50 μM of the indicated inhibitor. Bright field images were taken after four days of treatment to visualise the morphology of the cells (20X magnification, 0.4 NA). SW480 cells grown in 1% FBS treated with ZYQ-2-165 are dying (black arrows), while this effect is not seen when grown in 1% FBS + albumin. The effect is not seen with the inhibitor JW-2-80 nor the control compound JW-1-78. Scale bars: 1000 μm.

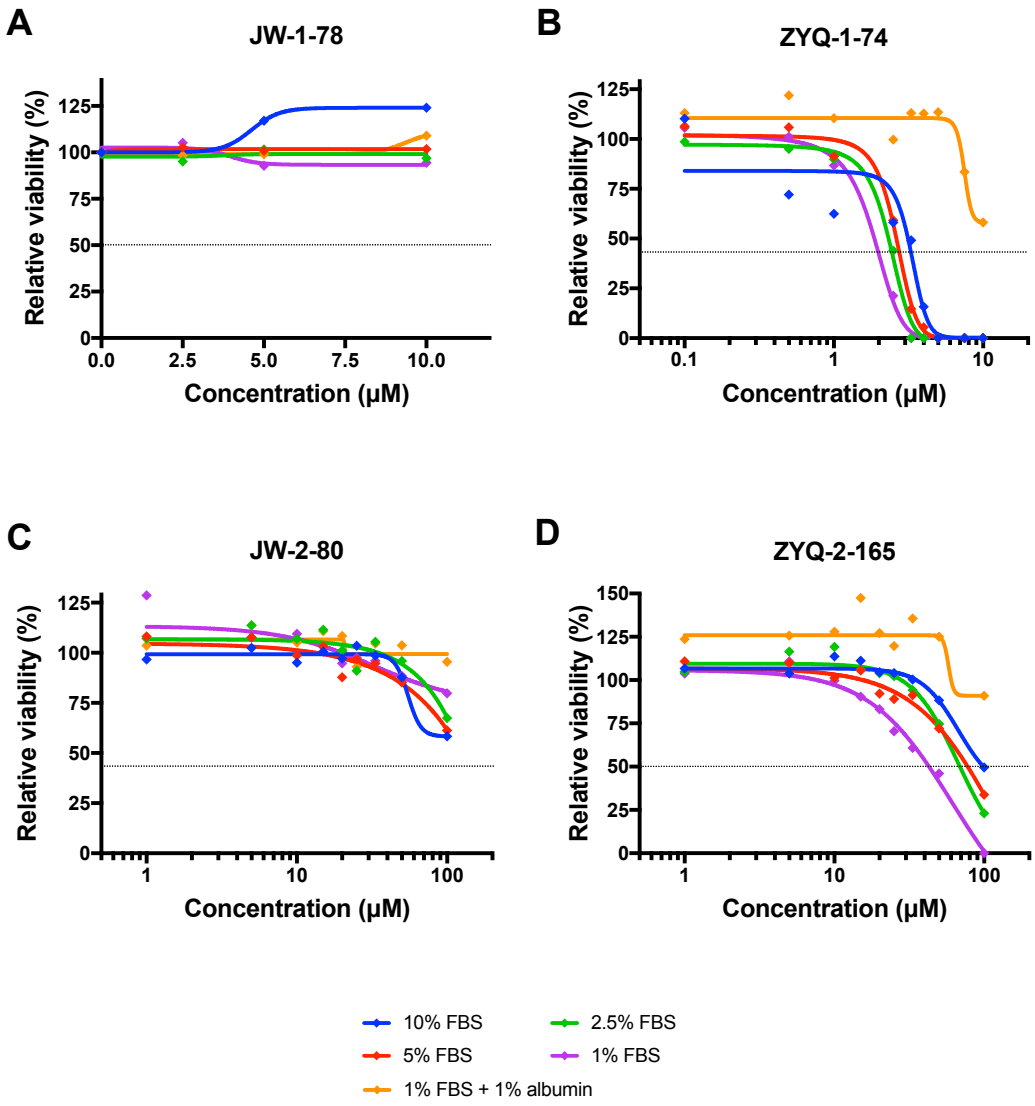


Figure 4.4 Dose-response curves to compounds JW-1-78, ZYQ-1-74, JW-2-80 and ZYQ-2-165 at different FBS concentrations
SW480 cells were treated with increasing concentrations of the compounds **A**) JW-1-78 (control), **B**) ZYQ-1-74, **C**) JW-2-80 and **D**) ZYQ-2-165 in different FBS concentrations (10%, 5%, 1%) or 1% FBS + 1% albumin. The SRB assay was performed in triplicate wells in a single experiment after 5 days (three DTs of SW480).

Overall, we showed that the FBS concentration in the growth medium affects the ZYQ-2-165 treatment, but this result was still not comparable with the experimental data obtained by the Ji lab with an IC_{50} of 18 μM in SW480 cells. Given these discrepancies in the efficacies of the compounds, we decided to not further evaluate the β-catenin – BCL9 inhibitors ZYQ-2-165 and JW-2-80.

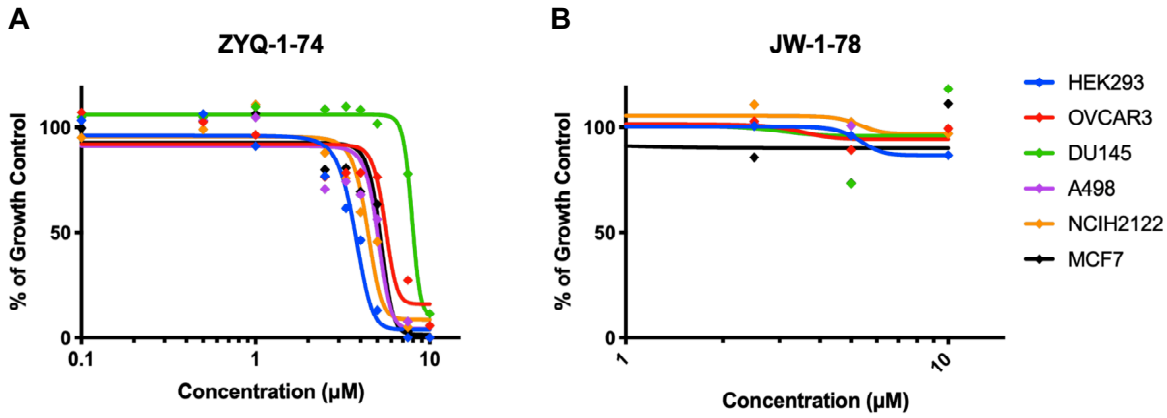
4.3.4 ZYQ-1-74 treatment of non-CRC cell lines

In order to assess the specificity of ZYQ-1-74 for the Wnt pathway, the compound was tested in cell lines originating from different tissues and fibroblasts (Table 4.3). HEK293 cells have low basal Wnt activity and need the addition of Wnt ligands to elicit a Wnt-signal (Newnham et al., 2015; Upadhyay et al., 2008), while other cell lines, such as MCF7, OVCAR3 and DU145, have been described as Wnt-dependent (Guturi et al., 2012; Rask et al., 2003; Schlange et al., 2007).

Cell line	Tissue of origin
HEK293	Human embryonic kidney
DU145	Prostate cancer
OVCAR3	Ovarian cancer
NCIH2122	Lung cancer
A498	Kidney cancer
MCF7	Breast cancer
CCD-18Co	myofibroblasts
WFB	fibroblasts
JB	fibroblasts

Table 4.3 Non-CRC cell lines used in experiments
List of cell lines from various different origins that were treated with the compound ZYQ-1-74.

As seen in Figure 4.5A, ZYQ-1-74 killed all cell lines from various different tissues at comparable concentrations to these for the CRC cell lines. The control compound JW-1-78 did not have any effect on any of the cell lines (Figure 4.5B). The IC_{50} values of ZYQ-1-74 are listed in Figure 4.5C.



C

Cell line	IC_{50} – ZYQ-1-74 (μM)
HEK293	3.7
OVCAR3	5.5
DU145	7.8
A498	5.0
NCIH2122	4.3
MCF7	5.2

Figure 4.5 Dose response curves of ZYQ-1-74 and JW-1-78 in cell lines from different tissues.
HEK293, OVCAR3, DU145, A498, NCIH2122 and MCF7 cell lines were treated with increasing concentrations of **A**) ZYQ-1-74 and **B**) JW-1-78. **C**) Table of ZYQ-1-74 IC_{50}s. All cell lines n = 1.

In order further assess the β-catenin-BCL9 interaction specificity of the compound ZYQ-1-74 in non-cancer cell lines, three fibroblast cell lines were treated with the inhibitor. Microarray data available in our lab showed high mRNA expression of β-catenin in the fibroblast cell lines CCD18-CO, JB_Fibro and WFB_Fibro, while BCL9 mRNA expression was very low (Figure 4.6).

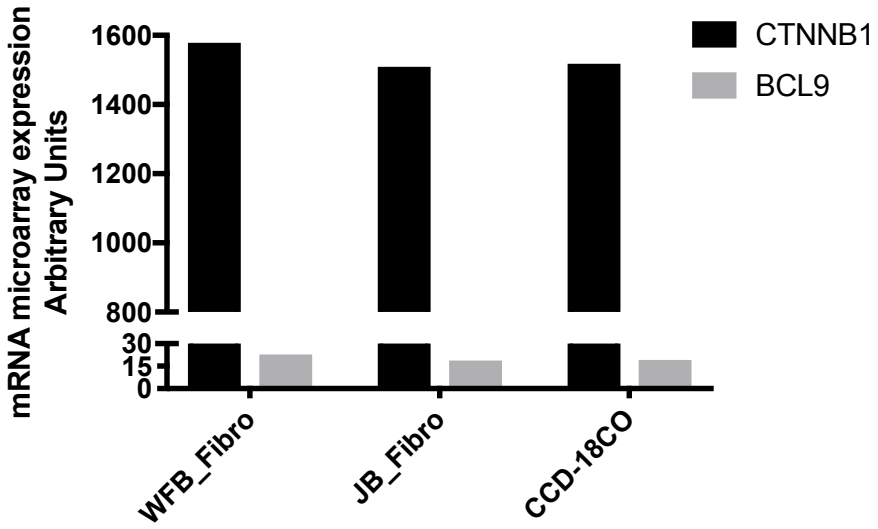


Figure 4.6 Microarray data for *β-catenin* and *BCL9* mRNA expression in fibroblasts
mRNA expression levels of β-catenin (*CTNNB1*) and *BCL9* in the fibroblast lines WFB, JB and CCD18-CO. β-catenin was abundantly expressed in all three fibroblast cell lines, while BCL9 had very low expression. mRNA expression in fibroblasts measured by the Affymetrix Human Genome U133 Plus 2.0 microarray (Hsia et al., 2016).

CCD18-CO, JB_Fibro and WFB_Fibro fibroblast cell lines were treated with the ZYQ-1-74 inhibitor and JW-1-78 control in growth medium supplemented with 10% FBS for 6 days. Viable cells were visually assessed by Calcein-AM staining. As seen in Figure 4.7, all three fibroblast cell lines were killed with increasing ZYQ-1-74 concentrations. No viable cells were visible at 5 μM ZYQ-1-74 treatment. This effect was not seen in cells treated with 10 μM of the control compound JW-1-78, which is comparable to the DMSO control treatment with healthy and growing fibroblasts.

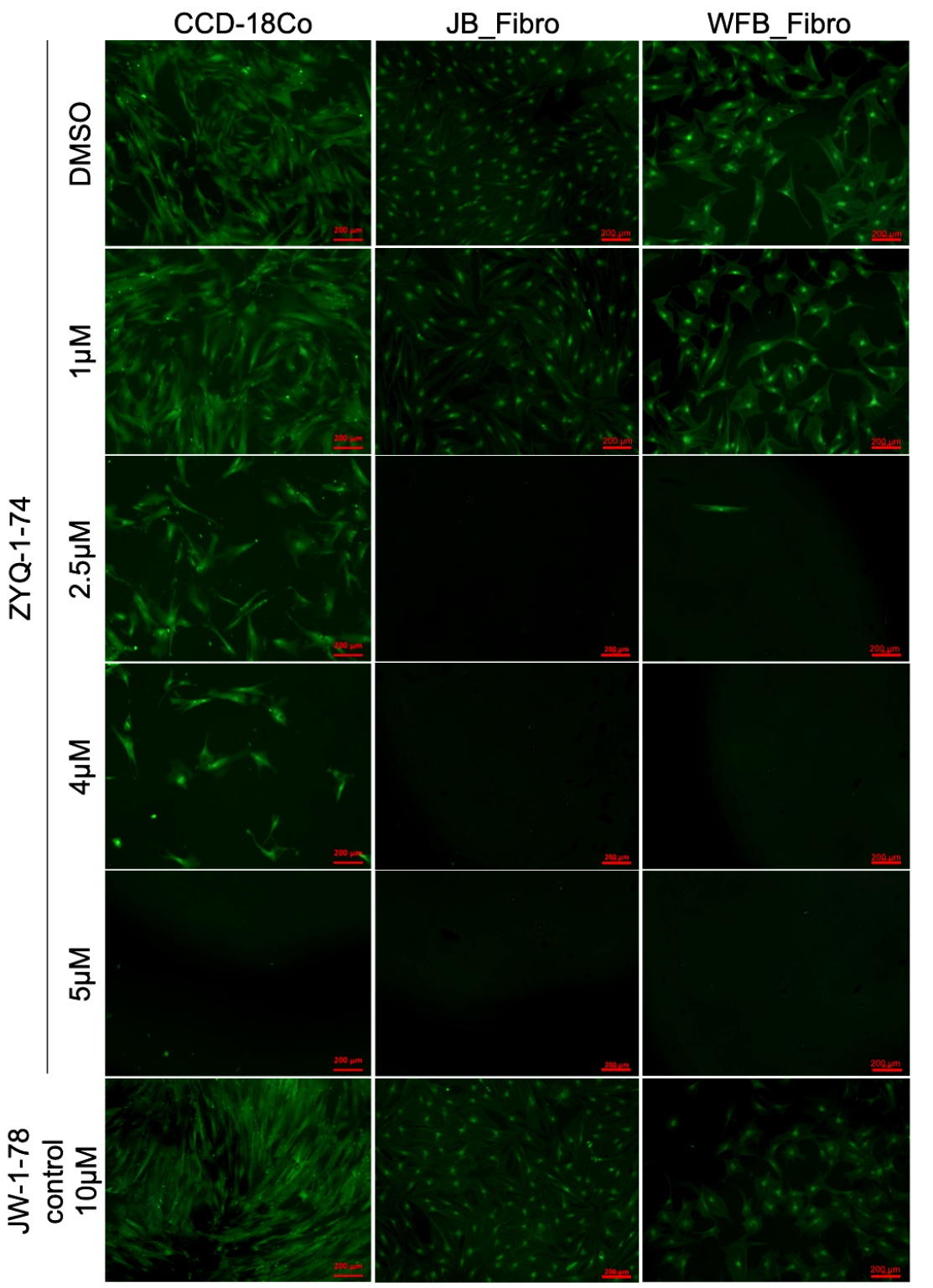


Figure 4.7 Calcein-AM staining of CCD18-CO, JB and WFB fibroblasts after ZYQ-1-74 treatment
The fibroblasts lines CCD18-CO, JB and WFB were treated with increasing concentrations of ZYQ-1-74 or JW-1-78 as control for 6 days in 10% FBS. The medium was removed and replaced with medium without FBS and Calcein-AM (1:1000) to assess the viability of the cells. The cells were incubated for 30 min at 37°C and imaged (green) at a magnification of 5X, 0.16 NA. Scale bars: 200 µm.

4.3.5 Assessment of WNT target genes upon β-catenin – BCL9 inhibitor treatment

In order to assess the Wnt pathway specificity of the given compounds, Wnt target genes were analysed following drug treatment. SW480 cells were treated with ZYQ-1-74 and ZYQ-2-165, as well as the control compound JW-1-78. The Wnt targets c-myc and Cyclin D1 were assessed by WB (Figure 4.8). Our previous experiments showed that ZYQ-1-74 has an IC_{50} of 3.4 μM for SW480 cells in 10% FBS cell culture medium (Table 4.2). If the compounds are specific to the Wnt pathway, we would expect a reduced expression of Wnt target genes at concentrations below the IC_{50}. The protein expression of the Wnt-target gene *c-myc* was not inhibited by ZYQ-1-74, while the expression of Cyclin D1 only started to be affected at 4 μM and abolished at 8 μM. In contrast, ZYQ-2-165 did not inhibit the protein expression of Cyclin D1, even at concentrations of 80 μM. In fact, the expression of Cyclin D1 seemed to be upregulated upon ZYQ-2-165 treatment. The c-myc expression was inhibited dose-dependently at 40 μM and 80 μM ZYQ-2-165. However, the same effect was observed in cells treated with the control compound JW-1-78, which should not have an effect on the Wnt pathway. It should be noted that this experiment was only performed once and if time and drug resources had permitted, the experiment would have been repeated to confirm the results.

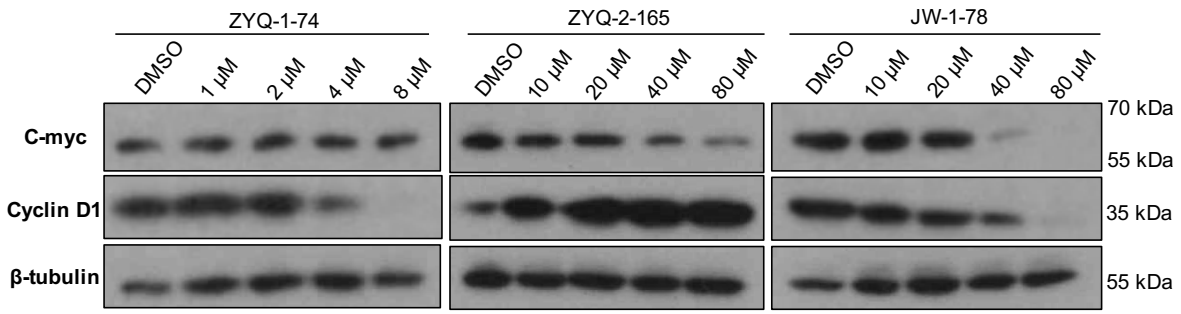


Figure 4.8 c-myc and Cyclin D1 WNT-target genes expression after ZYQ-1-74, ZYQ-2-165 and JW-1-78 treatment in SW480 cells
SW480 cells were grown in medium with 10% FBS and treated with the indicated concentrations of ZYQ-1-74, ZYQ-2-165 or JW-1-78. Forty-eight hours post-treatment, proteins were extracted using RIPA buffer and protein concentration was measured using the BCA assay. 25 μg of proteins were loaded per well. Membranes were probed with antibodies against CyclinD1 (36 kDa,1:600), c-myc (68 kDa, 1:300) and β-tubulin (55 kDa, 1:5000).

4.4 Discussion

In this chapter, three β-catenin – BCL9 inhibitors were tested on a panel of CRC cell lines with different APC and β-catenin statuses. Our experimental results with the β-catenin – BCL9 inhibitors showed some discrepancies with previously obtained data from our collaborators (Table 4.1), especially for the compounds ZYQ-2-165 and JW-2-80. This might be due to various factors: firstly, our collaborators were performing the drug treatments in culture medium containing 1% FBS. General cell culture and drug treatments are performed with 10% FBS in our lab to supplement cells with crucial growth factors. As seen in Figure 4.3, the effect of ZYQ-2-165 was FBS-dependent and could be reversed by the addition of 1% albumin. This indicated that the efficacy of the compound ZYQ-2-165 is affected by albumin. Interestingly, this effect was not seen with the compound JW-2-80, and we could not reproduce the data obtained by the Ji lab of IC_{50} of 22 μM and 26 μM in SW480 and HCT116 cells, respectively, when treating cells in 1% FBS cell culture medium.

Furthermore, it needs to be pointed out that the two labs used different cytotoxicity testing methodologies. While the Ji lab used the MTS assay, we performed our experiments using the SRB assay. The SRB assay is a whole cell end-point colorimetric assay. The dye binds to protein basic amino acid residues under mildly acidic conditions and can be released again for optical density measurement using weak bases (Skehan et al., 1990). The MTS assay is an adaptation from the MTT (3-(4,5-dimethylthiazol-2-yl)-2,5-diphenyltetrazolium bromide) assay, which relies on the Tetrazolium salt reduction by mitochondrial dehydrogenases to formazan (Berridge & Tan, 1993). Even though this assay is commonly used to assess cytotoxicity in drug testing, recent studies suggested that albumin and different cell

culture media (DMEM, RPMI or ISCOVES media) could have an effect on the assay outcome (Huang, Chen, & Walker, 2004; Talorete et al., 2007). Furthermore, it has been reported that cell lines differ in their abilities to reduce the MTT dye (Scudiero et al., 1988), with inaccuracies at high cell densities and variation with pH (Plumb, Milroy, & Kaye, 1989). In a direct comparison between the SRB and the MTT assay for an in vitro chemosensitivity study, the SRB assay resulted in a higher reproducibility and superior linearity with increasing cell density (Keepers et al., 1991). The different assay mechanisms and limitations might have been a contributing factor to the conflicting IC_{50} results of the β-catenin-BCL9 inhibitors between the labs. In addition, differences in cell culture practices between the labs could have potentially affect the cell line characteristics.

As previously mentioned in the introduction to this chapter, the Ji lab published their experimental results of their compounds after our lab concluded the testing on the panel of CRC cell lines. Based on the chemical structures provided (Appendix B.1), the compounds ZYQ-1-78 and ZYQ-2-165 are referred to as Compound 3 and Compound 29, respectively, in the publication by Zhang et al. (2018). In their study, it was concluded that ZYQ-1-78 (Compound 3) caused non-specific cytotoxicity as determined by a lactate dehydrogenase (LDH) cytotoxicity assay. This does agree with our findings of non-specific cell killing at an IC_{50} ranging from 2-10 μM in a panel of 28 colorectal cancer cell lines, 6 non-CRC cell lines from different tissues and fibroblast cells with low BCL9 expression. Our Wnt target expression analysis of Cyclin D1 and c-myc in SW480 cells after ZYQ-1-74 (Compound 3) treatment confirmed the reduction of Cyclin D1 at 8 μM drug concentration and was also described by the Ji lab. However, we could not confirm a significant reduction of the

c-myc WNT target gene expression after ZYQ-1-74 treatment. Furthermore, in our hands, while the drug ZYQ-2-165 (Compound 29) does lower the expression of c-myc Wnt target protein at 40 and 80 μM, we again could not confirm the inhibition of Cyclin D1 at the same concentrations seen in the data by the Ji lab. Cyclin D1 expression is known to be cell cycle dependent (Yang, Hitomi, & Stacey, 2006) and the changes seen in this experiment could be a consequence of an alternative effect on cell viability, as growth inhibitors also downregulate Cyclin D1 expression (Alao, 2007).

The Ji lab reported that ZYQ-2-165 is selective for cell lines with activated Wnt signalling with IC_{50}s of 41 μM and 55 μM in SW480 and HCT116 cells, respectively, while over 400 μM in non-small cell lung cancer cells A549 with normal Wnt status. We only tested the compound ZYQ-2-165 in Wnt-dependent colorectal cancer cell lines (Figure 4.2A). Therefore, we are unable to comment on the presented selectivity for WNT activated cell lines. Our reasoning for not pursuing the testing of ZYQ-2-165 in further studies was the high drug concentration (IC_{50} around 100 μM) needed to obtain any effect in SW480 and HCT116 colorectal cancer cells at 10% FBS concentration. The Ji lab does describe an IC_{50} of 41 $\pm$ 6.2 μM in SW480 cells (Zhang et al. 2018), which is similar to the result we obtained for the same compound and cell line in 1% FBS cell culture medium (IC_{50} of 50 μM). Furthermore, we showed that the effect of the compound ZYQ-2-165 is FBS dependent (Figure 4.3 and Figure 4.4).

A major limitation to this study was the limited amounts of available compounds and the large concentration required for the SRB assay. Therefore, the SRB assays for the inhibitors ZYQ-2-165 and JW-2-80 were only performed on a small number of cell

lines and mostly in a single experiment, except for SW480 and SW620 cell lines. Furthermore, we did not assess the selectivity of the compounds for the β-catenin–BCL9 interaction over the interaction of β-catenin–E-cadherin. This would have been useful to perform if the compounds were going to be developed and optimised any further.

Another limitation of small molecules targeting the Wnt pathway is the selectivity for cancer cells. As the Wnt pathway is crucial in normal cell function (Fevr et al., 2007), molecules targeting the Wnt pathway can cause major cytotoxicity, such as was previously shown in the development of Tankyrase Inhibitors (Zhong et al., 2015).

Based on the results presented in this chapter, we decided to not further pursue the evaluation of the β-catenin – BCL9 inhibitors. Instead, we shifted our research focus on identifying small antibody fragments to inhibit relevant β-catenin protein interactions to inhibit the Wnt pathway. This work is discussed in detail in Chapter 5.

Chapter 5

Intracellular Antibody Capture to identify small antibody fragments against β-catenin

CHAPTER 5: Intracellular Antibody Capture to identify small antibody fragments against β-catenin

5.1 Introduction

5.1.1 Yeast-Two-Hybrid systems

The Yeast-two-Hybrid (Y2H) system is a technique used to study protein-protein interactions (PPIs) in *Saccharomyces cerevisiae*. It was developed by Fields and Song in 1989 and has since become a popular method to identify binding proteins, as well as a tool to characterise and manipulate known interactions (Brückner et al., 2009).

The Y2H system exploits the fact that transcriptional activators often require both a DNA-binding domain (DBD) and a transactivation domain (AD). The transcriptional activator cannot function if the two domains do not interact physically. The Y2H methodology uses this property by fusing an antigen of interest (bait) to the DBD. The resultant fusion protein of interest is screened against a "prey", which is fused to an AD (Figure 5.1).

5.1.2 Intracellular Antibody Capture (IAC)

5.1.2.1 General methodology

The Intracellular Antibody Capture (IAC) is an adapted Y2H screening method designed for the isolation of functional VH or VL dAb from a cDNA library (Tanaka & Rabbitts, 2010b). The cDNA library of dAb is fused to the VP16 herpes simplex virus AD (prey) and can be screened in yeast against an *E.Coli* LexA-DBD antigen bait of interest. The interaction of the antibody fragment with the antigen of interest will form

a transcription factor complex activating the *HIS3* reporter gene (Figure 5.1). Yeast clones can be selected through this positive selection process and the cDNA encoding the dAb can be isolated from the yeast clones. This methodology enables selection of single-domain antibodies that fold correctly in the reducing cell environment (Visintin et al., 2008). For a detailed step-by-step procedure, refer to the Material and Methods chapter of this thesis.

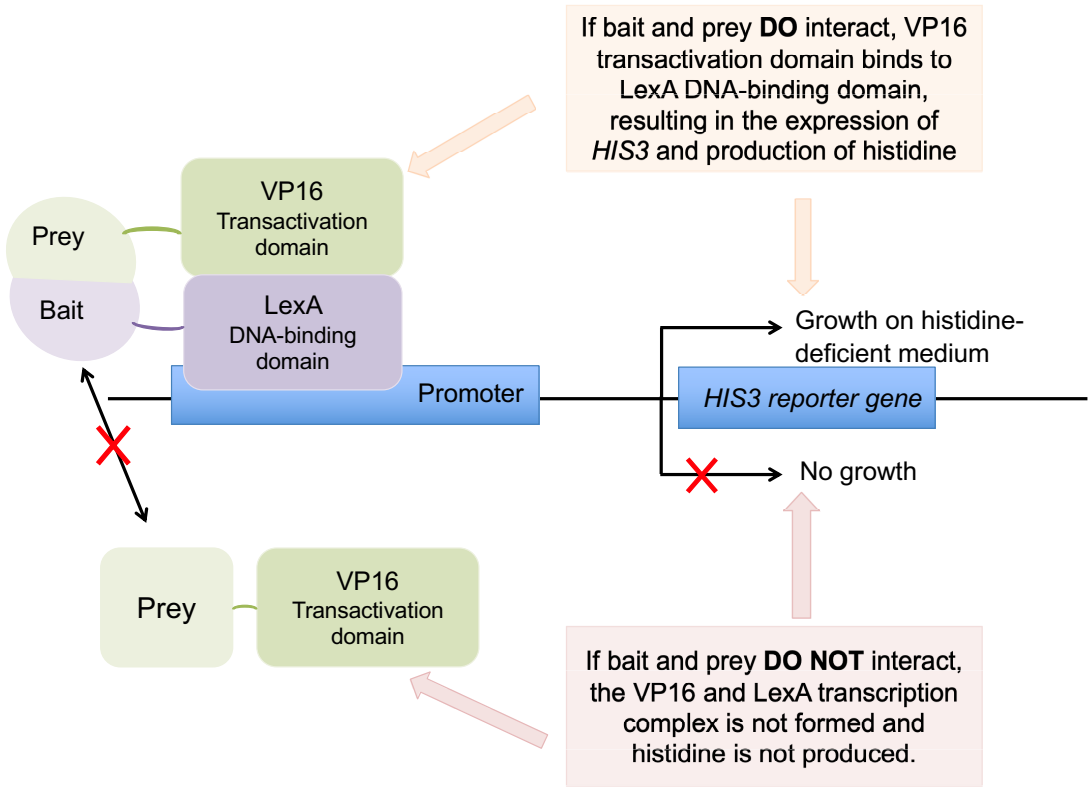


Figure 5.1 Schematic overview of the IAC mechanism of action
The bait of interest is fused to the LexA DNA-binding domain, while the prey is cloned in sequence with the VP16 transactivation domain. If the bait and prey bind, the interaction between the DBD and AD (transcription factor complex) will induce the expression of the *HIS3* reporter gene.

5.1.2.2 VH library

The Rabbitts laboratory has various human VH and VL single-domain libraries that can be used for this protocol (Tanaka & Rabbitts, 2010b). The libraries are based on an intracellular V-region consensus framework that is intrinsically stable and does not require disulphide bonds to fold correctly in their native secondary structure in the reducing environment of the cell (Tanaka & Rabbitts, 2003, 2008). All initial libraries for the IAC method are randomised for the CDR3 region (Tanaka & Rabbitts, 2010b). VH libraries are screened in preference to the VL library, as they have a greater diversity due to the variable length of 2 to 15 amino acids (AA) of the CDR3 region (Figure 5.2). In this study, the VH library VH4323/12 was used, with a diversity of approximately 2.1 x 10^6 clones (personal communications TH Rabbitts). This library has a CDR3 length of 12AA (Figure 5.2).

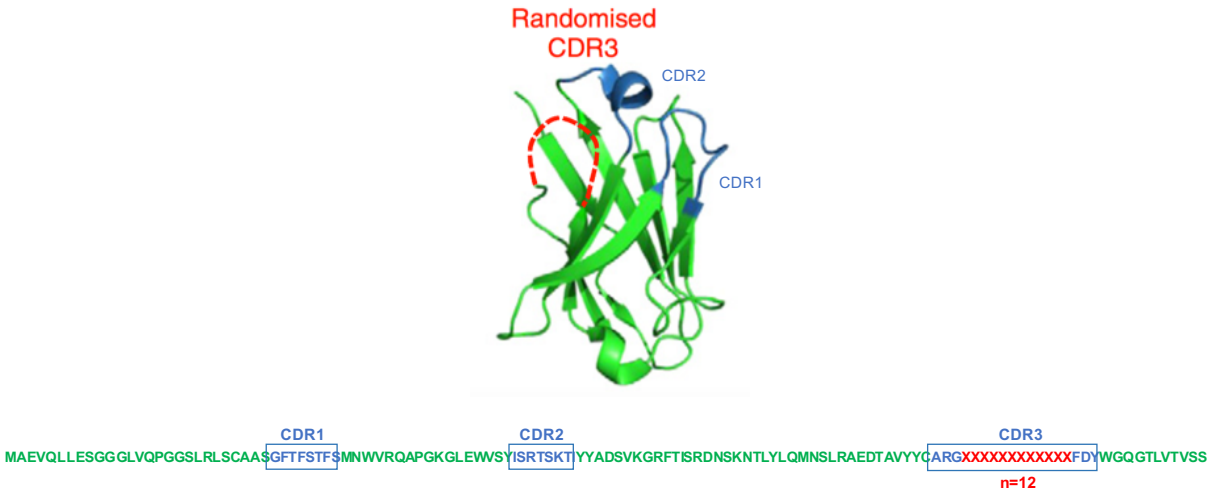


Figure 5.2 VH with randomised CDR3 region
Top: structure of a single variable heavy chain (VH), bottom: Amino acid sequence of the initial VH library. Green: VH consensus framework, blue: CDR1 and CDR2 loops, red: randomised CDR3 loop. Figure taken and adapted from Tanaka and Rabbitts (2010).

5.2 Aims

Up-to-date, there are no drugs in the clinic targeting the Wnt pathway, despite having a major role in cancer development (Cui et al., 2018). As the testing of the small molecule β-catenin-BCL9 inhibitors presented in Chapter 3 gave unsatisfactory results, we decided to explore further alternatives to inhibit β-catenin interactions in the growing field of intracellular antibodies.

The aim of this chapter was to identify intracellular single antibody domains (VHs) to inhibit oncogenic Wnt signalling. We screened a VH cDNA library using the IAC methodology against specific β-catenin target domains with known protein-protein interactions. This chapter describes the IAC process from identification and construction of the target bait constructs, through to the VH library screening and characterisation of antibody fragments against β-catenin.

5.3 Results

5.3.1 Selection of β-catenin target domains

The identification of potential bait β-catenin sequences was based on a thorough literature search and analysis of known β-catenin binding partners and structures. Table 5.1 summarises the four areas of β-catenin that were chosen as bait sequences. In order to maintain the endogenous structural conformation of each ArmR and allow interaction with the prey binding partners, the baits were designed such that each constructed domain contains the entire target ArmR plus an additional helix of the adjacent ArmR as a "linker". The amino acid sequence of the β-catenin ArmR regions was obtained from Huber, Nelson, & Weis (1997).

Bait Domain 1 (D1) represents the binding area of the transcriptional co-activator BCL9 on β-catenin. Various mutational and structural data have shown that the residues H358 and R359 in the Homology Domain 2 (HD2) of BCL9 specifically interacts with the binding "hotspots" residues D162 and D164 of β-catenin, which are located in the first Armadillo repeat (ArmR1) (Sampietro et al., 2006). As previously discussed, the specific and well-described interaction between these two proteins makes the interaction an interesting and valid target to disrupt the Wnt pathway (Sampietro et al., 2006; Takada et al., 2012). The β-catenin baits Domain 2 (D2) and Domain 3 (D3) include the TCF4 hotspot binding residue K312 and K435 (ArmR5 and ArmR8, respectively) (Fasolini et al., 2003a; Graham et al., 2001; Poy et al., 2001). Bait Domain 4 (D4) spans the entire C-terminal region of β-catenin from AA residue 503 to 781. This region was chosen as various transcriptional co-activators have been described to bind to this region of β-catenin (Hecht et al., 2000b; Valenta et al., 2012). Furthermore, the C-terminal region was also found to be

crucial in the nuclear translocation of β-catenin, which is important for the Wnt signal transmission (Koike et al., 2004).

Bait name	β-catenin AA residues	Comments
Domain 1 (D1)	126-189	BCL9 binding domain, corresponding to ArmR1 of β-catenin
Domain 2 (D2)	290-360	TCF4 binding domain, corresponding to ArmR5 of β-catenin
Domain 3 (D3)	424-488	TCF4 binding domain, corresponding to ArmR8 of β-catenin
Domain 4 (D4)	503-781	p300 and other transcription factor binding-sites, involved in nuclear translocation of β-catenin. Corresponding to ArmR10-C-terminal of β-catenin.

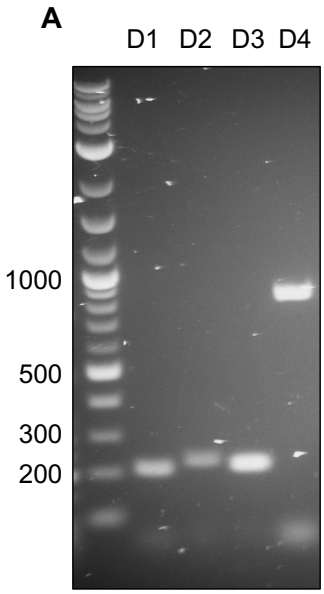
Table 5.1 List of β-catenin bait target domains
AA: amino acid

5.3.2 Cloning of bait and prey vectors

5.3.2.1 Construction of bait vectors

The cDNA sequence of HT29 colorectal cell line was used as a PCR template using a high-fidelity polymerase to obtain target β-catenin target regions. The PRC fragments were cloned in-frame with the DBD of the pBTM116 bait vector using the EcoRI/SalI restriction sites. The HT29 cell line cDNA was selected based on its wild-type β-catenin mutation status. Figure 5.3A shows the PCR results of the bait D1-D4 on a 1% agarose gel. All PCR products have the expected band size (Figure 5.3B).

A



B

PRC fragment	Expected size (bp)
D1	207
D2	228
D3	210
D4	852

Figure 5.3 PCR products of the β-catenin target regions for bait construction
A) The β-catenin target regions were obtained via PCR from a cDNA template from HT29 using the primers Domain 1_F and R, Domain 2_F and R, Domain 3_F and R and Domain 4_F and R (Table 2.5). PRC products were analysed by gel electrophoresis through a 1% agarose gel and the bands were all at the expected sizes, as summarised in **B**). The PCR products were purified for further downstream cloning processes.

PCR products were restriction-digested using EcoRI/SalI enzymes as described in Materials & Methods and cloned in-frame with LexA into the pBTM116 bait vector (Figure 5.4).

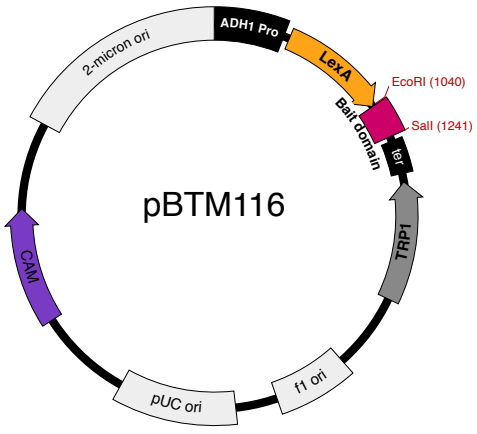


Figure 5.4 pBTM116 vector map
The β-catenin target regions were cloned in-frame with the LexA-DBD domain using EcoRI/SalI restriction sites. The pBTM116 vector has chloramphenicol and tryptophan for bacterial and yeast selection, respectively. The yeast alcohol dehydrogenase 1 (ADH1) promoter controls the expression of the LexA fusion protein.

The resulting bait vectors were sent for sequencing at the in-house WIMM Sequencing Facility to confirm the nucleotide sequence and the correct resulting in-frame fusion protein. Sequencing results can be found in Appendix C.1.

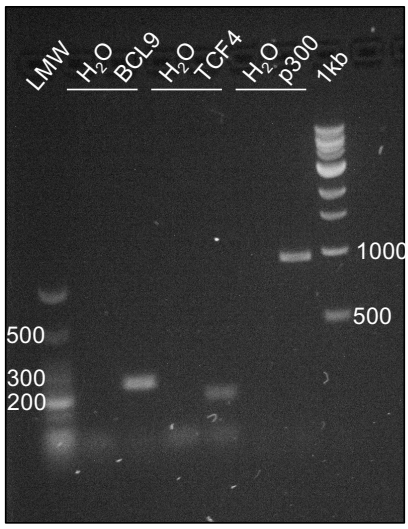
5.3.2.2 Construction of positive control vectors

In order to assess the correct function of the baits, "positive control" prey vectors were constructed using the known β-catenin binding partners (BCL9, TCF4 and p300). The binding regions of the β-catenin binding partners (Table 5.2) were identified from the literature (Fasolini et al., 2003a; Hecht et al., 2000b; Kramps et al., 2002; Poy et al., 2001; Sampietro et al., 2006) and amplified via PRC using HT29 cDNA as a template (Figure 5.5).

Control Prey name	AA residues on protein of interest	Comments
VP16-BCL9	321-391	HD2 domain of BCL9 binding to ArmR1 of β-catenin (Kramps et al., 2002)
VP16-TCF4	1-53	N-terminal of TCF4, binding to central ArmR region with hotspots in ArmR5 and ArmR8 (Fasolini et al., 2003a; Graham et al., 2001)
VP16-p300	1587-1891	Includes CH3 domain of p300, binding to AA residues 630-781 of β-catenin (Hecht et al., 2000b)

Table 5.2 List of β-catenin binding partner regions
AA: amino acid, HD2: homology domain 2, CH3: cysteine–histidine-rich region 3

A



B

PCR fragment	Expected size (bp)
BCL9	234
TCF4	180
p300	915

Figure 5.5 PCR products of the β-catenin interaction partners BCL9, TCF4 and p300 for positive control prey construction
A) HT29 cDNA sequence was used as template for the PCR. Primers BCL9_F and R, TCF4_F and R and p300_F and R (Table 2.5) were used for each reaction, respectively. PRC products were analysed by gel electrophoresis through a 1% agarose gel and the bands were all at the expected sizes, as listed in **B**). The PCR products were then purified for further downstream cloning processes. LMW: Low molecular weight ladder.

PRC products were digested and cloned in-frame with the AD of the prey vector pVP16 using the SfiI/NotI restriction sites (Figure 5.6). In this way the β-catenin binding sites of BCL9, TCF4 and p300 are replacing the VH sequence of the vector. These control preys were used to confirm the correct binding of the bait target domains D1-D4 to the known interaction partners before starting the VH library screen. All the resulting bait and prey vectors were sequenced to confirm the nucleotide sequence. Sequencing results can be found in Appendix C.2.

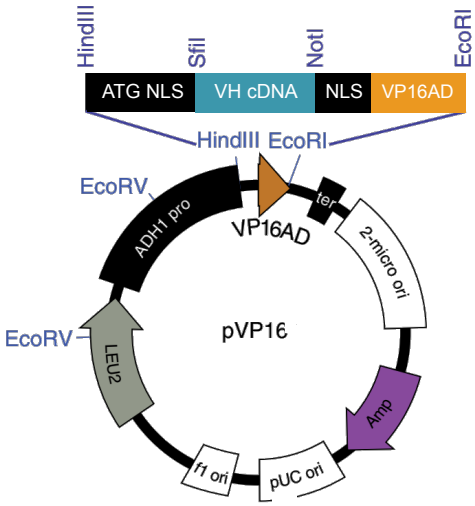


Figure 5.6 Vector map of VP16 prey vector
The prey vectors contain the VH cDNA library clones in-frame with the VP16-AD. For binding control vectors, the sequences of β-catenin binding partners were clones into the vector instead of VH cDNA using SfiI/NotI restriction sites. Ampicillin and Leucine was used for bacterial and yeast selection, respectively. NLS: nuclear localisation sequence. Figure adapted from Tanaka and Rabbitts 2010.

5.3.3 Characterisation of bait yeast lines

Bait vectors Domain 1-4 were transformed into L40 yeast (see Methods) to establish bait antigen yeast lines for validation and used for the library screen. As the pBTM116 bait vector carries the *trp1* gene, baits were grown on media lacking tryptophan (W), which compensates for the *trp1* gene mutation of L40 yeast. L40 yeast was also transformed with the pBTM116 empty vector (without β-catenin target sequence) as a control.

5.3.3.1 Auto-activation test

Auto-activation is the ability of some baits to activate the expression of the *HIS3* reporter gene in L40 yeast without an interaction with any prey. It is important to establish if the bait lines do auto-activate the reporter gene. If the *HIS3* reporter gene of L40 yeast is activated by the bait alone, the library screening conditions will be

affected. 3-amino-1,2,4-triazole (3-AT) is a competitive inhibitor of imidazoleglycerol-phosphate dehydratase, the enzyme encoded by the *HIS3* gene. Auto-activation of bait lines was assessed by growing the baits on selective plates lacking tryptophan (selection for baits) and histidine (reporter gene) with increasing concentrations of 3-AT (Figure 5.7). If the bait line grows on plates containing more than 30 mM 3-AT, the bait cannot be used for this screening protocol (Tanaka & Rabbitts, 2010b).

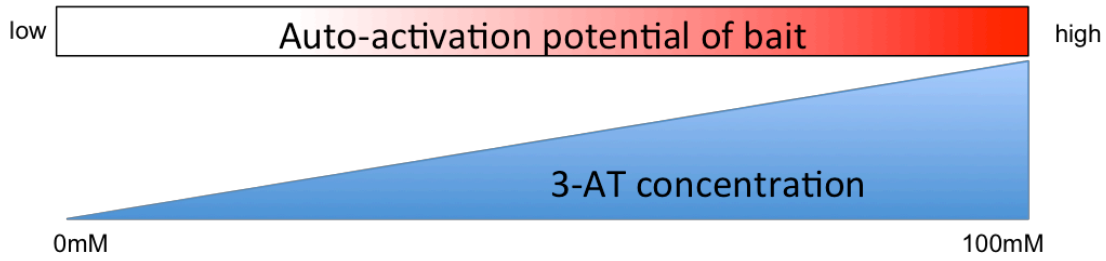


Figure 5.7 Schematic representation of bait auto-activation assessment by 3-AT
Baits growing on YC-WH plates with high 3-AT concentrations will have a high auto-activation potential.

The auto-activation test of the baits on selective YC-WH plate with increasing concentrations of 3-AT showed that baits D1, D2 and D3 did not auto-activate, while bait D4 was auto-activating in the absence of any prey (Figure 5.8). The empty pBTM116 (without β-catenin sequence) was used as control bait line and streaked on the same plates. The screening procedure has previously been optimised and baits growing on plates containing more than 30 mM 3-AT concentrations are not suitable for this procedure. Bait growing below this threshold should be screened on plates with the minimal 3-AT concentration that inhibits the auto-activation of *HIS3*. Therefore, bait D4 was not suitable for the IAC screen and not further characterised.

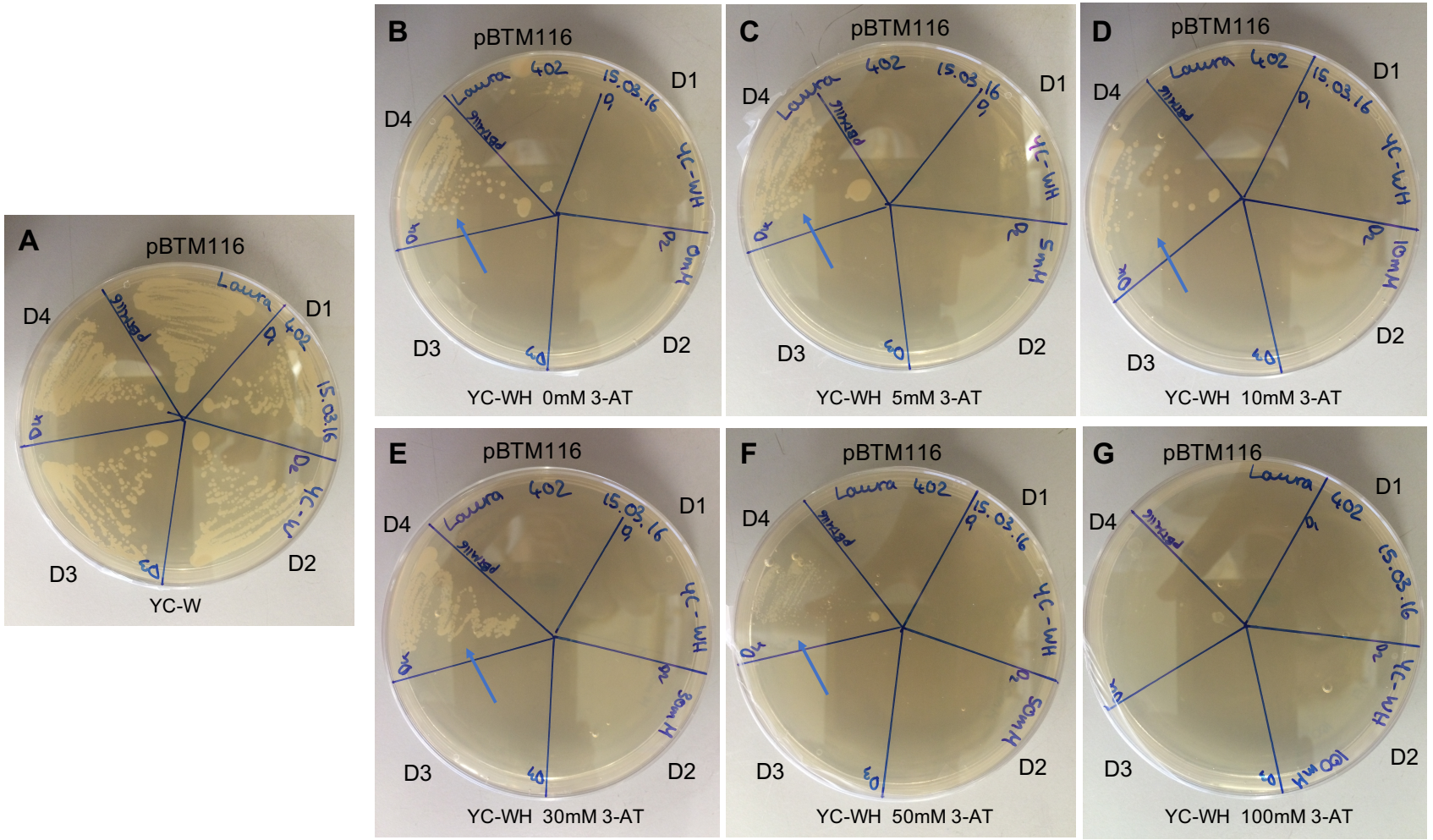
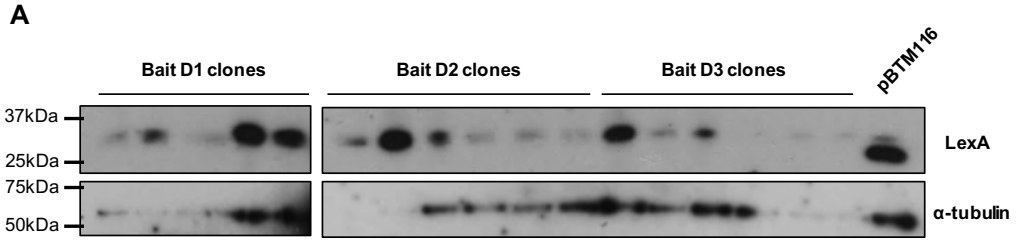


Figure 5.8 Auto-activation test of bait lines
D1, D2, D3, D4 bait lines, as well as pBTM116 control line were streaked onto selective plates lacking histidine (YC-WH) with increasing concentration of 3-AT. **A**) Growth control plate (YC-W). **B-G**) YC-WH plates with 0-100 mM 3-AT. D1, D2 and D3 plates did not auto-activate. D4 bait line grew on selective plates with up to 50 mM 3-AT (blue arrows).

5.3.3.2 Bait protein expression in yeast

The expressions of baits were assessed by Western Blot using an anti-LexA antibody against the DNA-binding domain of the fusion protein (Figure 5.9A). Clones of the yeast bait lines D1, D2, D3 and D4 were grown in 10 mL selective medium lacking tryptophan (YC-W) overnight at 30°C, 220 rpm and proteins were extracted (see Methods). Figure 5.9B indicates the expected sizes of the bait fusion proteins. The pBTM116 bait line was used as positive control.

A



B

Bait	Expected size (kDa)
D1	29.7
D2	30.4
D3	29.9
pBTM116	24.5

Figure 5.9 Bait line expression
A) Five clones of bait lines D1, D2 and D3 were tested for their expression of the LexA-β-catenin fusion protein by WB. Anti-LexA antibody (1:1000), α-tubulin (1:2000). **B**) Expected sizes of bait proteins in kDa. A clear shortcoming of this WB is the inconsistent expression of the tubulin loading control. Repeating the experiment did not result in a more uniform loading of proteins. A potential explanation for the variable amount of detectable protein is the protein extraction method: the yeast pellets were lysed, and proteins directly extracted using loading buffer without quantification of the extracted proteins (see Chapter 2). Using a commercial extraction buffer, such as Y-PER™ Yeast Protein Extraction Reagent (Thermo Scientific) would allow for extracted protein quantification and loading of equal amounts of protein.

5.3.3.3 Bait – positive control prey interaction

In order to assess the interaction of the bait lines and the positive control preys, they were co-transfected into L40 yeast. Two colonies of each transformation were streaked onto selective YC-WLH plates to assess bait-prey interactions. While it was

expected that the D1 bait line interacts with the VP16-BCL9 prey, D2 and D3 bait lines were predicted to interact with VP16-TCF4.

As seen on Figure 5.10A, co-transformants of D1 + VP16-BCL9 did grow on YC-WLH plates, indicating that the fusion protein bait D1 folded correctly and does interact with the positive control prey VP16-BCL9. As a negative control, the D1 bait line does not interact with the VP16-TCF4 prey. Overall, the bait auto-activation and interaction studies indicate that the bait D1 is suitable for the IAC VH screen. Furthermore, D2 and D3 bait lines co-transformed with VP16-TCF4 prey did not grow on YC-WLH plates (Figure 5.10B and C). Baits D2 and D3 contain the hotspots K312 and K435, respectively, which were shown to be important for the β-catenin-TCF4 interaction.

However, the chosen β-catenin domains D2 and D3 might not be sufficient to bind to TCF4 individually. To further assess this option, a bait containing the sequence from ArmR2 to ArmR9 could have been constructed. This bait would represent both domains 2 and 3, and span the entire β-catenin binding “groove”. However, since the bait D1 is already validated and commonly described as a valid β-catenin target region, baits D2 and D3 were not further optimised.

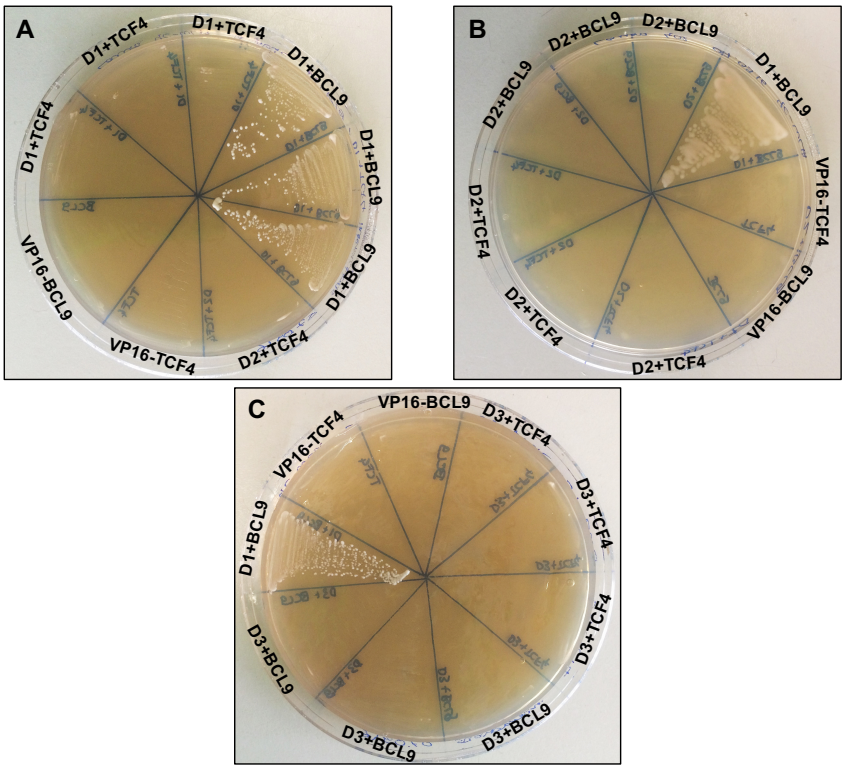


Figure 5.10 Bait line interactions with positive control preys
Bait lines D1, D2 and D3 were co-transformed with positive control prey VP16-BCL9 and VP16-TCF4. As the D1 bait contains the sequence of β-catenin Arm1R, it is expected to bind to VP16-BCL9, while D2 and D3 baits should bind to VP16-TCF4. Three yeast clones of each transformation were streaked on selective plates lacking tryptophan, leucine and histidine (YC-WLH) and incubated at 30°C for 3 days. **A**) Clones of the D1 + VP16-BCL9 co-transformation grow on YC-WLH plates. Clones from the D1+VP16-TCF4 co-transformation were streaked on the same plates as negative control, as well as VP16-BCL9 and VP16-TCF4 single prey lines. The D2 + VP16-TCF4 clone was supposed to serve as positive control, but as it can also be seen in B) and C), no interaction did occur between D2 bait and VP16-TCF4 prey. **B**) Clones of the D2 + VP16-TCF4 co-transformation did not grow on selective YC-WLH plates. D1 + VP16-BCL9 clone was used as positive control. **C**) Clones of the D3 + VP16-TCF4 co-transformation did not grow on selective YC-WLH plates. D1 + VP16-BCL9 clone was used as positive control.

5.3.4 Large-scale yeast transformation

The large-scale yeast transformation protocol is based on the Lithium acetate (LiAc) transformation method and the protocol by Tanaka and Rabbitts (2010) was followed. A total number of transformants that is approximately 10-times the library size should be screened in order to ensure the entire library has been covered. In this case, this would result in about 1.5 x 10^7 total yeast transformants for the 300 µg cDNA library

(Tanaka & Rabbitts, 2010). This leads to in an ideal transformation efficiency of 5.0 x 10^4 transformants/µg DNA.

Before performing a large-scale transformation using the VH library, the D1 bait clone 4 (Figure 5.9A) was transformed with the pVP16-BCL9 prey in order to test the transformation efficiency of the methodology. A large-scale transformation was performed as described using 300 µg of the pVP16-BCL9 prey vector. After 3 days of growth at 30°C on YC-WL plates, the number of colonies was counted on various dilution plates and the total number of transformants was determined to be 1.8 x 10^5, which was two magnitudes lower than the ideal number of screened transformants. This result prompted us to optimise the large-scale transformation protocol before performing the VH library screen.

5.3.5 Optimisation trials of large-scale transformation protocol

Various changes to the large-scale transformation protocol were made in attempts to improve the transformation efficiency of the procedure. These modifications included changing the size of the single stranded carrier DNA, altering the heat shock length for the transformation and comparing different D1 bait line clones. These optimisation attempts are described in the following sections.

5.3.5.1 Changes in the size of single-stranded carrier DNA

Single-stranded carrier DNA (ssDNA) is commonly used to improve the yeast transformation efficiency (Gietz & Schiestl, 2007a; Gietz et al., 1994; Schiestl & Gietz, 1989). In the trial large-scale transformations in this study 10 mg ssDNA were used, as outlined in the methodology (Tanaka & Rabbitts, 2010b).

Schiestl and Gietz (1989) described the importance of the ssDNA carrier size for an efficient yeast transformation. They reported that the most efficient carrier size was ranging from 15 to 2 kb, resulting in 5.5 x 10^4 transformants per µg DNA. Transformation efficiency was decreased to 1.9 x 10^4 transformants per µg DNA if the ssDNA size was reduced to about 500 bp (Schiestl & Gietz, 1989). This report prompted us to analyse the size of the commercially available carrier DNA (salmon sperm DNA) used in our study. As seen in Figure 5.11, the carrier DNA previously used in our experiments (termed “old” carrier DNA) had an average size of 100 bp.

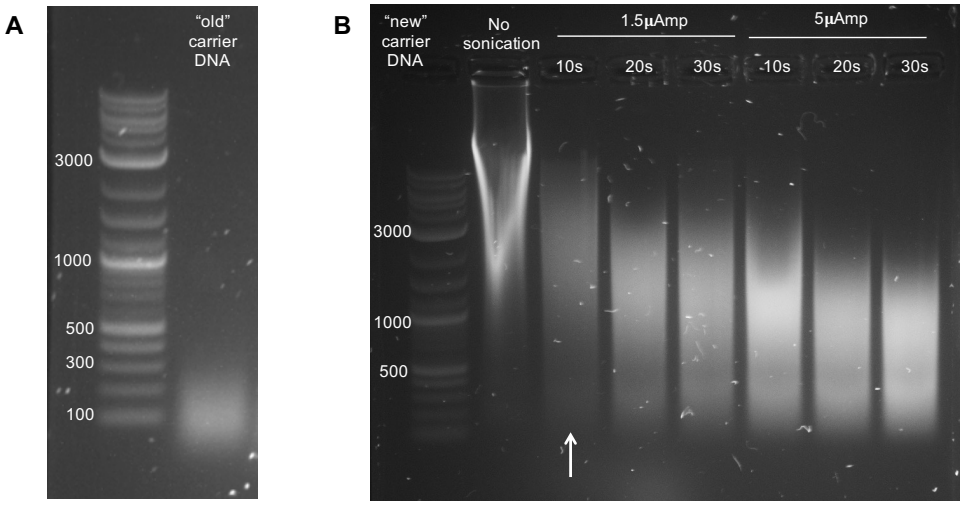


Figure 5.11 Single-stranded carrier DNA analysed on agarose gel
The size of the carrier DNA was analysed on 1% agarose gels. **A**) The “old” carrier DNA had an average size of 100 bp. **B**) The newly purchased ssDNA was sonicated at different intensities and the size of the resulting products were analysed. The white arrow indicates the optimal ssDNA size distribution.

New non-sonicated salmon sperm DNA was purchased, sonicated and analysed on an agarose gel to assess the size range (Figure 5.11B). ssDNA ranging from 1 kb - 6 kb was then used in three independent large-scale transformations of D1 bait comparing the “old” and “new” carrier DNA. The transformation efficiency was not improved by the new ssDNA; in fact, the transformation efficiency seemed to be better with the old carrier DNA (Table 5.3).

Transformation efficiencies: old vs new carrier DNA (transformants/µg)		
	Old carrier DNA (10-300 bp)	New carrier DNA
Trial 1	5.5×10^3	1.16×10^3
Trial 2	7.16×10^3	0.7×10^3
Trial 3	6.06×10^3	1.26×10^3

Table 5.3 Transformation efficiency results comparing old and new carrier DNA
Three independent large-scale transformation experiments were performed, comparing the effect of the old and new carrier DNA. Colonies were counted on YC-WL plates after three days growth at 30°C.Transformation efficiency is given as transformants per µg plasmid DNA used in the transformation reaction.

5.3.5.2 Comparison of transformation efficiencies of different bait clones

In order to test if the selected D1 bait clone 4 was contributing to the low transformation efficiency, the D1 bait clone 5 was transformed in a parallel experiment to compare transformation efficiencies between the clones. The transformation efficiencies were comparable between clone 4 and clone 5 (Table 5.4). In this experiment, the transformation efficiency was better in clone 5 compared to clone 4. However, both clones exhibited low transformation efficiencies in the previously observed range of magnitude (Table 5.3).

Transformation efficiency: D1 bait clone 4 vs D1 bait clone 5		
	D1 bait clone 4	D1 bait clone 5
Transformants/µg DNA	4.66×10^3	7.63×10^3

Table 5.4 Transformation efficiency results comparing D1 bait clones 4 and 5
D1 bait clone 4 and clone 5 were used in two parallel large-scale transformation experiments using 300 µg VP16-BCL9 prey vector. Colonies were counted on YC-WL plates after three days growth at 30°C. Transformation efficiency is given as transformants per µg plasmid DNA used in the transformation reaction.

5.3.5.3 Effect of heat shock step on the transformation efficiency

The heat shock step in the LiAc-PEG yeast transformation protocol has been reported to enhance the transformation efficiency by aiding DNA to cross the cell wall (Kawai, Hashimoto, & Murata, 2010). While the protocol by Tanaka and Rabbitts (2010) followed in this study includes at 15 min heat shock step at 42°C, longer heat shock times have been reported in the literature (Liu et al., 2017). In order to assess if increasing the heat shock time would have any positive effect on the number of transformants, the D1 bait line clone 5 was transformed with 300 µg VP16-BCL9 prey and heat shocked at 42°C for 15, 30 and 60 min. A 30 min heat shock did not have any notable difference on the total number of transformants compared to 15 min at 42°C. In contrast, the number of transformants dropped with a heat shock of 60 min (Table 5.5).

Transformation efficiencies of D1 bait clone 5 with different heat shock times			
	15 min	30 min	60 min
Transformants/µg DNA	1.96×10^3	1.26×10^3	0.23×10^3

Table 5.5 Transformation efficiency results comparing heat shock times
D1 bait clone 5 was transformed using 300 µg VP16-BCL9 prey vector and heat shocked for the indicated times at 42°C. Transformed yeast was plated on YC-WL plates and colonies were counted after three days at 30°C.

Various attempts to improve the transformation efficiency of the large-scale transformation protocol were unsuccessful. However, we decided to pursue to VH library screen with the sub-optimal transformation efficiency and see if we could obtain any VHs for potential further characterisation. The results of the library screen are described in the following section of this chapter.

5.3.6 VH library screen

The bait D1 clone 5 was screened against the VH library VH4323/12. The VH4323/12 library is randomised at the CDR3 with a length of 12 AA and a library diversity of 2.1 x 10^6 (personal communication TH Rabbitts). As the transformation efficiency has been low in the previous experiments and the D1 bait line did not auto-activate on YC-WLH plates (Figure 5.8), the library screen was performed on large screening plates with 0 mM 3-AT in order to obtain maximum positive hits and identify even weak VH binders against the bait. The detailed protocol of the large-scale transformation is described in Chapter 2.

Overall, the large-scale transformation of D1 bait clone 5 with the library VH4323/12 was performed with a transformation efficiency of 0.19 x 10^3 transformants/ µg DNA (approx. 5.7 x 10^5 total transformant yeast per 300 µg library DNA), according to the number of colonies growing on the control YC-WL plates (Appendix C.3).

After three to four days at 30°C, the screening plates were inspected for yeast colony growth. One hundred twenty-three colonies grew on the large YC-WLH screening plates. The clones were re-streaked on to small (3cm ∅) individual YC-WLH plates and incubated for 3 days at 30°C to confirm the positive interaction between bait and

prey. Out of the 123 clones, only 3 clones, termed VH49, VH55 and VH88, grew on the new YC-WLH plates. The other 120 clones either failed to grow on selective plates again (false positives on large screening plates) or turned out to be contaminants (growth in one day, yellow colour).

The positive library screen clones were grown in YC-L liquid medium to enrich for the prey (leucine selective marker). DNA was extracted from VH49, VH55 and VH88 clones and sequenced to confirm the correct sequence of the VH framework. All three identified VHs had the correct expected consensus framework sequence, with a randomised CDR3 region. The DNA sequences of all three clones can be found in Appendix C.4. Figure 5.12 shows the amino acid sequence of clones VH49, VH55 and VH88.

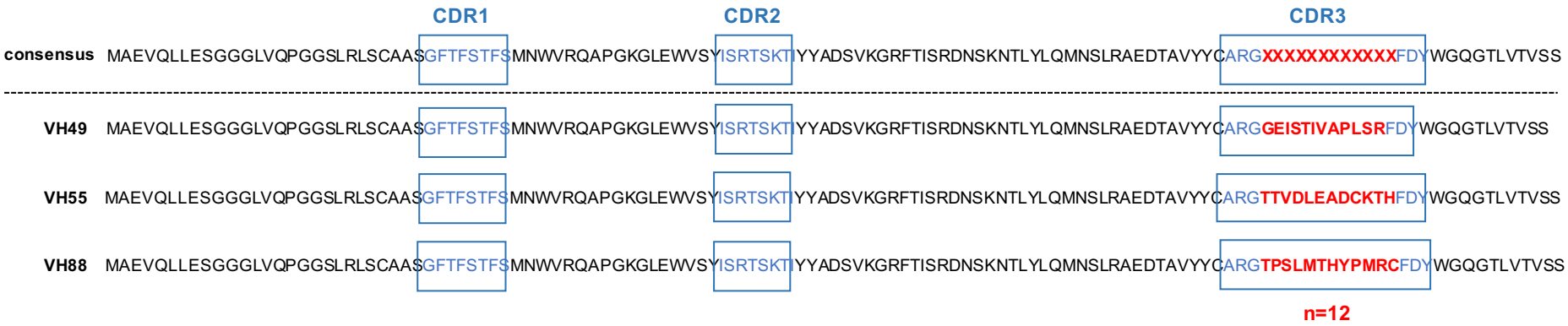


Figure 5.12 Amino acid sequence of VH49, VH55 and VH88
All three VHs identified through the VH library screen have the correct consensus framework sequence and identical CDR1 and CDR2 regions. As expected, the CDR3 region is randomised at 12 AA residues (red, n=12). The top sequence represents the consensus sequence of the VH library.

5.3.7 Characterisation of VHs after first round of library screen

The first step in the characterisation was to confirm that the VHs obtained in the library screen were "true-binders", meaning that they bind against the β-catenin part of the fusion protein and not against the DBD LexA (a schematic representation is given in Figure 5.13).

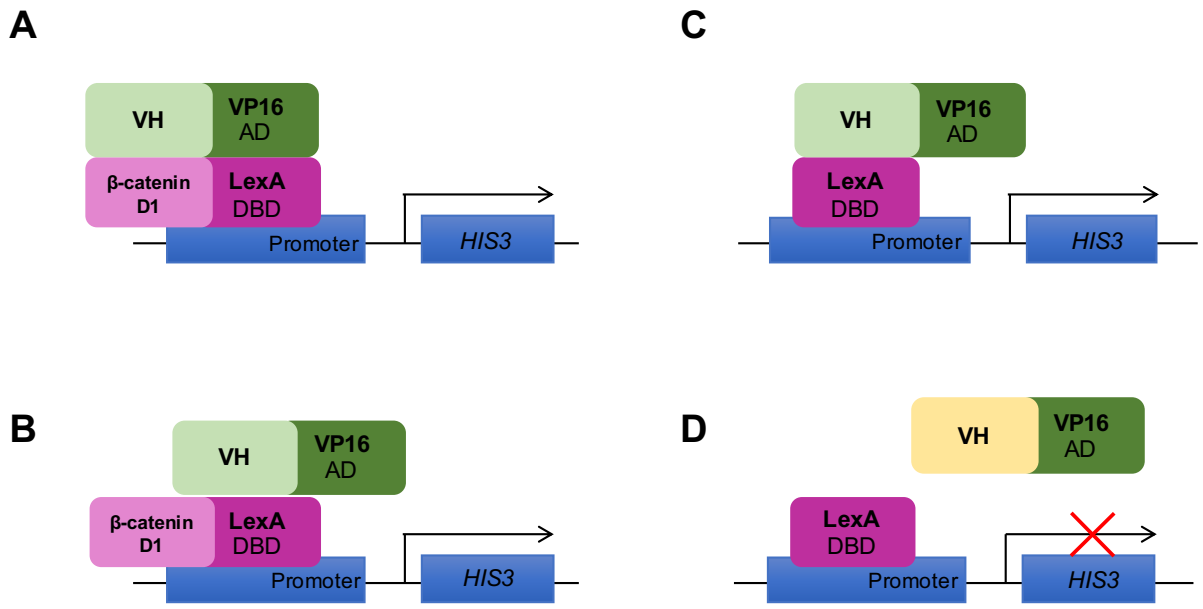


Figure 5.13 Schematic representation of VH binding to bait fusion protein
A-B) VH binding to both the β-catenin and LexA part of the bait fusion protein will activate the *HIS3* expression. **C**) VH binding to the LexA-DBD can be confirmed by co-transforming VH with the "empty vector control" (pBTM116 bait line) without the β-catenin sequence. **D**) If the VH does not bind to the LexA part of the fusion protein, *HIS3* expression does not occur.

In order to assess the specificity of VH49, VH55 and VH88 to the β-catenin domain of interest, the VHs vectors were transformed into the D1 bait line as well as the pBTM116 control line. VH59, a known LexA DBD-binder (obtained from the Rabbitts lab), was transformed into the pBTM116 bait line and used as a positive control. Two clones from each transformation (VHs + D1 bait line and VHs + pBTM116 control bait line) were streaked onto selective YC-WL and YC-WLH plates and incubated for 3 days at 30°C. As the clones contain both bait (tryptophan selection) and prey (leucine selection)

vectors, co-transformed clones should grow on plates lacking tryptophan and leucine. If the VHs bind to the bait vectors, they induce *HIS3* expression and grow on selective plates lacking histidine (YC-WLH).

As seen in Figure 5.14 (upper panel), all co-transformed clones grew well on control YC-WL plates, indicating that both baits (D1 and pBTM116) and VHs are expressed. The VHs prey lines on their own did not grow on YC-WL and served as negative controls. VH49, VH55 and VH88 were identified as DBD-binders, as they grew on YC-WLH plates when co-transformed with the DBD-only pBTM116 control bait line (Figure 5.14, lower panel). It should be noted that one of the D1+VH49 clones did not grow on the YC-WLH selective plates. It is unclear why the clone did not grow in this specific experiment, but the interaction between D1 bait and VH49 prey was confirmed again in separate experiments.

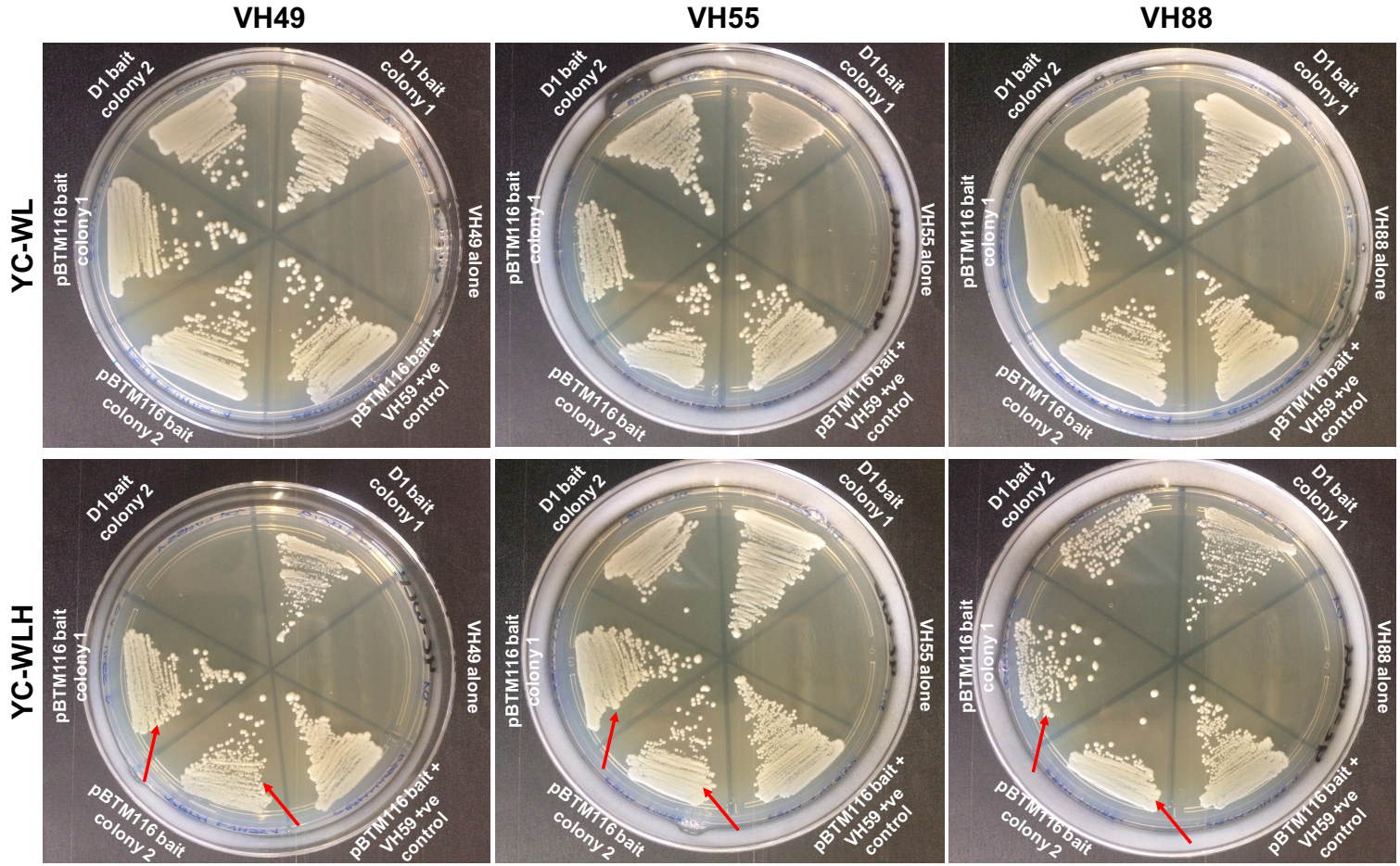


Figure 5.14 Interaction test of VH49, VH55 and VH88 with D1 and pBTM116 bait lines
VH49 (left), VH55 (middle) and VH88 (right) were transformed into D1 bait clone 5 and pBTM116 control bait line. The known DBD-binder VH59 was transformed into pBTM116 control bait line as positive control. Two clones of each transformation were streaked on YC-WL (growth control, upper panel) and YC-WLH (interaction plate, lower panel). VHs transformed into L40 yeast (prey alone, leucine selection) were used as negative control, as clones should not grow on YC-WL plates. Images were taken after 3 days at 30°C. Red arrows indicate the interaction between the VH and the pBTM116 bait line. If the interaction was specific to the D1 domain of interest, the pBTM116-VH clones should not grow on YC-WLH selection plates.

As all the VHs were identified as DBD-binders, we did not further pursue any characterisation and concluded the experiment. Figure 5.15 gives a final overview of the experimental results described in this chapter.

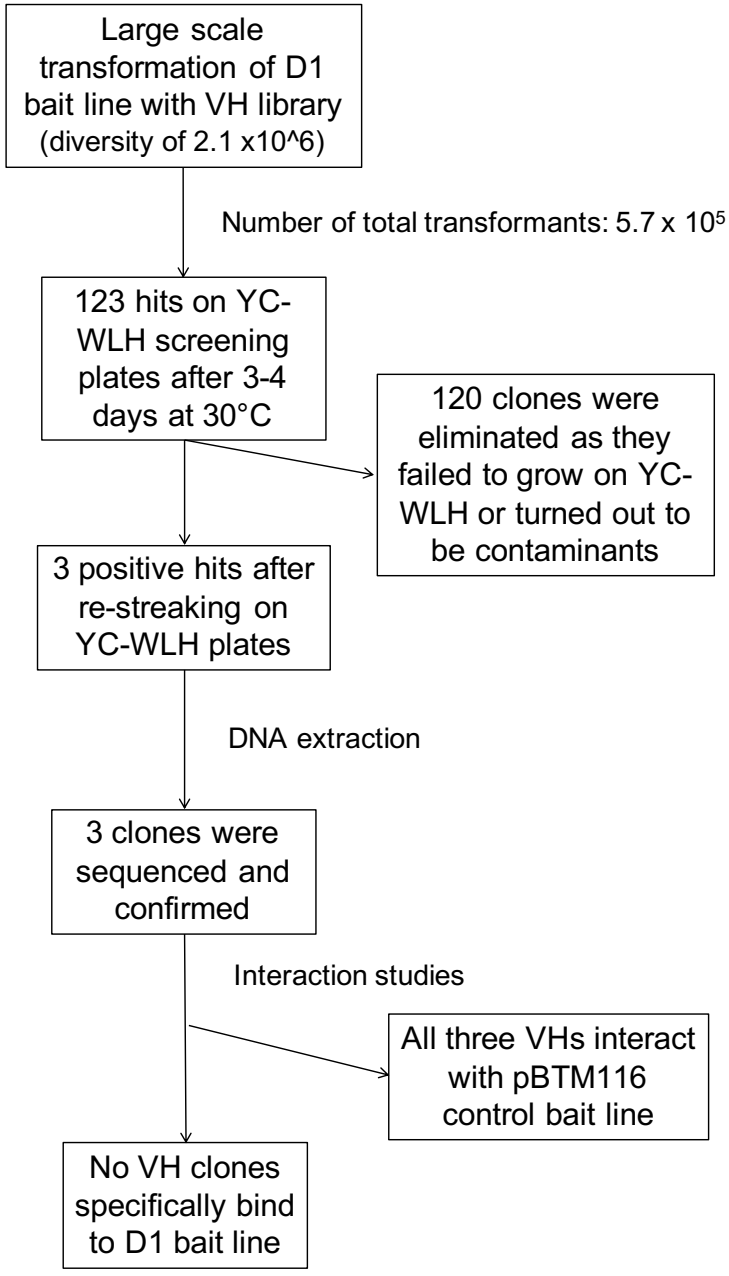


Figure 5.15 Flow- chart overview of the VH library screen results

5.4 Discussion

In this chapter, we described the single-domain antibody screen against a target domain of β-catenin using the IAC methodology. Several baits with potential β-catenin target domains were constructed with the corresponding interaction partners as positive control preys, as summarised in Table 5.1 and Table 5.2.

The bait lines were characterised through auto-activation tests and positive control prey interaction studies prior to the VH library screen. As the bait D4 auto-activates (Figure 5.8) and baits D2 and D3 do not interact with their positive control prey VP16-TCF4, only bait D1 was further pursued for the IAC VH library screen. Similarly to our auto-activation result, Hecht et al. (1999) found an auto-activation of the *lacZ* reporter gene expression of their LexA-fusion proteins containing the C-terminal AA residues 536-781 of β-catenin (D4 bait of this study includes residues 503-781). They concluded that the C-terminal region of β-catenin includes various transactivating subdomains, similar to the minimal transactivation domain of VP16. This would explain why the bait D4 auto-activates on selective plates in our study without the interaction with a prey.

The β-catenin bait constructs were designed based on the available structural data with interaction partners in the literature. While the positive interaction between the D1 bait and the VP16-BCL9 control prey was confirmed, the baits D2 and D3 did not bind to their positive control prey VP16-TCF4 (Figure 5.10). We hypothesise that the sequence fragments of β-catenin and TCF4 cloned into the pBTM116-bait and VP16-prey vectors did not lead to structurally correct and functioning domains that could interact. Furthermore, the TCF4 binding occurs along the large and dynamic

central region of β-catenin (Sampietro et al., 2006), with many other interaction partners involved in the same sites (Valenta et al., 2012). This makes the β-catenin-TCF4 interface difficult to target, albeit the interaction is very well characterised.

As seen in section 5.3.5 of this chapter, various optimisation attempts were made to improve the transformation efficiency of the large-scale transformation protocol. Neither the larger size of the single-stranded carrier DNA (Table 5.3), the different D1 bait line clone (Table 5.4) nor the heat shock length (Table 5.5) seemed to have improved the transformation conditions. It should be noted that only the LiAc-PEG transformation method was used in this study. Transformation by electroporation or a combined of Li-Ac-Electroporation could have been an alternative and improved methodology for the library screen (Becker & Guarente, 1991; Benatuil et al., 2010).

The large number of 120 false positive hits in the library screen might have been due to the fact that the screen was performed on YC-WLH plates with 0 mM 3-AT. Large library screens are generally performed at low concentration of 3-AT to avoid non-specific background growth (Caufield, Sakhawalkar, & Uetz, 2012), with the minimal 3-AT concentration determined on a case-by-case basis. However, since our transformation efficiency was already sub-optimal to begin with and the D1 bait line did not auto-activate (Figure 5.8), we decided to lower the stringency of the selection in order to identify even potentially weak VH binders. These could then have been affinity maturated in further screening rounds (Tanaka & Rabbitts, 2010b).

Three VH hits were identified through the library screen, VH49, VH55 and VH88. The VHs were tested against the pBTM116 bait line to assess their binding against the LexA-DBD region of the bait protein. It was concluded that all the identified VHs were

DBD-binders and not against the β-catenin part of the fusion protein. Due to these results, the subsequent affinity maturation of the VHs in further screening rounds were not pursued.

After obtaining the results from the VH library screen, further attempts were made to troubleshoot the poor yeast transformation efficiency. A previously studied bait line termed “myc bait” was obtained from the Rabbitts lab as a positive control, as it was successfully transformed using the IAC protocol with good transformation efficiency. The D1 bait and myc bait lines were transformed in a parallel experiment using the VP16-prey vector. The overall number of transformants was as low as in previous experiments and comparable for both D1 bait lines. Dr Wilawan Bunjobpol, a post-doctoral researcher in the Rabbitts laboratory, performed a large-scale transformation using the D1 bait in order to assess if the previously observed transformation efficiencies were due to technical issues. However, the transformation efficiency was not improved either in this experiment, with a result of 73 transformants/µg DNA (2.2×10^5 total transformants). A further optimisation could be to perform multiple smaller scale transformations with less DNA amount to achieve a higher yield and then pool the transformation reactions (Gietz & Schiestl, 2007b, 2007c).

Overall, we tried to identify small intracellular domain antibodies against β-catenin with the aim to further characterise their effect in a panel of colorectal cancer cell lines. However, after disappointing results and various optimisation attempts described in this chapter, we decided not to further develop this specific project. Instead, we focused our attention on a previously described Llama single domain antibody (VHH) against β-catenin (Newnham et al., 2015), with results described in following chapter.

Chapter 6

Characterisation of a Llama VHH against β-catenin

CHAPTER 6: Characterisation of a Llama VHH against β-catenin

6.1 Introduction

6.1.1 VHH against β-catenin

Recently, an intracellular VHH against β-catenin has been described. Newnham et al., (2015) immunised llamas with full-length recombinant human β-catenin with the aim of isolating intracellular VHHs targeting the protein. An immune phage display library of VHH domains was constructed from peripheral blood mononuclear cells from the immunised llamas. β-catenin-specific VHHs were enriched through various rounds of panning the phage library against biotinylated β-catenin both in solution and immobilised to immunotubes. β-catenin-binding of VHHs was further assessed by enzyme-linked immunosorbent assay (ELISA) and functional modifications of the VHHs to β-catenin were analysed using a HEK293 bioassay, which allows the assessment of Wnt-induced expression of the firefly luciferase reporter. An active intracellular VHH against β-catenin termed LL3 was isolated based on the ability to specifically inhibit the Wnt-signal, VHH fragment expression levels and sequence diversity (Newnham et al., 2015). The CDR3 region of LL3 was mutated to introduce alanine residues to create a non-binding control VHH, called LL3.CDRAAA. As seen in immunoprecipitation experiments performed by Newnham et al. (2015), scFc tagged LL3 did pull down β-catenin from HEK293 lysates, while LL3.CDRAAA-scFc did not (Figure 6.1). The sequences of LL3 and LL3.CDRAAA can be found in Appendix D.1. For simplicity, the wild-type and mutant VHHs are called LL3 and AAA, respectively, in this thesis.

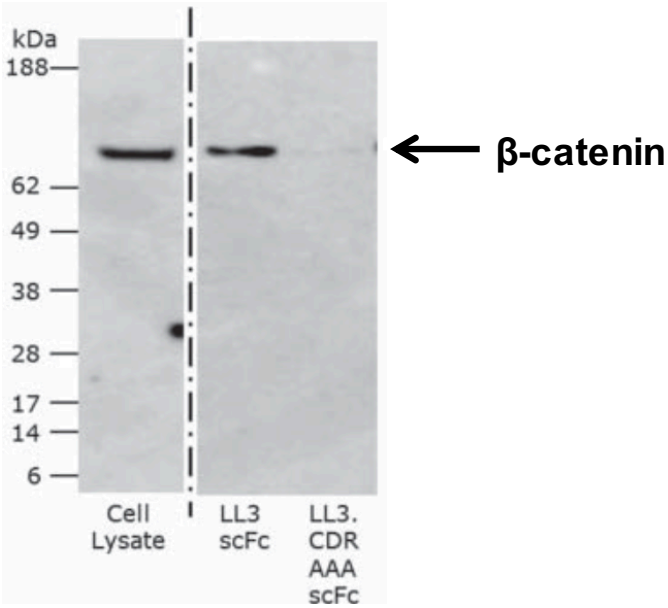


Figure 6.1 Immunoprecipitation of β-catenin by LL3-scFc
LL3 and AAA VHHs were tagged with a mouse scFc region. LL3-scFc and AAA-scFc were bound to sheep anti-mouse Fc Dynabeads® (Invitrogen) and incubated with HEK293 cell lysates overnight at 4°C. Beads were washed 3 times with cell lysis buffer and proteins were eluted by boiling in SDS sample buffer for 5 min. β-catenin detection by Western Blot showed that LL3 VHH does pull down β-catenin, while the mutant LL3.CDRAAA VHH does not. Figure adapted from Newnham et al., 2015.

Binding studies using different β-catenin fragments showed that LL3 binds between ArmR1 and ArmR6 of β-catenin (AA residues 164-390) (Newnham et al., 2015). This corresponds to the region where BCL9 and TCF4 are known to interact with β-catenin (Fasolini et al., 2003b; Sampietro et al., 2006). Further characterisation of LL3 indicated that the VHH was able to inhibit β-catenin-mediated Wnt signalling in HEK293 cells stably transfected with TCF-firefly Luciferase reporter constructs, while the mutant AAA did not (Newnham et al., 2015).

Overall, the data suggest that the VHH LL3 can specifically inhibit Wnt-mediated transcriptional activation by binding to β-catenin. It is the first time that an intracellular VHH has been described to target the Wnt signalling pathway. Further analyses needed to be performed to get a better understanding of the mechanism of action of the VHH.

6.2 Aim

The aim of this chapter was to further characterise the previously described VHHs against β-catenin. The main focus was to identify if LL3 had any functional effect, such as Wnt inhibition and cell killing, in SW480 colorectal cancer cells, and to narrow down the LL3 binding site on β-catenin to gain a better understanding on the mechanism of action of the VHH.

In order to answer these questions, the following steps were taken:

1. Confirm Wnt-mediated transcription inhibition by LL3 using the TOPflash assay.
2. Create and characterise stable inducible cell lines expressing the wild-type LL3 and mutant AAA to assess any functional effects of the VHHs.
3. Assess the binding site and binding kinetics of LL3 to β-catenin using recombinant proteins and pulldown assays.

6.3 Results

6.3.1 Expression of LL3 and AAA in SW480 cells

SW480 CRC cells were chosen for the characterisation of the VHHs LL3 and AAA because of their high baseline Wnt signal (APC mutant) and wild-type β-catenin status.

pNAFH-LL3 and pNAFH-AAA vectors (UCB Pharma) were received from Professor Rabbitts. The vector map of pNAFH-VHH is shown in Figure 6.2.

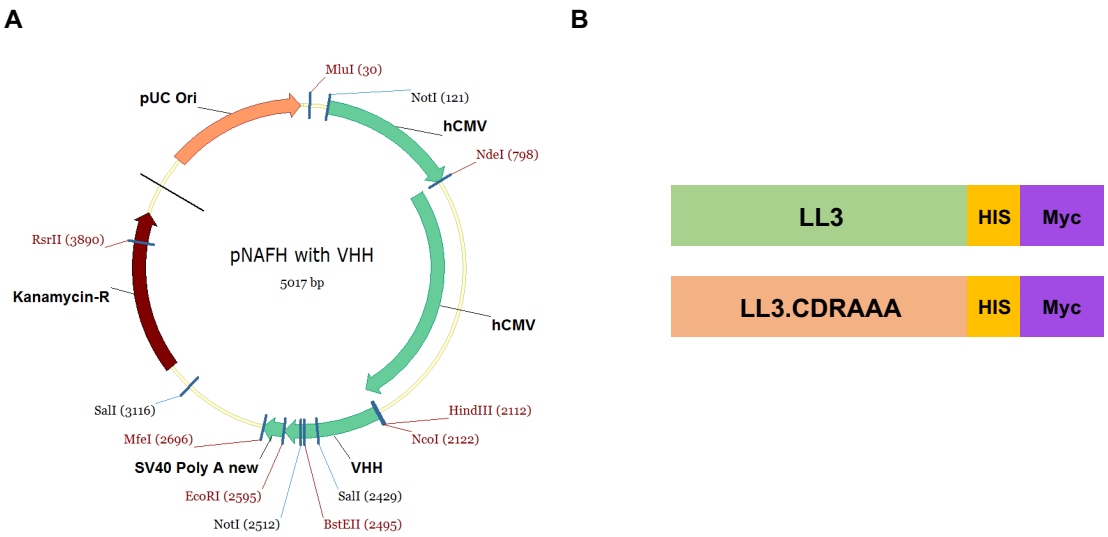


Figure 6.2 pNAFH-LL3 and pNAFH-AAA vector map and expected VHH structures
A) Vector map of pNAFH with VHH (LL3 or AAA) cloned into the HindIII/EcoRI sites. The vector map was received from Professor Terence Rabbitts, with permission from UCB Pharma. **B**) Schematic representation of the VHHs LL3 and AAA, with a HIS-tag and a myc-tag.

Vectors were sequenced at the WIMM in-house facilities to confirm the correct DNA sequence of both the wild-type LL3 and mutant AAA VHHs. Both constructs contain a HIS-tag and a myc-tag. In order to confirm the expression of the VHHs, the pNAFH-LL3 and pNAFH-AAA constructs were transfected into SW480 cells. The

expression of LL3 and AAA in SW480 cells was confirmed by WB and IF (Figure 6.3). The VHHs LL3 and AAA are expected at 16.9 kDa and 16.7 kDa, respectively.

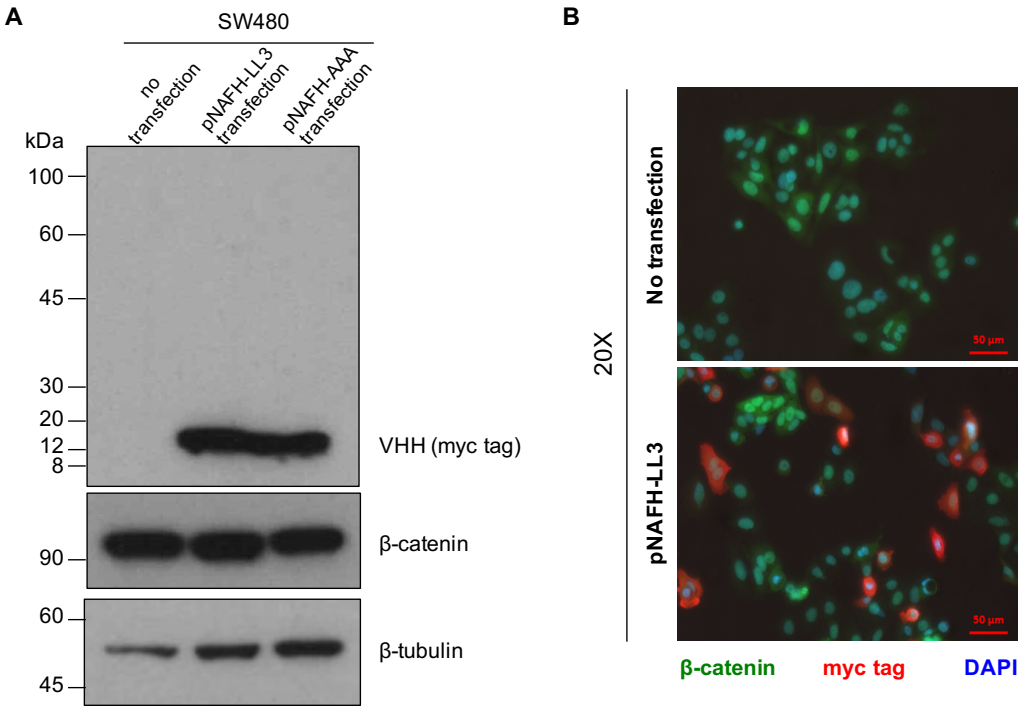


Figure 6.3 Expression of LL3 and AAA in SW480 cells
A) SW480 cells were transfected with pNAFH-LL3 and pNAFH-AAA vectors (1 µg each) using lipofectamine, and transfection medium was exchanged after 8 hrs. After 48 hrs, proteins were extracted using RIPA buffer and 30 µg of cell lysates were run an a 12% SDS acrylamide gel for separation. The membrane was probed with anti-myc-tag antibody (clone 9e10,1:5000, Cell Signaling) to detect the VHHs (17 kDa), as well as anti-β-catenin (1:8000, 92 kDa) and anti β-tubulin (1:6000). A lower exposure for β-catenin and the VHH detected by the myc-tag would have been of advantage to assess the expression levels of pNAFH-ll3 and pNAFH-AAA. **B**) pNAFH-LL3 vector was transfected into SW480 as described in A). After 48 hrs, the cells were fixed according to the methodology described in Chapter 2. Cells were stained using anti-myc tag (1:1000, Cell Signaling) and anti-β-catenin (1:300, abcam) antibodies. Images were taken using a Zeiss Observer z1 fluorescence microscope. Green: β-catenin, red: LL3 detected via myc-tag, blue: DAPI. Scale bars represent 50 µm, magnification 20X, 0.4 NA.

6.3.2 VHHs are expressed in the nucleus and cytoplasm

As the interaction site between LL3 and β-catenin and its mechanism of action is still unknown, it was important to get a better understanding of the localisation of the expressed VHHs throughout the cell. β-catenin is a protein that dynamically shuttles between the cytoplasm and the nucleus as part of its function in the Wnt pathway.

It is of interest to know if the VHHs are able to enter the nucleus, where LL3 could potentially inhibit β-catenin protein interactions with the transcription factor complex. We hypothesized that due to their small size (17 kDa), the VHHs are able to diffuse into the nucleus. Proteins larger than 60 kDa have previously been described to diffuse into the nucleus (Wang & Brattain, 2007).

In order to address the question of VHH localisation in the cell, total, cytoplasmic and nuclear protein fractions were isolated from transiently pNAFH-LL3 or pNAFH-AAA transfected SW480. As seen in Figure 6.4, the VHHs are expressed both in the cytoplasm and the nucleus, with Lamin A/C and β-tubulin as nuclear and cytoplasmic control, respectively.

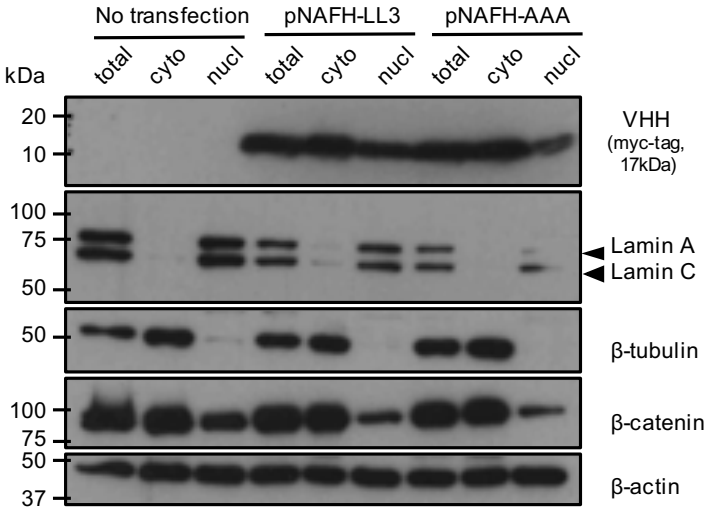


Figure 6.4 Cytoplasmic and nuclear expression of VHHs in transiently transfected SW480 cells
Total proteins as well as cytoplasmic and nuclear fractions were extracted from SW480 cells 48 hours post-transfection with pNAFH-LL3 and pNAFH-AAA, using RIPA lysis buffer and the N-PER protein extraction kit. Mock-transfected SW480 cells were used as negative control. Protein samples were separated on a SDS gel and membranes were probed with antibodies against myc-tag (VHHs), Lamin A/C (nuclear fraction), β-tubulin (cytoplasmic fraction), β-catenin and β-actin (total loading control).

These results show that the VHH LL3 is successfully expressed in the nucleus and so might have the potential to act on β-catenin in preventing the correct formation of the nuclear Wnt transcriptional complex.

6.3.3 WNT inhibition in SW480 cells by LL3

Previous TOPflash experiments by Newnham et al. (2015) showed that LL3 was able to inhibit the Wnt pathway, while the mutant version AAA did not. However, these experiments were performed in HEK293 cells, which needed to be co-transfected with Wnt1 in order to induce measurable Wnt signaling. (Newnham et al., 2015). The TOPflash experiments in this study were repeated with SW480 cells, which have endogenous Wnt transcriptional activity, as previously assessed by us (Chapter 3) and others (da Costa et al., 1999; Qu et al., 2016). SW480 cells were co-transfected with increasing concentrations of pNAFH-LL3 or pNAFH-AAA with TOPflash and FOPflash vectors, as well as a renilla construct for transfection control. An empty pNAFH vector without the LL3/AAA sequence was used to keep the DNA concentration constant in each well and a mock-transfection control was included. After 48 hours, the luciferase and renilla readings were taken and the Relative Luciferase Units (RLU, Luciferase/Renilla ratio) were calculated. As seen in Figure 6.5, LL3 dose-dependently inhibited the TOPflash signal up to approximately 50%, while AAA did not. The FOPflash vector with mutated TCF binding sites was used as negative control. Overall, these results confirmed the inhibitory activity of the VHH LL3 previously described by Newnham et al. (2015).

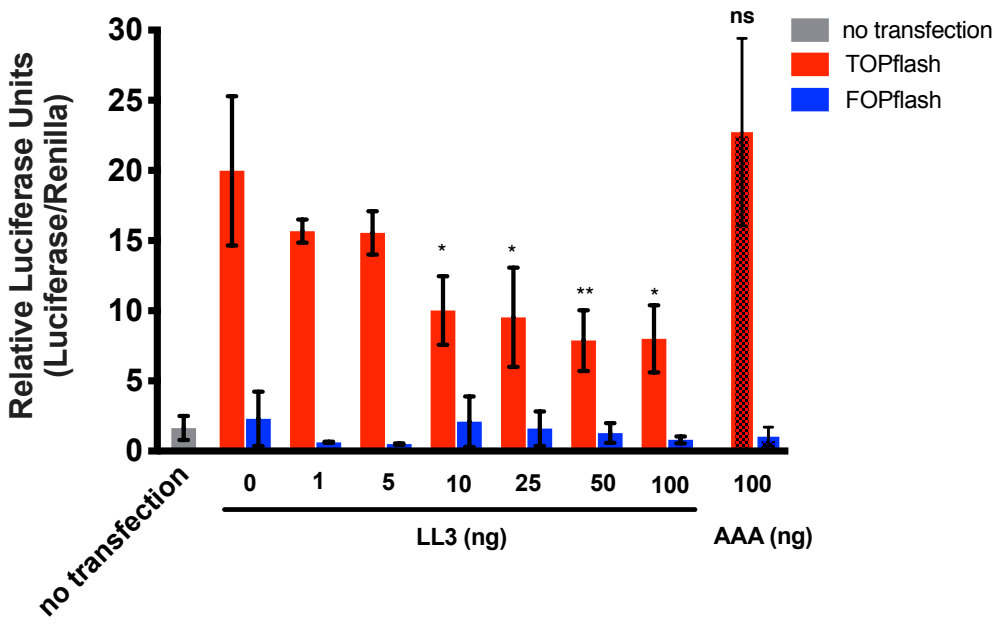


Figure 6.5 LL3 inhibits TOPflash signal in SW480 cells
LL3 inhibits the TOPflash signal in SW480 cells in a dose-dependent manner, while the mutant AAA does not. TOPflash assay was performed as described in the Materials and Methods chapter. All results were normalised to a blank control and Renilla was used as control for transfection efficiency. Results shown are from five independent experiments performed at least in duplicate. Unpaired t-test was used to analyse the statistical difference between baseline (0 ng LL3) and increasing concentrations of LL3. Error bars represent Standard Deviation, p-values: ns ≥0.05, * ≤0.05, ** ≤0.01. Ideally, the amount of LL3 and AAA should have been controlled for, for example through the addition of a quantifiable GFP-tag.

The reproducibility of the previously published Wnt-inhibition by LL3 in SW480 cells prompted us to investigate in more detail the mechanism of action of the VHH. The aim was to assess the effect of LL3 on cell survival and identify the LL3 binding site on β-catenin.

The use of VHH vector transfections was sub-optimal for further characterisations of the VHHs, as only a fraction of the cells were successfully transfected (see Figure 6.3B) and the expression would be only transient. Therefore, it was decided to create stably expressing cell lines using a doxycycline (DOX)-inducible lentivirus system.

6.3.4 Creation of stable VHH cell lines

The LL3 and AAA sequences were cloned in frame with the 2A self-cleaving peptide T2A and green-fluorescent protein (GFP) into the multicistronic TLCV2 lentiviral vector using the AgeI/BamHI restriction sites (Addgene #87360, vector received from the WIMM Lentiviral Facility, Figure 6.6A). This allowed the co-expression of the VHH proteins and GFP from a single transcript under the regulation of the same promoter (Figure 6.6B). The lentiviruses were produced by Dr Ryan Beveridge at the WIMM Lentivirus Facility.

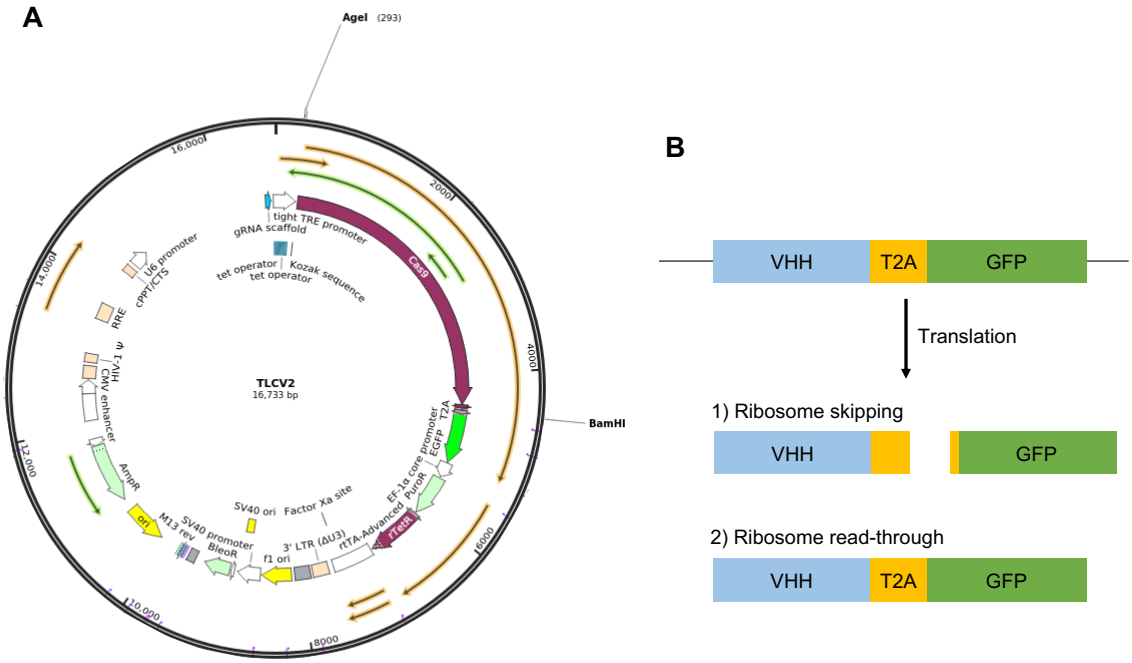


Figure 6.6 TLCV2 vector map
A) TLCV2 vector map. Adapted from the Addgene webpage. The VHHs of interest were cloned into the TLCV2 vector in frame with a T2A self-cleaving site and GFP instead of the Cas9 using the AgeI/BamHI restriction sites and under the control of the tight tetracycline-responsive element (TRE) promoter. **B**) Schematic representation of the multicistronic VHH-T2A-GFP construct. Ribosome skipping at the T2A sequence will result in the production of separate VHH and GFP proteins under the expression of the same promotor. In some cases, it can occur that the ribosome reads through the T2A site, resulting in a single protein product of the VHH fused to GFP. Figure adapted from Liu et al., 2017.

6.3.4.1 Lentiviral transduction of SW480

SW480 cells were transduced with increasing volumes (2.5, 5, 25 and 50 µL) of the lentivirus pTLCV2-LL3 or pTLCV2-AAA received from the WIMM Lentivirus facility. A puromycin killing curve was performed on parental SW480 cells to choose the antibiotic concentration for lentivirus transduced cells (Appendix D.2). After 3 days, transduced cells were selected using 1.2 µg/mL puromycin with SW480 parental cells as control (Figure 6.7).

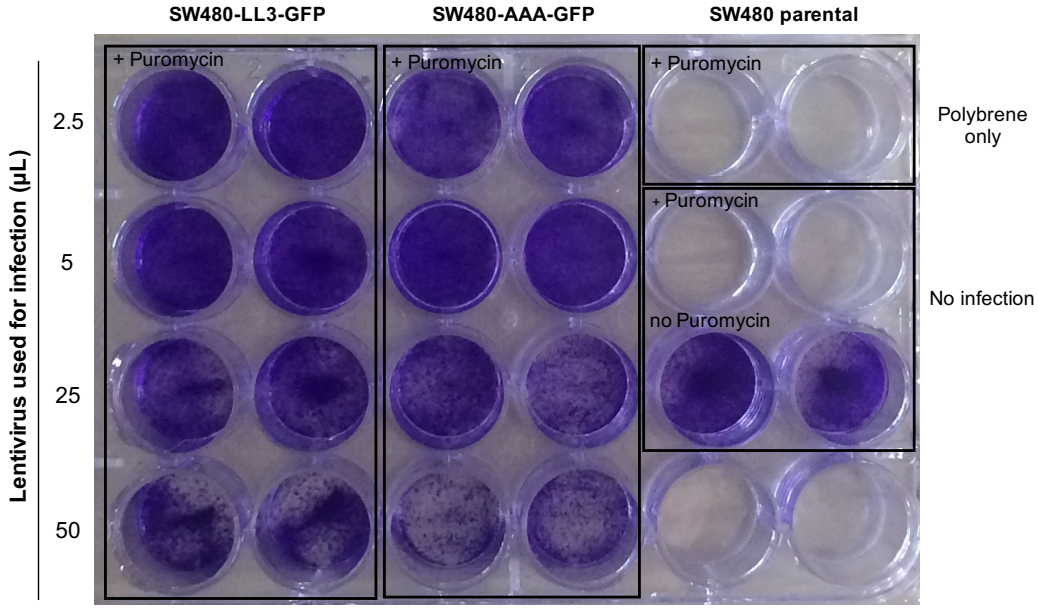


Figure 6.7 Puromycin selection of SW480-LL3-GFP and SW480-AAA-GFP bulk cell lines
After three days of lentiviral incubation, transduced SW480 cells were selected using 1.2 µg/mL puromycin until all SW480 parental control cells were dead. As seen in this crystal violet stain, SW480 parental cells were killed by the puromycin selection, while cells of the bulk lines SW480-LL3-GFP_2.5, SW480-LL3-GFP_5, SW480-LL3-GFP_25 and SW480-LL3-GFP_50 as well as SW480-AAA-GFP_2.5, SW480-AAA-GFP_5, SW480-AAA-GFP_25 and SW480-AAA-GFP_50 were successfully selected using puromycin. It is worth noting that the cell lines transduced with 50 µL lentivirus looked unhealthy under microscopic inspection and this is also reflected by the crystal violet stain, where a less dense staining could be observed by visual inspection.

Upon passaging the stable cell lines for routine cell culture, it was noted that the bulk cell lines SW480-LL3-GFP_50 and SW480-AAA-GFP_50 detached from cell culture flask easily, without the induction of the VHH constructs. Moreover, their

morphology looked unhealthy and rounded compared to the other stable clones (Figure 6.8) and many cells were observed floating. It was suspected that the high lentiviral concentration might affect normal cell functions due to high viral load and too many integration sites. Therefore, stable cell lines transduced with 25 and 50 µL of lentivirus were not used in further experiments.

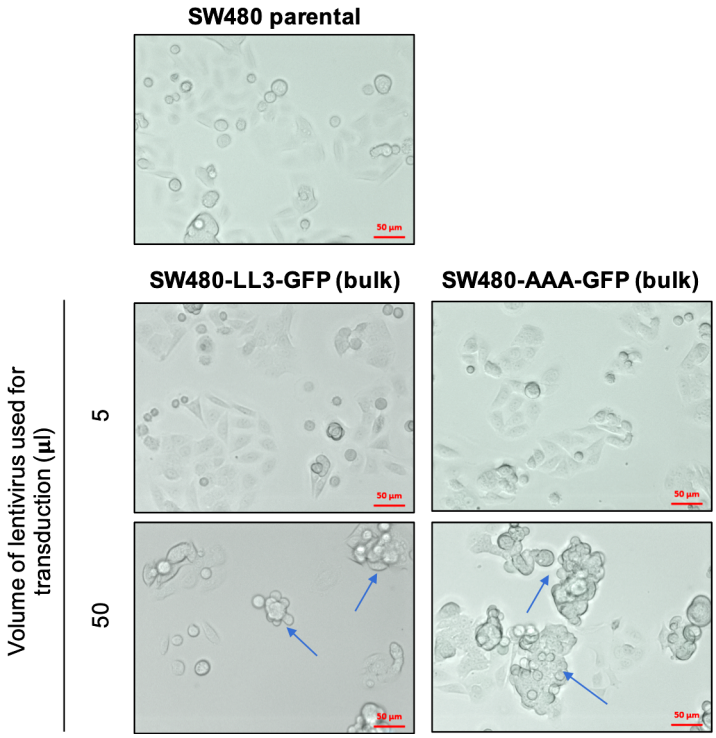


Figure 6.8 Brightfield images of stable cell lines SW480-LL3-GFP and SW480-AAA-GFP
Brightfield images were taken of SW480 parental as control and puromycin-selected stable cell lines SW480-LL3-GFP_5, SW480-LL3-GFP_50, SW480-AAA-GFP_5 and SW480-AAA-GFP_50 under normal cell culture conditions. As indicated by the blue arrows, SW480-LL3-GFP_50 and SW480-AAA-GFP_50 cells exhibited a more rounded and clustered morphology compared to the stable cell lines from transductions with lower lentivirus concentrations. Brightfield images at 20X magnification, 0.4 NA, scale bars represent 50 µm.

6.3.5 Expression of VHHs upon DOX induction

Puromycin selected stable bulk cell cultures SW480-LL3-GFP_2.5, SW480-LL3-GFP_5, SW480-AAA-GFP_2.5 and SW480-AAA-GFP_5, and SW480 parental cells were treated with 1 µg/mL DOX for 48 hrs to assess the VHH induction in the cell lines. Western Blot analyses show a good induction of both LL3 and AAA

(detected by the myc-tag) at the correct size of 17 kDa, as seen in Figure 6.9. The co-expression of GFP in DOX-induced cells was validated as well. SW480 parental cells were used as negative control. It is worth noting a faint signal below 50 kDa in DOX induced cells, which is believed to be the "read-through" product of VHH+GFP with an insufficient T2A cleavage of the VHH from the GFP product.

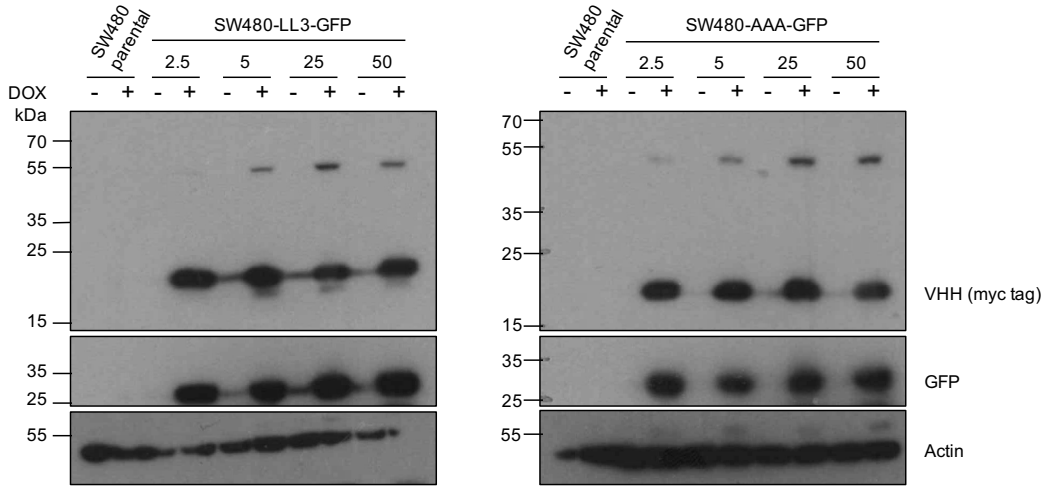


Figure 6.9 VHH expression of VHHs after DOX induction in stable cell lines
SW480 parental cells and stable bulk cell lines were treated with DMEM alone or supplemented with 1 µg/mL DOX for 48 hours. Proteins were run on a 14% SDS acrylamide gel and detected using anti-myc-tag antibody (1:6000), anti-GFP (1:500) and anti-actin (1:6000). Upon DOX induction, the VHHs could be detected in all transduced bulk cell lines at the expected size of 17 kDa, while absent in the SW480 parental control cells. GFP expression was used as induction control. Shorter time exposures would have been of advantage for interpretation of the results. It should be noted that a fainter band at about 50 kDa can be detected using the myc-tag antibody. This corresponds to the VHH-GFP "read-through" product, where the T2A ribosomal skipping site was not successful (described in Figure 6.6B).

Previous reports have identified putative unwanted side-effects of DOX, such as the impairment of mitochondrial functions (Moullan et al., 2015) and alteration of cellular proliferation (Ahler et al., 2013). In the preliminary experiment presented here, 1 µg/mL DOX was used as a starting point based on the advice from the lentiviral facility at the WIMM. Having shown successful VHH induction in the stable cell lines at 1 µg/mL DOX (Figure 6.9), more experiments were performed to assess the optimal DOX induction concentration. Furthermore, it was of interest to characterise

the VHH expression kinetics after DOX induction. In order to answer these questions, SW480 parental, SW480-LL3-GFP_2.5 and SW480-AAA-GFP_2.5 bulk cell lines were treated with increasing concentrations of DOX for 48 hrs and imaged for imaged for GFP (Figure 6.10). Proteins were extracted from the samples and analysed by WB (Figure 6.11). Both the GFP expression assessed by microscopy, as well as the Western Blot analysis shows that the VHHs can be successfully induced at concentrations starting at 10 ng/mL DOX. It was decided to perform all further experiments at 100 ng/mL DOX in order to ensure successful induction of the stable cell lines.

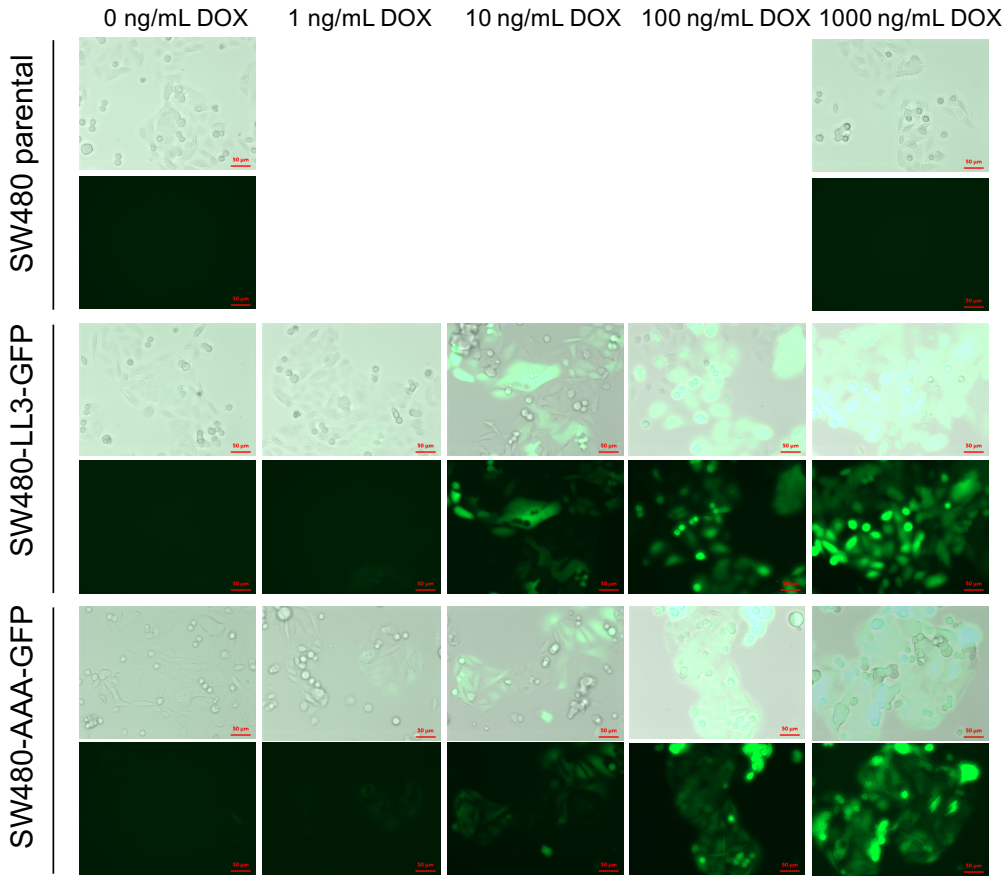


Figure 6.10 DOX titration – Immunofluorescence
SW480 parental cells, SW480-LL3-GFP_2.5 and SW480-AAA-GFP_2.5 bulk cell lines were seeded into a 96-well plate and treated with the indicated concentrations of DOX for 48 hrs. GFP signal was imaged using the Zeiss Observer z1 fluorescent microscope. Brightfield-GFP overlay is shown in the top panels, GFP channel alone in the lower panels. GFP expression was observed at concentrations starting from 10 ng/mL DOX. All images were taken with the same time exposure. Scale bars represent 50 µm, magnification 20X, NA = 0.4.

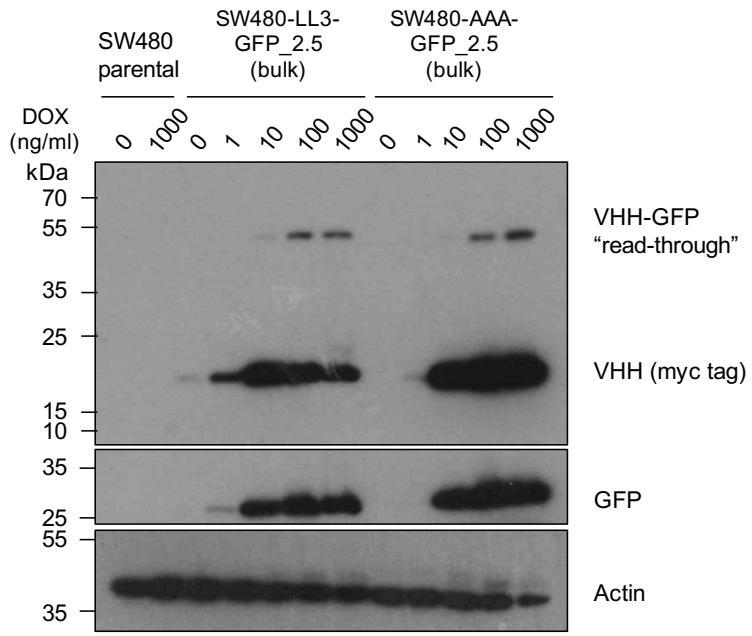


Figure 6.11 DOX titration in SW480-LL3-GFP_2.5 and SW480-AAA-GFP_2.5 cell lines
SW480 parental cells, SW480-LL3-GFP_2.5 and SW480-AAA-GFP_2.5 bulk cell lines were seeded into 6-well plates and treated with the indicated DOX concentrations for 48 hrs. Proteins were extracted using RIPA buffer and 30 µg were loaded onto a 14% SDS gel. The membrane was probed with antibodies against myc-tag (1:6000), GFP (1:500) and actin (1:6000). Detection of the VHHs were clear from 10 ng/mL DOX and consistent with the GFP signal. Once again, the VHH-GFP "read-through" product was observed at about 50 kDa. A shorter time exposure would have been beneficial for a better interpretation of the expression between different time points.

In a further attempt to characterise the DOX induction conditions of the stable cell lines, the SW480-LL3-GFP_2.5 bulk cell line was treated with 100 ng/mL DOX for 2, 8, 16, 24 and 48 hours. Cell lysates were analysed by Western Blot to detect the expression of LL3 at each time point. Figure 6.12 shows that LL3 is robustly expressed 8 hours post DOX treatment.

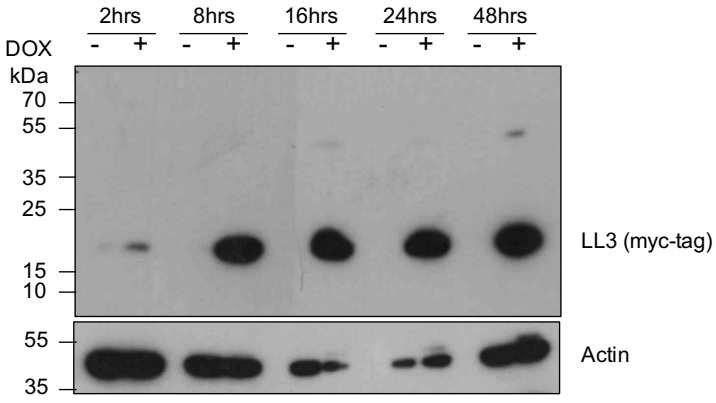


Figure 6.12 Time kinetics of VHH expression after DOX induction
SW480-LL3-GFP_2.5 bulk cell line was seeded into 6-well plates. The next day, cells were treated with either DMEM alone as control or DMEM with 100 ng/mL DOX. Proteins were extracted after the indicated times of treatments. Thirty µg of proteins were loaded for each protein onto a 14% SDS gel and the membrane was probed with antibodies against myc tag (1:6000) and actin (1:6000). A faint LL3 expression can be detected after 2 hrs DOX treatment, while the expression was clearly induced after 8 hrs DOX treatment. As previously described, a faint band at 50 kDa in the DOX induced samples can be detected, which corresponds to the LL3-GFP read-through product. A clear shortfall of this result is the unequal protein loading, as assessed by actin.

Furthermore, in order to confirm the VHH expression localisation in stable DOX-induced cell lines to be the same as in the transiently transfected cells (Figure 6.4), cytoplasmic and nuclear protein fractions were isolated from bulk cell lines SW480-LL3-GFP_2.5 and SW480-AAA-GFP_2.5 after 48 hrs of DOX treatment. In both cell lines, the VHHs are present in both the nuclear and cytoplasmic fraction of the DOX-induced cells (Appendix D.3), confirming previously observed results (Figure 6.4).

6.3.6 LL3 binds to β-catenin in SW480 cells

In previous immunoprecipitation experiments, the purified LL3 VHH (mobilised on beads) was shown to interact with cellular β-catenin from HEK293 lysates (Newnham et al., 2015). However, this result does not answer the question of whether LL3 is able to interact with β-catenin intracellularly, in the reducing environment of the cell.

To confirm that the interaction can occur within cells, a myc-tag pulldown assay was performed on the stable cell lines SW480-LL3-GFP_2.5 and SW480-AAA-GFP_2.5. The Western Blot in Figure 6.13 clearly shows that the VHH LL3 is able to pulldown β-catenin in the DOX induced sample, while the mutated VHH AAA does not. These results show that the VHHs are able to express correctly inside cells upon DOX induction and that LL3 binds to β-catenin in living cells. This confirms the previous results by Newnham et al., where the interaction was shown between purified LL3 and endogenous β-catenin.

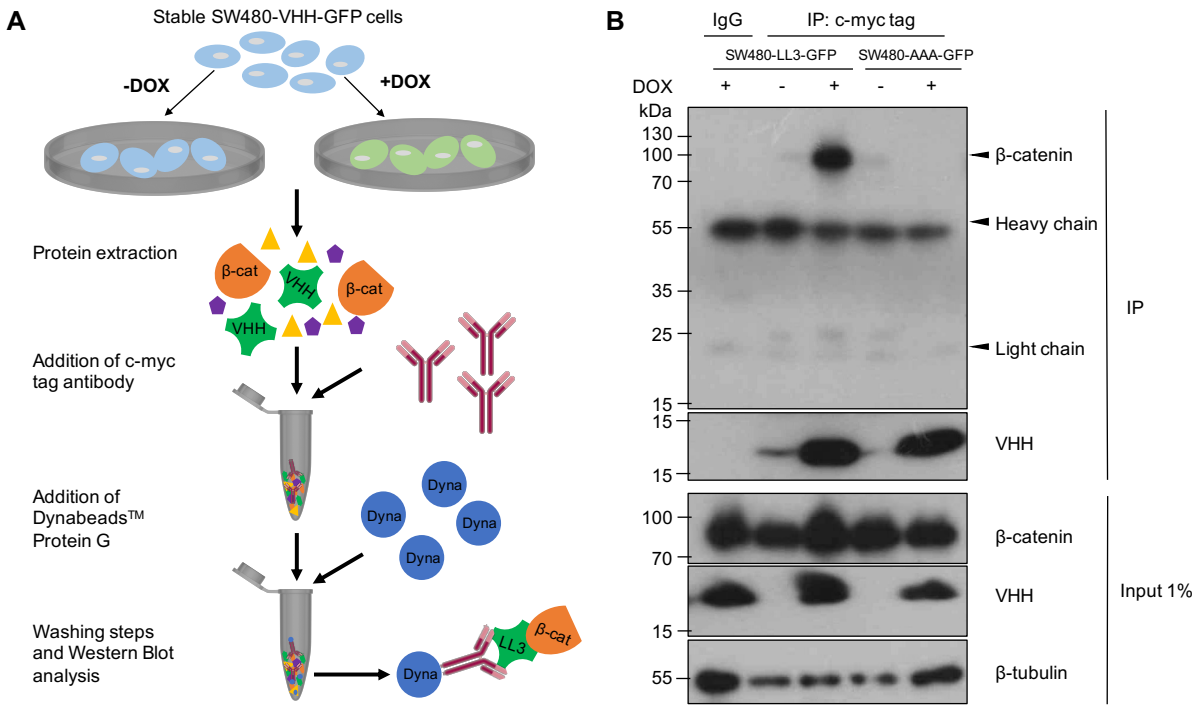


Figure 6.13 Pulldown assay of LL3 and AAA in the bulk cell lines SW480-LL3-GFP_2.5 and SW480-AAA-GFP_2.5
A) Schematic representation of experimental setup. **B**) LL3 pulled down β-catenin in DOX-induced SW480 cells, while AAA did not. SW480-LL3-GFP_2.5 and SW480-AAA-GFP_2.5 bulk cell lines were treated with 100 ng/mL DOX or control for 48 hrs. Proteins were extracted using the NP40 lysis buffer (20 mM Tris-HCl pH8, 200 mM NaCl, 1% NP40) and 500 µg of each cell lysate were used for the pulldown. Immunoprecipitations (IP) were performed as described in the Materials and Methods Chapter. IPs and the input controls (1%) were separated on a 12% SDS gel and the membrane was probed for β-catenin (1:6000), myc-tag (1:5000) and β-tubulin (1:6000). The immunoprecipitation experiment was performed three times and a representative result is given. A shorter time exposure would have been beneficial for interpretation.

6.3.7 Characterisation of SW480-LL3-GFP and SW480-AAA-GFP stable clones

The experiments with the stable bulk cultures exhibited good expression of the VHHs in both the cytoplasm and nucleus and confirmed the interaction of LL3 and β-catenin. Based on these results, it was decided to further assess the effect of the LL3 on cell growth and viability.

As the stable puromycin-selected cell lines are heterogeneous for lentivirus insertion sites and expression of the VHHs might vary from cell to cell, single clones were derived from the bulk cell lines SW480-LL3-GFP_2.5, SW480-LL3-GFP_5, SW480-AAA-GFP_2.5 and SW480-LL3-GFP_5 by single cell sorting (WIMM FACS Facilities, see Methods). After successful puromycin selection, a number of LL3 and AAA clones were selected for further experiments (Table 6.1).

	Clones								
SW480-LL3-GFP_2.5	3D6	2E3	3C5	2B10					
SW480-LL3-GFP_5	1F5	2D3	2G10	2D8	2B6	2G11	3B5	1C6	3E11
SW480-AAA-GFP_2.5	1B5	1E10							
SW480-AAA-GFP_5	2F8	2D9	1B4	2E5	2E6	3B2	1D5	1F3	2C11

Table 6.1 List of SW480-LL3-GFP and SW480-AAA-GFP clones used throughout this work
A total of four SW480-LL3-GFP_2.5 clones, nine SW480-LL3-GFP_5 clones, two SW480-AAA-GFP_2.5 clones and nine SW480-AA-GFP_5 clones were used in experiments throughout this study. All clones were selected through puromycin and showed positive GFP expression upon DOX treatment.

In order to confirm the correct DNA sequence, the LL3 and AAA regions of interest were amplified from cDNA of each clone using PCR (Figure 6.14), purified and sent for Sanger sequencing at the in-house WIMM Sequencing Facility.

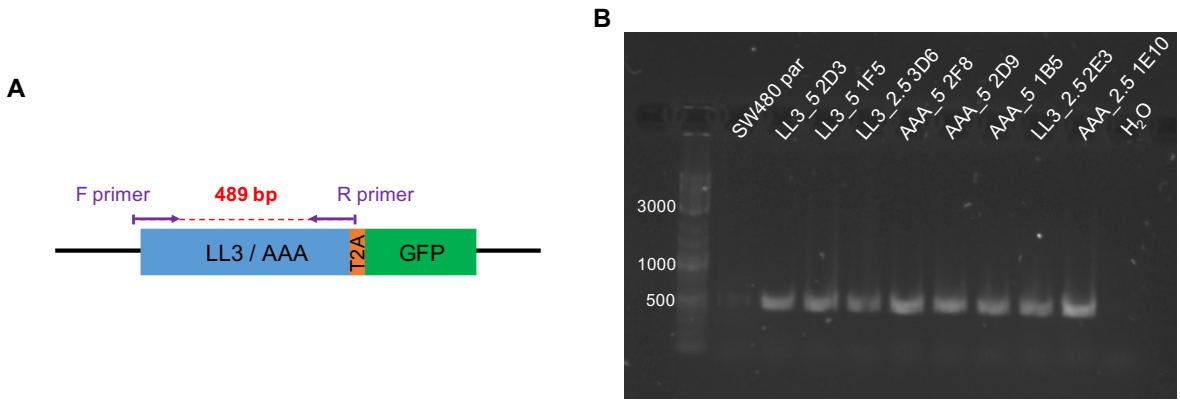


Figure 6.14 PCR product of LL3 and AAA from single clones for sequence confirmation
A) Schematic representation of the PCR products. **B**) cDNAs from the indicated DOX-treated clones were used as templates for the PCR using VHH-TLCV2_AgeI_F and VHH-GFP_TLCV2_BamHI_R primers and high-fidelity polymerase. cDNA from SW480 parental cells and a H_2O reaction were used as negative controls. A fraction of the PCR reactions was run on a 1% agarose gel for analysis. The expected fragments size of LL3 and AAA products is 489 bp. The PCR products were purified using a PCR purification kit (Qiagen) and sent for sequencing using the VHH-GFP_TLCV2_BamHI_R primer.

The following clones were sequenced: SW480-AAA-GFP 2D9, 1D5, 1F3, 1B5, 1E10, 2E6, 2E5, 1F9, 1B4, 2C11, 3B2 and SW480-LL3-GFP 1C6, 2D3, 1F5, 2D8, 2B6, 2E3, 1B10, 3C5, 2G10, 3D6, 2G11, 3B5. All clones contained the expected sequence. Figure 6.15 shows the differentiating sequence chromatograms of clones LL3 3D6 and AAA 2D9 as a representative example. The sequencing results for all clones can be found in Appendix D.4.

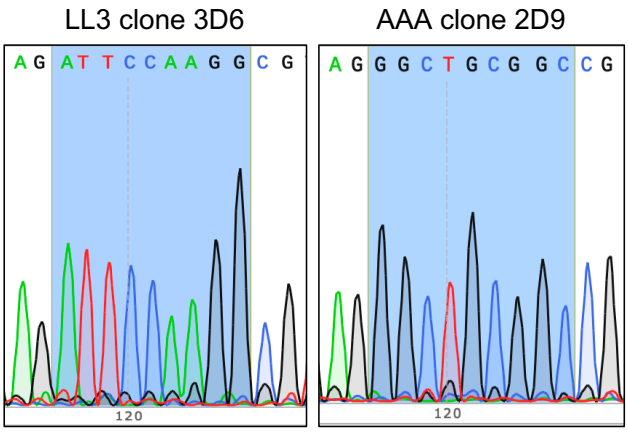


Figure 6.15 Sequencing chromatograms of AAA clone 2D9 and LL3 clone 3D6
LL3 and AAA area of interest were sequenced using the VHH-GFP_TLCV2_BamHI_R reverse primer. Highlighted in blue is the 9 bp reverse sequence differentiating the wild-type LL3 (ATTCCAAGG) from the mutant version AAA (GGCTGCGGC). This is equivalent to the forward sequence CCTTGGAAT and GCCGCAGCC for LL3 and AAA clones, respectively. Clones LL3-3D6 and AAA-2D9 are given as representative examples.

Fluorescence-activated cell sorting (FACS) analysis was used in order to assess what percentage of cells were successfully induced upon DOX treatment of each clone. As seen in the table in Figure 6.16A, GFP expression was induced in over 99% of cells in each DOX treated clone, compared to its untreated control. This indicates that all cells were transduced with the lentiviral construct. Figure 6.16B gives an example of the FACS data showing the GFP expression of LL3-GFP_5 clone 2D3 and AAA-GFP_5 clone 2D9 with and without DOX treatment (100 ng/mL, 48 hrs). In order to correlate the GFP signal with the VHH expression in the tested clones, proteins were extracted from the analysed cells and probed for the myc-tagged VHHs by Western Blot (Figure 6.16C). It can be clearly seen that the VHH expression in clone LL3 2D3 is significantly higher than the other LL3-clones.

A

Clone	DOX	% GFP +ive
LL3-GFP_2.5 **2E3**	-	0.2
	+	98.89
LL3-GFP_2.5 **3D6**	-	0.24
	+	99.8
LL3-GFP_5 **1F5**	-	0.35
	+	98.37
LL3-GFP_5 **2D3**	-	0.1
	+	99.48
AAA-GFP_2.5 **1B5**	-	0.17
	+	99.95
AAA-GFP_2.5 **1E10**	-	0.97
	+	99.49
AAA-GFP_5 **2F8**	-	0.24
	+	99.65
AAA-GFP_5 **2D9**	-	0.06
	+	98.96

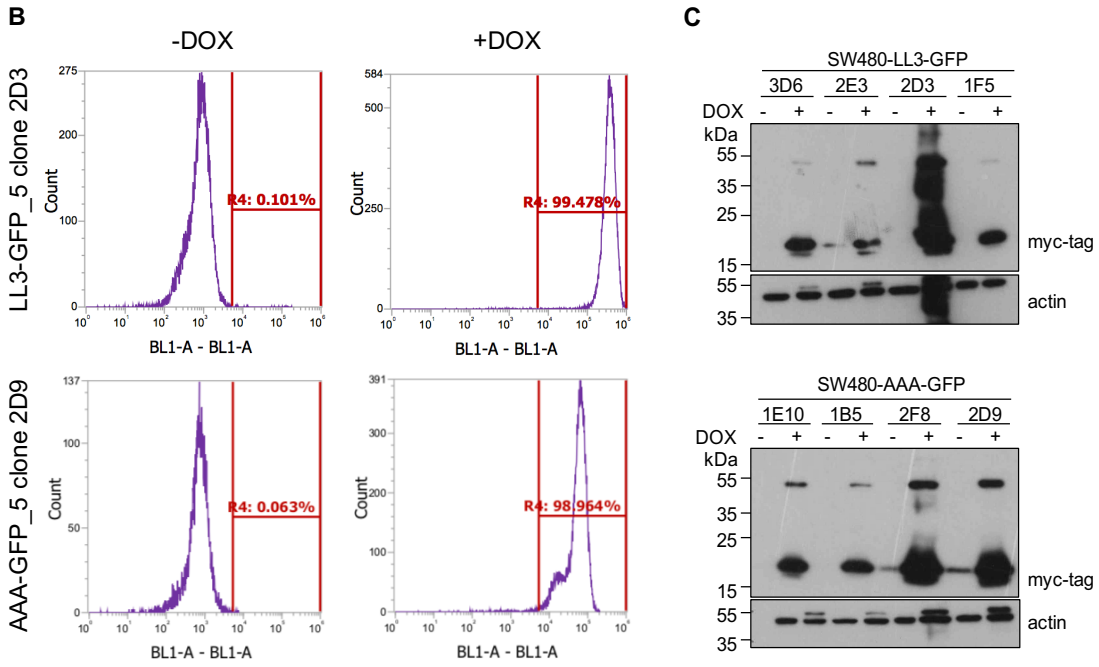


Figure 6.16 Examples of FACS analysis of LL3-GFP_5 clone 2D3 and AAA-GFP_5 clone 2D with and without DOX induction

150000 cells of different SW480-LL3-GFP_5 and SW480-AAA-GFP_5 clones were treated with DMEM with or without 100 ng/mL DOX for 48 hrs. Cells were trypsinised, washed and resuspended in 400 µL PBS on ice and stained with DAPI (1:1000) for 10 min. FACS analysis was performed by Dr Paul Sopp from the WIMM FACS Facility. **A**) Table indicating the percentage of GFP-positive cells in each clone with and without DOX treatment. **B**) Example of the GFP induction shift analysed by FACS analysis in clones LL3-GFP_5 clone 2D3 and AAA-GFP_5 clone 2D9. Left panels show GFP signal without DOX treatment, and the right panel with DOX treatment. Y-axis indicates number of counted cells, X-axis shows GFP signal. BL1-A: GFP channel. FACS data of other clones can be found in Appendix D.5. **C**) Western Blot of the FACS analysed cells. The VHHs were detected by the myc-tag. The band above the actin signal is the "read-through" product detected via the myc-tag antibody.

To further characterise the VHH expression in the stable clones upon DOX induction, protein lysates of various DOX treated clones were analysed by Western Blot (Figure 6.17). Eight SW480-LL3-GFP and eight SW480-AAA-GFP clones were analysed, alongside the SW480 parental control. SW480-LL3-GFP clone 2D3 expressed significantly more LL3 compared to other SW480-LL3-GFP clones. A similar result was previously noted in the FACS analysed cells (Figure 6.16). The VHH-GFP readthrough products are clearly visible in most of the clones, while the intensity of the signal varies notably between the clones.

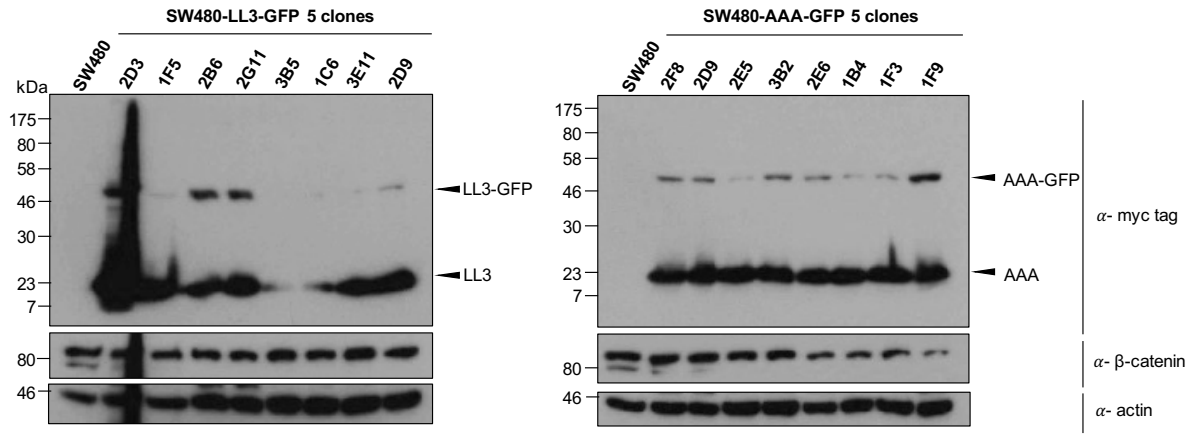


Figure 6.17 VHH baseline expression in various SW480-LL3-GFP_5 and SW480-AAA-GFP_5 clones analysed by Western Blot
Various SW480-LL3-GFP_5 and SW480-AAA-GFP_5 clones were treated with 100 ng/mL DOX for 48 hrs and proteins were extracted using RIPA buffer. Protein lysates (30 µg) were analysed by Western Blot by separating the proteins on a 12% SDS gel. Membranes were probed for the myc-tag to assess the VHH expression, β-catenin and actin.

6.3.7.1 β-catenin – LL3 interaction in single stable clones

In order to confirm that the VHH LL3 positively interacted with β-catenin in the single stable clones, myc-tag immunoprecipitation assays were performed in some SW480-LL3-GFP and SW480-AAA-GFP single clones. As expected, none of the mutant SW480-AAA-GFP clones showed any interaction with β-catenin. A clear binding between LL3 and β-catenin could be detected in all tested SW480-LL3-GFP

clones. Representative immunoprecipitation assays of SW480-LL3-GFP clone 3C5 and SW480-AAA-GFP clone 1F9 are shown in Figure 6.18. Pulldown assays of clones SW480-LL3-GFP clones 3C5, 3D6, 1F5, 2G10, 2D8 and SW480-AAA-GFP clones 1F9, 1B5, 2D9, 1B4 are represented in Appendix D.6. It should be noted that some clones showed detectable VHH expression in the absence of DOX induction, which was enriched through the myc-tag immunoprecipitation of the VHH. This might be due to the use of FBS that potentially contains traces of tetracycline and its derivatives. Specific tetracycline-free FBS should have been used to avoid the background induction.

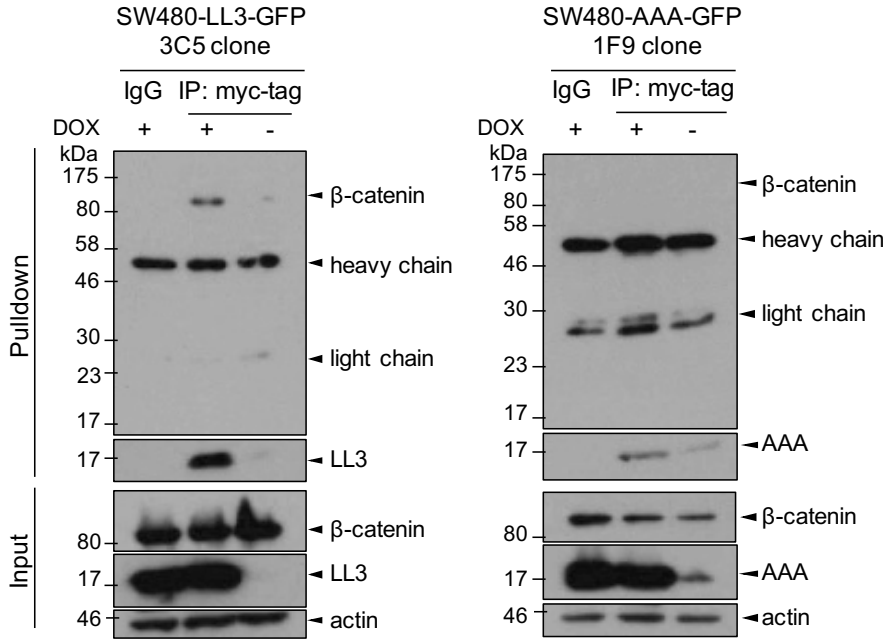


Figure 6.18 Myc-tag immunoprecipitation in single clones SW480-LL3 GFP 3C5 and SW480-AAA-GFP 1F9
Representative myc-tag immunoprecipitations of SW480-LL3-GFP clone 3C5 and SW480-AAA-GFP clone 1F9. Stable clones were treated with 100 ng/mL DOX or DMEM alone as control for 48 hrs. Proteins were extracted using NP40 lysis buffer. IP samples were separated on a 12% SDS gel and probed for the proteins of interest. The VHH LL3 expressed in the cell line SW480-LL3-GFP clone 3C5 is able to pulldown endogenous β-catenin, while no signal is present for the same protein in the mutant cell line SW480-AAA-GFP clone 1F9. Expected sizes for β-catenin: 92 kDa, LL3 and AAA: 17 kDa, actin: 42 kDa. The heavy chain and light chain from the myc-tag antibody used for the immunoprecipitation are expected at 50 kDa and 25 kDa, respectively. The VHHs are detected by the myc-tag.

6.3.7.2 SRB viability assay and cologeneic assay data of single clones expressing LL3 and AAA

As the positive interaction between LL3 and β-catenin was confirmed in isolated clones through immunoprecipitation experiments, the next aim was to assess if the stable clones showed any differential response regarding cell survival upon LL3 and AAA induction. Multiple clonal SW480-LL3-GFP_2.5, SW480-AAA-GFP_5, SW480-AAA-GFP_2.5 and SW480-AAA-GFP_5 cells were treated with increasing concentration of DOX (0 - 100 ng/mL) for 5 days (three DTs of parental SW480 cells) and tested by the SRB assay to assess the effect of the DOX treatment on the viability of the cells. Bulk cultures were also treated to get a better understanding if any seen effects are clone specific or applicable to the general cell population. Table 6.2 lists the clones treated in the SRB assays with their percentage cell survival compared to untreated control after 5 days of DOX treatment.

Stable cell line	Clone	Mean % cell survival at 100 ng/mL DOX compared to control (± SD)	p-value
SW480-LL3-GFP_2.5	bulk	101.5 (± 3.4)	0.490
	3C5	121.4 (± 23.5)	0.033
	2B10	111.8 (± 5.8)	0.0001
	3D6	97.2 (± 3.6)	0.258
	2E3	91.8 (± 7.5)	0.266
SW480-LL3-GFP_5	bulk	91.5 (± 5.7)	0.024
	2D8	91.9 (± 13.3)	0.137
	2G10	123.3 (± 23.6)	0.023
	2D3	0.47 (± 0.8)	<0.0001
	1F5	9.4 (± 8.7)	<0.0001
	3B5	90.8 (± 8.9)	0.084
	2B6	80.7 (± 9.1)	0.005
	2G11	96.2 (± 7.6)	0.431
	3E11	101.5 (± 1.7)	0.186
	1C6	99.0 (± 10.5)	0.880
SW480-AAA-GFP_2.5	bulk	99.2 (± 2.4)	0.598
	1E10	100.9 (± 4.7)	0.747
	1B5	99.8 (± 10.9)	0.980
SW480-AAA-GFP_5	bulk	91.2 (± 9.34)	0.107
	2D9	89.1 (± 16.5)	0.233
	2F8	68.7 (± 9.0)	0.0004
	1F9	110.0 (± 8.3)	0.015
	1B4	50.1 (± 24.3)	0.0005
	2E6	99.9 (± 13.9)	0.987
	3B2	105.9 (± 9.4)	0.335
	2C11	92.8 (± 3.5)	0.024
	2E5	71.7 (± 1.9)	0.002
	1D5	97.7 (± 11.0)	0.793
	1F3	95.8 (± 11.6)	0.658
SW480 parental	bulk	100.5 (± 2.8)	0.660

Table 6.2 Percentage cell survival at 100 ng/mL DOX treatment analysed by the SRB assay

Cells were treated with increasing DOX concentrations for three cell DTs (5 days). Cells were fixed and the percentage of surviving cells at 100 ng/mL was calculated compared to the untreated control using the SRB assay. Each clone was tested in triplicate in at least three independent biological experiments, standard deviation (±SD) given, p-values were calculated using two-tailed multiple t-tests, False Discovery Rate-adjusted p-values for multiple testing using the Benjamini, Krieger and Yekutieli corrections are given. Clones that show a discovery according to the multiple corrections are highlighted in orange.

In all of the tested SW480-LL3-GFP_2.5 and SW480-AAA-GFP_2.5 clones, the DOX induction showed no negative effect on viability compared to untreated control. Out of nine SW480-LL3-GFP_5 clones, two exhibited significant cell death at 100 ng/mL DOX. Specifically, clone 2D3 had no surviving cells five days post DOX treatment ($p<0.0001$), while the clone 1F5 only showed about 10% cell survival compared to untreated control ($p<0.0001$). Clone 2B6 showed 80% cell survival after three DTs, compared to untreated control ($p=0.002$). Interestingly, it is the 2D3 clone that was shown to repeatedly express higher amounts of LL3 in previous experiments (Figure 6.16 and Figure 6.17). On the other hand, three out of 10 tested SW480-AAA-GFP_5 clones, namely clones 2F8, 1B4 and 2E5, exhibited some degree of decreased cell viability upon DOX treatment. Most notably, clone 1B4 showed the highest degree of cell killing, with approximately 50% of cell survival after 5 days of DOX-treatment. Note the large standard deviation for the repeated experiments with this clone, indicating significant variability between the biological replicates (also visualised in Figure 6.19). The effect of DOX induction in some of the SW480-AAA-GFP clones raised the question of whether the observed cell death is due to the action of the VHH (nonspecific in the case of AAA), or due to toxicity induced because of the lentiviral integration sites in the specific clones. While some of the SW480-LL3-GFP_5 and SW480-AAA-GFP_5 clones showed significant cell death upon DOX induction, the bulk cultures did not exhibit the same effect. This supports the hypothesis that clonal heterogeneity of the lentiviral integration site plays an important role in the observed results.

All clones were further tested in Colony Formation Assays (CFA) to assess the ability of the clones to attach and form colonies. This was also used to support the findings from the SRB assay. Cells were seeded into 6-well plates in triplicate and treated with 100 ng/mL DOX or DMEM alone as growth control for 9 days. Images of the colonies were taken using a fluorescence microscope before fixation as a proof of GFP expression upon DOX treatment. The percentage of colony formation compared to untreated control was calculated. Representative examples of SW480 parental, SW480-LL3-GFP_5 clones 2D3 and 2G10 and SW480-AAA-GFP_5 clones 2D9 and 1B4 show a good agreement between the SRB and CFA data (Figure 6.19A and B, respectively). Some clones were able to form relatively large colonies that stained very well with the crystal violet stain (example clone 2D3), while other clones formed small colonies in the same time period (example clone 2G10).

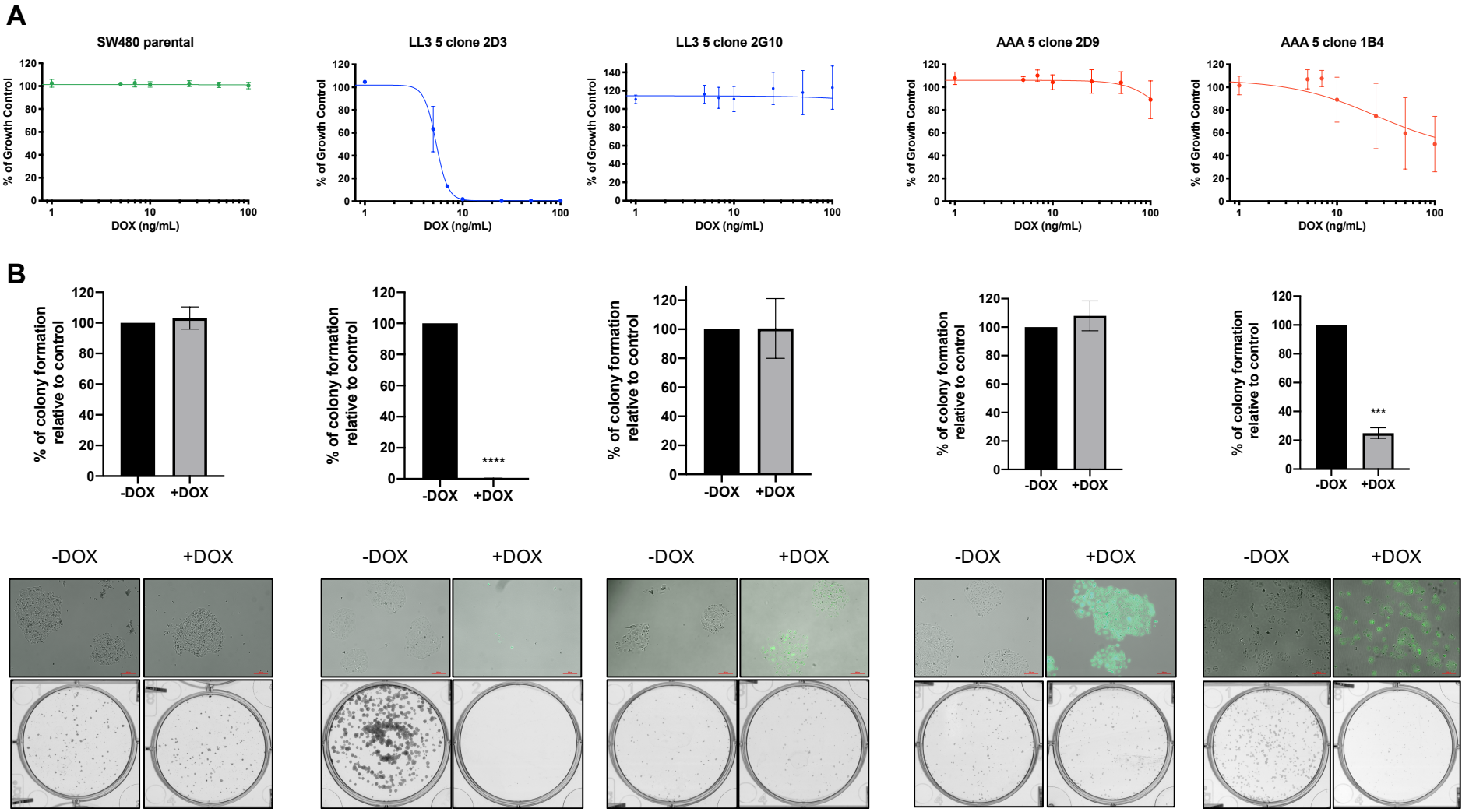


Figure 6.19 SRB and CFA assay data of representative clones

A) SRB survival curves for SW480 parental cells (green), SW480-LL3-GFP_5 clone 2D3 and SW480-LL3-GFP_5 clone 2G10 (blue), SW480-AAA-GFP_5 clone 2D9 and SW480-AAA-GFP_5 clone 1B4. **B**) CFA assay data of the above shown clones. Shown is the percentage of colony formation relative to untreated control. The upper panel of images shows the GFP induction in DOX treated samples before colony fixation, the lower panel shows representative wells with crystal violet-stained colonies. All experiments were performed in at least three independent biological experiments. The CFA results of other clones are summarised in Appendix D.7.

Based on these results, it is difficult to conclude that the cell killing in the SW480-LL3-GFP clones is related to the LL3 function on β-catenin, as a significant proportion of the tested SW480-AAA-GFP_5 clones showed cell toxicity as well. An empty lentivirus control (without the mutant AAA control) would have been useful to further clarify this potential toxicity problem. However, it should be noted that the LL3 clones 2D3 and 1F5 showed significantly more cell death at lower DOX concentrations compared to AAA clones. This suggests that there may be some effect of the LL3 antibody on viability, but in only a small proportion of the transfected clones. At 10 ng/mL DOX, no viable cells were detected for the 2D3 clone anymore, which stands in sharp contrast to the SW480-AAA-GFP_5 clone 1B4 where about 90% of the cells were still viable at the same DOX concentration.

6.3.7.3 WNT gene expression data

Even though we obtained inconclusive data from the viability assays, we wanted to assess the VHH induction effect on Wnt target genes. The expressions of the Wnt target genes *CCND1* (CyclinD1), *c-myc*, *AXIN2* and *ASCL2* were analysed by qRT-PCR upon 48 hours of DOX treatment in individual stable clones. As seen in Figure 6.20 (left panels), the different clones showed variable baseline expressions of the Wnt target genes (assessed by comparative converted ΔCt value (Hsia et al., 2016)). Furthermore, the expression levels between biological replicates also seemed to vary significantly (note the large standard deviations). However, when the fold change expression was calculated and normalised within each experiment, a sharp reduction especially of the Wnt target genes *AXIN2* and *ASCL2* became apparent in SW480-LL3-GFP clones (Figure 6.20, right panels). This decrease in target gene expression was also observed in SW480-LL3-GFP_2.5, which did not

show any significant cell death in previous experiments. It is important to note that the Wnt target genes were also affected in the higher lentiviral concentration clones SW480-AAA-GFP_5. This was especially true for the clones 2F8 and 1B4, which previously showed cell death in the viability assays. Therefore, the change in gene expression might actually be due to nonspecific cytotoxicity upon DOX induction, rather than the effect of the VHH. This is supported by the fact that the target genes in SW480-AAA-GFP_2.5 clones are not affected by the VHH induction, while a decrease of gene expression can be observed in SW480-LL3-GFP_2.5 clones. The Wnt target genes *CCND1* and *c-myc* exhibited a more variable inhibition pattern and were not inhibited to the same extend as *AXIN2* and *ASCL2*. While ASCL2 has mainly been associated with intestinal crypt stemness (Schuijers et al., 2015), *CCND1* and *c-myc* are involved in different cellular processes such as growth and proliferation (Dang, 1999; Herbst et al., 2014)

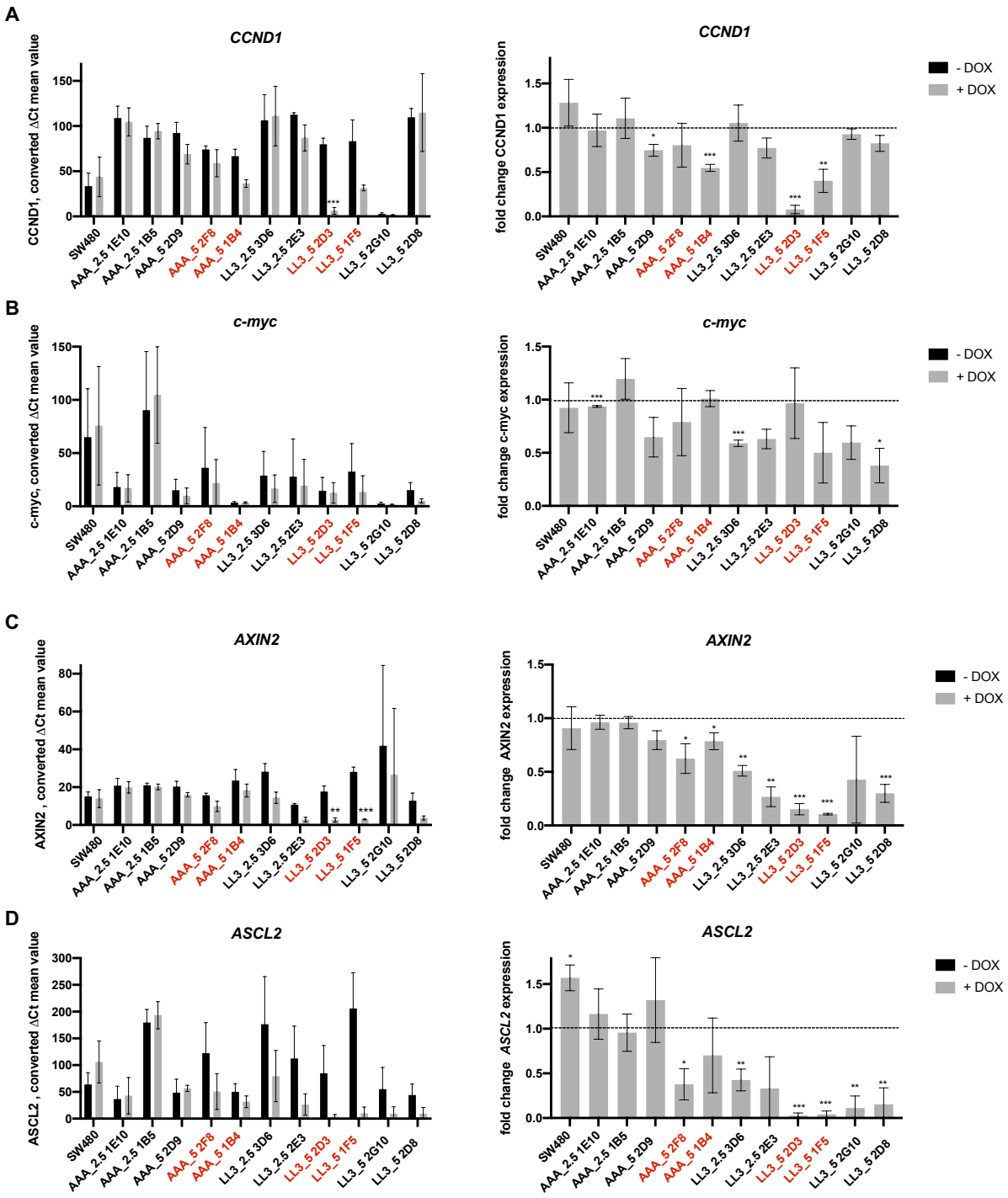


Figure 6.20 Expression of Wnt target genes
qRT-PCR analysis of Wnt target genes **A**) *CCND1* (CyclinD1), **B**) c-myc, **C**) *Axin2* and **D**) *ASCL2* in different stable clones upon 48 hours of DOX induction. Both comparative (converted ΔCt value) and fold change calculations are given for each target gene. For the fold change calculations, the untreated control within each experiment was normalised to 1 (---) and treated samples were compared to this value. Clones indicated in red have shown cell death after DOX treatment for 5 days in the SRB assay. Results shown from three independent biological experiments, except for clone LL3_2.5 2E3 n=2. Multiple t-tests were performed to assess statistical significance with Benjamini, Krieger and Yekutieli corrections for multiple testing. Error bars represent standard deviation, *p*-values are adjusted for multiple testing: * ≤0.01, **≤ 0.001 and ***≤ 0.0001.

6.3.7.4 β-catenin localisation in single clones

It was of interest to understand whether the expression of LL3 induced any changes in the subcellular localisation of β-catenin, especially in the context of Wnt target gene inhibition by LL3. In order to address this question, β-catenin was assessed by immunofluorescence in SW480-LL3-GFP_5 clones 2G10 and 2D3, SW480-AAA-GFP_5 clones 2D9 and 1B4 and SW480 parental cells upon DOX induction.

As visualised in Figure 6.21, all stable clones tested in this experiment expressed GFP upon DOX treatment, while the parental SW480 cells did not. β-catenin staining in SW480 parental cells was seen throughout the cells with a distinct accumulation in the nucleus (orange staining). This is in accordance with previous results obtained in SW480 cells (Chapter 3). In all lentiviral clones, GFP and the VHHs were successfully induced upon DOX treatment. It is clear from the images that the VHHs are expressed ubiquitously throughout the cell (Figure 6.21, red staining). Overall, in both the LL3- and AAA-lentiviral transduced clones, a membranous β-catenin localisation is apparent in addition to the nuclear and cytoplasmic staining, even without DOX treatment. Furthermore, the baseline cell-cell contact seems to be impacted in the lentiviral clones, as many exhibit empty “vacuoles” between cells (white arrows). Through initial visual assessment of the 2D images, the β-catenin localisation does not seem to be influenced by the DOX induction. However, it is difficult to make any clear statements on the β-catenin localisation based on these images. In order to make any conclusion on the β-catenin localisation upon DOX induction, 3D imaging and appropriate image

analysis should be performed to allow for the quantification of the protein in different subcellular compartments.

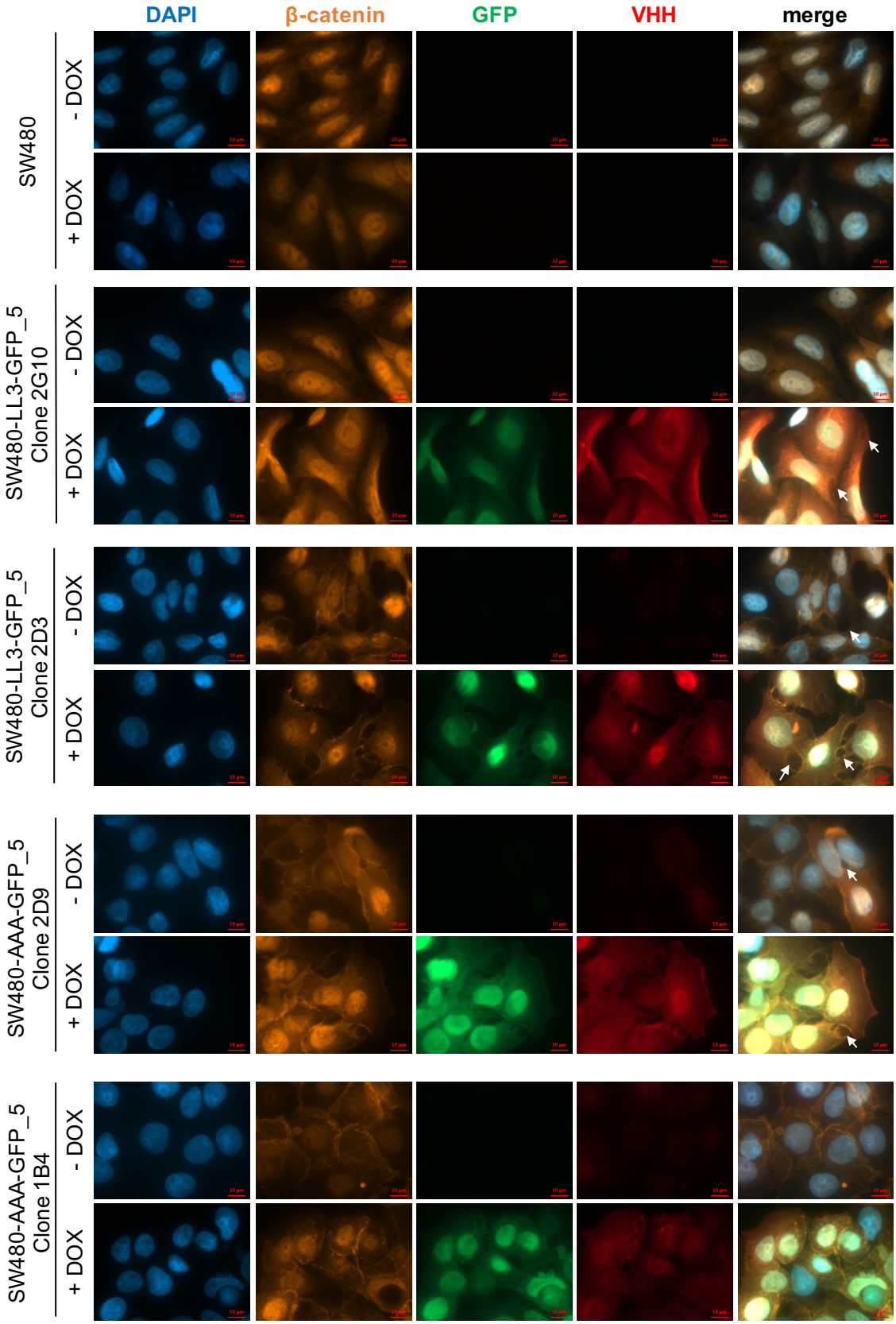


Figure 6.21 β-catenin localisation upon DOX induction in SW480 parental, SW480-AAA-GFP_5 clones 2D9 and 1B4 and SW480-LL3-GFP_5 clones 2G10 and 2D3 (previous page)
Indicated cell lines were treated with 100 ng/mL DOX or medium alone for 48 hrs. Cells were fixed and stained according to the methodology described in Chapter 2. Primary antibodies: β-catenin (rabbit) and myc tag (mouse). Secondary antibodies DAR AF555 and DAM AF647. Images were taken using the Zeiss Observer z1 fluorescence microscope. Blue: DAPI, green: GFP, orange: β-catenin, red: VHH. White arrows indicate commonly seen "vacuole"-like structures between the cells. 100X magnification, NA = 1.4, oil, scale bar is 10 µm

6.3.8 Assessment of LL3 Binding site on β-catenin

In the work by Newnham et al. (2015) it is described that the VHH LL3 binds to a HIS-tagged β-catenin fragment ranging from AA residues 164-390, which corresponds to Armadillo repeats 1-6 of β-catenin. This area of β-catenin is known to interact with various other proteins involved in the transcriptional activation of the Wnt pathway, namely BCL9, Pontin52 and TCF4 (Bauer, Huber, & Kemler, 1998; Bauer et al., 1998; Sampietro et al., 2006; Valenta et al., 2012). Here we aimed at defining the LL3 binding site on β-catenin more precisely in order to get an insight into the potential mechanism of action of the VHH.

6.3.8.1 VHH and full-length β-catenin recombinant protein purifications

In order to obtain purified LL3 and AAA proteins, the VHH sequences were cloned into a pGEX expression vector and sequenced (Appendix D.8). The resulting protein constructs contained a GST and HIS tag, which was separated from the VHH sequence by a TEV cleavage site (Figure 6.22A). The proteins were successfully expressed in C41 *E.coli* using IPTG induction and purified by the GST-tag using 4B Sepharose resin (Figure 6.22B). The GST/HIS-tag portion of the recombinant protein was cleaved using TEV protease (Figure 6.22C) and the

resulting VHH proteins were chromatography column purified (ÄKTA, GE Healthcare) by Dr Abimael Cruz Migoni and Andres Hueso Cuervo (Appendix D.9).

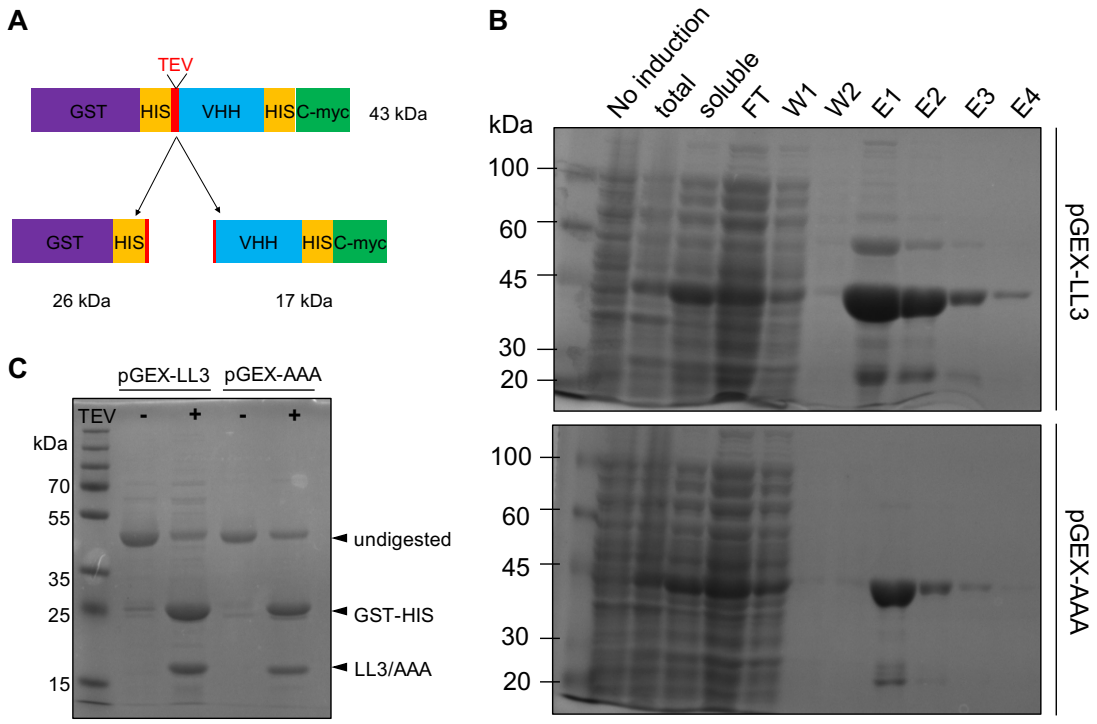


Figure 6.22 pGEX-LL3 and pGEX-AAA purifications
A) Schematic representation of the LL3 and AAA VHH recombinant protein construct. The TEV cleavage site is indicated in red and the TEV protease cleavage products with respective molecular weight are indicated below the full-length protein construct. **B**) Coomassie stain of IPTG induction samples and GST-purifications of pGEX-LL3 (above) and pGEX-AAA (below), both with an expected molecular weight of 43 kDa. FT = flow-through, W = wash, E = elution. **C**) Coomassie stain of TEV cleavage of the pGEX-LL3 and pGEX-AAA constructs. TEV protease was added (1:1000) to the respective proteins and incubated overnight at 4°C on a rotor. A fraction of each digest was separated on a 14% SDS gel, while the rest of the samples were chromatography column purified using an ÄKTA machine.

As it was previously shown that the VHH LL3 binds to β-catenin, a full length β-catenin recombinant protein was used in experiments as a positive binding control. The pGEX-Bcafl expression vector (Addgene, #24193) encoding the GST-tagged full length β-catenin (Bcatfl) was induced in C41 *E.coli* and the resulting protein purified by the GST-tag using Sepharose resin (Figure 6.23).

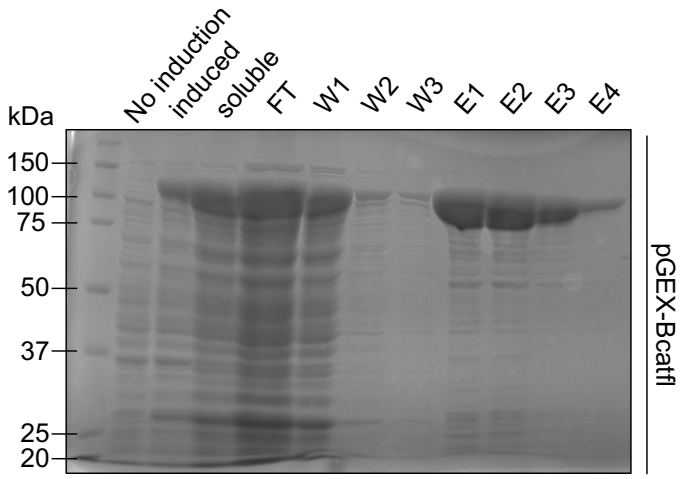


Figure 6.23 Coomassie stain of pGEX-Bcatfl recombinant protein purification
Bcatfl recombinant protein expression was induced with 0.8 mM IPTG overnight at 16°C. The soluble fraction was GST purified using 4B Sepharose resin in binding buffer (20 mM Tris-HCl pH8, 200mM NaCl, 5% glycerol) for 4 hours at 4°C. Resin and sample were poured into a purification column and the flow-through (FT) was collected. The resin was washed three times (W1-3) with binding buffer and eluted using 10 mM reduced glutathione in 50 mM Tris-HCl pH8 for 10 min at RT. Fractions of each step were analysed by SDS gel separation and Coomassie stain. Expected size of Bcatfl is 111 kDa.

In order to confirm the correct folding of the purified proteins, the interaction between the LL3 and Bcatfl proteins was assessed by a HIS-pulldown assay (Figure 6.24A). It was confirmed that the purified LL3 protein is able to pulldown Bcatfl. While Bcatfl did bind non-specifically to the HIS-Dynabeads™ when incubated and washed with Buffer A (20mM Tris-HCl pH8, 200mM NaCl, 5% glycerol, 0.5% NP40), this nonspecific binding could be abolished by using a more stringent Buffer B (20mM Tris-HCl pH8, 300mM NaCl, 5% glycerol, 1% NP40, 0.1% Triton, 30mM imidazole) (Figure 6.24B). The clear signal around 26 kDa in the LL3 + Bcatfl lane when probing with an anti-GST antibody is the TEV-cleaved GST-HIS fragment from the LL3 protein construct. Even though the TEV-cleaved GST-HIS-LL3 protein was purified using an AKTA column, the small size difference between the LL3 fraction (17 kDa) and GST-HIS fraction (about 26 kDa) made it difficult to solely purify the LL3 TEV-cleavage product without

GST-HIS contamination (schematic representation in Figure 6.22A). The GST-HIS product bound to the HIS-Dynabeads™ alongside the LL3 protein and could therefore also be detected by the anti-GST-tag antibody. To confirm the interaction between LL3 and β-catenin seen in this HIS pulldown optimisation, the HIS pulldown assay was repeated alongside the mutant AAA as negative control. As seen in Figure 6.24C, the wild-type VHH LL3 binds to β-catenin, while AAA does not. Once again, the residual GST-HIS fraction from the TEV digest could be detected on the blot using the anti-GST-tag antibody. Furthermore, the assay was repeated through a myc-tag immunoprecipitation (Figure 6.24D), leading to the same result.

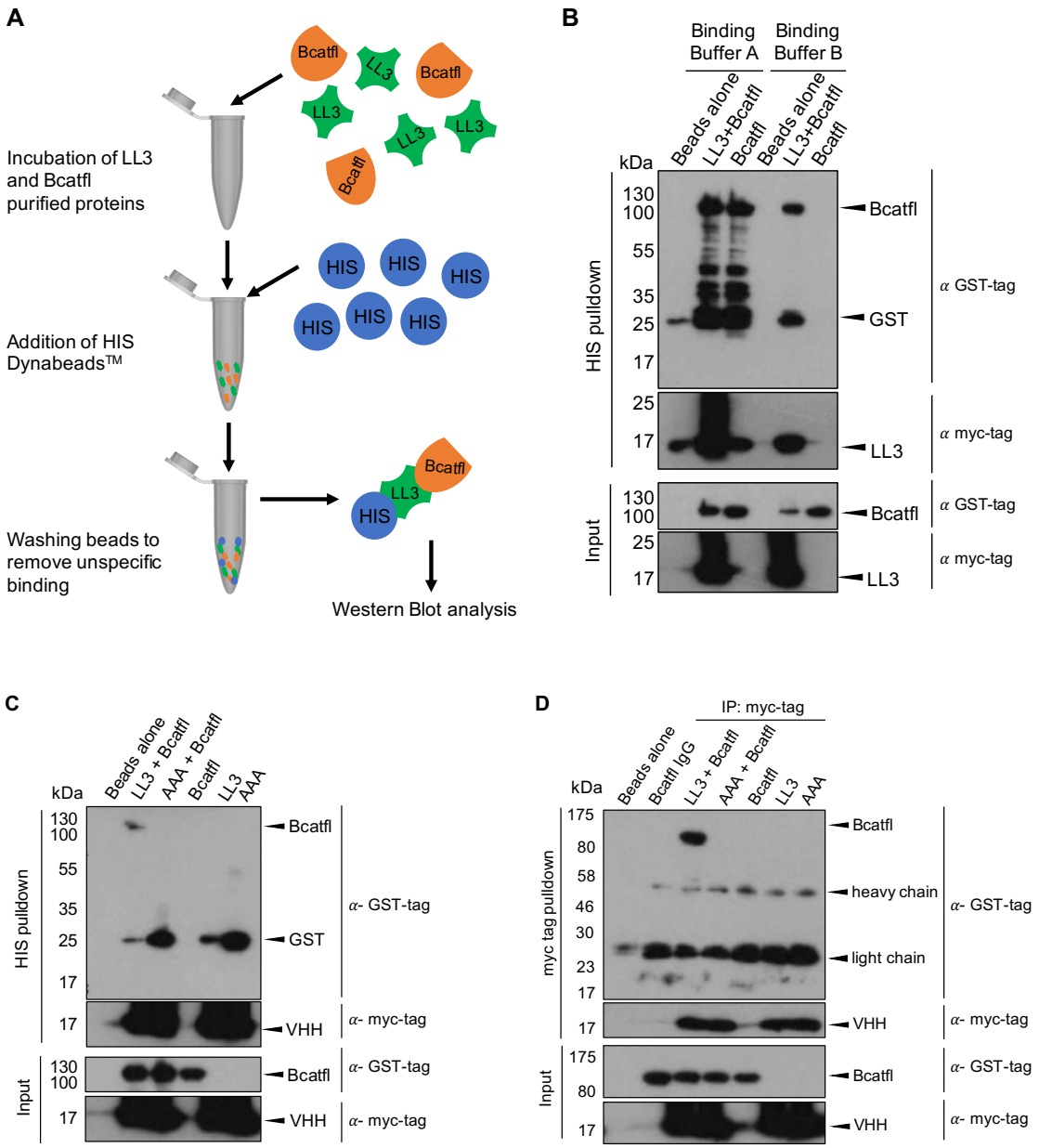


Figure 6.24 Pulldown assays to assess the LL3 - β-catenin interaction
A) Schematic representation of HIS-Dynabeads™ pulldown assay. **B**) Optimisation of HIS-Dynabeads™ pulldown assay to reduce nonspecific binding of the Bcatfl proteins to the beads. Assay was performed in binding / wash Buffer A (20mM Tris-HCl pH8, 200mM NaCl, 5% glycerol, 0.5% NP40) and a more stringent Buffer B (20mM Tris-HCl pH8, 300mM NaCl, 5% glycerol, 1% NP40, 0.1% Triton, 30mM imidazole). Nonspecific Bcatfl binding to the Dynabeads occurred with Buffer A, which was abolished using buffer B. The lower GST signal in the Buffer B condition at around 26 kDa on the GST-tag blot is the TEV-cleaved GST-HIS fraction contaminating the LL3 purified protein. **C**) The HIS-pulldown was repeated under the previously optimised condition to compare the binding of Bcatfl to wild-type LL3 and mutant AAA. Bcatfl can be detected at 111 kDa when incubated with LL3, but not with AAA. Once again, the GST signal at around 26 kDa is the TEV cleaved GST-HIS fraction of the VHH purified proteins. **D**) The experiment was repeated using a myc-tag pulldown in order to remove the GST-HIS contamination previously observed in the HIS-tag pulldowns. LL3 clearly interacted Bcatfl, while mutant AAA did not. A less exposed film would have been of advantage for interpretation.

As identified in the HIS-tag pulldown assays, the VHH proteins were still contaminated with residual GST-HIS fragments from the TEV digest. As this might interfere with further downstream experiments, the VHHs sequences were cloned into the pET-HIS-TEV-Avi-MCS vector, which does not contain the GST tag. The new constructs HIS-TEV-Avi-LL3 and HIS-TEV-Avi-AAA were sequenced (Appendix D.10) and proteins were expressed in *E.Coli* by IPTG induction. HIS-tag purification using Ni-NTA beads was performed and the correct size of the purified proteins (22 kDa) was confirmed by a Coomassie stain (Figure 6.25). The specific interaction between the new recombinant LL3 protein and Bcatfl was confirmed by pulldown assays. The proteins were further purified using a size exclusion chromatography column and analysed by Mass Spectrometry by Dr David Staunton (Biochemistry Department, University of Oxford). Mass Spectroscopy results can be found in Appendix D.11.

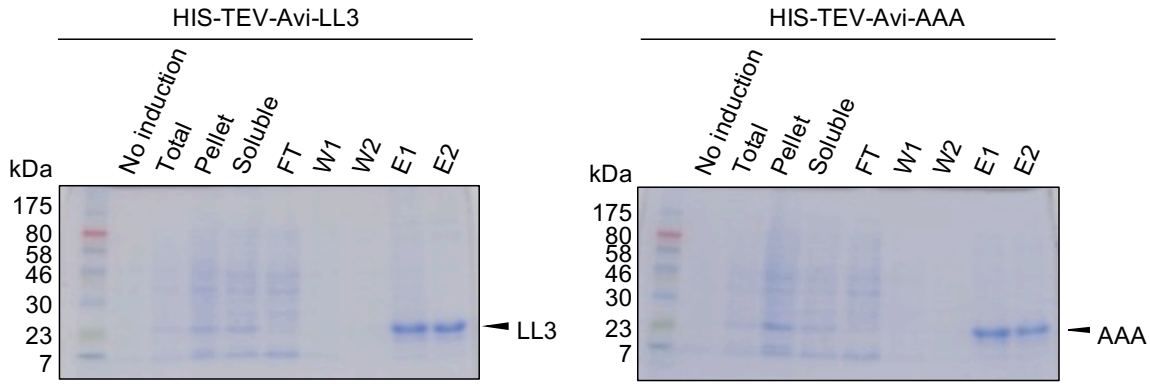


Figure 6.25 HIS-TEV-Avi-LL3 and HIS-TEV-Avi-AAA protein purifications
Coomassie stain of HIS-TEV-Avi-LL3 and HIS-TEV-Avi-AAA purifications using Ni-NTA beads for HIS-tag purifications. C41 *E.Coli* carrying the indicated vector were induced with 0.8 mM IPTG and grown overnight at 16°C. The bacterial pellet was sonicated and the insoluble (pellet) and soluble fractions were separated by centrifugation. FT: Flow-through, W: wash, E: Elution. LL3 and AAA purified proteins are expected at about 22 kDa.

6.3.8.2 β-catenin fragment recombinant protein purifications

The aim was to further map out the LL3 binding region on β-catenin using previously optimised pulldown assays with different β-catenin fragments. The β-catenin fragments were designed to cover different Armadillo repeats (ArmR) within the known LL3 binding area (Figure 6.26A). cDNA from HT29 cells served as PCR template for β-catenin fragment constructions (Figure 6.26B). The β-catenin fragments were cloned into the pGEX expression vector to create a GST-HIS-TEV-β-catenin fusion protein (Figure 6.26C). All vectors were sequenced to confirm correct insertion of the PCR fragments (Appendix D.12).

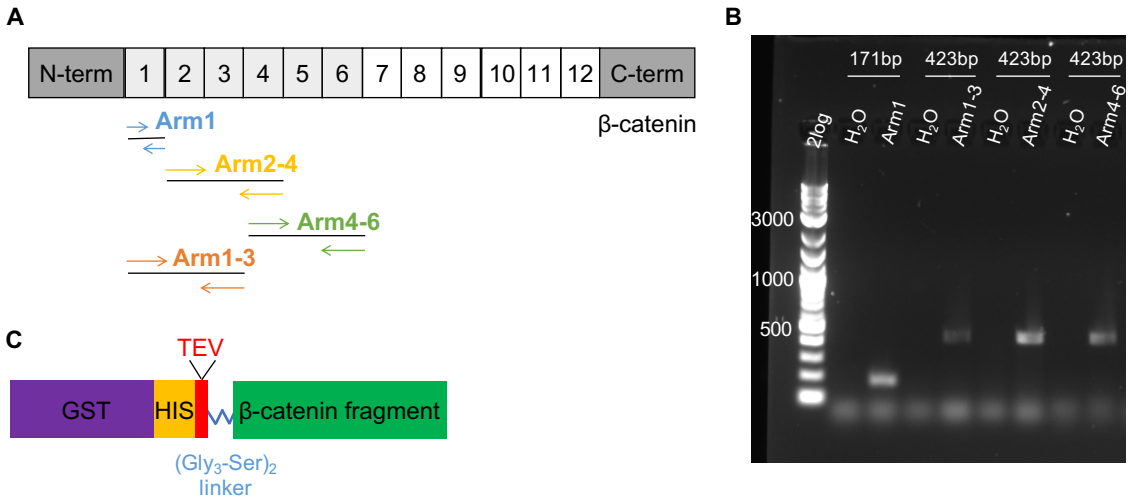
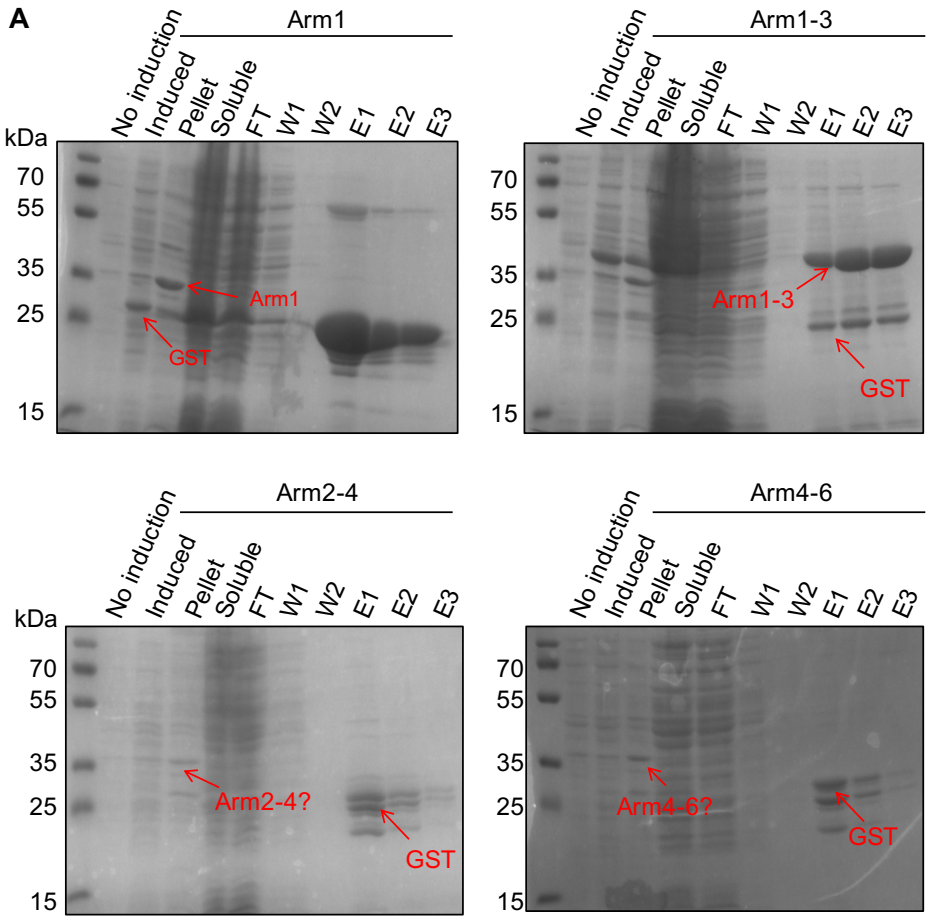


Figure 6.26 Design of β-catenin fragments
A) Various β-catenin fragments were designed to cover all ArmR between Arm1-6. This is the β-catenin region previously identified as LL3 binding site. The top grey schematic represents β-catenin with its 12 ArmR. **B**) PCR products of β-catenin fragments Arm1, Arm1-3, Arm2-4, Arm4-6, Arm5-6 and Arm1-6. Expected size is indicated above the lanes of the 1.2% agarose gel. **C**) Overview of recombinant protein structure once expressed in the pGEX expression vector. A Gly-Ser linker was added between the tags and the β-catenin fragments, as this helps to physically separate the two domains of the fusion protein (Chen, Zaro, & Shen, 2013).

β-catenin fragment vectors were transfected into C41 *E.Coli* for protein expression and induced by 1 mM IPTG overnight induction at 16°C. Only the pGEX-Arm1-3 fragment was successfully induced and purified by its GST tag (Figure 6.27). A

clearly induced band at 26 kDa is visible on the Coomassie stained gel, which is the GST on its own without the fused β-catenin Arm1-3 fraction.



B

pGEX-constructs	Expected size (kDa)
Arm1	33.60
Arm1-3	42.73
Arm2-4	42.60
Arm4-6	42.66

Figure 6.27 Purification of pGEX-ArmR fragments
A) Coomassie stains of SDS gels with induction and purification products of pGEX-Arm1, -Arm1-3, -Arm2-4 and -Arm4-6. **B**) Table with expected sizes of expressed constructs. FT: Flow-through, W1-2: wash, E1-3: elution. Arm1 is expressed at the correct size but is insoluble. Arm1-3 was successfully purified, while Arm2-4 and Arm4-6 were not induced after IPTG addition.

As we were unable to purify the different β-catenin fragments from our pGEX-constructs (other than Arm1-3), the company Promab Inc. (California) constructed new GST-tagged β-catenin fragments of the individual ArmRs: Arm1, Arm2, Arm3, Arm4, Arm5 and Arm6 (Appendix D.13).

6.3.8.3 LL3 binds to Arm1-3 of β-catenin

In order to refine the LL3 binding site on β-catenin, further GST pulldown assays were performed. In initial experiments, GST-tagged fragments Arm1-3, Arm1, Arm2 and Arm3 were tested for the interaction with LL3. GST on its own and Bcatfl were used as negative and positive controls, respectively. As seen in Figure 6.28, the Arm1-3 fragment is able to interact with LL3, just as the positive control of full-length β-catenin did. LL3 did not interact with the negative control GST or with the Sepharose beads on their own, and the negative control AAA did not bind to full-length β-catenin. Interestingly, while LL3 was able to bind to the combined Arm1-3, the VHH failed to interact with the individual fragments Arm1, Arm2 and Arm3. Even longer film exposures did not identify any weaker binding with the β-catenin fragments. As the relatively small ArmRs (6 - 7.5 kDa) were fused with the large GST-tag (26 kDa), it is a possibility that the conformation of these peptides masked the LL3 epitope and hindered the binding.

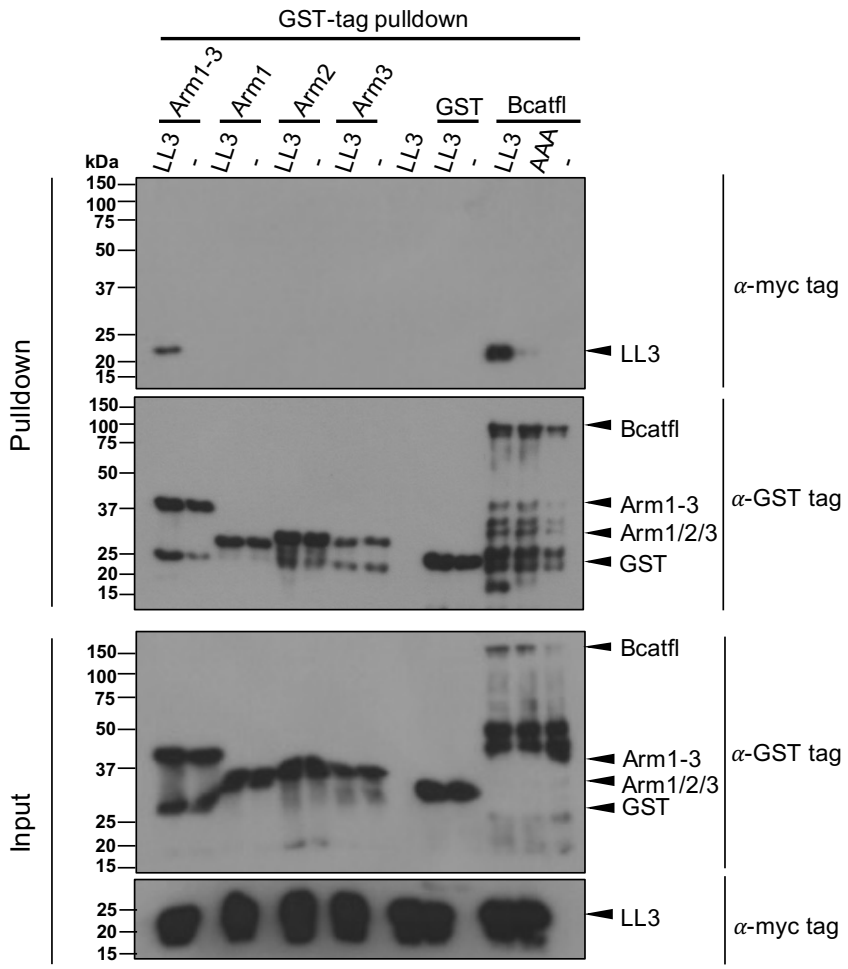


Figure 6.28 GST-pulldown assay with Arm1-3, Arm1, Arm2 and Arm3 β-catenin fragments

β-catenin fragments were incubated without VHHs for 1 hour at 4°C, rotating, before the addition of 4B Sepharose beads. After 1-hour incubation with the beads, the sepharose resin was washed three times and proteins were eluted using 10 mM reduced glutathione. Sample buffer was added, and samples boiled before SDS gel analysis. Membrane was probed with myc-tag and GST antibodies to detect the interaction of the proteins, VeriBlot-HRP (abcam) was used as secondary antibody. Arm1-3 pulled down LL3, but individual fragments Arm1, Arm2 and Arm3 did not. Experiment was repeated in three individual experiments and a representative example is given. Degradation of the Bcatfl protein is clearly seen as a smear in the last three lanes. A less exposed image of the WB would have benefited the interpretation of the results. Expected fragment sizes: LL3/AAA: 22 kDa, Bcatfl: 111 kDa, GST: 26 kDa, Arm1-3: 42.7 kDa, Arm1: 34 kDa, Arm2: 35.9 kDa, Arm3: 35.5 kDa.

As the individual Arm1, Arm2 and Arm3 fragments did not show any binding while the fused version Arm1-3 did, it was decided not to further test the fragments Arm4, Arm5, Arm6.

6.4 Discussion

In this chapter, we further characterised the wild-type VHH LL3 and mutant VHH AAA in SW480 colorectal cancer cells. It was successfully shown through immunoprecipitation experiments in inducible VHH-expressing cell lines that the VHHs can fold correctly in the reducing environment of the cells. Furthermore, we confirmed previously published data by Newnham et al. (2015) that the three alanine residue substitutions in the CDR3 loop of LL3 can ablate the binding to β-catenin (mutant AAA does not bind to full length β-catenin). More importantly, while binding studies were previously performed on purified proteins (Newnham et al., 2015), it was shown here that the interaction can occur in cells.

In this work, it was also shown that the LL3 can bind to the first three ArmRs of β-catenin. This is also the binding site of BCL9, Pontin52, E-cadherin and TCF4 (Bauer et al., 1998; Huber & Weis, 2001; Sampietro et al., 2006). Further work could include the pulldown assays of β-catenin binding partners to assess which of the interactions is affected by LL3. The VHHs are expressed throughout the cell (Figure 6.21). If the interaction between β-catenin and E-cadherin was targeted by LL3, one might expect a distinctive VHH accumulation at the cell membrane. It might therefore be less likely that the β-catenin/E-cadherin interaction is disrupted (Newnham et al., 2015).

6.4.1 Limitation of the study

While the goal was to specifically define the β-catenin binding site of LL3, we could only narrow down the binding site to Arm1-3. Ideally, an Arm4-6 fragment would have been needed as a control to confirm that the binding is specific to the first

three ArmR of β-catenin. The lack of suitable β-catenin fragments limited the efforts to identify the specific LL3 binding site. Small synthetic peptides of each ArmR could be used instead to assess the LL3 binding, using Surface Plasma Resonance (SPR) for example.

The creating of stable SW480-LL3-GFP and SW480-AAA-GFP cell lines using lentiviruses allowed us to study the effect of the VHH in an inducible system. However, as presented in this chapter, some of the puromycin selected stable cell lines showed signs of lentiviral toxicity. The same volume of the LL3 and AAA lentiviral supernatant was used to transduce the SW480 cells. As the viral titre of LL3 and AAA lentiviral supernatant we received by the lentiviral facility was unknown, there is the possibility that different concentrations of the viruses were used. In an ideal situation, the viral titre should have been calculated in order to determine the same multiplicity of infection (MOI) for both the LL3 and AAA infections.

If time had permitted, an analysis of the lentiviral insertion sites of each clone could have perhaps given a better understanding of the heterogeneity between clones. This would potentially help to explain why some of the clones showed cell death upon DOX induction, while others did not.

6.4.2 Future directions

The identification of novel antibodies against Wnt components has been one of the strategies to target the Wnt pathway (Fenderico et al., 2019; Gurney et al., 2012; Smith et al., 2013). In this context, the Llama VHH LL3 studied in this work is of

considerable interest (Newnham et al., 2015), as it targets β-catenin directly and potentially acts downstream of the β-catenin destruction complex. Identifying the exact binding-site of β-catenin will shed more light on its mechanism of action. As VHHs are frequently used as chaperones for crystal structures (Koide, 2009), and various structures of β-catenin itself have already been solved (Graham et al., 2000; Huber et al., 1997; Huber & Weis, 2001; Poy et al., 2001; Sampietro et al., 2006), it would be ideal to determine the crystal structure of the two interacting proteins. This structural information of this interaction could also be used to identify novel small molecules against the same interaction site.

We have shown here that the Wnt target genes *AXIN2* and *ASCL2* are inhibited by the induction of LL3, but not by AAA. In order to validate this Wnt inhibition, the TCF-mediated TOPflash assay could be used in different LL3- and AAA-clones to confirm this finding.

Overall, the use of VHHs to target the Wnt pathway offers great potential, especially because of their ability to target small epitopes that cannot be reached by conventional small molecules (Bannas, Hambach, & Koch-Nolte, 2017). The main challenge will be to find a way for targeted delivery of the VHHs, as discussed in the next chapter.

Chapter 7

General Discussion

CHAPTER 7: General Discussion

Over the past 30 years, the Wnt pathway has been a topic of great research focus, as it is implicated in many diseases, such as colorectal cancer, breast cancer, pancreatic cancer and leukaemia (Zhan et al., 2017). Yet, no Wnt-inhibitor is currently in clinical use, which reflects the complexity of targeting this pathway (Krishnamurthy & Kurzrock, 2018). In this work, different routes of Wnt-inhibition through targeting β-catenin were explored. These included the study of β-catenin/BCL9 inhibitor low molecular compounds, the attempt to identify small antibody domains against β-catenin using a Yeast-2-Hybrid system and the characterisation of a Llama VHH against β-catenin. Furthermore, we also used immunofluorescence staining of β-catenin in a panel of colorectal cancer cell lines to highlight the role of E-cadherin in the subcellular localisation of β-catenin.

7.1 E-cadherin associates with β-catenin subcellular localisation

In this work, β-catenin localisation was associated with the expression of E-cadherin in a panel of colorectal cancer cell lines. E-cadherin is able to sequester β-catenin to the cell membrane, where it forms a complex linking the cell-cell junction with the actin skeleton (Desai et al., 2013). As described in Chapter 3, cell lines with no or low *CDH1* mRNA expression, notably cell lines with an EMT phenotype such as CCO7 or COLO320DM, show nuclear β-catenin staining. Interestingly, the non-EMT cell line LS174T, which lacks E-cadherin protein expression due to two mutations in *CDH1* (Efstathiou et al., 1999), also exhibits nuclear localisation of β-catenin. It would be useful to

perform β-catenin immunofluorescence staining in HDC9 cells, which also lack E-cadherin protein expression (Figure 3.10) due to similar mutations.

Orsulic et al. (1999) showed a shift in β-catenin localisation from the nucleus to the membrane after transfection of full-length β-catenin into SW480 cells, while transfection of E-cadherin constructs lacking the β-catenin-binding domain did not have the same effect. Importantly, the work presented in this thesis supports previously reported results using endogenous E-cadherin expression levels, rather than exogeneous expression.

While the relevant role of E-cadherin in the localisation of β-catenin is well established (Gottardi et al., 2001; Orsulic et al., 1999), more work is required to understand the link between E-cadherin and the Wnt pathway and EMT. While loss of E-cadherin is often associated with increased TCF-mediated Wnt transcriptional activity and EMT (Heuberger & Birchmeier, 2010), analysis of Wnt activity did not show any association with the endogenous E-cadherin expression and mutation status in breast, gastric and pancreatic cancer cell lines (Caca et al., 1999; van de Wetering et al., 2001). This stands in contrast to studies where TCF/β-catenin mediated Wnt signalling was inhibited by exogenous E-cadherin binding to β-catenin (Gottardi et al., 2001; Orsulic et al., 1999; Stockinger et al., 2001). In light of these previous conflicting findings, and our results showing an association of endogenous E-cadherin expression and β-catenin subcellular localisation, it is of major interest to further investigate the relationship between E-cadherin expression and mutations affecting the Wnt pathway activity in the panel of colorectal cancer cell lines.

7.2 Small molecules targeting β-catenin to inhibit the Wnt pathway

With the aim to target β-catenin to inhibit the Wnt pathway, we tested β-catenin/BCL9 inhibitors from Dr. Haitao Ji (Moffitt Cancer Centre) in a panel of CRC cell lines (Chapter 4). The compound ZYQ-1-78 exhibited nonspecific cell killing. The tested CRC cell lines, independent of their APC and β-catenin mutation status, as well as cell lines derived from different tissues (breast, lung, prostate) and fibroblasts were killed at similar drug concentrations (Figure 4.5, Figure 4.7 and Table 4.2). This nonspecific cytotoxic drug action of ZYQ-1-78 was later confirmed through LDH cytotoxicity assays (Zhang et al. 2018).

Two further compounds tested on a small panel of CRC cell lines only showed effects on cell death at a high μM range of drug concentrations, which significantly limits their further development. More importantly, in our studies, the compound ZYQ-2-165 only appeared to have an effect when tested in cell culture medium with 1% FBS, as compared to the usual 10% FBS. This represents another hindrance for the further clinical development. Extensive alterations of the chemical properties and structures of the compounds may be necessary for the development of effective further β-catenin/BCL9 inhibitors.

Overall, intense research effort is currently placed on the identification of small molecular weight molecules to inhibit β-catenin protein-protein interactions to inhibit the Wnt pathway (Chen et al., 2009; Fang et al., 2016; Gandhirajan et al., 2010; Grossmann et al., 2012; Scarborough et al., 2017). While the Wnt pathway remains a prominent target, significant off-target effects have prevented further development of compounds (Krishnamurthy & Kurzrock, 2018; Zhong et al., 2015). A major concern remains how to selectively target

the Wnt pathway of only malignant cells without significantly affecting healthy cells.

7.3 Antibody - based approaches to target β-catenin

Over the past two decades, antibody-based approaches to targeting the Wnt pathway have advanced significantly. Antibodies against Wnt ligands (He et al., 2004; You et al., 2004) and Wnt pathway receptors (Gong et al., 2010; Gurney et al., 2012; Nickho et al., 2017) have previously been described. However, they target the pathway upstream of APC, which is commonly mutated and the leading cause of the elevated Wnt signal in colorectal cancer. Therefore, complexes downstream of the mutated APC and β-catenin proteins, such as the stabilisation of the β-catenin destruction complex or disruption of the β-catenin-TCF transcriptional complex, have been described as potentially superior targets for colorectal cancer (Masuda et al., 2015).

With increasing successes in the field of antibody engineering, single domain antibodies have been investigated for a broad range of diseases from Central Nervous System (CNS) disorders and viral infections to cancer diagnostics and therapy (Bélanger et al., 2019; Colby et al., 2004; De Vlieger et al., 2019; Iezzi et al., 2018). In light of these developments, our aim was to identify single domain antibodies (VH) against β-catenin with the potential to inhibit its protein interactions downstream of APC and β-catenin mutations (Chapter 5). In Chapter 6, we further characterised a previously described Llama VHH fragment against β-catenin (Newnham et al., 2015).

7.3.1 Suggestions for the identification of VHs against β-catenin

Our aim was to identify a VH against the first ArmR of β-catenin, a well-characterised binding site of the transcriptional co-activator BCL9 (de la Roche et al., 2008; Kramps et al., 2002). This interaction is downstream of the mutated APC or β-catenin proteins, and therefore an inhibition of β-catenin protein interactions by the VH should be independent of the APC or β-catenin mutation status. By using a yeast-two-hybrid system, we screened a β-catenin bait against a VH library based on a stable framework with a randomised CDR3 loop (Rabbitts laboratory). In spite of continuously low transformation efficiencies in our large-scale yeast transformations (Table 5.3), we identified three hits against our β-catenin bait. However, upon further characterisation, all three VHs were confirmed as binders to the DNA-binding domain pBTM116 of the fusion protein, instead of the β-catenin domain (Figure 5.14). A low transformation efficiency appeared to be the main technical issue in these experiments. Multiple efforts to increase the transformation efficiency in order to screen a larger fraction of the VH library were unsuccessful.

An alternative approach of CDR grafting could be considered. CDR grafting is a commonly used method for the humanisation of murine monoclonal antibodies (Bowers et al., 2013; Kettleborough et al., 1991; Safdari et al., 2013). As the VH library in this work is based on a stable consensus framework derived from human IgG (Tanaka & Rabbitts, 2010b), the CDR loops from another antibody raised against the target region of β-catenin could be inserted. In theory, the VH framework should then specifically bind against the β-catenin area of interest through the grafted loops.

While we were unable to identify VHs against β-catenin, the use of VHs remains a viable option to target the Wnt pathway intracellularly. As an alternative to the Intracellular-Antibody Capture Yeast-2-Hybrid methodology used in this study, future work could investigate the use of other library screening methodologies, such as phage display (Binyamin, Plaksin, & Reiter, 2002; Dudgeon et al., 2012; Ledsgaard et al., 2018).

7.3.2 LL3 VHH against β-catenin

Newnham et al. (2015) identified the first intracellular VHH against β-catenin termed LL3, through immunisation of a Llama using a full-length β-catenin recombinant protein. There is a very high sequence homology of β-catenin between species, highlighting the crucial function of the protein in development and cellular homeostasis. Given this high degree of sequence homology, it is surprising that organisms are able to produce antibodies against β-catenin. Figure 7.1 shows the AA sequence alignment of the Arm1-3 regions of different species, including humans, mice, zebrafish and alpaca.

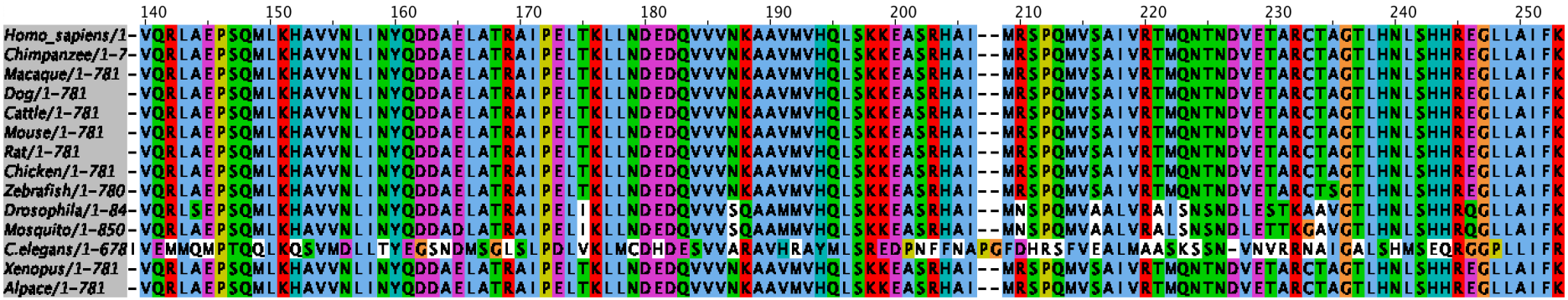


Figure 7.1 β-catenin sequence alignment between different species

β-catenin amino acid sequences were retrieved from National Centre for Biotechnology Information (NCBI, https://www.ncbi.nlm.nih.gov/) and aligned in the Jalview software using the MUSCLE multiple sequence alignment algorithm (Edgar, 2004). Amino acid residues 140-250 are represented in this figure, which corresponds approximately to the Arm1-3 region of β-catenin. A high sequence homology, especially between mammals, can be observed. Note the homology between the Alpaca (closely related to Llama) and the human sequence. Clustal X Colour Scheme was used: **blue** = hydrophobic, **red** = positive charge, **magenta** = negative charge, **green** = polar, **orange** = Glycines, **yellow** = Prolines, **cyan** = aromatic. White regions show non-conserved regions.

The VHH LL3 was shown to have a biological effect through the inhibition of the Wnt pathway assessed by the TCF-mediated TOPflash reporter assay. In Chapter 6 of this thesis, further characterisations of LL3 were performed using a stably expressing DOX-inducible cell line system. We showed that VHH LL3 is able to interact with β-catenin intracellularly (Figure 6.13) and that it is expressed both in the cytoplasm and nucleus upon DOX induction (Figure 6.4).

While we could refine the binding-site of the LL3 VHH to the first three ArmR of β-catenin, it is challenging to draw any conclusion as to the mechanisms of action of the VHH based on the data presented in Chapter 6. Our cytotoxicity data showed inconsistent results on some SW480 clones with stable introduction of the mutant VHH AAA, which also showed significant cell death upon DOX induction. Furthermore, only a proportion of the inducible SW480-LL3-clones exhibited cell-killing upon VHH induction, while a notable inhibition of the Wnt target genes *ASLC2* and *Axin2* was observed even in LL3 clones which were not killed after DOX induction (Figure 6.20). The observation of inhibition of Wnt target genes requires further investigations in order to confirm that the effect is LL3 specific.

7.3.3 Advantages of antibody fragments over monoclonal antibodies and small molecule inhibitors

The use of single domain antibodies (sdAb) such as VH and VHH as inhibitors has advantages compared to small molecule inhibitors or conventional monoclonal antibodies. While the large size of monoclonal antibodies is beneficial for lower renal clearance resulting in a relatively long serum half-life (Haraya, Tachibana, & Igawa, 2019), the small size of antibody fragments is potentially of great advantage

for reaching solid tumour sites (Li et al., 2016; Yokota et al., 1992). sdAb were shown to bind to “hidden epitopes”, which are difficult to target by small molecule screens (Visintin et al., 2008). Furthermore, due to the specific epitope binding, sdAb may only inhibit a specific PPI and function of a multifunctional target protein (Marschall & Dübel, 2016), which can reduce potential therapy side effects.

7.3.4 Limitations of antibody fragment-based therapies

Even though there are apparent advantages of intracellular antibodies over small molecule inhibitors, many unanswered questions currently limit their further therapeutic use. A main concern lies around the intracellular delivery of the sdAb. In order to continue the successful development of therapeutic intracellular VHs and VHHs, appropriate delivery mechanisms are required. Several key issues need to be taken into consideration: i) how to enable a targeted delivery of the intracellular fragments without affecting the healthy cells, ii) how to assure good expression levels of the antibody fragment in the target cells and iii) how to ensure that all malignant cells are successfully targeted.

Different delivery methodologies for intracellular antibody fragments are currently investigated and can be broadly grouped into viral and non-viral delivery, as summarised in Figure 7.2.

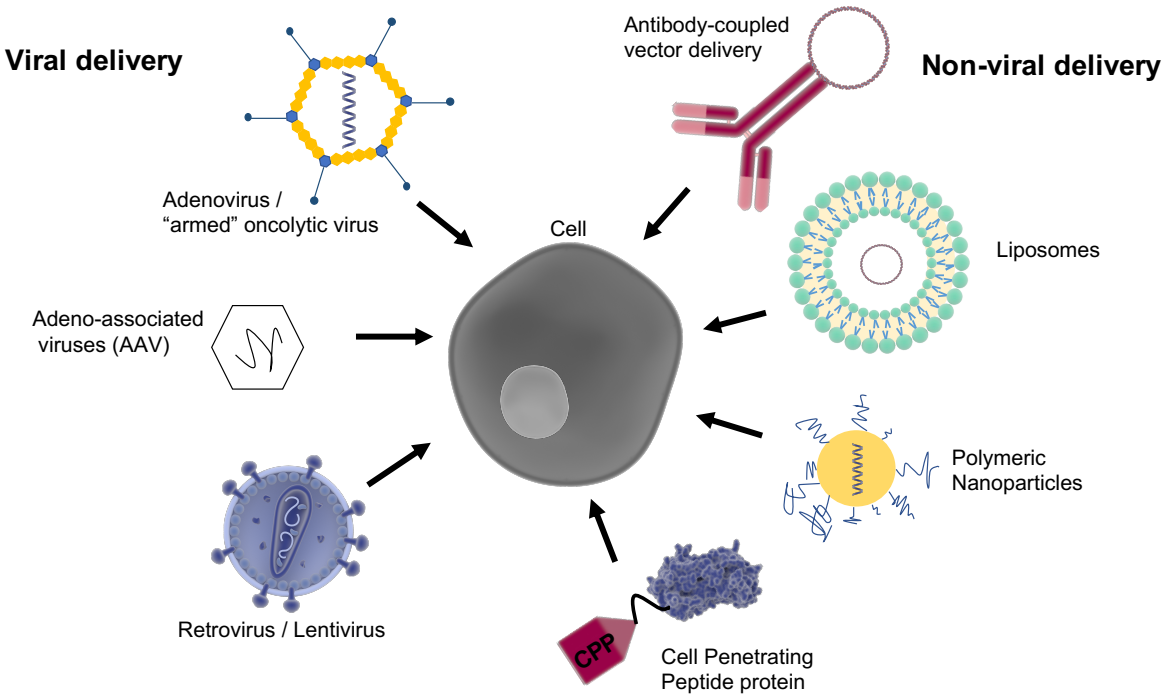


Figure 7.2 Currently investigated delivery options of intracellular antibodies. Delivery routes of intracellular antibody fragments currently being investigated can be divided into viral and non-viral delivery and are summarised in this figure. Investigations into non-viral delivery include the use of cell penetrating peptide (CPP)-tagged proteins or intracellular nucleic acid vector delivery through antibodies or nanoparticles. Figure adapted from Pérez-Martínez, Tanaka, & Rabbitts 2010.

While direct delivery of the intracellular sdAb protein to the cell using cell penetrating peptides such as HIV 1 trans-activating protein (Frankel & Pabo, 1988) is limited by proteasomal degradation, fast plasma clearance, limited cell specificity and the question if enough sdAb would reach the target cell for therapeutic use (Pérez-Martínez, Tanaka & Rabbitts, 2010), nucleic acid delivery of the expression vectors by non-viral delivery is also being investigated. However, the drawbacks with non-viral delivery systems include unknown levels and duration of expression as well as issues around the tissue specificity (Slastnikova et al., 2018).

Viral delivery of sdAb vectors have the advantage of long-term expression of the antibody fragments inside the cells. While lentivirus and retrovirus systems have previously been involved in safety concerns of oncogene activation and cancer

development (Aiuti et al., 2002), the use of adenoviruses and adeno-associated viruses (AAVs) are of great interest . Adenoviruses and AAVs are commonly used in gene therapy (Wold & Toth, 2014) and are currently in development for various different indications such as flu vaccines (www.greffex.com) or retinal dystrophy (Rodrigues et al., 2019).

Oncolytic viruses (OV) are natural or designed viruses with cancer cell preferential replication, resulting in cell lysis of the malignant target cells, while keeping healthy untransformed cells widely unaffected (Seymour & Fisher, 2016). Many clinical trials at various stages are currently ongoing (reviewed by Eissa et al. 2018), and first oncolytic viral therapies have been approved for clinical use for melanoma (Chesney et al., 2018; Garber, 2006; Russell & Peng, 2018), supporting their further development.

The cancer-targeting characteristic of OVs makes them ideal carriers for selective delivery of anti-cancer biologics. So-called “armed” oncolytic viruses, which deliver other anti-cancer therapeutics to the tumour site, may potentiate the inherent killing effect (Bauzon & Hermiston, 2014; Seymour & Fisher, 2016). In fact, there has been a surge of research in this field and increasing numbers of studies report enhanced therapeutic activity of OVs expressing immune checkpoint inhibitors such as anti-CTLA-4 (Dias et al., 2012) and anti-PD-L1 (Tanoue et al., 2017), as well as other anti-tumour antibodies, including anti-VEGF single domain antibodies (Adelfinger et al., 2015; Frentzen et al., 2009), the anti-HER2 antibody trastuzumab (Liikanen et al., 2016) and an EGFR-targeting bispecific T-cell engager (BiTE) (Fajardo et al., 2017). An OV delivering intracellular sdAb under

tissue-specific promoters and replicating inside the cell may ensure good expression of the antibody fragments to malignant targeted cells.

Overall, while intracellular antibody fragments are useful tools to explore potential targets in proof-of-concept studies (Beghein & Gettemans, 2017) and their specific delivery to target cells is currently being addressed, their use as cancer therapeutics needs to be further investigated. The main bottleneck in intracellular sdAb development remains the fact that it will be difficult, to successfully target every single cell of a tumour. Immune killing by conventional antibodies through surface attack on target cells can induce an immune response (Scott, Wolchok, & Old, 2012) and cell killing in neighbouring cells – a phenomenon called the bystander effect (WF Bodmer and D Ouaret personal communication, Ross et al., 2017). Intracellular inhibition of protein-protein interactions to block a signalling pathway by a sdAb will not result in this immunological bystander response and only the successfully targeted cells will be affected. The intracellular delivery of the sdAb by OVs, which inherently result in the lysis of tumour cells and elicit an immune response affecting neighbouring cells (de Graaf et al., 2018), may be a way forward. Therefore, the viability of this OV/sdAb combination approach needs to be further investigated.

References

References

Ackers, I., & Malgor, R. (2018). Interrelationship of canonical and non-canonical Wnt signalling pathways in chronic metabolic diseases. *Diabetes and Vascular Disease Research*, *15*(1), 3-13.

Adachi, S., Jigami, T., Yasui, T., Nakano, T., Ohwada, S., Omori, Y., … Akiyama, T. (2004). *Role of a BCL9-Related β-Catenin-Binding Protein, B9L, in Tumorigenesis Induced by Aberrant Activation of Wnt Signaling*. 6.

Adelfinger, M., Bessler, S., Frentzen, A., Cecil, A., Langbein-Laugwitz, J., Gentschev, I., & Szalay, A. (2015). Preclinical Testing Oncolytic Vaccinia Virus Strain GLV-5b451 Expressing an Anti-VEGF Single-Chain Antibody for Canine Cancer Therapy. *Viruses*, *7*(7), 4075–4092.

Ahler, E., Sullivan, W. J., Cass, A., Braas, D., York, A. G., Bensinger, S. J., … Christofk, H. R. (2013). Doxycycline Alters Metabolism and Proliferation of Human Cell Lines. *PLoS ONE*, *8*(5), e64561.

Aiuti, A., Slavin, S., Ficara, F., Deola, S., Mortellaro, A., Morecki, S., … Bordignon, C. (2002). Correction of ADA-SCID by Stem Cell Gene Therapy Combined with Nonmyeloablative Conditioning. *Science*, *296*(5577), 2410–2413.

Alao, J. P. (2007). The regulation of cyclin D1 degradation: Roles in cancer development and the potential for therapeutic invention. *Molecular Cancer*, *6*(1), 24.

Amit, S., Hatzubai, A., Birman, Y., Andersen, J. S., Ben-Shushan, E., Mann, M., … Alkalay, I. (2002). Axin-mediated CKI phosphorylation of β-catenin at Ser 45: A molecular switch for the Wnt pathway. *Genes & Development*, *16*, 1066–1076.

Arce, L., Yokoyama, N. N., & Waterman, M. L. (2006). Diversity of LEF/TCF action in development and disease. *Oncogene*, *25*(57), 7492–7504.

Baell, J. B. (2016). Feeling Nature's PAINS: Natural Products, Natural Product Drugs, and Pan Assay Interference Compounds (PAINS). *Journal of Natural Products*, *79*(3), 616–628.

Baell, J. B., & Walters, M. (2014). Chemical con artists foil drug discovery. *Nature*, *513*, 481–483.

Baldus, S. E. (2004). MUC1 and Nuclear b-Catenin Are Coexpressed at the Invasion Front of Colorectal Carcinomas and Are Both Correlated with Tumor Prognosis. *Clinical Cancer Research*, *10*(8), 2790–2796.

Bannas, P., Hambach, J., & Koch-Nolte, F. (2017). Nanobodies and Nanobody-Based Human Heavy Chain Antibodies As Antitumor Therapeutics. *Frontiers in Immunology*, *8*, 1603.

Barker, N., Huls, G., Korinek, V., & Clevers, H. (1999). Restricted High Level Expression of Tcf-4 Protein in Intestinal and Mammary Gland Epithelium. *The American Journal of Pathology*, *154*(1), 29–35.

Barker, N., van Es, J. H., Kuipers, J., Kujala, P., van den Born, M., Cozijnsen, M., … Clevers, H. (2007). Identification of stem cells in small intestine and colon by marker gene Lgr5. *Nature*, *449*(7165), 1003–1007.

Barretina, J., Caponigro, G., Stransky, N., Venkatesan, K., Margolin, A. A., Kim, S., … Garraway, L. A. (2012). The Cancer Cell Line Encyclopedia enables predictive modelling of anticancer drug sensitivity. *Nature*, *483*(7391), 603–607.

Basu, S., Cheriyamundath, S., & Ben-Ze'ev, A. (2018). Cell–cell adhesion: Linking Wnt/β-catenin signaling with partial EMT and stemness traits in tumorigenesis. *F1000Research*, *7*, 1488.

Bauer, A., Huber, O., & Kemler, R. (1998). Pontin52, an interaction partner of β-catenin, binds to the TATA box binding protein. *Proceedings of the National Academy of Sciences*, *95*(25), 14787–14792.

Bauer, Andreas, Chauvet, S., Huber, O., & Usseglio, F. (1998). Pontin52 and Reptin52 function as antagonistic regulators of β-catenin signalling activity. *Proc. Natl. Acad. Sci.*, *95*, 14787–14792.

Bauzon, M., & Hermiston, T. (2014). Armed Therapeutic Viruses – A Disruptive Therapy on the Horizon of Cancer Immunotherapy. *Frontiers in Immunology*, *5*.

Becker, D., & Guarente, L. (1991). High-efficiency transformation of yeast by electroporation. *Methods in Enzymology*, *194*, 182–187.

Beghein, E., & Gettemans, J. (2017). Nanobody Technology: A Versatile Toolkit for Microscopic Imaging, Protein–Protein Interaction Analysis, and Protein Function Exploration. *Frontiers in Immunology*, *8*, 771.

Behrens, J., Jerchow, B.-A., Würtele, M., Grimm, J., Asbrand, C., Wirtz, R., … Birchmeier, W. (1998). Functional Interaction of an Axin Homolog, Conductin, with β-Catenin, APC, and GSK3β. *Science*, *280*(5363), 596–599.

Behrens, J., von Kries, J. P., Kühl, M., Bruhn, L., Wedlich, D., Grosschedl, R., & Birchmeier, W. (1996). Functional interaction of p-catenin with the transcription factor LEF-1. *Nature*, *382*, 638–642.

Bélanger, K., Iqbal, U., Tanha, J., MacKenzie, R., Moreno, M., & Stanimirovic, D. (2019). Single-Domain Antibodies as Therapeutic and Imaging Agents for the Treatment of CNS Diseases. *Antibodies*, *8*(2), 27.

Belenkaya, T. Y., Han, C., Standley, H., Lin, X., Houston, D., Heasman, J., & Lin, X. (2002). Pygopus encodes a nuclear protein essential for Wingless/Wnt signaling. *Development*, *123*, 4089–4101.

Benatuil, L., Perez, J. M., Belk, J., & Hsieh, C.-M. (2010). An improved yeast transformation method for the generation of very large human antibody libraries. *Protein Engineering, Design and Selection*, *23*(4), 155–159.

Berridge, M., & Tan, A. (1993). Characterization of the cellular reduction of 3-(4,5-dimethylthiazol-2-yl)-2,5-diphenyltetrazolium bromide (MTT)-subcellular localization, substrate dependence, and involvement of mitochondrial electron transport in MTT Reduction. *Archives of Biochemistry and Biophysics*, *303*(2), 474–482.

Beumer, J., & Clevers, H. (2016). Regulation and plasticity of intestinal stem cells during homeostasis and regeneration. *Development*, *143*(20), 3639–3649.

Binyamin, L., Plaksin, D., & Reiter, Y. (2002). Single-Domain VH Antibody Fragments from a Phage Display Library. In M. Welschof & J. Krauss, *Recombinant Antibodies for Cancer Therapy* (Vol. 207, pp. 133–144). https://doi.org/10.1385/1-59259-334-8:133

Biocca, S., Ruberti, F., Tafani, M., Pierandrel-Amaldi, P., & Cattaneo, A. (1995). Redox State of Single Chain Fv Fragments Targeted to the Endoplasmic Reticulum, Cytosol and Mitochondria. *Bio/Technology*, *13*(10), 1110–1115.

Bodmer, W. F., Bailey, C. J., Bodmer, J., Bussey, H. J. R., Ellis, A., Gorman, P., … Spurr, N. K. (1987). Localization of the gene for familial adenomatous polyposis on chromosome 5. *Nature*, *328*(6131), 614–616.

Bodmer, W. F. (2006). Cancer genetics: Colorectal cancer as a model. *Journal of Human Genetics*, *51*(5), 391–396.

Bond, C., Marsters Jr, J., & Sidhu, S. (2003). Contributions of CDR3 to VHH Domain Stability and the Design of Monobody Scaffolds for Naive Antibody Libraries. *J. Mol. Biol.*, *332*, 643–655.

Bourhis, E., Tam, C., Franke, Y., Bazan, J. F., Ernst, J., Hwang, J., … Hannoush, R. N. (2010). Reconstitution of a Frizzled8·Wnt3a·LRP6 Signaling Complex Reveals Multiple Wnt and Dkk1 Binding Sites on LRP6. *Journal of Biological Chemistry*, *285*(12), 9172–9179.

Bowers, P. M., Neben, T. Y., Tomlinson, G. L., Dalton, J. L., Altobell, L., Zhang, X., … King, D. J. (2013). Humanization of Antibodies Using Heavy Chain Complementarity-determining Region 3 Grafting Coupled with *in Vitro* Somatic Hypermutation. *Journal of Biological Chemistry*, *288*(11), 7688–7696.

Brabletz, T., Jung, A., Reu, S., Porzner, M., Hlubek, F., Kunz-Schughart, L., … Kirchner, T. (2001). Variable β-catenin expression in colorectal cancers indicates tumor progression driven by the tumor environment. *PNAS*, *98*(18), 10356–10361.

Bracht, K., Nicholls, A. M., Liu, Y., & Bodmer, W. F. (2010). 5-Fluorouracil response in a large panel of colorectal cancer cell lines is associated with mismatch repair deficiency. *British Journal of Cancer*, *103*(3), 340–346.

Bratosin, D., Mitrofan, L., Palii, C., Estaquier, J., & Montreuil, J. (2005). Novel fluorescence assay using calcein-AM for the determination of human erythrocyte viability and aging. *Cytometry Part A*, *66A*(1), 78–84.

Bray, F., Ferlay, J., Soerjomataram, I., Siegel, R. L., Torre, L. A., & Jemal, A. (2018). Global cancer statistics 2018: GLOBOCAN estimates of incidence and mortality worldwide for 36 cancers in 185 countries. *CA: A Cancer Journal for Clinicians*, *68*(6), 394–424.

Brembeck, F. (2004). Essential role of BCL9-2 in the switch between β-catenin's adhesive and transcriptional functions. *Genes & Development*, *18*(18), 2225–2230.

Brembeck, F., Wiese, M., Zatula, N., Grigoryan, T., Dai, Y., Fritzmann, J., & Birchmeier, W. (2011). BCL9-2 Promotes Early Stages of Intestinal Tumor Progression. *Gastroenterology*, *141*(4), 1359-1370.e3.

Brückner, A., Polge, C., Lentze, N., Auerbach, D., & Schlattner, U. (2009). Yeast Two-Hybrid, a Powerful Tool for Systems Biology. *International Journal of Molecular Sciences*, *10*(6), 2763–2788.

Brunner, E., Peter, O., Schweizer, L., & Basler, K. (1997). Pangolin encodes a Lef-1 homologue that acts downstream of Armadillo to transduce the Wingless signal in Drosophila. *Nature*, *385*(6619), 829–833.

Bulinski, J. C., & Bossler, A. (1994). Purification and characterization of ensconsin, a novel microtubule stabilizing protein. *Journal of Cell Science*, *107*, 2839–2849.

Caca, K., Kolligs, F. T., Ji, X., Hayes, M., Qian, J., Yahanda, A., … Fearon, E. R. (1999). β- and γ-Catenin Mutations, but not E-Cadherin Inactivation, Underlie T-Cell Factor/Lymphoid Enhancer Factor Transcriptional Deregulation in Gastric and Pancreatic Cancer. *Cell Growth & Differentiation*, *10*, 369–376.

Cadigan, K. M., & Waterman, M. L. (2012). TCF/LEFs and Wnt Signaling in the Nucleus. *Cold Spring Harbor Perspectives in Biology*, *4*(11), a007906–a007906.

Caufield, J. H., Sakhawalkar, N., & Uetz, P. (2012). A comparison and optimization of yeast two-hybrid systems. *Methods*, *58*(4), 317–324.

Chaudhary, A. R., Lu, H., Krementsova, E. B., Bookwalter, C. S., Trybus, K. M., & Hendricks, A. G. (2019). MAP7 regulates organelle transport by recruiting kinesin-1 to microtubules. *Journal of Biological Chemistry*, *294*(26), 10160–10171.

Chen, B., Dodge, M. E., Tang, W., Lu, J., Ma, Z., Fan, C.-W., … Lum, L. (2009). Small molecule–mediated disruption of Wnt-dependent signaling in tissue regeneration and cancer. *Nature Chemical Biology*, *5*(2), 100–107.

Chen, J., Liu, J., Jin, R., Shen, J., Liang, Y., Ma, R., … Cai, X. (2014). Cytoplasmic and/or Nuclear Expression of β-Catenin Correlate with Poor Prognosis and Unfavorable Clinicopathological Factors in Hepatocellular Carcinoma: A Meta-Analysis. *PLoS ONE*, *9*(11), e111885.

Chen, P.-H., Chen, X., Lin, Z., Fang, D., & He, X. (2013). The structural basis of R-spondin recognition by LGR5 and RNF43. *Genes & Development*, *27*(12), 1345–1350.

Chen, X., Zaro, J. L., & Shen, W.-C. (2013). Fusion protein linkers: Property, design and functionality. *Advanced Drug Delivery Reviews*, *65*(10), 1357–1369.

Chen, Zecheng, Venkatesan, A. M., Dehnhardt, C. M., Santos, O. D., Santos, E. D., Ayral-Kaloustian, S., … Mansour, T. S. (2009). 2,4-Diamino-quinazolines as inhibitors of β-catenin/Tcf-4 pathway: Potential treatment for colorectal cancer. *Bioorganic & Medicinal Chemistry Letters*, *19*(17), 4980–4983.

Chen, Zhigang, He, X., Jia, M., Liu, Y., Qu, D., Wu, D., … Huang, J. (2013). β-catenin Overexpression in the Nucleus Predicts Progress Disease and Unfavourable Survival in Colorectal Cancer: A Meta-Analysis. *PLoS ONE*, *8*(5), e63854.

Cheng, H., & Leblond, C. P. (1974). Origin, differentiation and renewal of the four main epithelial cell types in the mouse small intestine V. Unitarian theory of the origin of the four epithelial cell types. *American Journal of Anatomy*, *141*(4), 537–561.

Cheng, H. & Leblond, C. P.,(1974). Origin, differentiation and renewal of the four main epithelial cell types in the mouse small intestine I. Columnar cell. *American Journal of Anatomy*, *141*(4), 461–479.

Chesney, J., Puzanov, I., Collichio, F., Singh, P., Milhem, M. M., Glaspy, J., … Kaufman, H. L. (2018). Randomized, Open-Label Phase II Study Evaluating the Efficacy and Safety of Talimogene Laherparepvec in Combination With Ipilimumab Versus Ipilimumab Alone in Patients With Advanced, Unresectable Melanoma. *Journal of Clinical Oncology*, *36*(17), 1658–1667.

Clevers, H. (2013). The Intestinal Crypt, A Prototype Stem Cell Compartment. *Cell*, *154*(2), 274–284.

Colby, D. W., Chu, Y., Cassady, J. P., Duennwald, M., Zazulak, H., Webster, J. M., … Wittrup, K. D. (2004). Potent inhibition of huntingtin aggregation and cytotoxicity by a disulfide bond-free single-domain intracellular antibody. *Proceedings of the National Academy of Sciences*, *101*(51), 17616–17621.

Cong, F., Schweizer, L., Chamorro, M., & Varmus, H. (2003). Requirement for a Nuclear Function of β-Catenin in Wnt Signaling. *Molecular and Cellular Biology*, *23*(23), 8462–8470.

Cong, F., & Varmus, H. (2004). Nuclear-cytoplasmic shuttling of Axin regulates subcellular localization of β-catenin. *Proceedings of the National Academy of Sciences*, *101*(9), 2882–2887.

Cottrell, S., Bodmer, W. F., Bicknell, D., & Kaklamanis, L. (1992). Molecular analysis of APC mutations in familial adenomatous polyposis and sporadic colon carcinomas. *The Lancet*, *340*(8820), 626–630.

Croce, J. C., & McClay, D. R. (2008). Evolution of the Wnt Pathways, *Methods Mol Biol., 469*, 3–18.

Crosnier, C., Stamataki, D., & Lewis, J. (2006). Organizing cell renewal in the intestine: Stem cells, signals and combinatorial control. *Nature Reviews Genetics*, *7*(5), 349–359.

Cui, C., Zhou, X., Zhang, W., Qu, Y., & Ke, X. (2018). Is β-Catenin a Druggable Target for Cancer Therapy? *Trends in Biochemical Sciences*, *43*(8), 623–634.

da Costa, L. T., He, T.-C., Yu, J., Sparks, A. B., Morin, P. J., Polyak, K., … Kinzler, K. W. (1999). CDX2 is mutated in colorectal cancer with normal APC/b-catenin signaling. *Oncogene*, *18*, 5010–5014.

Dang, C. V. (1999). C-Myc Target Genes Involved in Cell Growth, Apoptosis, and Metabolism. *Molecular and Cellular Biology*, *19*(1), 1–11.

Daniels, D. L., & Weis, W. I. (2002). ICAT inhibits β-catenin binding to tcf/lef-family transcription factors and the general coactivator p300 using independent structural modules. *Molecular Cell*, *10*(3), 573–584.

Daniels, D. L., & Weis, W. I. (2005). β-catenin directly displaces Groucho/TLE repressors from Tcf/Lef in Wnt-mediated transcription activation. *Nature Structural & Molecular Biology*, *12*(4), 364–371.

Dar, M. S., Singh, P., Singh, G., Jamwal, G., Hussain, S. S., Rana, A., … Dar, M. J. (2016). Terminal regions of β-catenin are critical for regulating its adhesion and transcription functions. *Biochimica et Biophysica Acta (BBA) - Molecular Cell Research*, *1863*(9), 2345–2357.

Davies, J., & Riechmann, L. (1996). Single antibody domains as small recognition units: Design and in vitro antigen selection of camelized, human VH domains with improved protein stability. *Protein Engineering, Design and Selection*, *9*(6), 531–537.

De, A. (2011). Wnt/Ca2+ signaling pathway: A brief overview. *Acta Biochimica et Biophysica Sinica*, *43*(10), 745–756.

De Genst, E., Silence, K., Decanniere, K., Conrath, K., Loris, R., Kinne, J., … Wyns, L. (2006). Molecular basis for the preferential cleft recognition by dromedary heavy-chain antibodies. *Proceedings of the National Academy of Sciences*, *103*(12), 4586–4591.

de Graaf, J. F., de Vor, L., Fouchier, R. A. M., & van den Hoogen, B. G. (2018). Armed oncolytic viruses: A kick-start for anti-tumor immunity. *Cytokine & Growth Factor Reviews*, *41*, 28–39.

de la Roche, M., Rutherford, T. J., Gupta, D., Veprintsev, D. B., Saxty, B., Freund, S. M., & Bienz, M. (2012). An intrinsically labile α-helix abutting the BCL9-binding site of β-catenin is required for its inhibition by carnosic acid. *Nature Communications*, *3*(1).

de la Roche, M., Worm, J., & Bienz, M. (2008). The function of BCL9 in Wnt/β-catenin signaling and colorectal cancer cells. *BMC Cancer*, *8*(1).

de Lau, W. B., Snel, B., & Clevers, H. C. (2012). The R-spondin protein family. *Genome Biology*, *13*(3), 242.

De Vlieger, D., Ballegeer, M., Rossey, I., Schepens, B., & Saelens, X. (2019). Single-Domain Antibodies and Their Formatting to Combat Viral Infections. *Antibodies*, *8*(1).

Deka, J., Wiedemann, N., Anderle, P., Murphy-Seiler, F., Bultinck, J., Eyckerman, S., … Aguet, M. (2010). Bcl9/Bcl9l Are Critical for Wnt-Mediated Regulation of Stem Cell Traits in Colon Epithelium and Adenocarcinomas. *Cancer Research*, *70*(16), 6619–6628.

Desai, R., Sarpal, R., Ishiyama, N., Pellikka, M., Ikura, M., & Tepass, U. (2013). Monomeric α-catenin links cadherin to the actin cytoskeleton. *Nature Cell Biology*, *15*(3), 261–273.

Desmyter, A., Transue, T., Ghahroudi, M., Thi, M.-H., Poortmans, F., Hamers, R., … Wyns, L. (1996). Crystal structure of a camel single-domain VH antibody fragment in complex with lysozyme. *Nature Structural Biology*, *3*(9), 803–811.

Dias, J. D., Hemminki, O., Diaconu, I., Hirvinen, M., Bonetti, A., Guse, K., … Hemminki, A. (2012). Targeted cancer immunotherapy with oncolytic adenovirus coding for a fully human monoclonal antibody specific for CTLA-4. *Gene Therapy*, *19*(10), 988–998.

Dietrich, C., Scherwat, J., Faust, D., & Oesch, F. (2002). Subcellular Localization of β-Catenin Is Regulated by Cell Density. *Biochemical and Biophysical Research Communications*, *292*(1), 195–199.

Dietrich, L., Rathmer, B., Ewan, K., Bange, T., Heinrichs, S., Dale, T. C., … Grossmann, T. N. (2017). Cell Permeable Stapled Peptide Inhibitor of Wnt Signaling that Targets β-Catenin Protein-Protein Interactions. *Cell Chemical Biology*, *24*(8), 958-968.e5.

Donini, M., Morea, V., Desiderio, A., Pashkoulov, D., Villani, M. E., Tramontano, A., & Benvenuto, E. (2003). Engineering Stable Cytoplasmic Intrabodies with Designed Specificity. *Journal of Molecular Biology*, *330*(2), 323–332.

Dudgeon, K., Rouet, R., Famm, K., & Christ, D. (2012). Selection of Human VH Single Domains with Improved Biophysical Properties by Phage Display. In D. Saerens & S. Muyldermans (Eds.), *Single Domain Antibodies* (pp. 383–397).

Edgar, R. C. (2004). MUSCLE: Multiple sequence alignment with high accuracy and high throughput. *Nucleic Acids Research*, *32*(5), 1792–1797.

Efstathiou, J. A., Liu, D., Wheeler, J. M. D., Kim, H. C., Beck, N. E., Ilyas, M., … Bodmer, W. F. (1999). Mutated epithelial cadherin is associated with increased tumorigenicity and loss of adhesion and of responsiveness to the motogenic trefoil factor 2 in colon carcinoma cells. *Proceedings of the National Academy of Sciences*, *96*(5), 2316–2321.

Eissa, I., Bustos-Villalobos, I., Ichinose, T., Matsumura, S., Naoe, Y., Miyajima, N., … Kasuya, H. (2018). The Current Status and Future Prospects of Oncolytic Viruses in Clinical Trials against Melanoma, Glioma, Pancreatic, and Breast Cancers. *Cancers*, *10*(10), 356.

El-Bahrawy, M., Poulsom, S. R., Rowan, A. J., Tomlinson, I. T., & Alison, M. R. (2004). Characterization of the E-cadherin/catenin complex in colorectal carcinoma cell lines: E-cadherin/catenin complex and colorectal carcinoma. *International Journal of Experimental Pathology*, *85*(2), 65–74.

Emami, K. H., Nguyen, C., Ma, H., Kim, D. H., Jeong, K. W., Eguchi, M., … Kahn, M. (2004). A small molecule inhibitor of β-catenin/CREB-binding protein transcription. *Proceedings of the National Academy of Sciences*, *101*(34), 12682–12687.

Fagotto, F., Funayama, N., Glück, U., & Gumbiner, B. M. (1996). Binding to cadherins antagonizes the signaling activity of beta-catenin during axis formation in Xenopus. *The Journal of Cell Biology*, *132*(6), 1105–1114.

Fagotto, F., Glück, U., & Gumbiner, B. M. (1998). Nuclear localization signal-independent and importin/karyopherin-independent nuclear import of b-catenin. *Current Biology*, *8*, 181–190.

Fajardo, C. A., Guedan, S., Rojas, L. A., Moreno, R., Arias-Badia, M., de Sostoa, J., … Alemany, R. (2017). Oncolytic Adenoviral Delivery of an EGFR-Targeting T-cell Engager Improves Antitumor Efficacy. *Cancer Research*, *77*(8), 2052–2063.

Fang, L., Zhu, Q., Neuenschwander, M., Specker, E., Wulf-Goldenberg, A., Weis, W. I., … Birchmeier, W. (2016). A Small-Molecule Antagonist of the β-Catenin/TCF4 Interaction Blocks the Self-Renewal of Cancer Stem Cells and Suppresses Tumorigenesis. *Cancer Research*, *76*(4), 891–901.

Fasolini, M., Wu, X., Flocco, M., Trosset, J. Y., Oppermann, U., & Knapp, S. (2003a). Hot spots in Tcf4 for the interaction with β-catenin. *Journal of Biological Chemistry*, *278*(23), 21092–21098.

Fearnhead, N., Britton, M., & Bodmer, W. F. (2001). The ABC of APC. *Human Molecular Genetics*, *10*(7), 721–733.

Fenderico, N., van Scherpenzeel, R. C., Goldflam, M., Proverbio, D., Jordens, I., Kralj, T., … Maurice, M. M. (2019). Anti-LRP5/6 VHHs promote differentiation of Wnt-hypersensitive intestinal stem cells. *Nature Communications*, *10*(1), 365.

Feng, M., Jin, J. Q., Xia, L., Xiao, T., Mei, S., Wang, X., … Zhu, A. X. (2019). Pharmacological inhibition of b-catenin/BCL9 interaction overcomes resistance to immune checkpoint blockades by modulating Treg cells. *Sci. Adv.*, 5, eaau5240.

Fevr, T., Robine, S., Louvard, D., & Huelsken, J. (2007). Wnt/ -Catenin Is Essential for Intestinal Homeostasis and Maintenance of Intestinal Stem Cells. *Molecular and Cellular Biology*, *27*(21), 7551–7559.

Fields, S., & Song, O. (1989). A novel genetic system to detect protein-protein interactions. *Nature*, *340*, 245–246.

Frankel, A., & Pabo, C. (1988). Cellular uptake of the tat protein from human immunodeficiency virus. *Cell*, *55*, 1189–1193.

Frentzen, A., Yu, Y. A., Chen, N., Zhang, Q., Weibel, S., Raab, V., & Szalay, A. A. (2009). Anti-VEGF single-chain antibody GLAF-1 encoded by oncolytic vaccinia virus significantly enhances antitumor therapy. *Proceedings of the National Academy of Sciences*, *106*(31), 12915–12920.

Fujii, N., You, L., Xu, Z., Uematsu, K., Shan, J., He, B., … Jablons, D. M. (2007). An Antagonist of Dishevelled Protein-Protein Interaction Suppresses β-Catenin-Dependent Tumor Cell Growth. *Cancer Research*, *67*(2), 573–579.

Galli, L. M., Barnes, T. L., Secrest, S. S., Kadowaki, T., & Burrus, L. W. (2007). Porcupine-mediated lipid-modification regulates the activity and distribution of Wnt proteins in the chick neural tube. *Development*, *134*(18), 3339–3348.

Gamallo, C., Palacios, J., Moreno, G., Calvo de Mora, J., Suárez, A., & Armas, A. (1999). β-Catenin Expression Pattern in Stage I and II Ovarian Carcinomas. *The American Journal of Pathology*, *155*(2), 527–536.

Gandhirajan, R. K., Staib, P. A., Minke, K., Gehrke, I., Plickert, G., Schlösser, A., … Kreuzer, K.-A. (2010). Small Molecule Inhibitors of Wnt/β-Catenin/Lef-1 Signaling Induces Apoptosis in Chronic Lymphocytic Leukemia Cells In Vitro and In Vivo. *Neoplasia*, *12*(4), 326-335.

Gao, C., & Chen, Y.-G. (2010). Dishevelled: The hub of Wnt signaling. *Cellular Signalling*, *22*(5), 717–727.

Garber, K. (2006). China Approves World's First Oncolytic Virus Therapy For Cancer Treatment. *Journal of the National Cancer Institute*, *98*(5), 298–300.

Garnett, M. J., Edelman, E. J., Heidorn, S. J., Greenman, C. D., Dastur, A., Lau, K. W., … Benes, C. H. (2012). Systematic identification of genomic markers of drug sensitivity in cancer cells. *Nature*, *483*(7391), 570–575.

Gay, D. M., Ridgway, R. A., Müller, M., Hodder, M. C., Hedley, A., Clark, W., … Sansom, O. J. (2019). Loss of BCL9/9l suppresses Wnt driven tumourigenesis in models that recapitulate human cancer. *Nature Communications*, *10*(1), 723.

Gee, L., Hartig, J., Law, L., Wittlieb, J., Khalturin, K., Bosch, T. C. G., & Bode, H. R. (2010). β-catenin plays a central role in setting up the head organizer in hydra. *Developmental Biology*, *340*(1), 116–124.

Gehart, H., & Clevers, H. (2019). Tales from the crypt: New insights into intestinal stem cells. *Nature Reviews Gastroenterology & Hepatology*, *16*(1), 19–34.

Gelmann, A., Desnoyers, R., Cagir, B., Weinberg, D., Boman, B. M., & Waldman, S. A. (2000). Colorectal cancer staging and adjuvant chemotherapy. *Expert Opinion on Pharmacotherapy*, *1*(4), 737–755.

Gietz, R. D., & Schiestl, R. H. (2007a). High-efficiency yeast transformation using the LiAc/SS carrier DNA/PEG method. *Nature Protocols*, *2*(1), 31–34.

Gietz, R. D., & Schiestl, R. H. (2007c). Large-scale high-efficiency yeast transformation using the LiAc/SS carrier DNA/PEG method. *Nature Protocols*, *2*(1), 38–41.

Gietz, R. D., Schiestl, R. H., Willems, A. R., & Woods, R. A. (1994). Studies on the transformation of intact yeast cells by the LiAc/SS-DNA/PEG procedure. *Yeast*, *11*(4), 355–360.

Gong, Y., Bourhis, E., Chiu, C., Stawicki, S., DeAlmeida, V. I., Liu, B. Y., … Costa, M. (2010). Wnt Isoform-Specific Interactions with Coreceptor Specify Inhibition or Potentiation of Signaling by LRP6 Antibodies. *PLoS ONE*, *5*(9), e12682.

Gottardi, C. J., Wong, E., & Gumbiner, B. M. (2001). E-Cadherin Suppresses Cellular Transformation by Inhibiting β-Catenin Signaling in an Adhesion-Independent Manner. *The Journal of Cell Biology*, *153*(5), 1049–1060.

Graham, T. A., Clements, W. K., Kimelman, D., & Xu, W. (2002). *The Crystal Structure of the β-Catenin / ICAT Complex Reveals the Inhibitory Mechanism of ICAT*. *10*, 563–571.

Graham, T. A., Weaver, C., Mao, F., Kimelman, D., & Xu, W. (2000). Crystal Structure of a β-Catenin/Tcf Complex. *Cell*, *103*, 885–896.

Graham, T., Ferkey, D., Mao, F., Kimelman, D., & Xu, W. (2001). TCF4 can specifically recognize β-catenin using alternative conformations. *Nature Structural Biology*, *8*(12).

Grigson, E. R., Ozerova, M., Pisklakova, A., Liu, H., Sullivan, D. M., & Nefedova, Y. (2015). Canonical Wnt Pathway Inhibitor ICG-001 Induces Cytotoxicity of Multiple Myeloma Cells in Wnt-Independent Manner. *PLOS ONE*, *10*(1), e0117693.

Groden, J., Thliveris, A., Samowitz, W., Carlson, M., Gelbert, L., Albertsen, H., … White, R. (1991). Identification and characterization of the familial adenomatous polyposis coli gene. *Cell*, *66*(3), 589–600.

Grossmann, T. N., Yeh, J. T.-H., Bowman, B. R., Chu, Q., Moellering, R. E., & Verdine, G. L. (2012). Inhibition of oncogenic Wnt signaling through direct targeting of β-catenin. *Proceedings of the National Academy of Sciences*, *109*(44), 17942–17947.

Gurney, A., Axelrod, F., Bond, C. J., Cain, J., Chartier, C., Donigan, L., … Hoey, T. (2012). Wnt pathway inhibition via the targeting of Frizzled receptors results in decreased growth and tumorigenicity of human tumors. *Proceedings of the National Academy of Sciences*, *109*(29), 11717–11722.

Guturi, K. K. N., Mandal, T., Chatterjee, A., Sarkar, M., Bhattacharya, S., Chatterjee, U., & Ghosh, M. K. (2012). Mechanism of β-Catenin-mediated Transcriptional Regulation of Epidermal Growth Factor Receptor Expression in Glycogen Synthase Kinase 3 β-inactivated Prostate Cancer Cells. *Journal of Biological Chemistry*, *287*(22), 18287–18296.

Haegel, H., Larue, L., Ohsugi, M., Fedorov, L., Herrenknecht, K., & Kemler, R. (1995). Lack of β-catenin affects mouse development at gastrulation. *Development*, *121*, 3529–3537.

Hahne, G., & Grossmann, T. N. (2013a). Direct targeting of beta-catenin: Inhibition of protein-protein interactions for the inactivation of Wnt signaling. *Bioorganic and Medicinal Chemistry*, *21*(14), 4020–4026.

Hahne, G., & Grossmann, T. N. (2013b). Direct targeting of β-catenin: Inhibition of protein–protein interactions for the inactivation of Wnt signaling. *Bioorganic & Medicinal Chemistry*, *21*(14), 4020–4026.

Hamers-Casterman, C., Atarhouch, T., Muyldermans, S., Robinson, G., Hammers, C., Songa, E. B., … Hamers, R. (1993). Naturally occurring antibodies devoid of light chains. *Nature*, *363*(6428), 446–448.

Hao, H.-X., Xie, Y., Zhang, Y., Charlat, O., Oster, E., Avello, M., … Cong, F. (2012). ZNRF3 promotes Wnt receptor turnover in an R-spondin-sensitive manner. *Nature*, *485*(7397), 195–200.

Haraya, K., Tachibana, T., & Igawa, T. (2019). Improvement of pharmacokinetic properties of therapeutic antibodies by antibody engineering. *Drug Metabolism and Pharmacokinetics*, *34*(1), 25–41.

Harb, J., Lin, P.-J., & Hao, J. (2019). Recent Development of Wnt Signaling Pathway Inhibitors for Cancer Therapeutics. *Current Oncology Reports*, *21*(12).

Harmsen, M. M., & De Haard, H. J. (2007). Properties, production, and applications of camelid single-domain antibody fragments. *Applied Microbiology and Biotechnology*, *77*(1), 13–22.

Harris, L., Larson, S., Hasel, K., & McPherson, A. (1997). Refined Structure of an Intact IgG2a Monoclonal Antibody. *Biochemistry*, *36*, 1581–1597.

Hart, M., Concordet, J.-P., Lassot, I., Albert, I., del los Santos, R., Durand, H., … Polakis, P. (1999). The F-box protein β-TrCP associates with phosphorylated β-catenin and regulates its activity in the cell. *Current Biology*, *9*(4), 207–211.

Hart, M. J., de los Santos, R., Albert, I., Rubinfeld, B., & Polakis, P. (1998). Downregulation of β-catenin by human Axin and its association with the APC tumor suppressor, b-catenin and GSK3β. *Current Biology*, *8*, 573–581.

He, B., You, L., Uematsu, K., Xu, Z., Lee, A. Y., Matsangou, M., … Jablons, D. M. (2004). A Monoclonal Antibody against Wnt-1 Induces Apoptosis in Human Cancer Cells. *Neoplasia*, *6*(1), 7–14.

Hecht, A., Litterst, C. M., Huber, O., & Kemler, R. (1999). Functional Characterization of Multiple Transactivating Elements in b-Catenin, Some of Which Interact with the TATA-binding Protein in Vitro. *The Journal of Biological Chemistry*, *274*, 18017–18025.

Hecht, A., Vleminckx, K., Stemmler, M. P., van Roy, F., & Kemler, R. (2000a). The p300/CBP acetyltransferases function as transcriptional coactivators of b-catenin in vertebrates. *The EMBO Journal*, *19*(9), 1839–1850.

Held, A., Glas, A., Dietrich, L., Bollmann, M., Brandstädter, K., Grossmann, T. N., … Bertrand, J. (2018). Targeting β-catenin dependent Wnt signaling via peptidomimetic inhibitors in murine chondrocytes and OA cartilage. *Osteoarthritis and Cartilage*, *26*(6), 818–823.

Henderson, B. R. (2000). Nuclear-cytoplasmic shuttling of APC regulates β-catenin subcellular localization and turnover. *Nature Cell Biology*, *2*(9), 653–660.

Herbst, A., Jurinovic, V., Krebs, S., Thieme, S. E., Blum, H., Göke, B., & Kolligs, F. T. (2014). Comprehensive analysis of β-catenin target genes in colorectal carcinoma cell lines with deregulated Wnt/β-catenin signaling. *BMC Genomics*, *15*(1), 74.

Hernández, A. R., Klein, A. M., & Kirschner, M. W. (2012). Kinetic Responses of β-Catenin Specify the Sites of Wnt Control. *Science*, 338 (6112), 1337-1340.

Heuberger, J., & Birchmeier, W. (2010). Interplay of Cadherin-Mediated Cell Adhesion and Canonical Wnt Signaling. *Cold Spring Harbor Perspectives in Biology*, *2*(2), a002915.

Hoffmans, R., & Basler, K. (2004). Identification and in vivo role of the Armadillo-Legless interaction. *Development*, *131*(17), 4393–4400.

Hoffmans, R., & Basler, K. (2007). BCL9-2 binds Arm/β-catenin in a Tyr142-independent manner and requires Pygopus for its function in Wg/Wnt signaling. *Mechanisms of Development*, *124*(1), 59-67.

Hoggard, L. R., Zhang, Y., Zhang, M., Panic, V., Wisniewski, J. A., & Ji, H. (2015). Rational Design of Selective Small-Molecule Inhibitors for β-Catenin/B-Cell Lymphoma 9 Protein–Protein Interactions. *Journal of the American Chemical Society*, *137*(38), 12249–12260.

Holliger, P., & Hudson, P. J. (2005). Engineered antibody fragments and the rise of single domains. *Nature Biotechnology*, *23*(9), 1126–1136.

Hortin, G. L., Sviridov, D., & Anderson, N. L. (2008). High-Abundance Polypeptides of the Human Plasma Proteome Comprising the Top 4 Logs of Polypeptide Abundance. *Clinical Chemistry*, *54*(10), 1608–1616.

Hrckulak, D., Kolar, M., Strnad, H., & Korinek, V. (2016). TCF/LEF Transcription Factors: An Update from the Internet Resources. *Cancers*, *8*(7), 70.

Hsia, L., Ashley, N., Ouaret, D., Wang, L. M., Wilding, J., & Bodmer, W. F. (2016). Myofibroblasts are distinguished from activated skin fibroblasts by the expression of AOC3 and other associated markers. *Proceedings of the National Academy of Sciences*, *113*(15), E2162–E2171.

Huang, K. T., Chen, Y. H., & Walker, A. M. (2004). Inaccuracies in MTS assays: Major distorting effects of medium, serum albumin, and fatty acids. *BioTechniques*, *37*(3), 406–412.

Huang, S.-M. A., Mishina, Y. M., Liu, S., Cheung, A., Stegmeier, F., Michaud, G. A., … Cong, F. (2009). Tankyrase inhibition stabilizes axin and antagonizes Wnt signalling. *Nature*, *461*(7264), 614–620.

Huber, A. H., Nelson, W. J., & Weis, W. I. (1997). Three-Dimensional Structure of the Armadillo Repeat Region of β-Catenin. *Cell*, *90*, 871–882.

Huber, A. H., & Weis, W. I. (2001). The Structure of the β-Catenin/E-Cadherin Complex and the Molecular Basis of Diverse Ligand Recognition by β-Catenin. *Cell*, *105*, 391–402.

Huber, O., Korn, R., McLaughlin, J., Ohsugi, M., Herrmann, B., & Kemler, R. (1996). Nuclear localization of β-catenin by interaction with transcription factor LEF-1. *Mechanisms of Development*, *59*, 3–10.

Huels, D., Ridgway, R., Radulescu, S., Leushacke, M., Campbell, A., Biswas, S., … Sansom, O. J. (2015). E-cadherin can limit the transforming properties of activating β-catenin mutations. *The EMBO Journal*, *34*, 2321–2333.

Huelsken, J., Vogel, R., Brinkmann, V., Erdmann, B., Birchmeier, C., & Birchmeier, W. (2000). Requirement for β-Catenin in Anterior-Posterior Axis Formation in Mice. *The Journal of Cell Biology*, *148*(3), 567–578.

Hugh, T. J., Dillon, S. A., O'Dowd, G., Getty, B., Pignatelli, M., Poston, G. J., & Kinsella, A. R. (1999). ß-catenin expression in primary and metastatic colorectal carcinoma. *Int. J. Cancer*, *82*, 504–511.

Hülsken, J., Birchmeier, W., & Behrens, J. (1994). E-cadherin and APC compete for the interaction with beta-catenin and the cytoskeleton. *The Journal of Cell Biology*, *127*(6), 2061–2069.

Humphries, A., & Wright, N. A. (2008). Colonic crypt organization and tumorigenesis. *Nature Reviews Cancer*, *8*(6), 415–424.

Hwang, S.-Y., Deng, X., Byun, S., Lee, C., Lee, S.-J., Suh, H., … Lee, S. W. (2016). Direct Targeting of β-Catenin by a Small Molecule Stimulates Proteasomal Degradation and Suppresses Oncogenic Wnt/β-Catenin Signaling. *Cell Reports*, *16*(1), 28–36.

Hyeon, J., Ahn, S., Lee, J. J., Song, D. H., & Park, C.-K. (2013). Prognostic Significance of BCL9 Expression in Hepatocellular Carcinoma. *Korean Journal of Pathology*, *47*(2), 130.

Iezzi, M. E., Policastro, L., Werbajh, S., Podhajcer, O., & Canziani, G. A. (2018). Single-Domain Antibodies and the Promise of Modular Targeting in Cancer Imaging and Treatment. *Frontiers in Immunology*, *9*, 273.

Igawa, T., Tsunoda, H., Kuramochi, T., Sampei, Z., Ishii, S., & Hattori, K. (2011). Engineering the variable region of therapeutic IgG antibodies. *MAbs*, *3*(3), 243–252.

Jasperson, K. W., Tuohy, T. M., Neklason, D. W., & Burt, R. W. (2010). Hereditary and Familial Colon Cancer. *Gastroenterology*, *138*(6), 2044–2058.

Jass, J. R., & Morson, B. C. (1987). Reporting colorectal cancer. *Journal of Clinical Pathology*, *40*(9), 1016–1023.

Jho, E. -h., Zhang, T., Domon, C., Joo, C.-K., Freund, J.-N., & Costantini, F. (2002). Wnt/β-Catenin/Tcf Signaling Induces the Transcription of Axin2, a Negative Regulator of the Signaling Pathway. *Molecular and Cellular Biology*, *22*(4), 1172–1183.

Jubb, A. M., Chalasani, S., Frantz, G. D., Smits, R., Grabsch, H. I., Kavi, V., … Koeppen, H. (2006). Achaete-scute like 2 (ascl2) is a target of Wnt signalling and is upregulated in intestinal neoplasia. *Oncogene*, *25*(24), 3445–3457.

Kabat, E., & Wu, T. T. (1991). Identical V Region Amino Acid Sequences and Segments of Sequences in Antibodies of Different Specificities. *The Journal of Immunology*, *147*, 1709–1719.

Kadowaki, T., Wilder, E., Klingensmith, J., Zachary, K., & Perrimon, N. (1996). The segment polarity gene porcupine encodes a putative multitransmembrane protein involved in Wingless processing. *Genes & Development*, *10*, 3116–3128.

Kageshita, T., Hamby, C. V., Ishihara, T., Matsumoto, K., Saida, T., & Ono, T. (2001). Loss of beta-catenin expression associated with disease progression in malignant melanoma. *British Journal of Dermatology*, *145*(2), 210–216.

Kaplon, H., & Reichert, J. M. (2019). Antibodies to watch in 2019. *MAbs*, *11*(2), 219–238. https://doi.org/10.1080/19420862.2018.1556465

Kartha, V. K., Alamoud, K. A., Sadykov, K., Nguyen, B.-C., Laroche, F., Feng, H., … Kukuruzinska, M. A. (2018). Functional and genomic analyses reveal therapeutic potential of targeting β-catenin/CBP activity in head and neck cancer. *Genome Medicine*, *10*(1), 54.

Kawai, S., Hashimoto, W., & Murata, K. (2010). Transformation of Saccharomyces cerevisiae and other fungi: Methods and possible underlying mechanism. *Bioengineered Bugs*, *1*(6), 395–403.

Kawamoto, S. A., Coleska, A., Ran, X., Yi, H., Yang, C.-Y., & Wang, S. (2012). Design of Triazole-Stapled BCL9 α-Helical Peptides to Target the β-Catenin/B-Cell CLL/lymphoma 9 (BCL9) Protein–Protein Interaction. *Journal of Medicinal Chemistry*, *55*(3), 1137–1146.

Keepers, Y., Pizao, P., Peters, G., van Ark-Otte, J., Winograd, B., & Pinedo, H. (1991). Comparison of the Sulforhodamine B Protein and Tetrazolium (MTT) Assays for in vitro Chemosensitivity Testing. *Eur J Cancer*, *27*(7), 897–900.

Kettleborough, C. A., Saldanha, J., Heath, V. J., Morrison, C. J., & Bendig, M. M. (1991). Humanization of a mouse monoclonal antibody by CDR–grafting: The importance of framework residues on loop conformation. *Protein Engineering, Design and Selection*, *4*(7), 773–783.

Kishida, S., Yamamoto, H., Hino, S.-I., Ikeda, S., Kishida, M., & Kikuchi, A. (1999). DIX Domains of Dvl and Axin Are Necessary for Protein Interactions and Their Ability To Regulate β-Catenin Stability. *Mol. Cell. Biol.*, 19(6), 4414-4422.

Knapp, S., Zamai, M., Volpi, D., Nardese, V., Avanzi, N., Breton, J., … Caiolfa, V. R. (2001). Thermodynamics of the high-affinity interaction of TCF4 with β-catenin. *Journal of Molecular Biology*, *306*(5), 1179–1189.

Köhler, G., & Milstein, C. (1975). Continuous cultures of fused cells secreting antibody of predefined specificity. *Nature*, *256*(5517), 495–497.

Koide, S. (2009). Engineering of recombinant crystallization chaperones. *Current Opinion in Structural Biology*, *19*(4), 449–457.

Koike, M., Kose, S., Furuta, M., Taniguchi, N., Yokoya, F., Yoneda, Y., & Imamoto, N. (2004). β-Catenin Shows an Overlapping Sequence Requirement but Distinct Molecular Interactions for Its Bidirectional Passage through Nuclear Pores. *Journal of Biological Chemistry*, *279*(32), 34038–34047.

Komekado, H., Yamamoto, H., Chiba, T., & Kikuchi, A. (2007). Glycosylation and palmitoylation of Wnt-3a are coupled to produce an active form of Wnt-3a. *Genes to Cells*, *12*(4), 521–534.

Koo, B.-K., Spit, M., Jordens, I., Low, T. Y., Stange, D. E., van de Wetering, M., … Clevers, H. (2012). Tumour suppressor RNF43 is a stem-cell E3 ligase that induces endocytosis of Wnt receptors. *Nature*, *488*(7413), 665–669.

Korinek, V., Barker, N., Moerer, P., van Donselaar, E., Huls, G., Peters, P. J., & Clevers, H. (1998). Depletion of epithelial stem-cell compartments in the small intestine of mice lacking Tcf-4. *Nature Genetics*, *19*(4), 379–383.

Korinek, V., Barker, N., Morin, P. J., van Wichen, D., de Weger, R., Kinzler, K. W., … Clevers, H. (1997). Constitutive Transcriptional Activation by a b-Catenin–Tcf Complex in APC-/- Colon Carcinoma. *Science*, *275*, 1784–1787.

Kramps, T., Peter, O., Brunner, E., Nellen, D., Froesch, B., Chatterjee, S., … Basler, K. (2002). Wnt/Wingless signaling requires BCL9/legless-mediated recruitment of pygopus to the nuclear β-catenin-TCF complex. *Cell*, *109*(1), 47–60.

Kramps, T., Peter, O., Brunner, E., Nellen, D., Froesch, B., Chatterjee, S., & Murone, M. (2002). Wnt/Wingless Signaling Requires BCL9/Legless-Mediated Recruitment of Pygopus to the Nuclear β-Catenin-TCF Complex. *Cell*, *109*, 47–60.

Krieghoff, E., Behrens, J., & Mayr, B. (2006). Nucleo-cytoplasmic distribution of β-catenin is regulated by retention. *Journal of Cell Science*, *119*(7), 1453–1463.

Krishnamurthy, N., & Kurzrock, R. (2018). Targeting the Wnt/beta-catenin pathway in cancer: Update on effectors and inhibitors. *Cancer Treatment Reviews*, *62*, 50–60.

Kurayoshi, M., Yamamoto, H., Izumi, S., & Kikuchi, A. (2007). Post-translational palmitoylation and glycosylation of Wnt-5a are necessary for its signalling. *Biochemical Journal*, *402*(3), 515–523.

Lapébie, P., Gazave, E., Ereskovsky, A., Derelle, R., Bézac, C., Renard, E., … Borchiellini, C. (2009). WNT/β-Catenin Signalling and Epithelial Patterning in the Homoscleromorph Sponge Oscarella. *PLOS ONE*, *4*(6), e5823.

Lau, T., Chan, E., Callow, M., Waaler, J., Boggs, J., Blake, R. A., … Costa, M. (2013). A Novel Tankyrase Small-Molecule Inhibitor Suppresses APC Mutation-Driven Colorectal Tumor Growth. *Cancer Research*, *73*(10), 3132–3144.

Ledsgaard, L., Kilstrup, M., Karatt-Vellatt, A., McCafferty, J., & Laustsen, A. (2018). Basics of Antibody Phage Display Technology. *Toxins*, *10*(236).

Lee, C. S., Bishop, E. S., Zhang, R., Yu, X., Farina, E. M., Yan, S., … He, T.-C. (2017). Adenovirus-mediated gene delivery: Potential applications for gene and cell-based therapies in the new era of personalized medicine. *Genes & Diseases*, *4*(2), 43–63.

Lee, N.-K., Zhang, Y., Su, Y., Bidlingmaier, S., Sherbenou, D. W., Ha, K. D., & Liu, B. (2018). Cell-type specific potent Wnt signaling blockade by bispecific antibody. *Scientific Reports*, *8*(1), 766.

Levy, L., Wei, Y., Labalette, C., Wu, Y., Renard, C.-A., Buendia, M. A., & Neuveut, C. (2004). Acetylation of β-Catenin by p300 Regulates β-Catenin-Tcf4 Interaction. *Molecular and Cellular Biology*, *24*(8), 3404–3414.

Li, T. W. H., Peng, H., Yang, H., Kurniawidjaja, S., Panthaki, P., Zheng, Y., … Lu, S. C. (2014). S-Adenosylmethionine and Methylthioadenosine Inhibit -Catenin Signaling by Multiple Mechanisms in Liver and Colon Cancer. *Molecular Pharmacology*, *87*(1), 77–86.

Li, X.-Q., Yang, X.-L., Zhang, G., Wu, S.-P., Deng, X.-B., Xiao, S.-J., … Xiao, G.-H. (2013). Nuclear β-catenin accumulation is associated with increased expression of Nanog protein and predicts poor prognosis of non-small cell lung cancer. *Journal of Translational Medicine*, *11*(1), 114.

Li, Z., Krippendorff, B.-F., Sharma, S., Walz, A. C., Lavé, T., & Shah, D. K. (2016). Influence of molecular size on tissue distribution of antibody fragments. *MAbs*, *8*(1), 113–119.

Liikanen, I., Ta htinen, S., Guse, K., Gutmann, T., Savola, P., Oksanen, M., … Hemminki, A. (2016). Oncolytic Adenovirus Expressing Monoclonal Antibody Trastuzumab for Treatment of HER2-Positive Cancer. *Molecular Cancer Therapeutics*, *15*(9), 2259–2269.

Ling, X.-H., Chen, Z.-Y., Luo, H.-W., Liu, Z.-Z., Liang, Y.-K., Chen, G.-X., … Zhong, W.-D. (2016). BCL9, a coactivator for Wnt/β-catenin transcription, is targeted by miR-30c and is associated with prostate cancer progression. *Oncology Letters*, *11*(3), 2001–2008.

Liu, C., Li, Y., Semenov, M., Han, C., Baeg, G.-H., Tan, Y., … He, X. (2002). Control of β-Catenin Phosphorylation/Degradation by a Dual-Kinase Mechanism. *Cell*, *108*, 837–847.

Liu, F. (2005). Distinct roles for Xenopus Tcf/Lef genes in mediating specific responses to Wnt/β-catenin signalling in mesoderm development. *Development*, *132*(24), 5375–5385.

Liu, G., Lanham, C., Buchan, J. R., & Kaplan, M. E. (2017). High-throughput transformation of Saccharomyces cerevisiae using liquid handling robots. *PLOS ONE*, *12*(3).

Liu, W., Dong, X., Mai, M., Seelan, R. S., Taniguchi, K., Krishnadath, K. K., … Thibodeau, S. N. (2000). Mutations in AXIN2 cause colorectal cancer with defective mismatch repair by activating β-catenin/TCF signalling. *Nature Genetics*, *26*(2), 146–147.

Liu, Y., & Bodmer, W. F. (2006). Analysis of P53 mutations and their expression in 56 colorectal cancer cell lines. *Proceedings of the National Academy of Sciences*, *103*(4), 976–981. https://doi.org/10.1073/pnas.0510146103

Liu, Z., Chen, O., Wall, J. B. J., Zheng, M., Zhou, Y., Wang, L., … Liu, J. (2017). Systematic comparison of 2A peptides for cloning multi-genes in a polycistronic vector. *Scientific Reports*, *7*(1), 2193.

Loussouarn, M., Krieger-Liszkay, A., Svilar, L., Bily, A., Birtić, S., & Havaux, M. (2017). Carnosic Acid and Carnosol, Two Major Antioxidants of Rosemary, Act through Different Mechanisms. *Plant Physiology*, *175*(3), 1381–1394.

Lynch, H. T. (2003). Hereditary Colorectal Cancer. *The New England Journal of Medicine*, 348(10), 912-932.

Lyou, Y., Habowski, A. N., Chen, G. T., & Waterman, M. L. (2017). Inhibition of nuclear Wnt signalling: Challenges of an elusive target for cancer therapy. *British Journal of Pharmacology*, *174*(24), 4589–4599.

Maher, M. T., Flozak, A. S., Stocker, A. M., Chenn, A., & Gottardi, C. J. (2009). Activity of the β-catenin phosphodestruction complex at cell–cell contacts is enhanced by cadherin-based adhesion. *The Journal of Cell Biology*, *186*(2), 219–228.

Mani, M., Carrasco, D. E., Zhang, Y., Takada, K., Gatt, M. E., Dutta-Simmons, J., … Carrasco, D. R. (2009). BCL9 Promotes Tumor Progression by Conferring Enhanced Proliferative, Metastatic, and Angiogenic Properties to Cancer Cells. *Cancer Research*, *69*(19), 7577–7586.

Mann, B., Gelos, M., Siedow, A., Hanski, M. L., Gratchev, A., Ilyas, M., … Hanski, C. (1999). Target genes of β-catenin- T cell-factor/lymphoid-enhancer-factor signaling in human colorectal carcinomas. *Proceedings of the National Academy of Sciences*, *96*(4), 1603–1608.

Mao, J., Wang, J., Liu, B., Pan, W., Farr, G. H., Flynn, C., … Wu, D. (2001). Low-Density Lipoprotein Receptor-Related Protein-5 Binds to Axin and Regulates the Canonical Wnt Signaling Pathway. *Molecular Cell*, *7*(4), 801–809.

Marikawa, Y., & Elinson, R. P. (1998). β-TrCP is a negative regulator of the Wnt/β-catenin signaling pathway and dorsal axis formation in Xenopus embryos. *Mechanisms of Development*, 77, 75-80.

Marschall, A. L. J., & Dübel, S. (2016). Antibodies inside of a cell can change its outside: Can intrabodies provide a new therapeutic paradigm? *Computational and Structural Biotechnology Journal*, *14*, 304–308.

Masuda, M., Sawa, M., & Yamada, T. (2015). Therapeutic targets in the Wnt signaling pathway: Feasibility of targeting TNIK in colorectal cancer. *Pharmacology & Therapeutics*, *156*, 1–9.

Matsuo, Y., Asakawa, K., Toda, T., & Katayama, S. (2006). A Rapid Method for Protein Extraction from Fission Yeast. *Bioscience, Biotechnology, and Biochemistry*, *70*(8), 1992–1994.

Menon, M., Elliott, R., Bowers, L., Balan, N., Rafiq, R., Costa-Cabral, S., … Lord, C. J. (2019). A novel tankyrase inhibitor, MSC2504877, enhances the effects of clinical CDK4/6 inhibitors. *Scientific Reports*, *9*(1), 201.

Meran, L., Baulies, A., & Li, V. S. W. (2017). Intestinal Stem Cell Niche: The Extracellular Matrix and Cellular Components. *Stem Cells International*, *2017*.

Mikels, A. J., & Nusse, R. (2006). Wnts as ligands: Processing, secretion and reception. *Oncogene*, *25*(57), 7461–7468.

Miyagishi, M., Fujii, R., Hatta, M., Yoshida, E., Araya, N., Nagafuchi, A., … Fukamizu, A. (2000). Regulation of Lef-mediated Transcription and p53-dependent Pathway by Associating β-Catenin with CBP/p300. *Journal of Biological Chemistry*, *275*(45), 35170–35175.

Miyamoto, S., & Rosenberg, D. W. (2011). Role of Notch signaling in colon homeostasis and carcinogenesis. *Cancer Science*, *102*(11), 1938–1942.

Miyoshi, Y., Nagse, H., Ando, H., Horii, A., Ichii, S., Nakatsuru, S., … Nakamura, Y. (1992). Somatic mutations of the APC gene in colorectal tumors: Mutation cluster region in the APC gene. *Human Molecular Genetics*, *1*(4), 229–233.

Moor, A. E., Anderle, P., Cantù, C., Rodriguez, P., Wiedemann, N., Baruthio, F., … Aguet, M. (2015). BCL9/9L-β-catenin Signaling is Associated With Poor Outcome in Colorectal Cancer. *EBioMedicine*, *2*(12), 1932–1943.

Morin, P. J., Sparks, A. B., Korinek, V., Barker, N., Clevers, H., Vogelstein, B., & Kinzler, K. W. (1997). Activation of ß-Catenin–Tcf Signaling in Colon Cancer by Mutations in β-Catenin or APC. *Science*, *275*, 1787–1790.

Moullan, N., Mouchiroud, L., Wang, X., Ryu, D., Williams, E. G., Mottis, A., … Auwerx, J. (2015). Tetracyclines Disturb Mitochondrial Function across Eukaryotic Models: A Call for Caution in Biomedical Research. *Cell Reports*, *10*(10), 1681–1691.

Mouradov, D., Sloggett, C., Jorissen, R. N., Love, C. G., Li, S., Burgess, A. W., … Sieber, O. M. (2014). Colorectal Cancer Cell Lines Are Representative Models of the Main Molecular Subtypes of Primary Cancer. *Cancer Research*, *74*(12), 3238–3247.

Mukai, T., Fujita, S., & Morita, Y. (2019). Tankyrase (PARP5) Inhibition Induces Bone Loss through Accumulation of Its Substrate SH3BP2. *Cells*, *8*(2), 195.

Muyldermans, S., Atarhouch, T., Saldanha, J., Barbosa, J. A. R. G., & Hamers, R. (1994). Sequence and structure of VH domain from naturally occurring camel heavy chain immunoglobulins lacking light chains. *Protein Engineering*, *7*(9), 1129–1135.

Nagase, H., & Nakamura, Y. (1993). Mutations of theAPC adenomatous polyposis coli) gene. *Human Mutation*, *2*(6), 425–434.

Nagy, B., Tóth, L., Molnár, P., Méhes, G., Thurzó, L., Póka, R., & Hernádi, Z. (2017). Nuclear β-catenin positivity as a predictive marker of long-term survival in advanced epithelial ovarian cancer. *Pathology - Research and Practice*, *213*(8), 915–921.

Nakamura, T., Hamada, F., Ishidate, T., Anai, K., Kawahara, K., Toyoshima, K., & Akiyama, T. (1998). Axin, an inhibitor of the Wnt signalling pathway, interacts with β-catenin, GSK-3β and APC and reduces the β-catenin level. *Genes to Cells*, *3*(6), 395–403.

Nelson, A. L., & Reichert, J. M. (2009). Development trends for therapeutic antibody fragments. *Nature Biotechnology*, *27*(4), 331–337.

Newnham, L. E., Wright, M. J., Holdsworth, G., Kostarelos, K., Robinson, M. K., Rabbitts, T. H., & Lawson, A. D. (2015). Functional inhibition of β-catenin-mediated Wnt signaling by intracellular VHH antibodies. *MAbs*, *7*(1), 180–191.

Nickho, H., Younesi, V., Aghebati-Maleki, L., Motallebnezhad, M., Majidi Zolbanin, J., Movassagh Pour, A., & Yousefi, M. (2017). Developing and characterization of single chain variable fragment (scFv) antibody against frizzled 7 (Fzd7) receptor. *Bioengineered*, *8*(5), 501–510.

Novellasdemunt, L., Antas, P., & Li, V. S. W. (2015). Targeting Wnt signaling in colorectal cancer. A Review in the Theme: Cell Signaling: Proteins, Pathways and Mechanisms. *American Journal of Physiology-Cell Physiology*, *309*(8), C511–C521.

Nusse, R., & Varmus, H. E. (1982). Many tumors induced by the mouse mammary tumor virus contain a provirus integrated in the same region of the host genome. *Cell*, *31*(1), 99–109.

Omer, C., Miller, P., Diehl, R., & Kral, A. (1999). Identification of Tcf4 residues involved in high-affinity beta-catenin binding. *Biochemical and Biophysical Research Communications*, *256*, 584–590.

Orsulic, S., Huber, O., Aberle, H., Arnold, S., & Kemler, R. (1999). E-cadherin binding prevents β-catenin nuclear localization and β-catenin LEF1-mediated transactivation. *Journal of Cell Science*, *112*, 1237–1245.

Pan, P., Yu, J., & Wang, L.-S. (2018). Colon Cancer: What We Eat. *Surgical Oncology Clinics of North America*, *27*(2), 243–267.

Parker, D. S., Jemison, J., & Cadigan, K. M. (2002). Pygopus, a nuclear PHD-finger protein required for Wingless signaling in Drosophila. *Development*, *129*, 2565–2576.

Pérez-Martínez, D., Tanaka, T., & Rabbitts, T. H. (2010). Intracellular antibodies and cancer: New technologies offer therapeutic opportunities. *BioEssays*, *32*(7), 589–598.

Pinto, D., Gregorieff, A., Begthel, H., & Clevers, H. (2003). Canonical Wnt signals are essential for homeostasis of the intestinal epithelium. *Genes & Development*, *17*(14), 1709–1713.

Plumb, J. A., Milroy, R., & Kaye, S. B. (1989). Effects of the pH Dependence of 3-(4,5-Dimethylthiazol-2-yl)-2,5-diphenyl- tetrazolium Bromide-Formazan Absorption on Chemosensitivity Determined by a Novel Tetrazolium-based Assay. *Cancer Research*, *49*, 4435–4440.

Potten, C.S., Hume, W.J., Reid, P, Cairns (1978). The Segregation of DNA in Epithelial Stem Cells. Cell, 15, 899-906.

Potten, C. S., Kellett, M., Roberts, S. A., Rew, D. A., & Wilson, G. D. (1992). Measurement of in vivo proliferation in human colorectal mucosa using bromodeoxyuridine. *Gut*, *33*(1), 71–78. https://doi.org/10.1136/gut.33.1.71

Poy, F., Lepourcelet, M., Shivdasani, R. A., & Eck, M. J. (2001). Structure of a human Tcf4–β-catenin complex. *Nature Structural Biology*, *8*(12), 1053–1057.

Proba, K., Wörn, A., Honegger, A., & Plückthun, A. (1998). Antibody scFv Fragments Without Disulfide Bonds Made by Molecular Evolution. *J. Mol. Biol.*, *275*, 245–253.

Qi, Z., Li, Y., Zhao, B., Xu, C., Liu, Y., Li, H., … Chen, Y.-G. (2017). BMP restricts stemness of intestinal Lgr5+ stem cells by directly suppressing their signature genes. *Nature Communications*, *8*(1), 13824.

Qu, Y., Gharbi, N., Yuan, X., Olsen, J. R., Blicher, P., Dalhus, B., … Ke, X. (2016). Axitinib blocks Wnt/β-catenin signaling and directs asymmetric cell division in cancer. *Proceedings of the National Academy of Sciences*, *113*(33), 9339–9344.

Rask, K., Nilsson, A., Brännström, M., Carlsson, P., Hellberg, P., Janson, P.-O., … Sundfeldt, K. (2003). Wnt-signalling pathway in ovarian epithelial tumours: Increased expression of β-catenin and GSK3β. *British Journal of Cancer*, *89*(7), 1298–1304.

Rijsewijk, F., Wagenaar, E., Parren, P., & Weigel, D. (1987). The Drosophila Homolog of the Mouse Mammary Oncogene int-1 Is Identical to the Segment Polarity Gene wingless. *Cell*, *50*, 649–657.

Rodrigues, G. A., Shalaev, E., Karami, T. K., Cunningham, J., Slater, N. K. H., & Rivers, H. M. (2019). Pharmaceutical Development of AAV-Based Gene Therapy Products for the Eye. *Pharmaceutical Research*, *36*(2), 29.

Rosin-Arbesfeld, R., Cliffe, A., Brabletz, T., & Bienz, M. (2003). Nuclear export of the APC tumour suppressor controls b-catenin function in transcription. *The EMBO Journal*, *22*(5), 1101–1113.

Ross, S. L., Sherman, M., McElroy, P. L., Lofgren, J. A., Moody, G., Baeuerle, P. A., … Arvedson, T. (2017). Bispecific T cell engager (BiTE®) antibody constructs can mediate bystander tumor cell killing. *PLOS ONE*, *12*(8), e0183390.

Russell, L., & Peng, K.-W. (2018). The emerging role of oncolytic virus therapy against cancer. *Chinese Clinical Oncology*, *7*(2), 16–16.

Safdari, Y., Farajnia, S., Asgharzadeh, M., & Khalili, M. (2013). Antibody humanization methods – a review and update. *Biotechnology and Genetic Engineering Reviews*, *29*(2), 175–186.

Sakanaka, C. (2002). Phosphorylatipn and Regulation of β-Catenin by Casein Kinase ε. *J. Biochem.*, *132*(5), 697-703.

Sampietro, J., Dahlberg, C. L., Cho, U. S., Hinds, T. R., Kimelman, D., & Xu, W. (2006). Crystal Structure of a β-Catenin/BCL9/Tcf4 Complex. *Molecular Cell*, *24*(2), 293–300.

Sang, P., Zhang, M., Shi, Y., Li, C., Abdulkadir, S., Li, Q., … Cai, J. (2019). Inhibition of β-catenin/B cell lymphoma 9 protein−protein interaction using α-helix–mimicking sulfono-γ-AApeptide inhibitors. *Proceedings of the National Academy of Sciences*, *116*(22), 10757–10762.

Sanson, B., White, P., & Vincent, J.-P. (1996). Uncoupling cadherin-based adhesion from wingless signalling in Drosophila. *Nature*, *383*(6601), 627–630.

Sato, T., van Es, J. H., Snippert, H. J., Stange, D. E., Vries, R. G. van den Born, M., Barker, N., Shroyer, N., van de Wetering, M., Clevers H. (2011). Paneth cells constitite the niche for Lgr5 stem cells in intestinal crypts. *Nature*, 469, 415-419.

Scarborough, H. A., Helfrich, B. A., Casás-Selves, M., Schuller, A. G., Grosskurth, S. E., Kim, J., … DeGregori, J. (2017). AZ1366: An Inhibitor of Tankyrase and the Canonical Wnt Pathway that Limits the Persistence of Non–Small Cell Lung Cancer Cells Following EGFR Inhibition. *Clinical Cancer Research*, *23*(6), 1531–1541.

Schiestl, R. H., & Gietz, R. D. (1989). High efficiency transformation of intact yeast cells using single stranded nucleic acids as a carrier. *Current Genetics*, *16*(5–6), 339–346.

Schippers, K. J., & Nichols, S. A. (2018). Evidence of Signaling and Adhesion Roles for β-Catenin in the Sponge Ephydatia muelleri. *Molecular Biology and Evolution*, *35*(6), 1407–1421.

Schlange, T., Matsuda, Y., Lienhard, S., Huber, A., & Hynes, N. E. (2007). Autocrine WNT signaling contributes to breast cancer cell proliferation via the canonical WNT pathway and EGFR transactivation. *Breast Cancer Research*, *9*(5), R63.

Schmalhofer, O., Brabletz, S., & Brabletz, T. (2009). E-cadherin, β-catenin, and ZEB1 in malignant progression of cancer. *Cancer and Metastasis Reviews*, *28*(1–2), 151–166.

Schuijers, J., Junker, J. P., Mokry, M., Hatzis, P., Koo, B.-K., Sasselli, V., … Clevers, H. (2015). Ascl2 Acts as an R-spondin/Wnt-Responsive Switch to Control Stemness in Intestinal Crypts. *Cell Stem Cell*, *16*(2), 158–170.

Schwarz-Romond, T., Metcalfe, C., & Bienz, M. (2007). Dynamic recruitment of axin by Dishevelled protein assemblies. *Journal of Cell Science*, *120*(14), 2402–2412.

Scott, A. M., Wolchok, J. D., & Old, L. J. (2012). Antibody therapy of cancer. *Nature Reviews Cancer*, *12*(4), 278–287.

Scudiero, D., Shoemaker, R. H., Paul, K. D., Monks, A., Tierney, S., Nofziger, T. H., & Currens, M. J. (1988). Evaluation of a soluble Tetrazolium/Formazan assay for cell growth and drug sensitivity in culture using human and other tumor cell lines. *Cancer Research*, *48*, 4827–4833.

Sekiya, T., Nakamura, T., Kazuki, Y., Oshimura, M., Kohu, K., Tago, K., … Akiyama, T. (2002). Overexpression of Icat Induces G2 Arrest and Cell Death in Tumor Cell Mutants for Adenomatous Polyposis Coli, β-catenin, or Axin. *Cancer Research*, *62*, 3322–3326.

Seo, M. J., Jeong, K. J., Leysath, C. E., Ellington, A. D., Iverson, B. L., & Georgiou, G. (2009). Engineering antibody fragments to fold in the absence of disulfide bonds. *Protein Science*, *18*(2), 259–267.

Seymour, L. W., & Fisher, K. D. (2016). Oncolytic viruses: Finally delivering. *British Journal of Cancer*, *114*(4), 357–361.

Shan, J., Shi, D.-L., Wang, J., & Zheng, J. (2005). Identification of a Specific Inhibitor of the Dishevelled PDZ Domain. *Biochemistry*, *44*(47), 15495–15503.

Shapiro, L., & Weis, W. I. (2009). Structure and Biochemistry of Cadherins and Catenins. *Cold Spring Harbor Perspectives in Biology*, *1*(3), a003053–a003053.

Sharma, R. P., & Chopra, V. L. (1976). Effect of the wingless (wg1) mutation on wing and haltere development in Drosophila melanogaster. *Developmental Biology*, *48*(2), 461–465.

Shimoyama, Y., Nagafuchi, A., & Hirohashi, S. (1992). Cadherin Dysfunction in a Human Cancer Cell Line: Possible Involvement of Loss of a-Catenin Expression in Reduced Cell-Cell Adhesiveness. *Cancer Research*, *52*, 5770–5774.

Shin, S. H., Lim, D. Y., Reddy, K., Malakhova, M., Liu, F., Wang, T., … Dong, Z. (2017). A Small Molecule Inhibitor of the β-Catenin-TCF4 Interaction Suppresses Colorectal Cancer Growth In Vitro and In Vivo. *EBioMedicine*, *25*, 22–31.

Siegel, R. L., Miller, K. D., & Jemal, A. (2019). Cancer statistics, 2019. *CA Cancer Journal for Clinicians*, *69*(1), 7–34.

Singh, S., Kumar, N. K., Dwiwedi, P., Charan, J., Kaur, R., Sidhu, P., & Chugh, V. K. (2018). Monoclonal Antibodies: A Review. *Current Clinical Pharmacology*, *13*(2), 85–99.

Skehan, P., Storeng, R., Scudiero, D., Monks, A., McMahon, J., Vistica, D., … Boyd, M. R. (1990). New Colorimetric Cytotoxicity Assay for Anticancer-Drug Screening. *JNCI Journal of the National Cancer Institute*, *82*(13), 1107–1112.

Slastnikova, T. A., Ulasov, A. V., Rosenkranz, A. A., & Sobolev, A. S. (2018). Targeted Intracellular Delivery of Antibodies: The State of the Art. *Frontiers in Pharmacology*, *9*, 1208.

Smith, D. C., Rosen, L. S., Chugh, R., Goldman, W., Xu, L., & Kapoun, A. (2013). First-in-human evaluation of the human monoclonal antibody vantictumab (OMP-18R5; anti- Frizzled) targeting the WNT pathway in a phase I study for patients with advanced solid tumors. *Journal of Clinical Oncology*, *31*(no.15_suppl), 2540–2540.

Snyder, C., & Hampel, H. (2019). Hereditary Colorectal Cancer Syndromes. *Seminars in Oncology Nursing*, *35*(1), 58–78.

Sparks, A. B., Morin, P. J., Vogelstein, B., & Kinzler, K. W. (1998). *Mutational Analysis of the APC/ß-Catenin/Tcf Pathway in Colorectal Cancer*. *58*, 1130–1134.

Steinhart, Z., & Angers, S. (2018). Wnt signaling in development and tissue homeostasis. *Development*, *145*(11), dev146589.

Steinhusen, U., Badock, V., Bauer, A., Behrens, J., Wittman-Liebold, B., Dörken, B., & Bommert, K. (2000). Apoptosis-induced Cleavage of β-Catenin by Caspase-3 Results in Proteolytic Fragments with Reduced Transactivation Potential. *Journal of Biological Chemistry*, *275*(21), 16345–16353.

Stockinger, A., Eger, A., Wolf, J., Beug, H., & Foisner, R. (2001). E-cadherin regulates cell growth by modulating proliferation-dependent β-catenin transcriptional activity. *The Journal of Cell Biology*, *154*(6), 1185–1196.

Stoffel, E., Mukherjee, B., Raymond, V. M., Tayob, N., Kastrinos, F., Sparr, J., … Gruber, S. B. (2009). Calculation of Risk of Colorectal and Endometrial Cancer Among Patients With Lynch Syndrome. *Gastroenterology*, *137*(5), 1621–1627.

Strohl, W. R. (2018). Current progress in innovative engineered antibodies. *Protein & Cell*, *9*(1), 86–120.

Sun, Y., Kolligs, F. T., Hottiger, M. O., Mosavin, R., Fearon, E. R., & Nabel, G. J. (2000). Regulation of β-catenin transformation by the p300 transcriptional coactivator. *PNAS*, *97*(23), 12613–12618.

Sustmann, C., Flach, H., Ebert, H., Eastman, Q., & Grosschedl, R. (2008). Cell-Type-Specific Function of BCL9 Involves a Transcriptional Activation Domain That Synergizes with -Catenin. *Molecular and Cellular Biology*, *28*(10), 3526–3537.

Tago, K., Nakamura, T., Nishita, M., Hyodo, J., Nagai, S., Murata, Y., … Akiyama, T. (2000). Inhibition of Wnt signaling by ICAT, a novel β-catenin—Interacting protein. *Genes & Development*, *14*, 1741–1749.

Takada, K., Zhu, D., Bird, G. H., Sukhdeo, K., Zhao, J.-J., Mani, M., … Carrasco, D. R. (2012). Targeted Disruption of the BCL9/ β-Catenin Complex Inhibits Oncogenic Wnt Signaling. *Science Translational Medicine*, *4*(148), 148ra117.

Takemaru, K.-I., & Moon, R. T. (2000). The Transcriptional Coactivator CBP Interacts with β-Catenin to Activate Gene Expression. *The Journal of Cell Biology*, *149*(2), 249–254.

Talorete, T. P. N., Bouaziz, M., Sayadi, S., & Isoda, H. (2007). Influence of medium type and serum on MTT reduction by flavonoids in the absence of cells. *Cytotechnology*, *52*(3), 189–198.

Tamai, K., Semenov, M., Kato, Y., Spokony, R., Liu, C., Katsuyama, Y., … He, X. (2000). LDL-receptor-related proteins in Wnt signal transduction. *Nature*, *407*(6803), 530–535.

Tamai, K., Zeng, X., Liu, C., Zhang, X., Harada, Y., Chang, Z., & He, X. (2004). A Mechanism for Wnt Coreceptor Activation. *Molecular Cell*, *13*(1), 149–156.

Tanaka, N., Mashima, T., Mizutani, A., Sato, A., Aoyama, A., Gong, B., … Seimiya, H. (2017). APC Mutations as a Potential Biomarker for Sensitivity to Tankyrase Inhibitors in Colorectal Cancer. *Molecular Cancer Therapeutics*, *16*(4), 752–762.

Tanaka, & Rabbitts. (2010a). Interfering with RAS-effector protein interactions prevent RAS-dependent tumour initiation and causes stop-start control of cancer growth. *Oncogene*, *29*(45), 6064–6070.

Tanaka, T., Lobato, M. N., & Rabbitts, T. H. (2003). Single Domain Intracellular Antibodies: A Minimal Fragment For Direct In Vivo Selection of Antigen-specific Intrabodies. *Journal of Molecular Biology*, *331*(5), 1109–1120.

Tanaka, T., & Rabbitts, T. H. (2003). Intrabodies based on intracellular capture frameworks that bind the RAS protein with high affinity and impair oncogenic transformation. *The EMBO Journal*, *22*(5), 1025–1035.

Tanaka, T., & Rabbitts, T. H. (2008). Functional Intracellular Antibody Fragments Do Not Require Invariant Intra-domain Disulfide Bonds. *Journal of Molecular Biology*, *376*(3), 749–757.

Tanaka, T., & Rabbitts, T. H. (2010b). Protocol for the selection of single-domain antibody fragments by third generation intracellular antibody capture. *Nature Protocols*, *5*(1), 67–92.

Tanaka, Williams, & Rabbitts, T. H. (2007). Tumour prevention by a single antibody domain targeting the interaction of signal transduction proteins with RAS. *The EMBO Journal*, *26*(13), 3250–3259.

Tanoue, K., Rosewell Shaw, A., Watanabe, N., Porter, C., Rana, B., Gottschalk, S., … Suzuki, M. (2017). Armed Oncolytic Adenovirus–Expressing PD-L1 Mini-Body Enhances Antitumor Effects of Chimeric Antigen Receptor T Cells in Solid Tumors. *Cancer Research*, *77*(8), 2040–2051.

Tate, J. G., Bamford, S., Jubb, H. C., Sondka, Z., Beare, D. M., Bindal, N., … Forbes, S. A. (2019). COSMIC: The Catalogue Of Somatic Mutations In Cancer. *Nucleic Acids Research*, *47*(D1), D941–D947.

Tetsu, O., & McCormick, F. (1999). B-Catenin regulates expression of cyclin D1 in colon carcinoma cells. *Nature*, *398*, 422–426.

Thanikachalam, K., & Khan, G. (2019). Colorectal Cancer and Nutrition. *Nutrients*, *11*, 164.

The Cancer Genome Atlas Network. (2012). Comprehensive molecular characterization of human colon and rectal cancer. *Nature*, *487*(7407), 330–337.

Thorvaldsen, T. E. (2017). Targeting Tankyrase to Fight WNT-dependent Tumours. *Basic & Clinical Pharmacology & Toxicology*, *121*(2), 81–88.

Thrasivoulou, C., Millar, M., & Ahmed, A. (2013). Activation of Intracellular Calcium by Multiple Wnt Ligands and Translocation of β-Catenin into the Nucleus: A Convergent Model of Wnt/Ca^{2+} and Wnt/β-catenin Pathways. *Journal of Biological Chemistry*, *288*(50), 35651–35659.

Tsukiyama, T., Fukui, A., Terai, S., Fujioka, Y., Shinada, K., Takahashi, H., … Hatakeyama, S. (2015). Molecular Role of RNF43 in Canonical and Noncanonical Wnt Signaling. *Molecular and Cellular Biology*, *35*(11), 2007–2023.

Umar, S. (2010). Intestinal Stem Cells. *Current Gastroenterology Reports*, *12*(5), 340–348.

Upadhyay, G., Goessling, W., North, T. E., Xavier, R., Zon, L. I., & Yajnik, V. (2008). Molecular association between β-catenin degradation complex and Rac guanine exchange factor DOCK4 is essential for Wnt/β-catenin signaling. *Oncogene*, *27*(44), 5845–5855.

Valenta, T., Hausmann, G., & Basler, K. (2012). The many faces and functions of β-catenin: β-Catenin: a life by, beyond, and against the Wnt canon. *The EMBO Journal*, *31*(12), 2714–2736.

Vallner, J. J. (1977). Binding of Drugs by Albumin Plasma Protein. *Journal of Pharmaceutical Sciences*, *66*(4), 447–465.

van Amerongen, R., & Nusse, R. (2009). Towards an integrated view of Wnt signaling in development. *Development*, *136*(19), 3205–3214.

van de Wetering, M., Barker, N., Harkes, I. C., Hollestelle, A., Klijn, J. G. M., Clevers, H., & Schutte, M. (2001). Mutant E-cadherin Breast Cancer Cells Do Not Display Constitutive Wnt Signaling. *Cancer Research*, *61*, 278–284.

van Es, J. H., Haegebarth, A., Kujala, P., Itzkovitz, S., Koo, B.-K., Boj, S. F., … Clevers, H. (2012). A Critical Role for the Wnt Effector Tcf4 in Adult Intestinal Homeostatic Self-Renewal. *Molecular and Cellular Biology*, *32*(10), 1918–1927.

Vermeulen, L., De Sousa E Melo, F., van der Heijden, M., Cameron, K., de Jong, J. H., Borovski, T., … Medema, J. P. (2010). Wnt activity defines colon cancer stem cells and is regulated by the microenvironment. *Nature Cell Biology*, *12*(5), 468–476.

Vichai, V., & Kirtikara, K. (2006). Sulforhodamine B colorimetric assay for cytotoxicity screening. *Nature Protocols*, *1*(3), 1112–1116.

Visintin, M., Melchionna, T., Cannistraci, I., & Cattaneo, A. (2008). In vivo selection of intrabodies specifically targeting protein–protein interactions: A general platform for an "undruggable" class of disease targets. *Journal of Biotechnology*, *135*(1), 1–15.

von Kries, J. P., Winbeck, G., Asbrand, C., Schwarz-Romond, T., Sochnikova, N., Dell'Oro, A., … Birchmeier, W. (2000). Hot spots in β-catenin for interactions with LEF-1, conductin and APC. *Nature Structural Biology*, *7*(9), 800–807.

Vu, T., & Datta, P. (2017). Regulation of EMT in Colorectal Cancer: A Culprit in Metastasis. *Cancers*, *9*(171).

Waaler, J., Machon, O., Tumova, L., Dinh, H., Korinek, V., Wilson, S. R., … Krauss, S. (2012). A Novel Tankyrase Inhibitor Decreases Canonical Wnt Signaling in Colon Carcinoma Cells and Reduces Tumor Growth in Conditional APC Mutant Mice. *Cancer Research*, *72*(11), 2822–2832.

Wang, C., Dai, J., Sun, Z., Shi, C., Cao, H., Chen, X., … Han, X. (2015). Targeted inhibition of disheveled PDZ domain via NSC668036 depresses fibrotic process. *Experimental Cell Research*, *331*(1), 115–122.

Wang, L., Rambau, P. F., Kelemen, L. E., Anglesio, M. S., Leung, S., Talhouk, A., & Köbel, M. (2019). Nuclear β-catenin and CDX2 expression in ovarian endometrioid carcinoma identify patients with favourable outcome. *Histopathology*, *74*(3), 452–462.

Wang, R., & Brattain, M. G. (2007). The maximal size of protein to diffuse through the nuclear pore is larger than 60 kDa. *FEBS Letters*, *581*(17), 3164–3170.

Wei, W., Chua, M.-S., Grepper, S., & So, S. (2010). Small molecule antagonists of Tcf4/β-catenin complex inhibit the growth of HCC cells *in vitro* and *in vivo*. *International Journal of Cancer*, 126, 2426-2436.

Weiner, G. J. (2015). Building better monoclonal antibody-based therapeutics. *Nature Reviews Cancer*, *15*(6), 361–370.

Wells, J. A., & McClendon, C. L. (2007). Reaching for high-hanging fruit in drug discovery at protein–protein interfaces. *Nature*, *450*(7172), 1001–1009.

Wiese, K. E., Nusse, R., & van Amerongen, R. (2018). Wnt signalling: Conquering complexity. *Development*, *145*(12), dev165902.

Wilding, J. L., McGowan, S., Liu, Y., & Bodmer, W. F. (2010). Replication error deficient and proficient colorectal cancer gene expression differences caused by 3'UTR polyT sequence deletions. *Proceedings of the National Academy of Sciences*, *107*(49), 21058–21063.

Willert, K., & Nusse, R. (2012). Wnt Proteins. *Cold Spring Harbor Perspectives in Biology*, *4*(9), a007864.

Willis, T., Zalcberg, I., Coignet, L., Wlodarska, I., Stul, M., Jadayel, D., … Dyer, M. (1998). Molecular Cloning of Translocation t(1;14)(q21;q32) Defines a Novel Gene (BCL9) at Chromosome 1q21. *Blood*, *91*(6), 1873–1881.

Wisniewski, J. A., Yin, J., Teuscher, K. B., Zhang, M., & Ji, H. (2016). Structure-Based Design of 1,4-Dibenzoylpiperazines as β-Catenin/B-Cell Lymphoma 9 Protein–Protein Interaction Inhibitors. *ACS Medicinal Chemistry Letters*, *7*(5), 508–513.

Wold, W., & Toth, K. (2014). Adenovirus Vectors for Gene Therapy, Vaccination and Cancer Gene Therapy. *Current Gene Therapy*, *13*(6), 421–433.

Wong, S. C. C., Lo, E. S. F., Lee, K. C., Chan, J. K. C., & Hsiao, W. L. W. (2004). Prognostic and Diagnostic Significance of β-Catenin Nuclear Immunostaining in Colorectal Cancer. *Clinical Cancer Research*, *10*(4), 1401–1408.

Wörn, A., & Plückthun, A. (1998). An intrinsically stable antibody scFv fragment can tolerate the loss of both disulfide bonds and fold correctly. *FEBS Letters*, *427*(3), 357–361.

Xu, J. L., & Davis, M. M. (2000). Diversity in the CDR3 Region of VH Is Sufficient for Most Antibody Specificities. *Immunity*, *13*(1), 37–45.

Yadav, S., Verma, P. J., & Panda, D. (2014). C-Terminal Region of MAP7 Domain Containing Protein 3 (MAP7D3) Promotes Microtubule Polymerization by Binding at the C-Terminal Tail of Tubulin. *PLoS ONE*, *9*(6), e99539.

Yamagishi, H., Kuroda, H., Imai, Y., & Hiraishi, H. (2016). Molecular pathogenesis of sporadic colorectal cancers. *Chinese Journal of Cancer*, *35*(1), 4.

Yan, K. S., Janda, C. Y., Chang, J., Zheng, G. X. Y., Larkin, K. A., Luca, V. C., … Kuo, C. J. (2017). Non-equivalence of Wnt and R-spondin ligands during Lgr5+ intestinal stem-cell self-renewal. *Nature*, *545*(7653), 238–242.

Yanagawa, S., van Leeuwen, F., Wodarz, A., Klingensmith, J., & Nusse, R. (1995). The dishevelled protein is modified by wingless signaling in Drosophila. *Genes & Development*, *9*(9), 1087–1097.

Yang, K., Hitomi, M., & Stacey, D. W. (2006). Variations in cyclinD1 leves through the cell cycle determine the proliferative fate of a cell. *Cell Division*, *1*(1), 32.

Yang, X., Gu, Q., Lin, L., Li, S., Zhong, S., Li, Q., & Cui, Z. (2015). Nucleoporin 62-Like Protein Activates Canonical Wnt Signaling through Facilitating the Nuclear Import of β-Catenin in Zebrafish. *Molecular and Cellular Biology*, *35*(7), 1110–1124.

Yang, Y., & Mlodzik, M. (2015). Wnt-Frizzled/Planar Cell Polarity Signaling: Cellular Orientation by Facing the Wind (Wnt). *Annual Review of Cell and Developmental Biology*, *31*(1), 623–646.

Yasgar, A., Simeonov, A., & Coussens, N. P. (2016). AlphaScreen-Based Assays: Ultra-High-Throughput Screening for Small-Molecule Inhibitors of Challenging Enzymes and Protein-Protein Interactions. *Methods Mol Biol*, *1439*, 77–98.

Yokota, T., Milenic, D. E., Whitlow, M., & Schlom, J. (1992). Rapid Tumor Penetration of a Single-Chain Fv and Comparison with Other Immunoglobulin Forms. *Cancer Research*, *52*, 3402–3408.

Yokoya, F., Imamoto, N., Tachibana, T., & Yoneda, Y. (1999). β-Catenin Can Be Transported into the Nucleus in a Ran-unassisted Manner. *Molecular Biology of the Cell*, *10*, 13.

You, L., He, B., Xu, Z., Uematsu, K., Mazieres, J., Fujii, N., … Jablons, D. M. (2004). An Anti-Wnt-2 Monoclonal Antibody Induces Apoptosis in Malignant Melanoma Cells and Inhibits Tumor Growth. *Cancer Research*, *64*(15), 5385–5389.

Zeng, S., Seifert, A. M., Zhang, J. Q., Cavnar, M. J., Kim, T. S., Balachandran, V. P., … DeMatteo, R. P. (2017). Wnt/β-catenin Signaling Contributes to Tumor Malignancy and Is Targetable in Gastrointestinal Stromal Tumor. *Molecular Cancer Therapeutics*, *16*(9), 1954–1966.

Zeng, X., Tamai, K., Doble, B., Li, S., Huang, H., Habas, R., … He, X. (2005). A dual-kinase mechanism for Wnt co-receptor phosphorylation and activation. *Nature*, *438*(7069), 873–877.

Zhai, L., Chaturvedi, D., & Cumberledge, S. (2004). Drosophila Wnt-1 Undergoes a Hydrophobic Modification and Is Targeted to Lipid Rafts, a Process That Requires Porcupine. *Journal of Biological Chemistry*, *279*(32), 33220–33227.

Zhan, T., Rindtorff, N., & Boutros, M. (2017). Wnt signaling in cancer. *Oncogene*, *36*(11), 1461–1473.

Zhang, M., Wang, Z., Zhang, Y., Guo, W., & Ji, H. (2018). Structure-Based Optimization of Small-Molecule Inhibitors for the β-Catenin/B-Cell Lymphoma 9 Protein–Protein Interaction. *Journal of Medicinal Chemistry*, *61*(7), 2989–3007.

Zhang, S., Wang, Z., Shan, J., Yu, X., Li, L., Lei, R., … Wang, X. (2016). Nuclear expression and/or reduced membranous expression of β-catenin correlate with poor prognosis in colorectal carcinoma: A meta-analysis. *Medicine*, *95*(49), e5546.

Zhang, Y., Liu, B., Zhao, Q., Hou, T., & Huang, X. (2014). Nuclear localization of β-catenin is associated with poor survival and chemo-/radioresistance in human cervical squamous cell cancer. *Int J Clin Exp Pathol*, *7*(7), 3908–3917.

Zhao, Z.-M., Reynolds, A. B., & Gaucher, E. A. (2011). The evolutionary history of the catenin gene family during metazoan evolution. *BMC Evolutionary Biology*, *11*(1), 198.

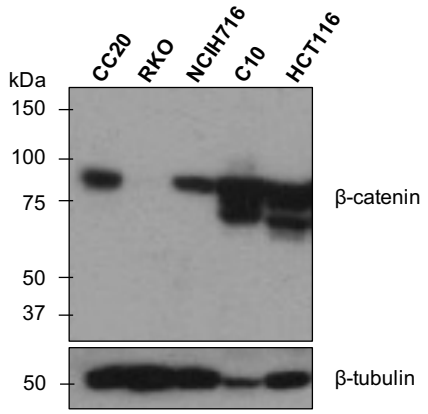
Zhong, Y., Katavolos, P., Nguyen, T., Lau, T., Boggs, J., Sambrone, A., … Schutten, M. (2015). Tankyrase Inhibition Causes Reversible Intestinal Toxicity in Mice with a Therapeutic Index < 1. *Toxicologic Pathology*, *44*(2), 267–278.

Appendices

Appendices

Appendix A - Supplementary data for Chapter 3

Appendix A.1 β-catenin expression in CC20, RKO, NCIH716, C10 and HCT116
Repeated β-catenin expression in panel of CRC cell lines assessed by Western Blot. β-tubulin is used as loading control. RKO cells are negative for β-catenin at protein expression level.

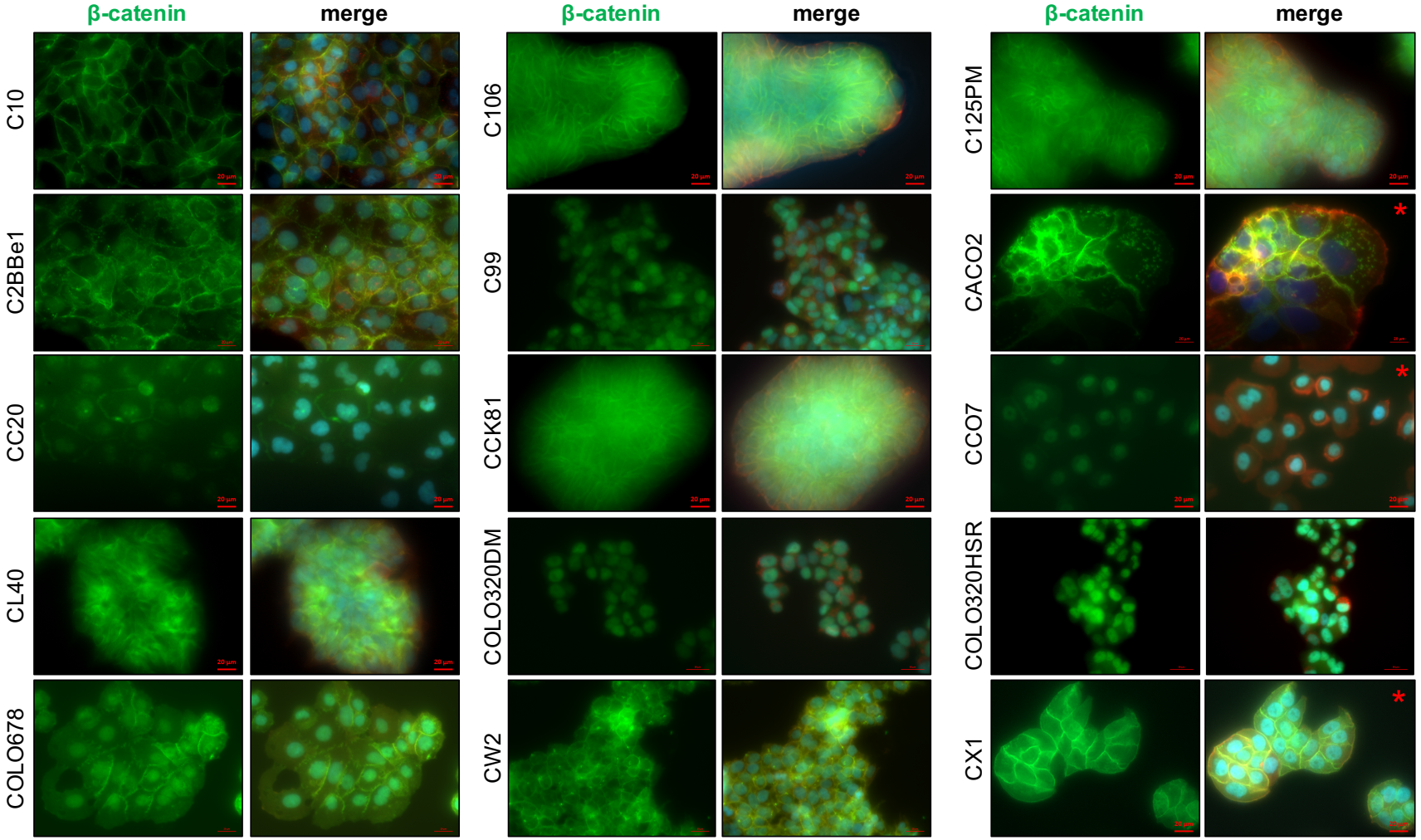


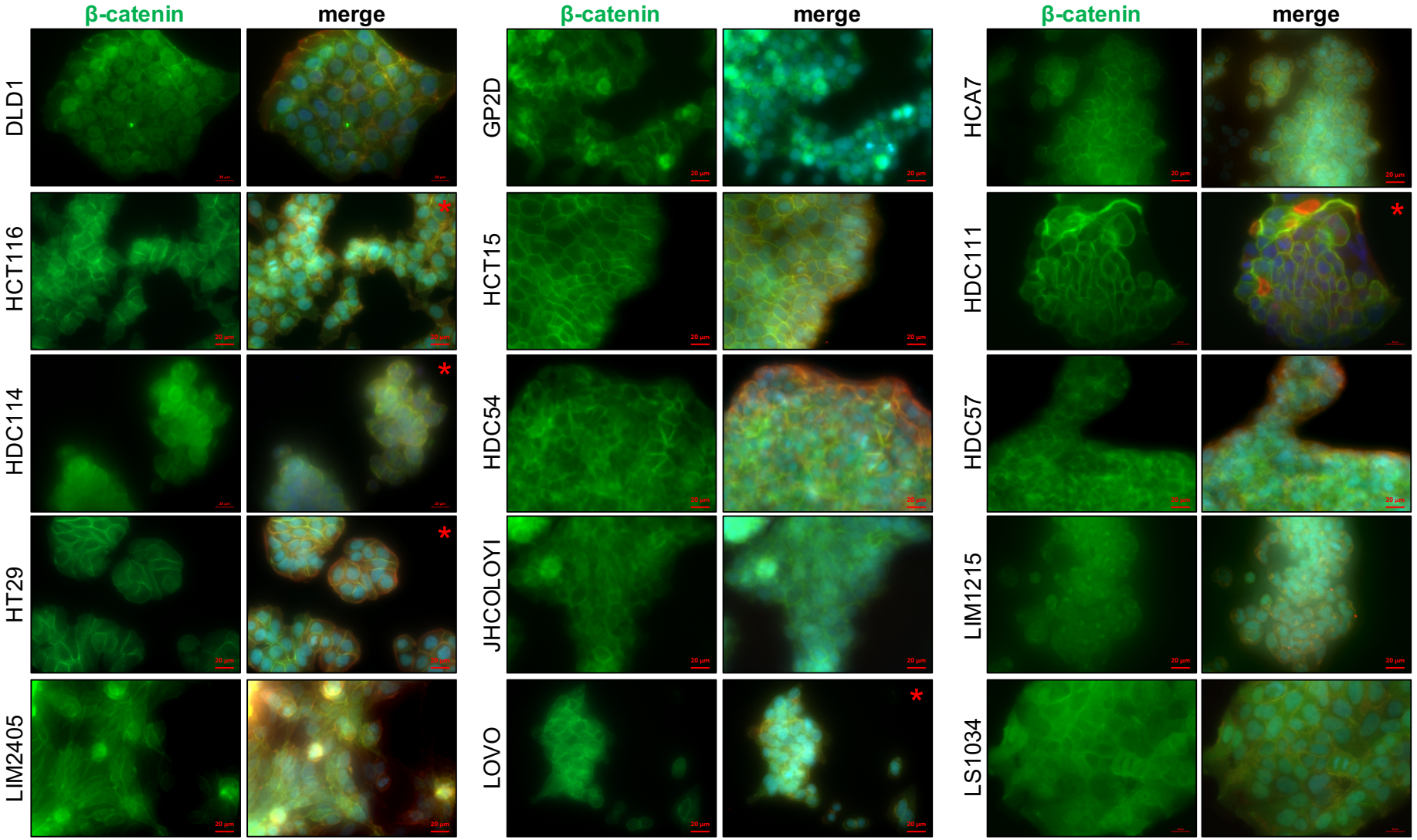
Appendix A.2 p53, BRAF and KRAS mutation statuses
List of known p53, BRAF and KRAS mutations in all stained CRC cell lines. 1 = wild-type, 2 = mutation in mutation cluster region (codon 12 & 13 for KRAS), 3 = mutation outside cluster region, ? = unknown. Replication error (RER) deficient: RER+, RER proficient: RER- (Mouradov et al., 2014; Wilding et al., 2010).

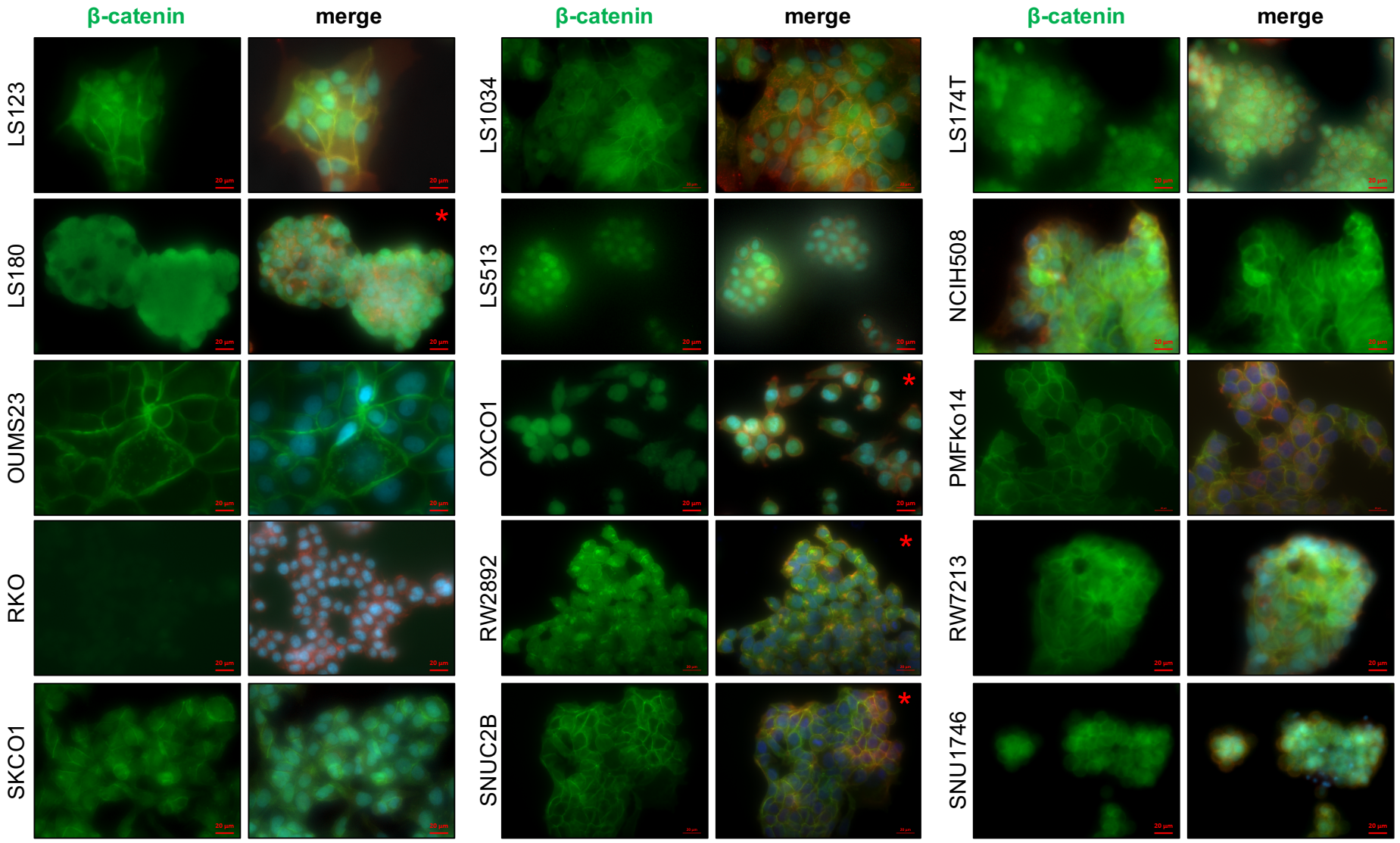
cell line	RER status	p53	KRAS codon 12&13	BRAF	cell line	RER status	p53	KRAS codon 12&13	BRAF
C10	-	2	1	1	LIM1215	+	1	1	1
C106	-	2	2	1	LIM2405	+	1	1	2
C125PM	-	2	3	1	LOVO	+	1	2	1
C2BBe1	-	2	1	1	LS1034	-	2	3	1
C99	-	1	1	1	LS123	-	2	2	1
CACO2	-	2	1	1	LS174T	+	1	2	3
CC07	-	2	2	1	LS180	+	1	2	3
CC20	-	2	1	1	LS513	-	1	2	3
CCK81	+	2	1	3	NCIH508	-	2	1	3
CL40	?	2	2	1	OUMS23	?	2	1	2
COLO320DM	-	2	1	1	OXCO1	-	2	?	2
COLO320HSR	-	2	1	1	PMFKo14	?	2	?	?
COLO678	-	1	2	1	RKO	+	1	1	2
CW2	+	1	3	1	RW2892	-	1	3	1
CX1	-	2	1	2	RW7213	-	1	2	1
DLD1	+	2	2	1	SKCO1	-	1	2	1
GP2D	+	1	2	3	SNU1746	+	1	2	?
HCA7	+	2	1	1	SNUC2B	+	2	2	1
HCT116	+	1	2	1	SW1417	-	2	1	2
HCT15	+	2	2	1	SW403	-	2	2	2
HDC111	-	?	2	1	SW48	+	1	1	1
HDC114	-	2	1	1	SW480	-	2	2	1
HDC54	-	2	1	1	SW620	-	2	2	1
HDC57	-	2	1	1	T84	-	?	2	1
HT29	-	2	1	2	VACO4A	-	2	2	1
JHCOLOY1	?	?	?	?	WIDR	-	2	1	2

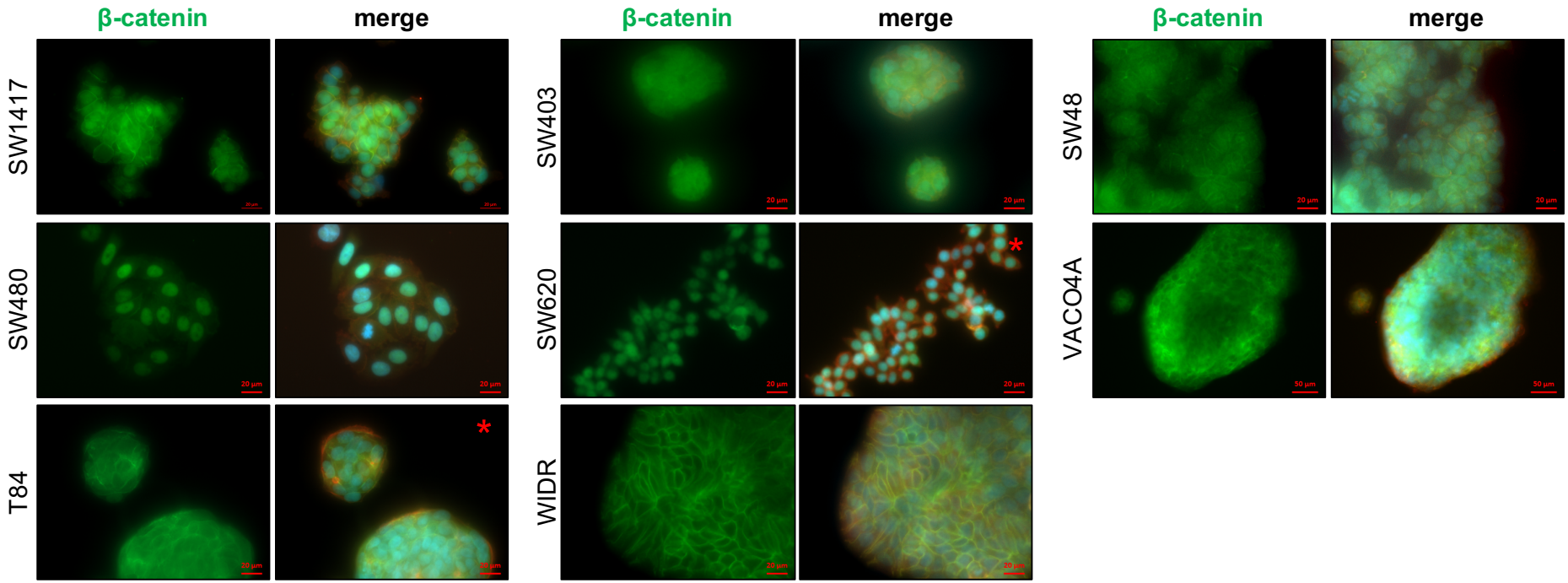
Appendix A.3 Immunofluorescence of β-catenin in a panel of 52 CRC cell lines

The images on the following four pages represent the β-catenin staining (green) and the overlay with DAPI (blue) and EpCAM (red) in a panel of CRC cell lines. Cell lines indicated with a " * " were stained for F-actin (red) instead of EpCAM. Images were taken using a Zeiss Observer z1 fluorescence microscope, magnification 20X, NA = 0.4, scale bars: 20 µm. Images on next four pages.




β-catenin
merge
DLD1
HCT116
HDC114
HT29
LIM2405
GP2D
HCT15
HDC54
JHCOLOYI
LOVO
HCA7
HDC111
HDC57
LIM1215
LS1034
*
20 µm


β-catenin
merge
LS123
LS180
OUMS23
RKO
SKCO1
LS1034
LS513
OXCO1
RW2892
SNUC2B
LS174T
NCIH508
PMFKo14
RW7213
SNU1746
*
20 μm


β-catenin
merge
SW1417
SW480
T84
SW403
SW620
WIDR
SW48
VACO4A
*
20 µm
50 µm

Appendix A.4 β-catenin localisation scores for 52 CRC cell lines by three assessors
β-catenin localisation scores: 1 = clearly membrane, 2 = cytoplasmic mostly membrane, 3 = cytoplasmic mostly nuclear, 4 = nuclear, 5 = non-quantifiable, 6= no staining. Cell lines with different scores in similar sub-groupings were categorised with the most common score (for example one score 2 and two scores 1 for the same cell line were categorised as 1).

Cell line	A 1	A 2	A 3	Cons.	Cell line	A1	A2	A3	Cons.
C10	1	1	1	1	LIM1215	3	5	3	3
C106	1	2	1	1	LIM2405	1	1	1	1
C125PM	1	2	1	1	LOVO	1	1	1	1
C2BBe1	1	1	1	1	LS1034	1	5	3	No
C99	4	3	3	3	LS123	1	5	1	1
CACO2	1	2	1	1	LS174T	4	4	4	4
CC20	3	4	5	No	LS180	5	5	5	5
CCK81	1	2	1	1	LS513	4	4	4	4
CCO7	4	4	4	4	NCIH508	1	2	2	2
CL40	1	1	2	1	OUMS23	1	1	1	1
COLO320DM	4	4	4	4	OXCO1	4	3	4	4
COLO320HSR	4	4	4	4	PMFKo14	1	1	2	1
COLO678	5	5	1	No	RKO	6	6	6	6
CW2	1	1	1	1	RW2892	3	5	5	5
CX1	1	1	1	1	RW7213	2	1	1	1
DLD1	5	5	1	No	SKCO1	1	1	2	1
GP2D	1	2	2	2	SNu1476	1	1	1	1
HCA7	1	1	1	1	SNUC2B	1	1	1	1
HCT116	1	2	2	2	SW1417	1	5	1	1
HCT15	1	1	1	1	SW403	2	5	5	5
HDC111	1	1	1	1	SW48	1	5	5	5
HDC114	1	2	2	2	SW480	4	4	4	4
HDC54	2	1	1	1	SW620	4	4	4	4
HDC57	1	1	1	1	T84	1	2	4	No
HT29	1	1	1	1	VACO4A	1	7	5	No
JHCOLOY1	1	2	1	1	WIDR	1	1	1	1

Appendix A.5 Correlation between β-catenin localisation and position of APC and β-catenin mutations
2 X 2 contingency tables for mutation location of APC and β-catenin for β-catenin localisation subgroups membrane (1) vs nuclear (4). *P*-values for Fisher's exact test for the 2 x 2 tables are given. MRC: Mutation Cluster Region of APC. Ex3: Exon3, hotspot mutation region of β-catenin.

Correlation of β-catenin cellular localisation with position of APC and β-catenin mutation – subgroups 1 vs 4

P=0.34	APC		
	WT	MT in MRC	MT out MRC
β-catenin localisation			
membrane	2	15	2
nuclear	2	3	1

P=0.166	β-catenin		
	WT	MT in Ex3	MT out Ex3
β-catenin localisation			
membrane	12	0	5
nuclear	3	1	1

Appendix A.6 List of significant differentially expressed probe-sets in correlation with β-catenin membrane (localisation scores 1 and 2) vs nuclear (localisation scores 3 and 4)
p-values uncorrected for multiple comparisons are given.

Gene Symbol	Membrane / low gene expression	Membrane / high gene expression	Nuclear / low gene expression	Nuclear / high gene expression	p-value
CDH1--1	0	24	5	2	0.0001235
CDH1--2	0	24	5	2	0.0001235
C1orf172	1	23	5	2	0.0006940
AP1M2--1	0	24	4	3	0.0011123
AKT3--2	24	0	3	4	0.0011123
nan--711	24	0	3	4	0.0011123
MAP7--3	0	24	4	3	0.0011123
RAB25	0	24	4	3	0.0011123
AP1M2--2	0	24	4	3	0.0011123
MAP7--1	0	24	4	3	0.0011123
MAP7--2	0	24	4	3	0.0011123
GRHL2	0	24	4	3	0.0011123
IRF6--1	0	24	4	3	0.0011123
LOC100506844	24	0	3	4	0.0011123
nan--5366	24	0	3	4	0.0011123
OVOL1--2	0	24	4	3	0.0011123
AIM1	0	24	4	3	0.0011123
SPINT1--1	0	24	4	3	0.0011123
MARVELD3--2	2	22	5	2	0.0022684
CD24--4	2	22	5	2	0.0022684
DAPK1--1	8	16	7	0	0.0024471
FHL1--1	23	1	3	4	0.0050673
ZEB1--3	23	1	3	4	0.0050673
DSC2--2	1	23	4	3	0.0050673
RTEL1 /// TNFRSF6B	23	1	3	4	0.0050673
S100A14	1	23	4	3	0.0050673
FHOD3	23	1	3	4	0.0050673
F11R--3	1	23	4	3	0.0050673
MAST4--6	23	1	3	4	0.0050673
KLF9--3	23	1	3	4	0.0050673
nan--23	23	1	3	4	0.0050673
TRAF3IP2--2	1	23	4	3	0.0050673
FHL1--2	21	3	2	5	0.0056358
FHL1--5	21	3	2	5	0.0056358
SPIN3--3	15	9	0	7	0.0067976

Gene Symbol	Membrane / low gene expression	Membrane / high gene expression	Nuclear / low gene expression	Nuclear / high gene expression	p-value
CLDN7	0	24	3	4	0.0077864
DNAJC18--2	24	0	4	3	0.0077864
SNAP25--2	24	0	4	3	0.0077864
C20orf194--2	24	0	4	3	0.0077864
EPCAM	0	24	3	4	0.0077864
TMEM136--2	24	0	4	3	0.0077864
BSPRY--2	0	24	3	4	0.0077864
C3orf55--2	24	0	4	3	0.0077864
C1orf106	0	24	3	4	0.0077864
TMEM125	0	24	3	4	0.0077864
DSC2--3	0	24	3	4	0.0077864
MEST	0	24	3	4	0.0077864
GALNT3--1	0	24	3	4	0.0077864
MSRB3--4	24	0	4	3	0.0077864
C3orf34--2	24	0	4	3	0.0077864
ESRP2--1	0	24	3	4	0.0077864
LLGL2--2	0	24	3	4	0.0077864
TPM1--6	0	24	3	4	0.0077864
SLC16A2	24	0	4	3	0.0077864
ST14--2	0	24	3	4	0.0077864
PKP3--2	0	24	3	4	0.0077864
CCDC46--2	24	0	4	3	0.0077864
LTBP2--2	24	0	4	3	0.0077864
OXR1--3	24	0	4	3	0.0077864
SMARCA4--9	0	24	3	4	0.0077864
TRPC1--1	24	0	4	3	0.0077864
MAL2	0	24	3	4	0.0077864
PKP3--1	0	24	3	4	0.0077864
CD24--2	4	20	5	2	0.0117851
CD24--3	4	20	5	2	0.0117851
CD24--5	4	20	5	2	0.0117851
CD24--6	4	20	5	2	0.0117851
ELMO3	2	22	4	3	0.0138140
CLDN11--1	22	2	3	4	0.0138140
nan--7559	2	22	4	3	0.0138140
DTX4	2	22	4	3	0.0138140
AKT3--1	22	2	3	4	0.0138140
CDH3	2	22	4	3	0.0138140
nan--5171	22	2	3	4	0.0138140
ELF3--1	2	22	4	3	0.0138140

Gene Symbol	Membrane / low gene expression	Membrane / high gene expression	Nuclear / low gene expression	Nuclear / high gene expression	p-value
BSPRY--1	2	22	4	3	0.0138140
STARD10--2	2	22	4	3	0.0138140
VIM--2	22	2	3	4	0.0138140
nan--5999	2	22	4	3	0.0138140
FXYD3--2	2	22	4	3	0.0138140
FBXO17 /// SARS2	22	2	3	4	0.0138140
TMEM136--1	22	2	3	4	0.0138140
HDGFRP3--6	19	5	2	5	0.0218476
ZNF331--1	19	5	2	5	0.0218476
EHF--5	5	19	5	2	0.0218476
POF1B--3	5	19	5	2	0.0218476
PARP9--2	11	13	7	0	0.0245013
SPIN3--4	12	12	0	7	0.0261395
MANSC1	1	23	3	4	0.0278086
MSRB3--3	23	1	4	3	0.0278086
MYO6--2	1	23	3	4	0.0278086
nan--8774	1	23	3	4	0.0278086
SLC22A4	23	1	4	3	0.0278086
TGM2--3	23	1	4	3	0.0278086
PPARG	1	23	3	4	0.0278086
SERPINE1--3	23	1	4	3	0.0278086
TGM2--2	23	1	4	3	0.0278086
DENND2D	1	23	3	4	0.0278086
AXL--1	23	1	4	3	0.0278086
MAPK13--1	1	23	3	4	0.0278086
SYBU	1	23	3	4	0.0278086
CHST11--2	23	1	4	3	0.0278086
CHST11--3	23	1	4	3	0.0278086
OSBPL6--1	23	1	4	3	0.0278086
ESRP2--2	1	23	3	4	0.0278086
TMC4	1	23	3	4	0.0278086
EPB41L5--3	1	23	3	4	0.0278086
HOXD10--2	23	1	4	3	0.0278086
S100P	1	23	3	4	0.0278086
RGS4--1	23	1	4	3	0.0278086
C16orf45--2	23	1	4	3	0.0278086
ESRP1--2	1	23	3	4	0.0278086
MAST4--2	23	1	4	3	0.0278086
ERCC1--1	23	1	4	3	0.0278086

Gene Symbol	Membrane / low gene expression	Membrane / high gene expression	Nuclear / low gene expression	Nuclear / high gene expression	p-value
AFAP1L2	23	1	4	3	0.0278086
SLC5A3--1	23	1	4	3	0.0278086
ITGA1--2	23	1	4	3	0.0278086
GNG11	23	1	4	3	0.0278086
MYO5C	1	23	3	4	0.0278086
ZFP36L2--2	8	16	6	1	0.0281151
POF1B--2	8	16	6	1	0.0281151
CLDN11--2	21	3	3	4	0.0292081
IWS1--1	3	21	4	3	0.0292081
FERMT2--1	21	3	3	4	0.0292081
ZNF518A--1	3	21	4	3	0.0292081
CD24--1	3	21	4	3	0.0292081
PRR15L	3	21	4	3	0.0292081
LOC283278	3	21	4	3	0.0292081
RBM47--2	3	21	4	3	0.0292081
NAV3--3	21	3	3	4	0.0292081
LMO7--4	3	21	4	3	0.0292081
FAM101B--1	21	3	3	4	0.0292081
WNT5A--2	21	3	3	4	0.0292081
EPB41L4B--1	3	21	4	3	0.0292081
PRR15	3	21	4	3	0.0292081
FA2H--1	3	21	4	3	0.0292081
ERBB3--3	3	21	4	3	0.0292081
NBEA--1	21	3	3	4	0.0292081
HEG1--1	21	3	3	4	0.0292081
ST14--1	3	21	4	3	0.0292081
ERBB3--5	3	21	4	3	0.0292081
IKBIP--1	21	3	3	4	0.0292081
MAST4--4	21	3	3	4	0.0292081
PRSS8	3	21	4	3	0.0292081
C20orf46	13	11	7	0	0.0331194
OASL--1	13	11	7	0	0.0331194
OASL--2	13	11	7	0	0.0331194
ERO1L--1	9	15	6	1	0.0372512
PROM1	9	15	6	1	0.0372512
HS6ST2--3	9	15	6	1	0.0372512
FAM126A--1	15	9	1	6	0.0372512
HS6ST2--2	9	15	6	1	0.0372512
APCDD1	15	9	1	6	0.0372512
SPANXC	24	0	5	2	0.0451612

Gene Symbol	Membrane / low gene expression	Membrane / high gene expression	Nuclear / low gene expression	Nuclear / high gene expression	p-value
TTC28--1	24	0	5	2	0.0451612
E2F7--2	24	0	5	2	0.0451612
KRT86 /// LOC100509764	24	0	5	2	0.0451612
NEGR1--2	24	0	5	2	0.0451612
C9orf9--1	24	0	5	2	0.0451612
KRT18	0	24	2	5	0.0451612
MEX3B	24	0	5	2	0.0451612
SNAP25--1	24	0	5	2	0.0451612
TTC28--2	24	0	5	2	0.0451612
CLDN4--2	0	24	2	5	0.0451612
IGFBP7--1	24	0	5	2	0.0451612
YPEL1--1	24	0	5	2	0.0451612
FGD1	24	0	5	2	0.0451612
CNKSR1	0	24	2	5	0.0451612
PDLIM3--1	24	0	5	2	0.0451612
SMARCA4--6	0	24	2	5	0.0451612
C14orf101--1	0	24	2	5	0.0451612
SSRP1--1	0	24	2	5	0.0451612
ZMAT3--2	24	0	5	2	0.0451612
DLX1--2	24	0	5	2	0.0451612
CORO2B	24	0	5	2	0.0451612
COLEC11	24	0	5	2	0.0451612
nan--7447	24	0	5	2	0.0451612
PHLDA2--2	0	24	2	5	0.0451612
CREB5--2	24	0	5	2	0.0451612
POLR2E--1	0	24	2	5	0.0451612
IGFBP7--2	24	0	5	2	0.0451612
DLL3--1	24	0	5	2	0.0451612
RAB20--1	0	24	2	5	0.0451612
MCOLN3--1	24	0	5	2	0.0451612
MGC16121--2	24	0	5	2	0.0451612
MPV17L2	0	24	2	5	0.0451612
SPANXA1 /// SPANXA2 /// SPANXB1 /// SPANXB2 /// SPANXC /// SPANXF1	24	0	5	2	0.0451612
MYO1D--2	0	24	2	5	0.0451612
SMARCA4--8	0	24	2	5	0.0451612
LOC644450--3	24	0	5	2	0.0451612
nan--5673	24	0	5	2	0.0451612

Gene Symbol	Membrane / low gene expression	Membrane / high gene expression	Nuclear / low gene expression	Nuclear / high gene expression	p-value
OSBPL6--3	24	0	5	2	0.0451612
SEC14L4--2	24	0	5	2	0.0451612
DKK3--1	24	0	5	2	0.0451612
ITGA1--1	24	0	5	2	0.0451612
SERPINB1--1	0	24	2	5	0.0451612
SNAP25--3	24	0	5	2	0.0451612
WNT5A--3	24	0	5	2	0.0451612
IRF6--3	0	24	2	5	0.0451612
F11R--1	0	24	2	5	0.0451612
CTSS--1	24	0	5	2	0.0451612
HOXC9	24	0	5	2	0.0451612
DRAP1	24	0	5	2	0.0451612
MYLIP--1	0	24	2	5	0.0451612
CCDC88A--2	24	0	5	2	0.0451612
CNTNAP1	24	0	5	2	0.0451612
KRT19--1	0	24	2	5	0.0451612
MARVELD2--1	0	24	2	5	0.0451612
C14orf132--1	24	0	5	2	0.0451612
WRB	0	24	2	5	0.0451612
nan--5442	24	0	5	2	0.0451612
RAB17	0	24	2	5	0.0451612
MYLIP--3	0	24	2	5	0.0451612
PAX8--1	24	0	5	2	0.0451612
LOC100505880	24	0	5	2	0.0451612
AK5--2	24	0	5	2	0.0451612
BCAP29--5	24	0	5	2	0.0451612
SRGN--3	24	0	5	2	0.0451612
ZEB1--2	24	0	5	2	0.0451612
NID1--2	24	0	5	2	0.0451612
AASS--1	24	0	5	2	0.0451612
ERCC1--2	24	0	5	2	0.0451612
SRGN--2	24	0	5	2	0.0451612
CDS1--3	0	24	2	5	0.0451612
RGS4--3	24	0	5	2	0.0451612
ANO4--2	24	0	5	2	0.0451612
HTATIP2--1	0	24	2	5	0.0451612
CCDC136--2	24	0	5	2	0.0451612
ACPL2--1	0	24	2	5	0.0451612
LDB2	24	0	5	2	0.0451612
FZD8--3	24	0	5	2	0.0451612

Gene Symbol	Membrane / low gene expression	Membrane / high gene expression	Nuclear / low gene expression	Nuclear / high gene expression	p-value
SRSF3--3	0	24	2	5	0.0451612
ALPK2	24	0	5	2	0.0451612
MGC16121 /// MIR503	24	0	5	2	0.0451612
GFPT2	24	0	5	2	0.0451612
REEP2	24	0	5	2	0.0451612
CDS1--1	0	24	2	5	0.0451612
TSPAN13	0	24	2	5	0.0451612
ANGPT1--3	24	0	5	2	0.0451612
CD40--1	24	0	5	2	0.0451612
NEGR1--4	24	0	5	2	0.0451612
LRRC8C--4	24	0	5	2	0.0451612
NRG1--1	24	0	5	2	0.0451612
KPNA5--1	24	0	5	2	0.0451612
MAP3K12--1	24	0	5	2	0.0451612
HOOK1--2	0	24	2	5	0.0451612
MGC16121--1	24	0	5	2	0.0451612
CYP24A1	24	0	5	2	0.0451612
SMARCA4--3	0	24	2	5	0.0451612
C3orf34--1	24	0	5	2	0.0451612
MYLIP--6	0	24	2	5	0.0451612
EDIL3--3	24	0	5	2	0.0451612
C20orf194--1	24	0	5	2	0.0451612
PADI2--2	24	0	5	2	0.0451612
SERINC2	0	24	2	5	0.0451612
TRPC1--2	24	0	5	2	0.0451612
RTKN--1	0	24	2	5	0.0451612
GPR64	24	0	5	2	0.0451612
CDS1--4	0	24	2	5	0.0451612
LSR	0	24	2	5	0.0451612
MSRB3--1	24	0	5	2	0.0451612
PLEK2	0	24	2	5	0.0451612
FOXG1--1	24	0	5	2	0.0451612
KRT8--1	0	24	2	5	0.0451612
AFF3--3	24	0	5	2	0.0451612
HP1BP3--4	0	24	2	5	0.0451612
GABRG2--2	24	0	5	2	0.0451612
ITGA10	24	0	5	2	0.0451612
ELK3--1	24	0	5	2	0.0451612
LAD1--2	0	24	2	5	0.0451612

Gene Symbol	Membrane / low gene expression	Membrane / high gene expression	Nuclear / low gene expression	Nuclear / high gene expression	p-value
AMOTL1--2	24	0	5	2	0.0451612
METTL9--3	24	0	5	2	0.0451612
DNER	24	0	5	2	0.0451612
MAD1L1	24	0	5	2	0.0451612
SLC12A4--2	24	0	5	2	0.0451612
RLBP1	24	0	5	2	0.0451612
HSPB3	24	0	5	2	0.0451612
RCAN3--2	0	24	2	5	0.0451612

Appendix A.7 List of significant differentially expressed probe-sets in correlation with β-catenin membrane (localisation scores 1) vs nuclear (localisation scores 4)
p-values uncorrected for multiple comparisons are given

Gene Symbol	Membrane / low gene expression	Membrane / high gene expression	Nuclear / low gene expression	Nuclear / high gene expression	p-value
CDH1--1	0	20	5	1	9.12E-05
CDH1--2	0	20	5	1	9.12E-05
MARVELD3--2	1	19	5	1	0.0005255
CD24--4	1	19	5	1	0.0005255
F11R--3	0	20	4	2	0.0010033
RAB25	0	20	4	2	0.0010033
nan--5366	20	0	2	4	0.0010033
AKT3--2	20	0	2	4	0.0010033
AP1M2--1	0	20	4	2	0.0010033
nan--711	20	0	2	4	0.0010033
RTEL1 /// TNFRSF6B	20	0	2	4	0.0010033
GRHL2	0	20	4	2	0.0010033
IRF6--1	0	20	4	2	0.0010033
AP1M2--2	0	20	4	2	0.0010033
AIM1	0	20	4	2	0.0010033
OVOL1--2	0	20	4	2	0.0010033
MAP7--3	0	20	4	2	0.0010033
LOC100506844	20	0	2	4	0.0010033
FHL1--1	20	0	2	4	0.0010033
MAP7--1	0	20	4	2	0.0010033
MAP7--2	0	20	4	2	0.0010033
SPINT1--1	0	20	4	2	0.0010033
FHL1--2	18	2	1	5	0.0017634
CD24--2	2	18	5	1	0.0017634
CD24--6	2	18	5	1	0.0017634
CD24--3	2	18	5	1	0.0017634
CD24--5	2	18	5	1	0.0017634
FHL1--5	18	2	1	5	0.0017634
ZFP36L2--2	6	14	6	0	0.0040133
DAPK1--1	6	14	6	0	0.0040133
nan--23	19	1	2	4	0.0046518
STARD10--2	1	19	4	2	0.0046518
TRAF3IP2--2	1	19	4	2	0.0046518
C1orf172	1	19	4	2	0.0046518
ZEB1--3	19	1	2	4	0.0046518

Gene Symbol	Membrane / low gene expression	Membrane / high gene expression	Nuclear / low gene expression	Nuclear / high gene expression	p-value
FBXO17 /// SARS2	19	1	2	4	0.0046518
DTX4	1	19	4	2	0.0046518
LOC283278	1	19	4	2	0.0046518
DSC2--2	1	19	4	2	0.0046518
CD24--1	1	19	4	2	0.0046518
S100A14	1	19	4	2	0.0046518
FXYD3--2	1	19	4	2	0.0046518
PKP3--2	0	20	3	3	0.0076923
PKP3--1	0	20	3	3	0.0076923
C3orf55--2	20	0	3	3	0.0076923
TPM1--6	0	20	3	3	0.0076923
MEST	0	20	3	3	0.0076923
BSPRY--2	0	20	3	3	0.0076923
ST14--2	0	20	3	3	0.0076923
GALNT3--1	0	20	3	3	0.0076923
MANSC1	0	20	3	3	0.0076923
LTBP2--2	20	0	3	3	0.0076923
TMEM125	0	20	3	3	0.0076923
C3orf34--2	20	0	3	3	0.0076923
C1orf106	0	20	3	3	0.0076923
CLDN7	0	20	3	3	0.0076923
TRPC1--1	20	0	3	3	0.0076923
OSBPL6--1	20	0	3	3	0.0076923
ESRP2--1	0	20	3	3	0.0076923
SLC16A2	20	0	3	3	0.0076923
S100P	0	20	3	3	0.0076923
MAL2	0	20	3	3	0.0076923
LLGL2--2	0	20	3	3	0.0076923
SNAP25--2	20	0	3	3	0.0076923
TMEM136--2	20	0	3	3	0.0076923
MSRB3--4	20	0	3	3	0.0076923
EPCAM	0	20	3	3	0.0076923
CCDC46--2	20	0	3	3	0.0076923
C20orf194--2	20	0	3	3	0.0076923
DSC2--3	0	20	3	3	0.0076923
DNAJC18--2	20	0	3	3	0.0076923
EHF--5	4	16	5	1	0.0096685
POF1B--3	4	16	5	1	0.0096685
TMEM136--1	18	2	2	4	0.0129044

Gene Symbol	Membrane / low gene expression	Membrane / high gene expression	Nuclear / low gene expression	Nuclear / high gene expression	p-value
CDH3	2	18	4	2	0.0129044
AKT3--1	18	2	2	4	0.0129044
FAM101B--1	18	2	2	4	0.0129044
LMO7--4	2	18	4	2	0.0129044
ERBB3--3	2	18	4	2	0.0129044
ERBB3--5	2	18	4	2	0.0129044
RBM47--2	2	18	4	2	0.0129044
FERMT2--1	18	2	2	4	0.0129044
nan--5171	18	2	2	4	0.0129044
PRR15	2	18	4	2	0.0129044
BSPRY--1	2	18	4	2	0.0129044
nan--7559	2	18	4	2	0.0129044
CLDN11--1	18	2	2	4	0.0129044
PTPRS--3	18	2	2	4	0.0129044
VIM--2	18	2	2	4	0.0129044
nan--5999	2	18	4	2	0.0129044
ELF3--1	2	18	4	2	0.0129044
ST14--1	2	18	4	2	0.0129044
ELMO3	2	18	4	2	0.0129044
PRR15L	2	18	4	2	0.0129044
POF1B--2	7	13	6	0	0.0149068
FAM126A--1	13	7	0	6	0.0149068
MUC20--2	5	15	5	1	0.0184250
MECOM--3	5	15	5	1	0.0184250
nan--7439	5	15	5	1	0.0184250
ELF3--2	5	15	5	1	0.0184250
MYO6--1	5	15	5	1	0.0184250
UBE2E2	11	9	0	6	0.0237458
HMGCS2--1	9	11	6	0	0.0237458
SPIN3--3	11	9	0	6	0.0237458
PARP9--2	9	11	6	0	0.0237458
SERPINE1--3	19	1	3	3	0.0277592
CCDC3	19	1	3	3	0.0277592
MYO6--2	1	19	3	3	0.0277592
TGM2--2	19	1	3	3	0.0277592
CHST11--2	19	1	3	3	0.0277592
KLF9--3	19	1	3	3	0.0277592
AXL--1	19	1	3	3	0.0277592
SIRPA--3	19	1	3	3	0.0277592
TGM2--3	19	1	3	3	0.0277592

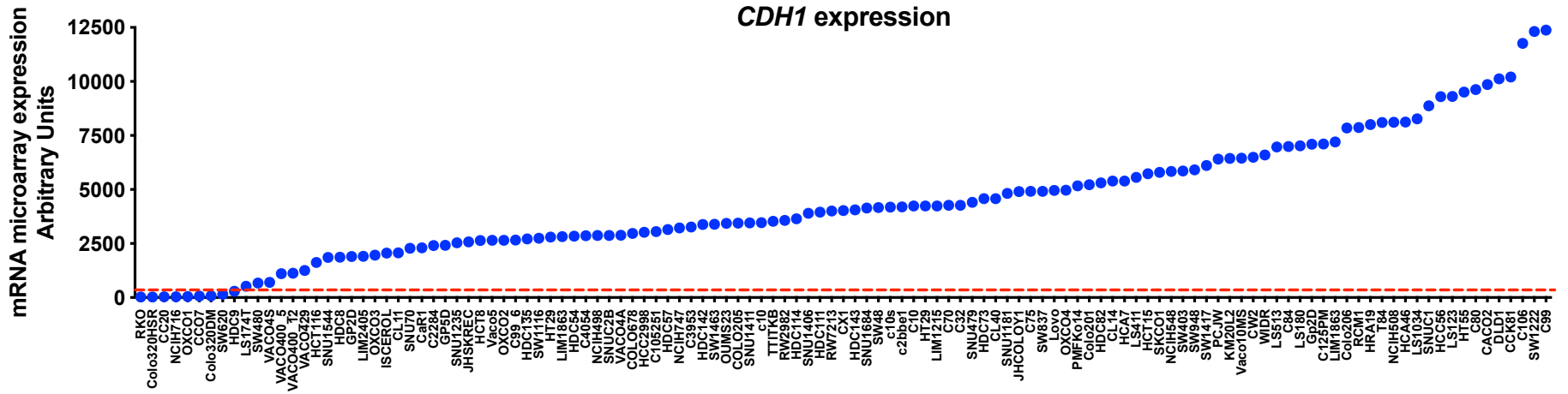
Gene Symbol	Membrane / low gene expression	Membrane / high gene expression	Nuclear / low gene expression	Nuclear / high gene expression	p-value
GNG11	19	1	3	3	0.0277592
MAPK13--1	1	19	3	3	0.0277592
SLC22A4	19	1	3	3	0.0277592
nan--5966	19	1	3	3	0.0277592
OGDHL	19	1	3	3	0.0277592
ANK3--1	1	19	3	3	0.0277592
POLR3G--2	19	1	3	3	0.0277592
FHOD3	19	1	3	3	0.0277592
MYO5C	1	19	3	3	0.0277592
MSRB3--3	19	1	3	3	0.0277592
SYBU	1	19	3	3	0.0277592
PPARG	1	19	3	3	0.0277592
ESRP1--2	1	19	3	3	0.0277592
RGS4--1	19	1	3	3	0.0277592
HOXD10--2	19	1	3	3	0.0277592
EPB41L5--3	1	19	3	3	0.0277592
MAGEE1--2	19	1	3	3	0.0277592
ESRP2--2	1	19	3	3	0.0277592
LGALS1	19	1	3	3	0.0277592
ERCC1--1	19	1	3	3	0.0277592
CHST11--3	19	1	3	3	0.0277592
ITGA1--2	19	1	3	3	0.0277592
DENND2D	1	19	3	3	0.0277592
C16orf45--2	19	1	3	3	0.0277592
MAST4--6	19	1	3	3	0.0277592
AFAP1L2	19	1	3	3	0.0277592
TJP2--1	1	19	3	3	0.0277592
TMC4	1	19	3	3	0.0277592
UBXN10--3	19	1	3	3	0.0277592
nan--8774	1	19	3	3	0.0277592
ANKRD22--1	3	17	4	2	0.0277592
FAM195B	17	3	2	4	0.0277592
MUC13--1	3	17	4	2	0.0277592
GJC1--1	17	3	2	4	0.0277592
WNT5A--2	17	3	2	4	0.0277592
HEG1--1	17	3	2	4	0.0277592
IKBIP--1	17	3	2	4	0.0277592
EPB41L4B--1	3	17	4	2	0.0277592
ITGB6--3	3	17	4	2	0.0277592
TSPAN8	3	17	4	2	0.0277592

Gene Symbol	Membrane / low gene expression	Membrane / high gene expression	Nuclear / low gene expression	Nuclear / high gene expression	p-value
AGR2--1	3	17	4	2	0.0277592
KRTCAP3	3	17	4	2	0.0277592
SH3YL1--2	3	17	4	2	0.0277592
MGAT4A--3	3	17	4	2	0.0277592
DOK4--2	3	17	4	2	0.0277592
MUC13--2	3	17	4	2	0.0277592
TMEM30B--1	3	17	4	2	0.0277592
HNMT--4	3	17	4	2	0.0277592
ZNF518A--1	3	17	4	2	0.0277592
NAV3--3	17	3	2	4	0.0277592
FA2H--1	3	17	4	2	0.0277592
MUC1--1	3	17	4	2	0.0277592
PCOLCE2	17	3	2	4	0.0277592
nan--10731	3	17	4	2	0.0277592
FSD1	17	3	2	4	0.0277592
NBEA--1	17	3	2	4	0.0277592
CLDN11--2	17	3	2	4	0.0277592
KIAA1543--1	3	17	4	2	0.0277592
ANKRD22--2	3	17	4	2	0.0277592
PRSS8	3	17	4	2	0.0277592
KLF5--2	0	20	2	4	0.0461538
LAPTM5--2	20	0	4	2	0.0461538
KLF5--1	0	20	2	4	0.0461538
VCAN--5	20	0	4	2	0.0461538
DLX1--2	20	0	4	2	0.0461538
COLEC11	20	0	4	2	0.0461538
CDKL3--2	20	0	4	2	0.0461538
GPR64	20	0	4	2	0.0461538
CNKSR1	0	20	2	4	0.0461538
RTKN--1	0	20	2	4	0.0461538
MGC16121--2	20	0	4	2	0.0461538
nan--5442	20	0	4	2	0.0461538
SMARCA4--3	0	20	2	4	0.0461538
LOC644450--3	20	0	4	2	0.0461538
FGD1	20	0	4	2	0.0461538
KRT8--1	0	20	2	4	0.0461538
MARVELD2--1	0	20	2	4	0.0461538
E2F7--2	20	0	4	2	0.0461538
OXR1--3	20	0	4	2	0.0461538
F11R--1	0	20	2	4	0.0461538

Gene Symbol	Membrane / low gene expression	Membrane / high gene expression	Nuclear / low gene expression	Nuclear / high gene expression	p-value
MYLIP--3	0	20	2	4	0.0461538
CDS1--1	0	20	2	4	0.0461538
HMGA2--6	20	0	4	2	0.0461538
ZEB1--2	20	0	4	2	0.0461538
TRPC1--2	20	0	4	2	0.0461538
MEX3B	20	0	4	2	0.0461538
nan--5981	20	0	4	2	0.0461538
LOC100505880	20	0	4	2	0.0461538
AMOTL1--2	20	0	4	2	0.0461538
SLC12A4--2	20	0	4	2	0.0461538
RGS4--3	20	0	4	2	0.0461538
MCOLN3--1	20	0	4	2	0.0461538
ITGA1--1	20	0	4	2	0.0461538
NEGR1--4	20	0	4	2	0.0461538
CNTNAP1	20	0	4	2	0.0461538
LAPTM5--1	20	0	4	2	0.0461538
SRGN--3	20	0	4	2	0.0461538
NEGR1--2	20	0	4	2	0.0461538
HOXC9	20	0	4	2	0.0461538
ELK3--1	20	0	4	2	0.0461538
LDB2	20	0	4	2	0.0461538
HTATIP2--1	0	20	2	4	0.0461538
REEP2	20	0	4	2	0.0461538
DLL3--1	20	0	4	2	0.0461538
C14orf132--1	20	0	4	2	0.0461538
MAP3K12--1	20	0	4	2	0.0461538
RAB17	0	20	2	4	0.0461538
nan--5673	20	0	4	2	0.0461538
GABRG2--2	20	0	4	2	0.0461538
ITGA10	20	0	4	2	0.0461538
HSPB3	20	0	4	2	0.0461538
NID1--2	20	0	4	2	0.0461538
AFF3--3	20	0	4	2	0.0461538
EPOR--6	20	0	4	2	0.0461538
C3orf34--1	20	0	4	2	0.0461538
TTC28--1	20	0	4	2	0.0461538
CYP24A1	20	0	4	2	0.0461538
WNT5A--3	20	0	4	2	0.0461538
SRGN--2	20	0	4	2	0.0461538
SH3BGRL2	0	20	2	4	0.0461538

Gene Symbol	Membrane / low gene expression	Membrane / high gene expression	Nuclear / low gene expression	Nuclear / high gene expression	p-value
HOOK1--2	0	20	2	4	0.0461538
nan--6417	20	0	4	2	0.0461538
C14orf101--1	0	20	2	4	0.0461538
RLBP1	20	0	4	2	0.0461538
MAD1L1	20	0	4	2	0.0461538
NRG1--1	20	0	4	2	0.0461538
EDIL3--3	20	0	4	2	0.0461538
C20orf194--1	20	0	4	2	0.0461538
SMARCA4--9	0	20	2	4	0.0461538
LSR	0	20	2	4	0.0461538
FOXG1--1	20	0	4	2	0.0461538
BCAP29--5	20	0	4	2	0.0461538
PLEK2	0	20	2	4	0.0461538
GFPT2	20	0	4	2	0.0461538
SNAP25--1	20	0	4	2	0.0461538
STX17--1	0	20	2	4	0.0461538
KPNA5--1	20	0	4	2	0.0461538
CD40--1	20	0	4	2	0.0461538
RAB20--1	0	20	2	4	0.0461538
ANGPT1--3	20	0	4	2	0.0461538
YPEL1--1	20	0	4	2	0.0461538
SMARCA4--6	0	20	2	4	0.0461538
PDLIM3--1	20	0	4	2	0.0461538
CCDC136--2	20	0	4	2	0.0461538
CLDN4--2	0	20	2	4	0.0461538
MYLIP--1	0	20	2	4	0.0461538
KRT19--1	0	20	2	4	0.0461538
ANO4--2	20	0	4	2	0.0461538
TSPAN13	0	20	2	4	0.0461538
SMARCA4--8	0	20	2	4	0.0461538
SPANXC	20	0	4	2	0.0461538
IRF6--3	0	20	2	4	0.0461538
nan--7447	20	0	4	2	0.0461538
IGFBP7--2	20	0	4	2	0.0461538
IGFBP7--1	20	0	4	2	0.0461538
SEC14L4--2	20	0	4	2	0.0461538
PADI2--2	20	0	4	2	0.0461538
OSBPL6--3	20	0	4	2	0.0461538
C9orf64--2	0	20	2	4	0.0461538
ERCC1--2	20	0	4	2	0.0461538

Gene Symbol	Membrane / low gene expression	Membrane / high gene expression	Nuclear / low gene expression	Nuclear / high gene expression	p-value
ALPK2	20	0	4	2	0.0461538
MSRB3--1	20	0	4	2	0.0461538
DNER	20	0	4	2	0.0461538
MGC16121 /// MIR503	20	0	4	2	0.0461538
MYLIP--6	0	20	2	4	0.0461538
KRT18	0	20	2	4	0.0461538
C9orf9--1	20	0	4	2	0.0461538
LAD1--2	0	20	2	4	0.0461538
SPANXA1 /// SPANXA2 /// SPANXB1 /// SPANXB2 /// SPANXC /// SPANXF1	20	0	4	2	0.0461538
AASS--1	20	0	4	2	0.0461538
FZD8--3	20	0	4	2	0.0461538
AK5--2	20	0	4	2	0.0461538
CCDC88A--2	20	0	4	2	0.0461538
TTC28--2	20	0	4	2	0.0461538
MGC16121--1	20	0	4	2	0.0461538
KRT86 /// LOC100509764	20	0	4	2	0.0461538
DKK3--1	20	0	4	2	0.0461538
SNAP25--3	20	0	4	2	0.0461538
MYO1D--2	0	20	2	4	0.0461538
CDS1--4	0	20	2	4	0.0461538
LRRC8C--4	20	0	4	2	0.0461538
CREB5--2	20	0	4	2	0.0461538
METTL9--3	20	0	4	2	0.0461538
CDS1--3	0	20	2	4	0.0461538
SERPINB1--1	0	20	2	4	0.0461538
DRAP1	20	0	4	2	0.0461538
PAX8--1	20	0	4	2	0.0461538
ACPL2--1	0	20	2	4	0.0461538
SERINC2	0	20	2	4	0.0461538
CORO2B	20	0	4	2	0.0461538



Appendix A.8 CDH1 microarray expression data

CDH1 expression in a panel of CRC cell lines ranked by increasing expression. Red line indicates the arbitrary microarray expression unit 200. This is generally considered as low in our lab (Haoyu Liu, DPhil Thesis, 2017, Bodmer Lab). EMT cell lines, such as COLO320HSR and OXCO1 cells, express low *CDH1* message.

Appendix A.9 EMT expression markers in RKO, OXCO1, SW480, SW620, LS174T and LS180 cell lines

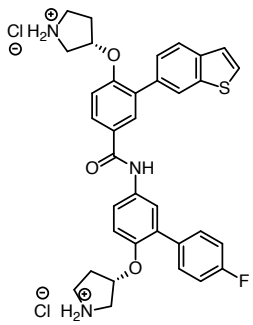
EMT associated gene expression levels in typical EMT cell lines (RKO and OXCO1), "borderline EMT" cell lines (SW480 and SW620) and non-EMT cell lines (LS174T and LS180). Values were obtained from the Affymetrix U133+2 microarray data.

Gene	EMT		"borderline EMT"		Non-EMT	
	RKO	OXCO1	SW480	SW620	LS174T	LS180
E-cadherin (*CDH1*)	25	50	673	158	529	6753
Claudin7 (*CLDN7*)	63	186	1472	77	2608	2559
Claudin3 (*CLDN3*)	122	753	305	220	2768	1903
ZEB1	1177	401	131	188	7	8
Vimentin (*VIM*)	157	3718	1556	1867	31	40

Appendix B - Supplementary data for Chapter 4

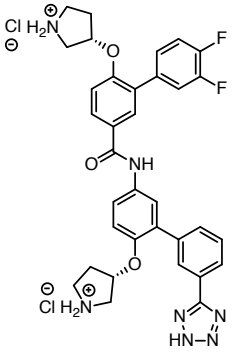
Appendix B.1 Chemical structures of β-catenin/BCL9 inhibitors

Chemical structures of ZYQ-174, ZYQ-2-165, JW-02-80 and JW-1-78. Publication references are given below each structure. Figure obtained by Dr Haitao Ji, with permission to publish.



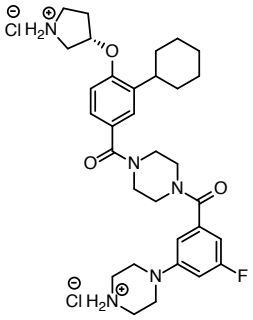
ZYQ-1-74

J. Med. Chem. 2018, 61, 2989−3007



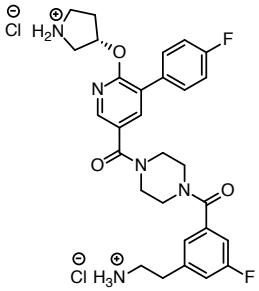
ZYQ-2-165

J. Med. Chem. 2018, 61, 2989−3007



JW-02-80

ACS Med. Chem. Lett. 2016, 7, 508−513



JW-1-78

ACS Med. Chem. Lett. 2016, 7, 508−513

Appendix C - Supplementary data for Chapter 5

Appendix C.1 Bait vectors sequencing results
pBTM116-D1, pBTM116-D2, pBTM116-D3 and pBTM116-D4 vectors were sequenced using the pBTM116_F_seq primer. pBTM116-D4 was also sequenced using the pBTM116_R_seq primer and reverse complement sequence is given as well. The restriction sites EcoRI (GAATTC) and SalI (GTCGAC) are highlighted in light blue. β-catenin domains of interest are marked in green. Stop codon in red. Appendix is two pages long.

pBTM116-D1: Forward sequencing

CAAGCCGAAGTTTAAACCAATTTGTCGTAGATCTTCGTCAGCAGAGCTTCACCATTGAAGGGCTGGCGG
TTGGGGTTATTCGCAACGGCGACTGGCTGGAATTCGCTGAACCATCACAGATGCTGAAACATGCAGTT
GTAAACTTGATTAACTATCAAGATGATGCAGAACTTGCCACACGTGCAATCCCTGAACTGACAAAACTG
CTAAATGACGAGGACCAGGTGGTGGTTAATAAGGCTGCAGTTATGGTCCATCAGCTTTCTAAAAAGGAA
GCTTCCAGACACGCTATCATGTGAGTCGACCTGCAGCCAAGCTAATTCCGGGCGAATTTCTTATGATTT
ATGATTTTTATTATTAAATAAGTTATAAAAAAAAATAAGTGTATACAAATTTTAAAGTGACTCTTAGGTTTTA
AAACGAAAATTCTTATTCTTGAGTAACTCTTTCCTGTAGGTCAGGTTGCTTTCTCAGGTATAGCATGAGG
TCGCTCTTATTGACCACACCTCTACCGGCATGCCGGCAAGTGCACAAACAATACTTAAATAAATACTACT
CAGTAATAACCTATTTCTTAGCATTTTTGACGAAATTTGCTATTTTGTTAGAGTCTTTTACACCATTTGTCT
CCACACCTCCGCTTACATCAACACCAATAACGCCATTTAATCTAAGCGCATCACCAACATTTTCT

pBTM116-D2: Forward sequencing

TTGCCCAAGTTTAAAACAAATTTTTCGTAGATCTTCGTCAGCAGAGCTTCACCATTGAAGGGCTGGCGG
TTGGGGTTATTCGCAACGGCGACTGGCTGGAATTCAATGTTAAATTCTTGGCTATTACGACAGACTGCC
TTCAAATTTTAGCTTATGGCAACCAAGAAAGCAAGCTCATCATACTGGCTAGTGGTGGACCCCAAGCTT
TAGTAAATATAATGAGGACCTATACTTACGAAAAACTACTGTGGACCACAAGCAGAGTGCTGAAGGTGC
TATCTGTCTGCTCTAGTAATAAGCCGGCTATTGTAGAAGCTTGAGTCGACCTGCAGCCAAGCTAATTCC
GGGCGAATTTCTTATGATTTATGATTTTTATTATTAAATAAGTTATAAAAAAAAATAAGTGTATACAAATTTT
AAAGTGACTCTTAGGTTTTAAAACGAAAATTCTTATTCTTGAGTAACTCTTTCCTGTAGGTCAGGTTGCTT
TCTCAGGTATAGCATGAGGTCGCTCTTATTGACCACACCTCTACCGGCATGCCGGCAAGTGCACAAAC
AATACTTAAATAAATACTACTCAGTAATAACCTATTTCTTAGCATTTTTGACGAAATTTGCTATTTTGTTAG
AGTCTTTTACACCATTTGTCTCCACACCTCCGCTTACATCAACACCAATAACGCCATTTAATCTAAG

pBTM116-D3: Forward sequencing

AGAAGTTTTAAACCAATTGTCGTAGATCTTCGTCAGCAGAGCTTCACCATTGAAGGGCTGGCGGTTGGG
GTTATTCGCAACGGCGACTGGCTGGAATTCCTTTCTAACCTCACTTGCAATAATTATAAGAACAAGATGA
TGGTCTGCCAAGTGGGTGGTATAGAGGCTCTTGTGCGTACTGTCCTTCGGGCTGGTGACAGGGAAGAC
ATCACTGAGCCTGCCATCTGTGCTCTTCGTCATCTGACCAGCCGACACCAAGAAGCAGAGATGGCCCA
GAATGCAGTTCGCCTTCACTGAGTCGACCTGCAGCCAAGCTAATTCCGGGCGAATTTCTTATGATTTAT
GATTTTTATTATTAAATAAGTTATAAAAAAAAATAAGTGTATACAAATTTTAAAGTGACTCTTAGGTTTTAAA
ACGAAAATTCTTATTCTTGAGTAACTCTTTCCTGTAGGTCAGGTTGCTTTCTCAGGTATAGCATGAGGTC
GCTCTTATTGACCACACCTCTACCGGCATGCCGGCAAGTGCACAAACAATACTTAAATAAATACTACTCA
GTAATAACCTATTTCTTAGCATTTTTGACGAAATTTGCTATTTTGTTAGAGTCTTTTACACCATTTGTCTCC
ACACCTCCGCTTACATCAACACCAATAACGCCATTTAATCTAAGCGCATCACCAACATTTTCTGGCGTCA
GTCCACCAGCTAACATAAAATGTAAGCTTTCGGGGCTCTCTTGCCTTCCAACCCAGTCAGAAATCGAGT
TCCA

pBTM116-D4: Forward sequencing

TTTTCCCGAGTTTTAACCATTTGTCGTAGATCTTCGTCAGCAGAGCTTCACCATTGAAGGGCTGGCGGT
TGGGGTTATTCGCAACGGCGACTGGCTGGAATTCCACTGGCCTCTGATAAAGGCTACTGTTGGATTGA
TTCGAAATCTTGCCCTTTGTCCCGCAAATCATGCACCTTTGCGTGAGCAGGGTGCCATTCCACGACTAG
TTCAGTTGCTTGTTCGTGCACATCAGGATACCCAGCGCCGTACGTCCATGGGTGGGACACAGCAGCAA
TTTGTGGAGGGGGTCCGCATGGAAGAAATAGTTGAAGGTTGTACCGGAGCCCTTCACATCCTAGCTCG
GGATGTTCACAACCGAATTGTTATCAGAGGACTAAATACCATTCCATTGTTTGTGCAGCTGCTTTATTCT
CCCATTGAAAACATCCAAAGAGTAGCTGCAGGGGTCCTCTGTGAACTTGCTCAGGACAAGGAAGCTGC
AGAAGCTATTGAAGCTGAGGGAGCCACAGCTCCTCTGACAGAGTTACTTCACTCTAGGAATGAAGGTG
TGGCGACATATGCAGCTGCTGTTTTGTTCCGAATGTCTGAGGACAAGCCACAAGATTACAAGAAACGGC
TTTCAGTTGAGCTGACCAGCTCTCTCTTCAGAACAGAGCCAATGGCTTGGAATGAGACTGCTGATCTTG
GACTTGATATTGGTGCCCAGGGAGAACCCCTTGGATATCGCCAGGATGATCCTAGCTATCGTTCTTTTC
ACTCTGGTGGATATGGCCAGGATGCCTTGGGTATGGACCCCA

Reverse sequencing

TAAAGCACCTTTGAACTACAGGAAGAGTTACTCAAGAATAAGAATTTTCGTTTTAAAACCTAAGAGTCAC
TTTAAAATTTGTATACACTTATTTTTTTTATAACTTATTTAATAATAAAAATCATAAATCATAAGAAATTCGC
CCGGAATTAGCTTGGCTGCAGGTCGACTTACAGGTCAGTATCAAACCAGGCCAGCTGATTGCTGTCAC
CTGGAGGCAGCCCATCCATGAGGTCCTGGGCATGCCCCAGATCTGGCAGCCCATCAACTGGATAGTC
AGCACCAGGGTGGTGGCCACCCATCTCATGTTCCATCATGGGGTCCATACCCAAGGCATCCTGGCCAT
ATCCACCAGAGTGAAAAGAACGATAGCTAGGATCATCCTGGCGATATCCAAGGGGTTCTCCCTGGGCA
CCAATATCAAGTCCAAGATCAGCAGTCTCATTCCAAGCCATTGGCTCTGTTCTGAAGAGAGAGCTGGTC
AGCTCAACTGAAAGCCGTTTCTTGTAATCTTGTGGCTTGTCCTCAGACATTCGGAACAAAACAGCAGCT
GCATATGTCGCCACACCTTCATTCCTAGAGTGAAGTAACTCTGTCAGAGGAGCTGTGGCTCCCTCAGCT
TCAATAGCTTCTGCAGCTTCCTTGTCCTGAGCAAGTTCACAGAGGACCCCTGCAGCTACTCTTTGGATG
TTTTCAATGGGAGAATAAAGCAGCTGCACAAACAATGGAATGGTATTTAGTCCTCTGATAACAATTCGGT
TGTGAACATCCCGAGCTAGGATGTGAAAGGGCTCCGGTACAACCTTT

pBTM116-D4: Reverse complement

AAAGGTTGTACCGGAGCCCTTTCACATCCTAGCTCGGGATGTTCACAACCGAATTGTTATCAGAGGACT
AAATACCATTCCATTGTTTGTGCAGCTGCTTTATTCTCCCATTGAAAACATCCAAAGAGTAGCTGCAGGG
GTCCTCTGTGAACTTGCTCAGGACAAGGAAGCTGCAGAAGCTATTGAAGCTGAGGGAGCCACAGCTCC
TCTGACAGAGTTACTTCACTCTAGGAATGAAGGTGTGGCGACATATGCAGCTGCTGTTTTGTTCCGAAT
GTCTGAGGACAAGCCACAAGATTACAAGAAACGGCTTTCAGTTGAGCTGACCAGCTCTCTCTTCAGAAC
AGAGCCAATGGCTTGGAATGAGACTGCTGATCTTGGACTTGATATTGGTGCCCAGGGAGAACCCCTTG
GATATCGCCAGGATGATCCTAGCTATCGTTCTTTTCACTCTGGTGGATATGGCCAGGATGCCTTGGGTA
TGGACCCCATGATGGAACATGAGATGGGTGGCCACCACCCTGGTGCTGACTATCCAGTTGATGGGCTG
CCAGATCTGGGGCATGCCCAGGACCTCATGGATGGGCTGCCTCCAGGTGACAGCAATCAGCTGGCCT
GGTTTGATACTGACCTGTAAGTCGACCTGCAGCCAAGCTAATTCCGGGCGAATTTCTTATGATTTATGAT
TTTTATTATTAAATAAGTTATAAAAAAAATAAGTGTATACAAATTTTAAAGTGACTCTTAGGTTTTAAAACG
AAAATTCTTATTCTTGAGTAACTCTTCCTGTAGTTCAAAGGTGCTTTA

Appendix C.2 Sequencing results of positive control prey vectors

Positive control vectors pVP16-BCL9 and pVP16-TCF4 were sequenced using the VP16_F_seq and VP16_R_seq primers. Restriction sites SfiI (GGCCNNNNNGGCC) and NotI (GCGGCCGC) are highlighted in light blue, insert of interest in green. pVP16-p300 vector was not sequenced, as bait interaction partner D4 auto-activated.

pVP16-BCL9: Forward sequencing

GGTGACACTATAGAACTCGATTTCCACC**ATG**GCGCCGAAAAAAAAGAGAAAAGTGGCCCAGCCGGCCA
GCAATAGCTCTTCAGCAGATCCCAAAGCCCCTCCGCCTCCACCAGTGTCCAGTGGCGAGCCCCCCACA
CTGGGAGAGAATCCCGATGGCCTATCTCAGGAGCAGCTGGAGCACCGGGAGCGCTCCTTACAAACTC
TCAGAGATATCCAGCGCATGCTTTTTCCTGATGAGAAAGAATTCACAGGAGCACAAAGTGGGGGACCG
CAGCAGAATGCGGCCGCCTCGAGCTCCGCCATGGCACCCAAGAAGAAGCGGAAGGTCCCAGGTGTAC
CGAGCTCGAATTGCATCGATACGGCCCCCCCGACCGATGTCAGCCTGGGGGACG

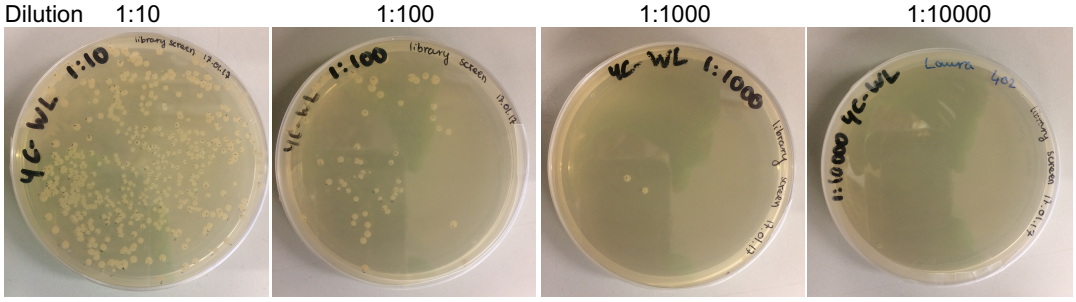
pVP16-TCF4: Forward sequencing

GTGAACTATAGAACTCGATTTCCACC**ATG**GCGCCGAAAAAAAAGAGAAAAGTGGCCCAGCCGGCCATG
CCGCAGCTGAACGGCGGTGGAGGGGATGACCTAGGCGCCAACGACGAACTGATTTCCTTCAAAGACG
AGGGCGAACAGGAGGAGAAGAGCTCCGAAAACTCCTCGGCAGAGAGGGATTTAGCTGATGTCAAATC
GTCTCTAGTCAATGAATCAGAAGCGGCCGCCTCGAGCTCCGCCATGGCACCCAAGAAGAAGCGGAAG
GTCCCAGGTGTACCGAGCTCGAATTGCATCGATACGGCCCCCCCGACCGATGTCAGCCTGGGGGACG
AGCTCCACTTAGACGGCGAGGACGTGGCGATGGCGCATGCCGACGCGCTAGACGA

Appendix C.3 Serial dilution of large-scale library screen on YC-WL growth control plates

A) Transformed yeast from the library screen was plated at the indicated dilutions on YC-WL growth control plates and incubated at 30°C for 3 days. B) Colonies on each plate were counted and total number of transformants was calculated. For example, 584 colonies grew on the 1:10 dilution plate. The dilution was performed from a 10 mL overall volume of transformed yeast (1:100). Therefore, the number of colonies is multiplied by the dilution factors to get the approximate number of total transformants: 584 x 10 x 100 = 5.86 x 10^5.

A



B

YC-WL plates	# colonies after 3 days at 30°C	Total number of transformants
1:10	584	5.86 x 10^5
1:100	57	5.7 x 10^5
1:1000	4	5 x 10^4
1:10000	0	-

Appendix C.4 Sequencing results of VH49, VH55 and VH88
The VHs VH49, VH55 and VH88 were sequenced using the pVP16_F_seq primer. Restriction enzyme sites SfiI and NotI are highlighted in blue, the VH sequence of interest is green.

VH49: Forward sequence

AAGGATACAATCAGTCCAAGCTTATTTAGGTGACACTATAGAACTCGATTTCCACCATGGCGCCGAAAA
AAAAGAGAAAAGTGGCCCAGCCGGCCATGGCCGAGGTGCAGCTGTTGGAGTCTGGGGGAGGCTTGGT
ACAGCCTGGGGGGTCCCTGAGACTCTCCTGTGCAGCCTCTGGATTCACCTTTAGTACCTTTAGCATGAA
CTGGGTCCGCCAGGCTCCAGGGAAGGGGCTGGAGTGGGTTTCATACATTAGTAGGACGTCGAAGACG
ATATACTATGCAGACTCTGTGAAGGGCCGATTCACCATCTCCAGAGACAATTCCAAGAACACACTGTAT
CTGCAAATGAACAGCCTGAGAGCCGAGGACACGGCTGTCTATTACTGTGCGAGAGGGGGGGAGATTT
CGACTATTGTTGCGCCTTTGTCTCGGTTTGACTACTGGGGCCAGGGAACCCTGGTCACCGTCTCGAG**C**
GCGGCCGC**CTC**GAGCTCCGCCATGGCACCCAAGAAGAAGCGGAAGGTCCCAGGTGTACCGAGCTCG
AATTGCATCGATACGGCCCCCCCGACCGATGTCAGCCTGGGGGACGAGCTCCACTTAGACGGCGAGG
ACGTGGCGATGGCGCATGCCGACGCGCTAGACGATTTCGATCTGGACATGTTGGGGGGACGGGGATT
CCCCGGGTCCGGGAT

VH55: Forward sequence

AGCTCCAAGCTTATTTAGGTGACACTATAGAACTCGATTTCCACCATGGCGCCGAAAAAAAAGAGAAAA
GTGGCCCAGCCGGCCATGGCCGAGGTGCAGCTGTTGGAGTCTGGGGGAGGCTTGGTACAGCCTGGG
GGGTCCCTGAGACTCTCCTGTGCAGCCTCTGGATTCACCTTTAGTACCTTTAGCATGAACTGGGTCCGC
CAGGCTCCAGGGAAGGGGCTGGAGTGGGTTTCATACATTAGTAGGACGTCGAAGACGATATACTATGC
AGACTCTGTGAAGGGCCGATTCACCATCTCCAGAGACAATTCCAAGAACACACTGTATCCGCAAATGAA
CAGCCTGAGAGCCGAGGACACGGCTGTCTATTACTGTGCGAGAGGGACGACGGTTGATCTTGAGGCT
GATTGTAAGACTCATTTTGACTACTGGGGCCAGGGAACCCTGGTCACCGTCTCGAGCGCGGCCGCCTC
GAGCTCCGCCATGGCACCCAAGAAGAAGCGGAAGGTCCCAGGTGTACCGAGCTCGAATTGCATCGAT
ACGGCCCCCCCGACCGATGTCAGCCTGGGGGACGAGCTCCACTTAGACGGCGAGGACGTGGCGATG
GCGCATGCCGACGCGCTAGACGATTTCGATCTGGACATGTTGGGGGACGGGGATTCCCCGGGTCCGG
GATTTACCCCCCCACGACTCCGCCCCCTACGGCGCTCTGGATATGGGCCGACTTCGAGTTTGAGCA

VH88: Forward sequence

ATCAAGCTCCAGCTTATTTAGGTGACACTATAGAACTCGATTTCCACCATGGTGGCCGAAAAAAAAGAG
AAAAGTGGCCCAGCCGGCCATGGCCGAGGTGCAGCTGTTGGAGTCTGGGGGAGGCTTGGTACAGCCT
GGGGGGTCCCTGAGACTCTCCTGTGCAGCCTCTGGATTCACCTTTAGTACCTTTAGCATGAACTGGGT
CCGCCAGGCTCCAGGGAAGGGGCTGGAGTGGGTTTCATACATTAGTAGGACGTCGAAGACGATATACT
ATGCAGACTCTGTGAAGGGCCGATTCACCATCTCCAGAGACAATTCCAAGAACACACTGTATCTGCAAA
TGAACAGCCTGAGAGCCGAGGACACGGCTGTCTATTACTGTGCGAGAGGGACGCCTTCGCTTATGACG
CATTATCCGATGAGGTGTTTTGACTACTGGGGCCAGGGAACCCTGGTCACCGTCTCGAGCGCGGCCG
CCTCGAGCTCCGCCATGGCACCCAAGAAGAAGCGGAAGGTCCCAGGTGTACCGAGCTCGAATTGCAT
CGATACGGCCCCCCCGACCGATGTCAGCCTGGGGGACGAGCTCCACTTAGACGGCGAGGACGTGGC
GATGGCGCATGCCGACGCGCTAGACGATTTCGATCTGGACATGTTGGGGGACGGGGATTCCCCGGGT
CCGGGATTTACCCCCCACGACTCCGCCCCCTACGGCGCTCTG

Appendix D - Supplementary data for Chapter 6

Appendix D.1 DNA and Amino Acid sequences of LL3 and LL3.CDRAAA
Highlighted in yellow are the differential sequences between the VHHs LL3 and LL3.CDRAAA. The HIS-tag location is highlighted in blue, while the myc-tag is visualised in green. Sequences were obtained from Professor Terence Rabbitts (Weatherall Institute of Molecular Medicine, Oxford), with permission from UCB Pharma.

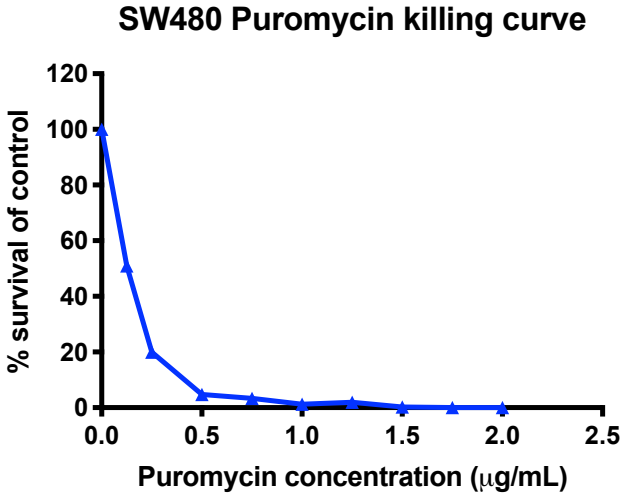
LL3:

```
 K  L  A  T  M  A  Q  V  Q  L  V  Q  S  G  G  G  L  V  Q  A  G  D  S
AAGCTTGCCACCATGGCTCAGGTGCAGCTGGTCCAGTCTGGGGGAGGGCTGGTGCAGGCTGGGGACTCTC
L  R  L  A  C  A  A  S  E  G  T  F  R  T  N  V  M  G  W  F  R  Q  A  P
TGAGACTCGCCTGTGCAGCCTCTGAAGGCACCTTCAGAACCAATGTTATGGGTTGGTTCCGCCAGGCTCC
  G  K  E  R  E  F  V  A  A  I  S  W  S  G  G  I  T  H  Y  S  N  S  V
AGGGAAGGAGCGTGAGTTTGTAGCAGCTATCAGTTGGAGTGGTGGTATCACGCACTATTCAAATTCCGTG
 K  G  R  F  A  I  S  R  D  N  A  K  N  T  V  Y  L  Q  M  N  S  L  K
AAGGGCCGATTCGCCATCTCCAGAGACAACGCCAAGAACACGGTGTATCTGCAAATGAACAGCCTGAAAC
P  E  D  T  A  V  Y  Y  C  A  A  D  P  S  T  T  P  W  N  L  R  V  R  V
CTGAGGACACGGCCGTTTATTACTGTGCAGCAGATCCGTCGACCACGCCTTGGAATCTCAGGGTGCGCGT
  N  E  Y  E  Y  W  G  Q  G  T  Q  V  T  V  S  S  A  A  A  H  H  H  H
CAATGAGTACGAGTACTGGGGCCAGGGGACCCAGGTCACCGTCTCCAGCGCGGCCGCCCATCACCATCAC
 H  H  G  A  A  E  Q  K  L  I  S  E  E  D  L  N  G  A  A  .  .  E  F
CATCACGGGGCCGCAGAACAAAAACTCATCTCAGAAGAGGATCTGAATGGGGCCGCATAGTAAGAATTC
```

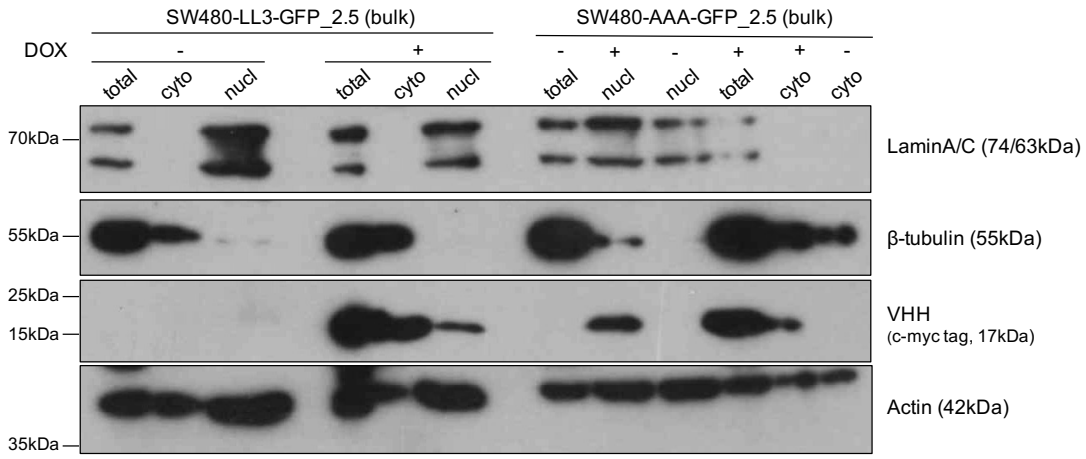
LL3.CDRAAA :

```
 K  L  A  T  M  A  Q  V  Q  L  V  Q  S  G  G  G  L  V  Q  A  G  D  S
AAGCTTGCCACCATGGCTCAGGTGCAGCTGGTCCAGTCTGGGGGAGGGCTGGTGCAGGCTGGGGACTCTC
L  R  L  A  C  A  A  S  E  G  T  F  R  T  N  V  M  G  W  F  R  Q  A  P
TGAGACTCGCCTGTGCAGCCTCTGAAGGCACCTTCAGAACCAATGTTATGGGTTGGTTCCGCCAGGCTCC
  G  K  E  R  E  F  V  A  A  I  S  W  S  G  G  I  T  H  Y  S  N  S  V
AGGGAAGGAGCGTGAGTTTGTAGCAGCTATCAGTTGGAGTGGTGGTATCACGCACTATTCAAATTCCGTG
 K  G  R  F  A  I  S  R  D  N  A  K  N  T  V  Y  L  Q  M  N  S  L  K
AAGGGCCGATTCGCCATCTCCAGAGACAACGCCAAGAACACGGTGTATCTGCAAATGAACAGCCTGAAAC
P  E  D  T  A  V  Y  Y  C  A  A  D  P  S  T  T  A  A  A  L  R  V  R  V
CTGAGGACACGGCCGTTTATTACTGTGCAGCAGATCCGTCGACCACGGCCGCAGCCCTCAGGGTGCGCGT
  N  E  Y  E  Y  W  G  Q  G  T  Q  V  T  V  S  S  A  A  A  H  H  H  H
CAATGAGTACGAGTACTGGGGCCAGGGGACCCAGGTCACCGTCTCCAGCGCGGCCGCCCATCACCATCAC
 H  H  G  A  A  E  Q  K  L  I  S  E  E  D  L  N  G  A  A  .  .  E  F
CATCACGGGGCCGCAGAACAAAAACTCATCTCAGAAGAGGATCTGAATGGGGCCGCATAGTAAGAATTC
```

Appendix D.2 Puromycin killing curve in SW480
SW480 cells were seeded in duplicates and treated with a pyromycin concentration range from 0-2 µg/mL for three days. Cell survival was assessed by the SRB assay. All cells were dead at a puromycin concentration of 1 µg/mL and it was decided to perform the puromycin selection of stable clones at a concentration of 1.2 µg/mL.

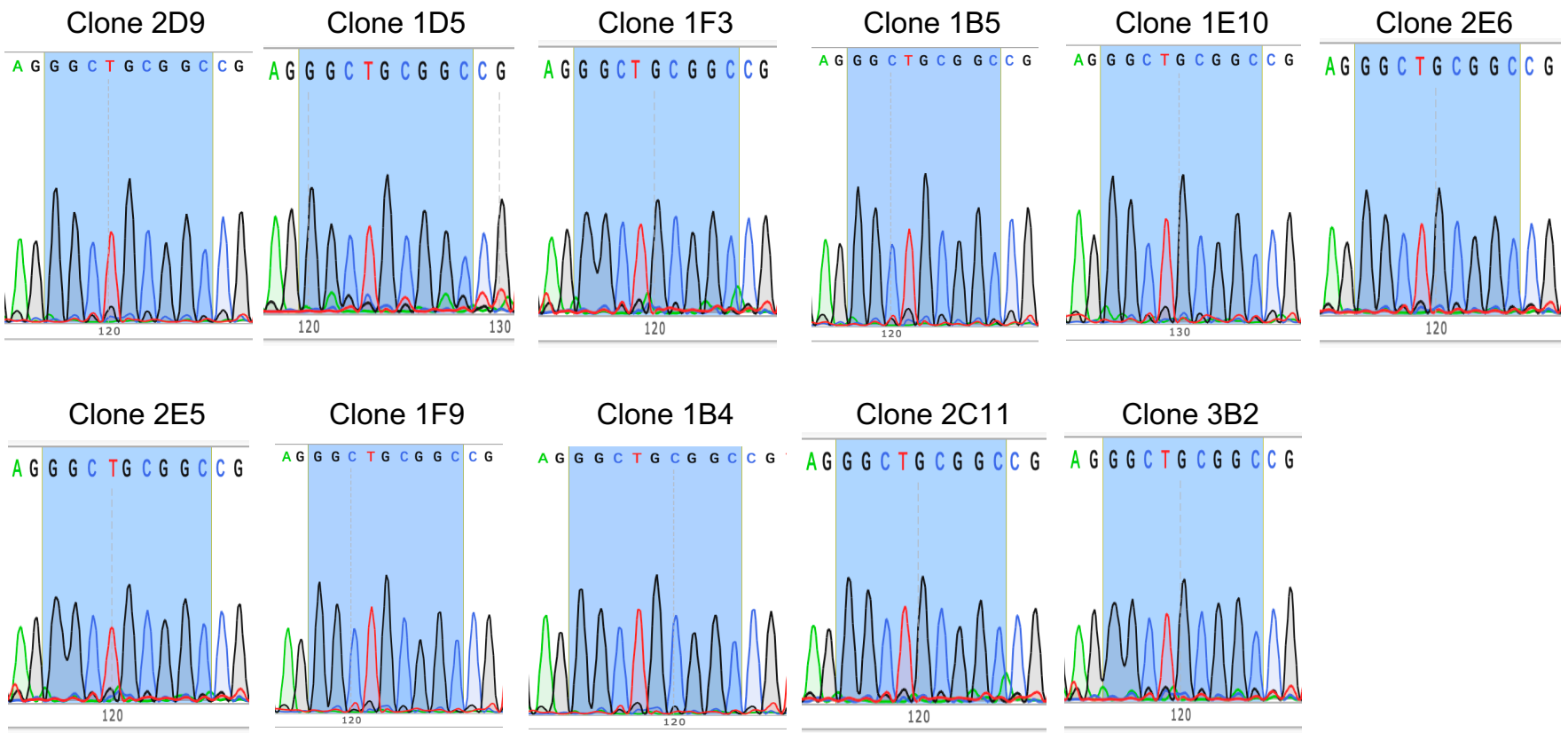


Appendix D.3 Cytoplasmic and nuclear VHHs expression in stable SW480 cells
SW480-LL3-GFP_2.5 and SW480-AAA-GFP_2.5 bulk cell lines were treated with 100 ng/mL DOX or with DMEM alone as negative control. After 48 hrs, cytoplasmic and nuclear proteins were extracted using the N-PER protein extraction kit, while the total proteins were extracted using RIPA buffer. Thirty µg of each protein sample were loaded onto a 14% SDS gel. Lamin A/C (1:3000) was used to control for nuclear fractions, while β-tubulin (1:5000) was used to detect the cytoplasmic portion. Actin (1:1000) was used as loading control. The experiment was performed twice.



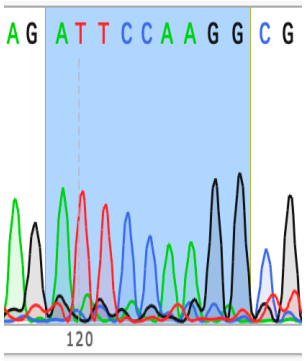
Appendix D.4 Sequencing data of individual SW480-AAA-GFP and SW480-LL3-GFP clones
Clones were sequenced using the LL3_GFP_TLCV2_BamHI_R reverse primer. Highlighted in blue is the 9 bp reverse sequence differentiating the wild-type LL3 (ATTCCAAGG) from the mutant version AAA (GGCTGCGGC). This is equivalent to the forward sequence CCTTGGAAT and GCCGCAGCC for LL3 and AAA clones, respectively. All sequenced clones have the expected sequences. Sanger sequencing was performed at the Sequencing Facility at the WIMM. Figure goes over two pages.

SW480-AAA-GFP clones

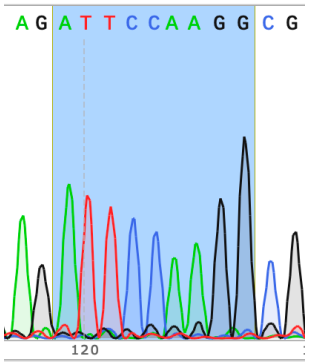


SW480-LL3-GFP clones

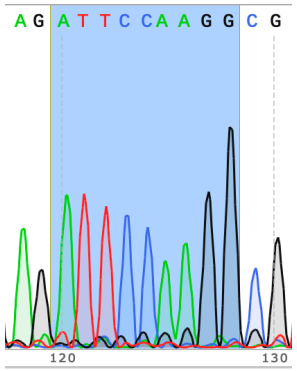
Clone 1C6



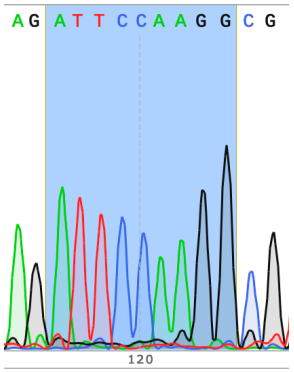
Clone 2D3



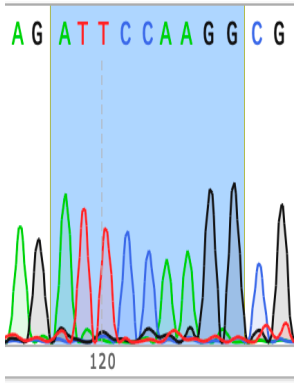
Clone 1F5



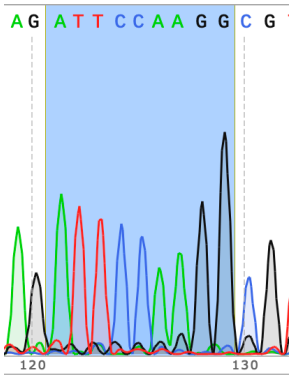
Clone 2D8



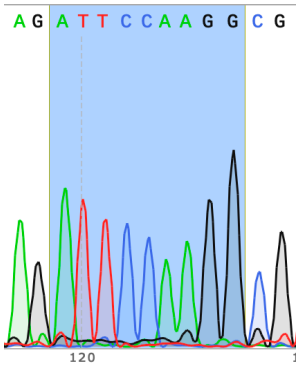
Clone 2B6



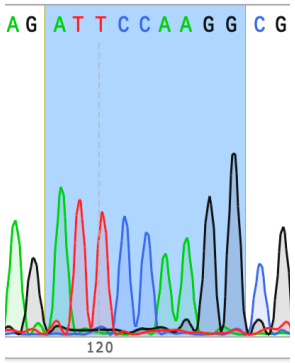
Clone 2E3



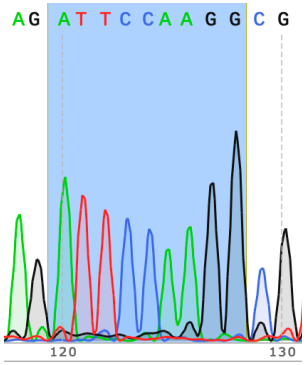
Clone 1B10



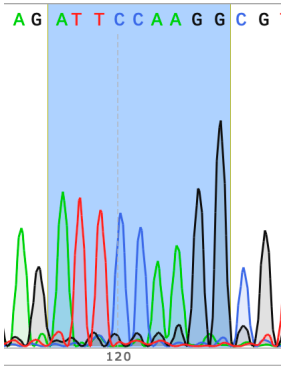
Clone 3C5



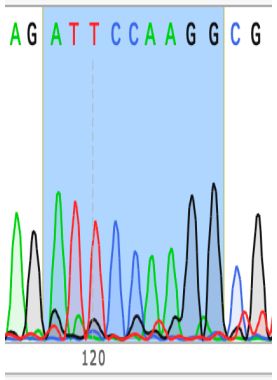
Clone 2G10



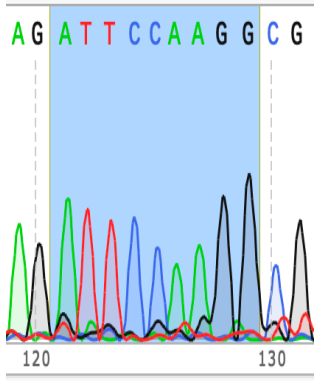
Clone 3D6



Clone 2G11

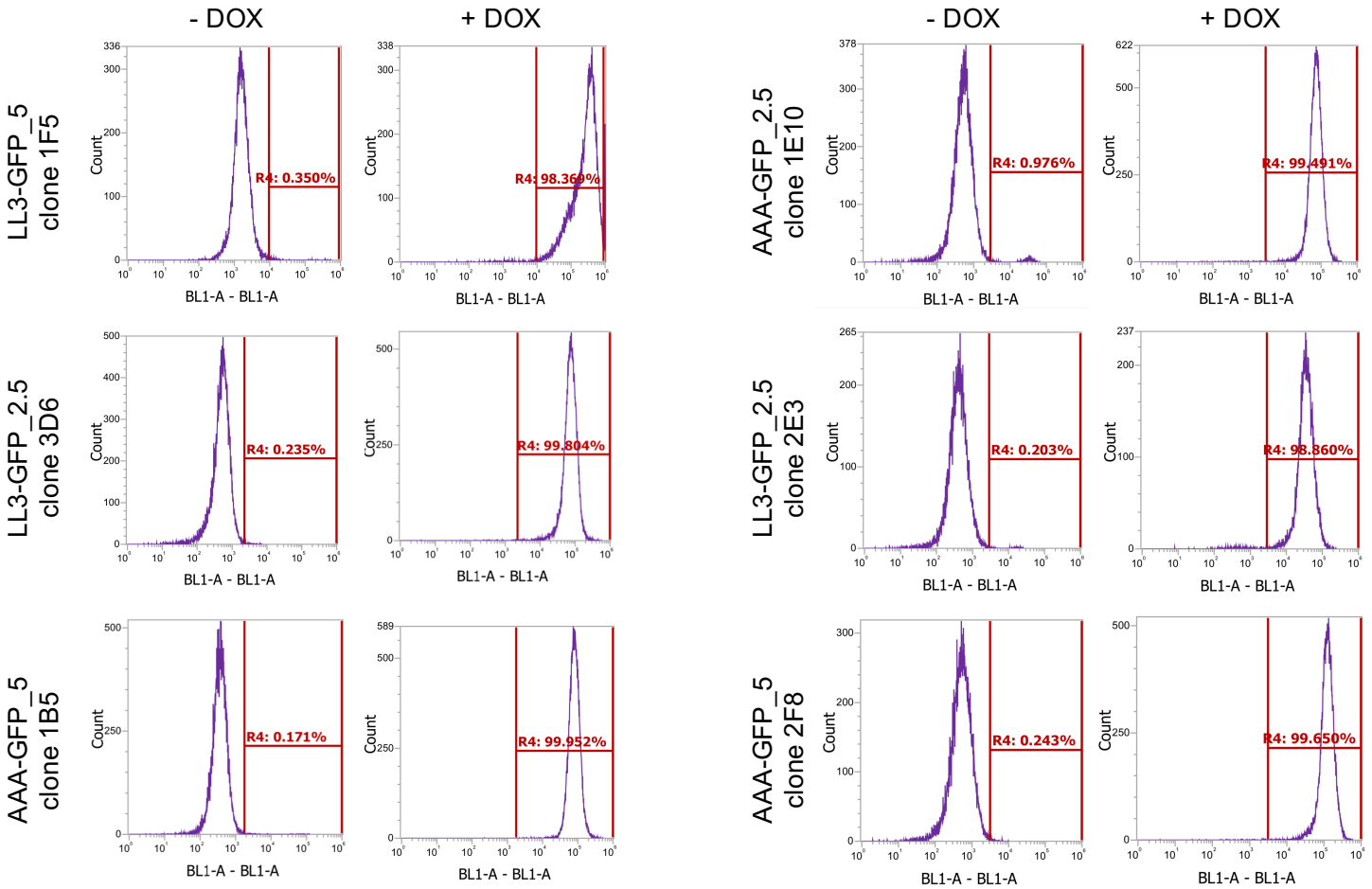


Clone 3B5



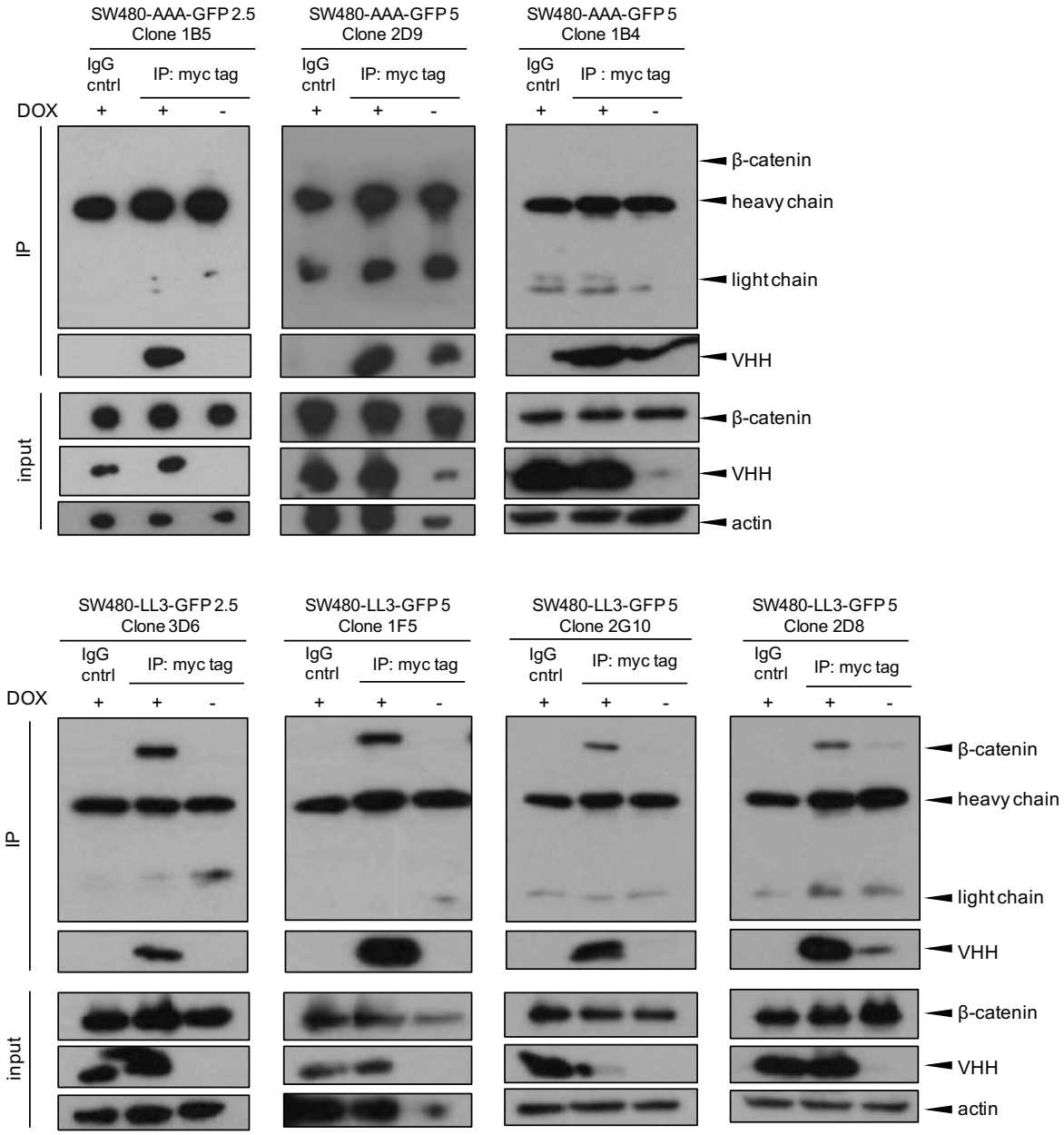
Appendix D.5 FACS data of DOX-induced clones

LL3-GFP clones 1F5, 3D6, 2E3 and AAA-GFP clones 1B5, 1E10, 2F8 were analysed by FACS 48 hrs after DOX induction. Y-axis indicates number of counted cells, X-axis shows GFP signal. BL1-A: GFP channel.



Appendix D.6 Myc-tag immunoprecipitations of stable SW480-AAA-GFP and SW480-LL3-GFP clones

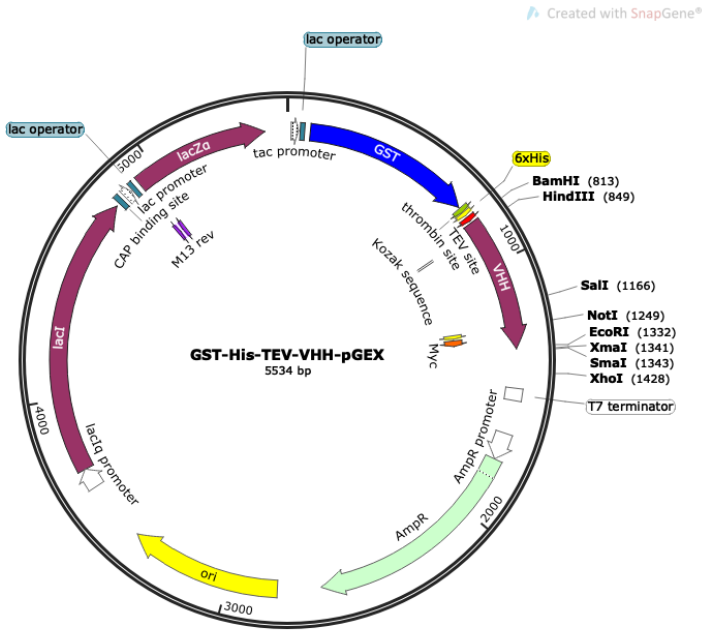
Myc-tag immunoprecipitations were performed on the following clones with and without DOX treatment: SW480-AAA-GFP clones 1B5, 2D9, 1B4 and SW480-LL3-GFP clones 3D6, 1F5, 2G10, 2D8. VHH were detected using a myc-tag antibody. Note that in clones SW480-AAA-GFP 2D9 and SW480-LL3-GFP 2D8 there is significant VHH background expression even without DOX induction.



Appendix D.7 Colony formation assay results for all tested clones
Mean percentage colony formation at 100 ng/mL DOX treatment is given. Experiments were repeated at least in three independent experiments, except for bulk cultures, which were performed in duplicate experiments. p-values were calculated using two-tailed multiple t-tests, False Discovery Rate-adjusted p-values for multiple testing using the Benjamini, Krieger and Yekutieli corrections are given. Clones that show a significant discovery according to the multiple corrections are highlighted in orange.

Stable cell line	Clone	Mean % colony formation at 100 ng/mL DOX relative to control (± SD)	p-value
SW480-LL3-GFP_2.5	bulk	90.96 (± 0.20)	0.0002
	3C5	110.4 (± 6.21)	0.015
	2B10	113.0 (± 7.76)	0.016
SW480-LL3-GFP_5	bulk	85.60 (± 0.16)	<0.0001
	2D8	108.36 (± 4.82)	0.004
	2G10	100.59 (± 20.6)	0.956
	2D3	0.34 (± 0.15)	<0.0001
	1F5	22.87 (± 23.13)	0.0005
	3B5	93.63 (± 3.23)	0.027
	2B6	110.02 (± 6.64)	0.059
	2G11	90.57 (± 8.86)	0.139
	3E11	133.6 (± 7.86)	0.002
	1C6	100.59 (± 8.45)	0.910
SW480-AAA-GFP_2.5	bulk	95.6 (± 1.82)	0.075
	1E10	113.82 (± 11.98)	0.063
	1B5	97.29 (± 7.81)	0.513
SW480-AAA-GFP_5	bulk	77.92 (± 4.06)	0.017
	2D9	107.93 (± 10.50)	0.397
	2F8	58.80 (± 16.58)	0.002
	1F9	108.93 (± 7.85)	0.063
	1B4	24.98 (± 3.63)	<0.0001
	2E6	101.98 (± 1.58)	0.092
	3B2	103.04 (± 1.61)	0.031
	2C11	80.69 (± 10.11)	0.029
	2E5	72.24 (± 23.54)	0.237
	1D5	98.59 (± 3.94)	0.662
	1F3	95.60 (± 10.52)	0.615
SW480 parental	bulk	103.2 (± 7.26)	0.354

Appendix D.8 GST-His-TEV-VHH-pGEX vector map and sequencing results
Top: VHH LL3 and LL3.CDRAAA were clones in frame with GST into the pGEX vector using the BamHI/XmaI restriction sites. A TEV site can be used to cleave the VHH fraction from the GST-HIS-tag. Bottom: Sequencing results of the inserted fragments are given. Highlighted in light blue are the restriction sites BamHI/XmaI, in green the VHH sequences. Inserts were sequenced using the pGEX_seq_F sequencing primer.



Sequencing results of GST-His-TEV-LL3-pGEX, F primer:

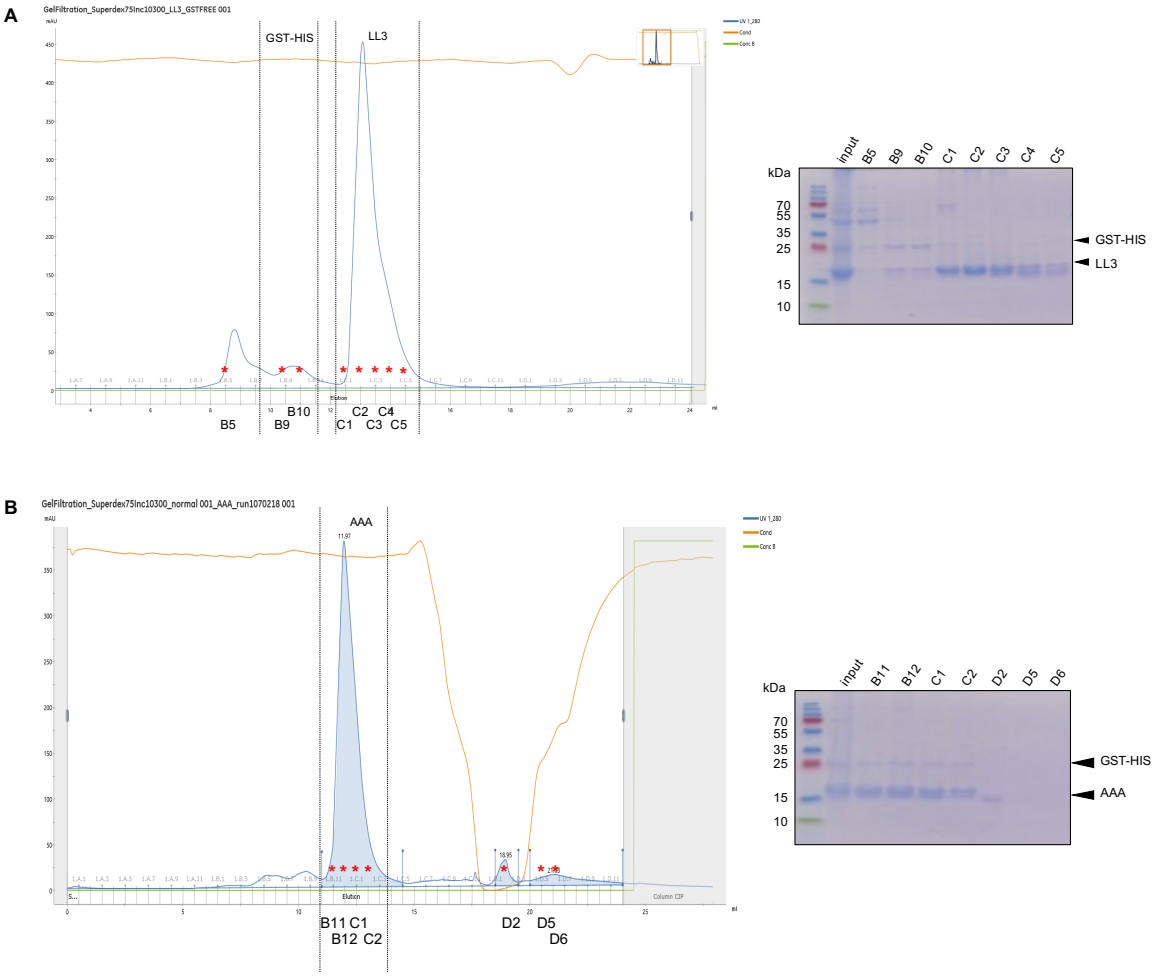
GCATCCTCAATCGGATCTGGTTCCGCGTGGATCTCACCACCATCACCATCACGGATCGGAAAACCTGT
ATTTCCAGGGCGGATCCGGTGGCGGAGGGTCAGGTGGCGGAGGGTCAAAGCTTGCCACCATGGCTCA
GGTGCAGCTGGTCCAGTCTGGGGGAGGGCTGGTGCAGGCTGGGGACTCTCTGAGACTCGCCTGTGC
AGCCTCTGAAGGCACCTTCAGAACCAATGTTATGGGTTGGTTCCGCCAGGCTCCAGGGAAGGAGCGTG
AGTTTGTAGCAGCTATCAGTTGGAGTGGTGGTATCACGCACTATTCAAATTCCGTGAAGGGCCGATTCG
CCATCTCCAGAGACAACGCCAAGAACACGGTGTATCTGCAAATGAACAGCCTGAAACCTGAGGACACG
GCCGTTTATTACTGTGCAGCAGATCCGTCGACCACGCCTTGGAATCTCAGGGTGCGCGTCAATGAGTA
CGAGTACTGGGGCCAGGGGACCCAGGTCACCGTCTCCAGCGCGGCCGCCCATCACCATCACCATCAC
GGGGCCGCAGAACAAAAACTCATCTCAGAAGAGGATCTGAATGGGGCCGCATAGTAAGAATTCTGACC
CGGGAAGCTTCGCCAGGGTTTTCCCAGTCGAGCTCGATATCGGTACCAGCGGATAACAATTTCACATC
CGGATTCGCGAACGCGTCTCGAGGGCTGCTAACAAAGCCCGAAAGGAAGCTGAGTTGGCTGCTGCCA
CCGCTGAGCAATAACTAGCATAACCCCTTTGGGGCCTCTAAACGGTCTTGAGGGGTTTTTTGCTGAAAG
GAGACTATAGCAGATAGTCTGAAGACGAAAGGCCTCGTGATACGCCCTTATTTTTTTTTATTAGT

Sequencing results of GST-His-TEV-AAA-pGEX, F primer:

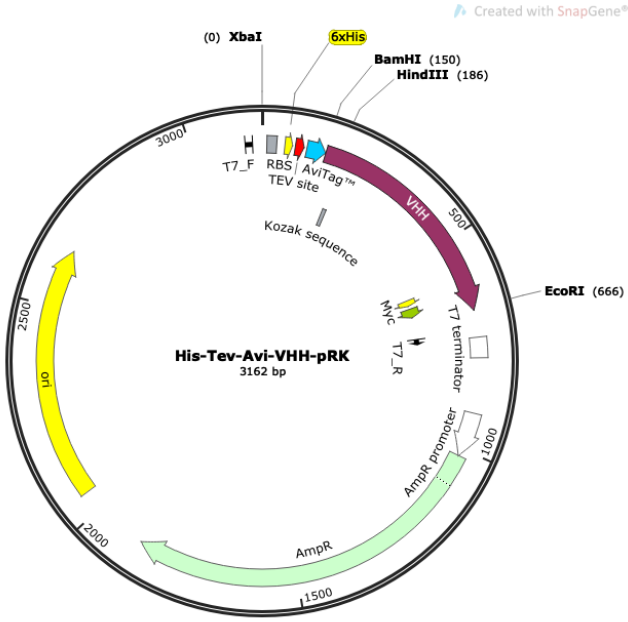
GCATCCTCAATCGGATCTGGTTCCGCGTGGATCTCACCACCATCACCATCACGGATCGGAAAACCTGT
ATTTCCAGGGCGGATCCGGTGGCGGAGGGTCAGGTGGCGGAGGGTCAAAGCTTGCCACCATGGCTCA
GGTGCAGCTGGTCCAGTCTGGGGGAGGGCTGGTGCAGGCTGGGGACTCTCTGAGACTCGCCTGTGC
AGCCTCTGAAGGCACCTTCAGAACCAATGTTATGGGTTGGTTCCGCCAGGCTCCAGGGAAGGAGCGTG
AGTTTGTAGCAGCTATCAGTTGGAGTGGTGGTATCACGCACTATTCAAATTCCGTGAAGGGCCGATTCG
CCATCTCCAGAGACAACGCCAAGAACACGGTGTATCTGCAAATGAACAGCCTGAAACCTGAGGACACG
GCCGTTTATTACTGTGCAGCAGATCCGTCGACCACGGCCGCAGCCCTCAGGGTGCGCGTCAATGAGTA
CGAGTACTGGGGCCAGGGGACCCAGGTCACCGTCTCCAGCGCGGCCGCCCATCACCATCACCATCAC
GGGGCCGCAGAACAAAAACTCATCTCAGAAGAGGATCTGAATGGGGCCGCATAGTAAGAATTCTGACC
CGGGAAGCTTCGCCAGGGTTTTCCCAGTCGAGCTCGATATCGGTACCAGCGGATAACAATTTCACATC
CGGATTCGCGAACGCGTCTCGAGGGCTGCTAACAAAGCCCGAAAGGAAGCTGAGTTGGCTGCTGCCA
CCGCTGAGCAATAACTAGCATAACCCCTTGGGGCCTCTAAACGGGTCTTGAGGGGTTTTTTTGCTGAAA
GGAGAACCTATAGCTGATTATCTGGAGGACGAAAGGCCT

Appendix D.9 Chromatography column purification results

TEV digested LL3 (A) and AAA (B) were purified on a Superdex75inc10300 column. Fractions indicated with a red star were analysed by Coomassie stain on an SDS gel. The expected VHH fragment size is 17 kDa.



Appendix D.10 His-Tev-Avi-VHH-pRK vector map and sequencing results
Top: VHH LL3 and LL3.CDRAAA were clones in frame with the HIS- and Avi-tag into the His-Tev-Avi-MCS-pRK vector using the BamHI/EcoRI restriction sites. A TEV site can be used to cleave the Avi-VHH fraction from the HIS-tag. Bottom: Sequencing results of the inserted fragments are given. Highlighted in light blue are the restrictionsites BamHI/EcoRi, in green the VHH sequences. Inserts were sequenced using the HisTEVAviMCS_seq_F and HisTEVAviMCS_seq_R sequencing primers.



Sequencing results: His-TEV-Avi-LL3, Reverse complement sequence, R primer:

TGTCAGAGTTTTCACCGTCATCACCGAAACGCGCGAGGGCAGGATCTCGATCCCGCGAAATTAATACG
ACTCACTATAGGGAGACCACAACGGTTTCCCTCTAGAAATAATTTTGTTTAACTTTAAGAAGGAGATATA
CATATGAGAGGATCGCATCACCATCACCATCACGGGTCTGAAAACCTGTATTTCCAGGGCGGATCTGG
CCTGAACGACATCTTCGAGGCTCAGAAAATCGAATGGCACGAGGGATCCGGTGGCGGAGGGTCAGGT
GGCGGAGGGTCAAAGCTTGCCACCATGGCTCAGGTGCAGCTGGTCCAGTCTGGGGGAGGGCTGGTG
CAGGCTGGGGACTCTCTGAGACTCGCCTGTGCAGCCTCTGAAGGCACCTTCAGAACCAATGTTATGGG
TTGGTTCCGCCAGGCTCCAGGGAAGGAGCGTGAGTTTGTAGCAGCTATCAGTTGGAGTGGTGGTATCA
CGCACTATTCAAATTCCGTGAAGGGCCGATTCGCCATCTCCAGAGACAACGCCAAGAACACGGTGTAT
CTGCAAATGAACAGCCTGAAACCTGAGGACACGGCCGTTTATTACTGTGCAGCAGATCCGTCGACCAC
GCCTTGGAATCTCAGGGTGCGCGTCAATGAGTACGAGTACTGGGGCCAGGGGACCCAGGTCACCGTC
TCCAGCGCGGCCGCCCATCACCATCACCATCACGGGGCCGCAGAACAAAAACTCATCTCAGAAGAGG
ATCTGAATGGGGCCGCATGAGAATCCGATCCGGCGCACC

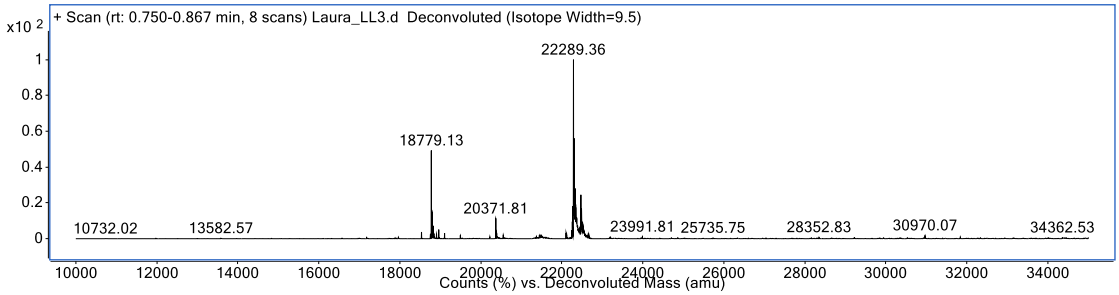
Sequencing results: His-TEV-Avi-AAA, F primer:

GCGATTTTCTCTCTAATACATCCGGGACGAACCTGGTATTTCCAGGGCGGATCTGGCCTGAACGACATC
TTCGAGGCTCAGAAAATCGAATGGCACGAG**GGATCC**GGTGGCGGAGGGTCAGGTGGCGGAGGGTCA
AAGCTTGCCACCATGGCTCAGGTGCAGCTGGTCCAGTCTGGGGGAGGGCTGGTGCAGGCTGGGGACT
CTCTGAGACTCGCCTGTGCAGCCTCTGAAGGCACCTTCAGAACCAATGTTATGGGTTGGTTCCGCCAG
GCTCCAGGGAAGGAGCGTGAGTTTGTAGCAGCTATCAGTTGGAGTGGTGGTATCACGCACTATTCAAA
TTCCGTGAAGGGCCGATTCGCCATCTCCAGAGACAACGCCAAGAACACGGTGTATCTGCAAATGAACA
GCCTGAAACCTGAGGACACGGCCGTTTATTACTGTGCAGCAGATCCGTCGACCACGGCCGCAGCCCT
CAGGGTGCGCGTCAATGAGTACGAGTACTGGGGCCAGGGGACCCAGGTCACCGTCTCCAGCGCGGC
CGCCCATCACCATCACCATCACGGGGCCGCAGAACAAAAACTCATCTCAGAAGAGGATCTGAATGGGG
CCGCATGAGAATTCCGATCCGGCTGCTAACAAAGCCCGAAAGGAAGCTGAGTTGGCTGCTGCCACCG
CTGAGCAATAACTAGCATAACCCCTTGGGGCCTCTAAACGGGTCTTGAGGGGTTTTTTGCTGAAAGGA
GGAACTATATCCCGGATAATTTCTTGAGACGAAAGGGTCTCGTGATACGCCTATTTTTATAGGTATTGTC
ATGATTATTATGGGTTTCTTTAGACGTCAAGTGGGCACTTTTTCCG

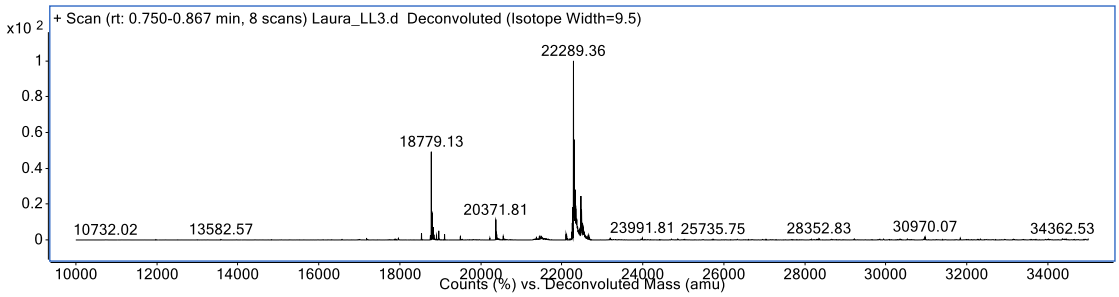
Appendix D.11 Electronspray Ionization Mass Spectroscopy data for His-TEV-Avi-AAA, His-TEV-Avi-LL3 and pGEX-Bcatfl

Data was obtained by Dr David Staunton (Molecular Biophysics Suite, Biochemistry Department, Oxford).

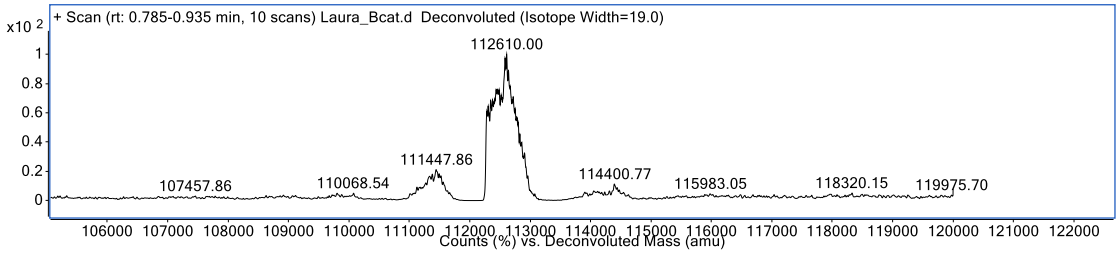
His-TEV-Avi-AAA (22.11 kDa):



His-TEV-Avi-LL3 (22.29 kDa):



pGEX-Bcatfl (111 kDa):



Appendix D.12 Sequencing results of pGEX-ArmR fragments

ArmR regions of interest were cloned into the GST-HIS-TEV-pGEX vector. pGEX-constructs were sequenced using the pGEX_seq_F and pGEX_seq_R primers. Highlighted in blue are the restriction sites BamHI/XmaI and in green the β-catenin ArmR regions of interest.

pGEX-Arm1:

CCACTTCCTCAATCGGATCTGGTTCCGCGTGGATCTCACCACCATCACCATCACGGATCGGAAAACCTGTA
TTTCCAGGGCGGATCCGGTGGCGGAGGGTCAGGTGGCGGAGGGTCATTGATTAACTATCAAGATGATGCA
GAACTTGCCACACGTGCAATCCCTGAACTGACAAAACTGCTAAATGACGAGGACCAGGTGGTGGTTAATAA
GGCTGCAGTTATGGTCCATCAGCTTTCTAAATGACCCGGGAAGCTTCGCCAGGGTTTTCCCAGTCGAGCTC
GATATCGGTACCAGCGGATAACAATTTCACATCCGGATTCGCGAACGCGTCTCGAGGGCTGCTAACAAAG
CCCGAAAGGAAGCTGAGTTGGCTGCTGCCACCGCTGAGCAATAACTAGCATAACCCCTTGGGGCCTCTAA
ACGGGTCTTGAGGGGTTTTTTGCTGAAAGGAGGAACTATAGCCGGATAATTCTTGAAGACGAAAGGGCCTC
GTGATACGCCTATTTTTATAGGTTAATGTCATGATAATAATGGTTTCTTAGACGTCAGGTGGCACTTTTCGG
GGAAATGTGCGCGGAACCCCTATTTGTTTATTTTTCTAAATACATTCAAATATGTATCCGCTCATGAGACAAT
AACCCTGAT

pGEX-Arm1-3:

TCATCTCCAATCGGATCTGGTTCCGCGTGGATCTCACCACCATCACCATCACGGATCGGAAAACCTGTATT
TCCAGGGCGGATCCGGTGGCGGAGGGTCAGGTGGCGGAGGGTCATTGATTAACTATCAAGATGATGCAG
AACTTGCCACACGTGCAATCCCTGAACTGACAAAACTGCTAAATGACGAGGACCAGGTGGTGGTTAATAAG
GCTGCAGTTATGGTCCATCAGCTTTCTAAAAAGGAAGCTTCCAGACACGCTATCATGCGTTCTCCTCAGAT
GGTGTCTGCTATTGTACGTACCATGCAGAATACAAATGATGTAGAAACAGCTCGTTGTACCGCTGGGACCT
TGCATAACCTTTCCCATCATCGTGAGGGCTTACTGGCCATCTTTAAGTCTGGAGGCATTCCTGCCCTGGTG
AAAATGCTTGGTTCACCAGTGGATTCTGTGTTGTTTTATGCCATTACAACTCTCCACAACCTTTTATTATGAC
CCGGGAAGCTTCGCCAGGGTTTTCCCAGTCGAGCTCGATATCGGTACCAGCGGATAACAATTTCACATCC
GGATTCGCGAACGCGTCTCGAGGGCTGCTAACAAAGCCCGAAAGGAAGCTGAGTTGGCTGCTGCCACCG
CTGAGCAATAACTAGCATAACCCCTTGGGGCCTCTAAACGGGTCTTGAGGGGTTTTTTGCTGAAAGGAGGA
ACTATAGCCGGATAATTCTTGAAGACGAAAGGGCCTCGTGATACGCCTATTTTTATAGGTTAATGTCATGAT
AATAATGGGTTTCTT

pGEX-Arm2-4:

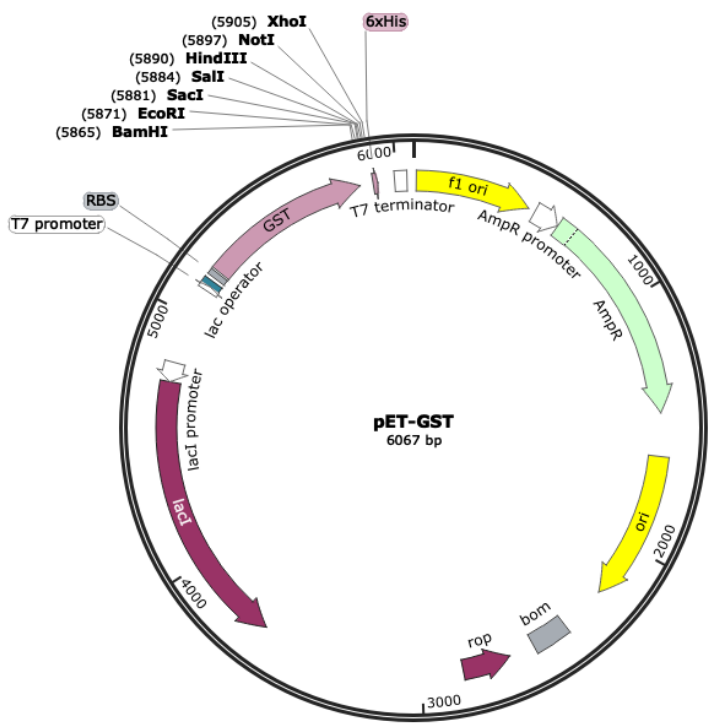
CATCCTCAATCGGATCTGGTTCCGCGTGGATCTCACCACCATCACCATCACGGATCGGAAAACCTGTATTT
CCAGGGCGGATCCGGTGGCGGAGGGTCAGGTGGCGGAGGGTCAAAGGAAGCTTCCAGACACGCTATCAT
GCGTTCTCCTCAGATGGTGTCTGCTATTGTACGTACCATGCAGAATACAAATGATGTAGAAACAGCTCGTTG
TACCGCTGGGACCTTGCATAACCTTTCCCATCATCGTGAGGGCTTACTGGCCATCTTTAAGTCTGGAGGCA
TTCCTGCCCTGGTGAAAATGCTTGGTTCACCAGTGGATTCTGTGTTGTTTTATGCCATTACAACTCTCCACA
ACCTTTTATTACATCAAGAAGGAGCTAAAATGGCAGTGCGTTTAGCTGGTGGGCTGCAGAAAATGGTTGCC
TTGCTCAACAAAACAAATGTTAAATTCTTGGCTATTACGACAGACTGCCTTCAAATTTTAGCTTATTGACCCG
GGAAGCTTCGCCAGGGTTTTCCCAGTCGAGCTCGATATCGGTACCAGCGGATAACAATTTCACATCCGGAT
TCGCGAACGCGTCTCGAGGGCTGCTAACAAAGCCCGAAAGGAAGCTGAGTTGGCTGCTGCCACCGCTGA
GCAATAACTAGCATAACCCCTTGGGGCCTCTAAACGGGTCTTGAGGGGTTTTTTGCTGAAAGGAGGAACTA
TAGCCGGATAATTCTTGAAGACGAAAGGGCCTCGTGATACGCCTATTTTTATAGGTTAATGTCATGATAATA
ATGGTTTCTTAGA

pGEX-Arm4-6, Reverse complement sequence:

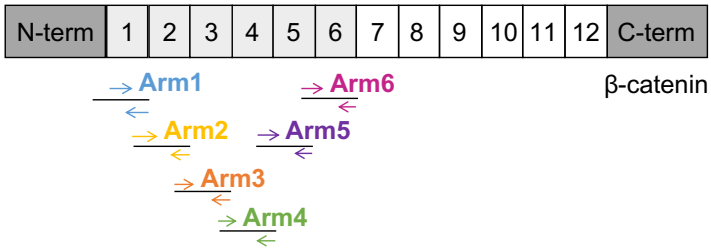
GCCGTTTTTGGATTATTTAAGATTACCGGTGTTTTCGAGAATTGCATATAGTAAAAGACTTTTGAAACTCTCA
AAGTTGATTTTCTTAGCAAGCTACTGAAATGCTGAAAATGTTCGAAGATCGTTTATGTCATAAAACATATTTA
AATGGTGATCATGTAACCCATCCTGACTTCATGTTGTATGACGCTCTTGATGTTGTTTTATACATGGACCCA
ATGTGCCTGGATGCGTTCCCAAAATTAGTTTGTTTTAAAAAACGTATTGAAGCTATCCCACAAATTGATAAGT
ACTTGAAATCCAGCAAGTATATAGCATGGCCTTTGCAGGGCTGGCAAGCCACGTTTGGTGGTGGCGACCA
TCCTCCAAAATCGGATCTGGTTCCGCGTGGATCTCACCACCATCACCATCACGGATCGGAAAACCTGTATT
TCCAGGGCGGATCCGGTGGCGGAGGGTCACATCAAGAAGGAGCTAAAATGGCAG
TGCGTTTAGCTGGTGGGCTGCAGAAAATGGTTGCCTTGCTCAACAAAACAAATGTTAAATTCTTGGCTATTA
CGACAGACTGCCTTCAAATTTTAGCTTATGGCAACCAAGAAAGCAAGCTCATCATACTGGCTAGTGGTGGA
CCCCAAGCTTTAGTAAATATAATGAGGACCTATACTTACGAAAAACTACTGTGGACCACAAGCAGAGTGCTG
AAGGTGCTATCTGTCTGCTCTAGTAATAAGCCGGCTATTGTAGAAGCTGGTGGAATGCAAGCTTTAGGACT
TCACCTGACAGATCCAAGTCAACGTCTTGTTCAGAACTGTCTTTGGACTCTCAGGAATCTTTCAGATTGACC
CGGGAAGCTCGCCAGGTAGCCCGTAGAC

Appendix D.13 Information on pET-GST-ArmR constructs from Promab Inc.
A) Vector map of pET-GST construct. ArmR fragments were cloned into the vector using the BamHI/XhoI restriction sites. Vector information received by Promab Inc. **B**) Schematic representation of the individual ß-catenin ArmR fragments. Each fragment has an overlap with the previous ArmR in order to be able to map out the LL3 binding site. **C**) Table indicates the expected fragment sizes (kDa). **D**) Coomassie stain of purified pET-GST-ArmR constructs.

A



B



C

pET-constructs	Expected size (kDa)
Arm1	34
Arm2	35.9
Arm3	35.5
Arm4	35.7
Arm5	35.7
Arm6	35.7
GST control	26

D

